Syntheses, Characterization and Reactivity of *trans*-Dioxorhenium(V) and -(VI) Complexes

Thesis by

John C. Brewer

In Partial Fulfillment of the Requirements

for the Degree of

Doctor of Philosophy

California Institute of Technology

Pasadena, California

1991

(Submitted October 17, 1990)

People see only what they are prepared to see.

—RALPH WALDO EMERSON, *Journals*, 1863

Acknowledgments

I arrived at Caltech a stranger and now as I prepare to leave five years later, I realize I am truly fortunate to have met so many remarkable individuals. No human being could possibly survive this experience without the enduring support, love and companionship provided by friends and family. I think the least I can do is acknowledge those who have made my experience special here.

First I would like to thank Terry Collins for his enthusiasm and encouragement during my early Caltech years. The Collins group was indispensable in getting me started in my doctoral research. Yogi and Jeff Peake shared their scientific talents. Erich Uffleman was a source of many interesting chemistry discussions and good company on late-night donut runs to Winchell's. Brian Treco, in addition to being a caring friend, taught me the 'ins and outs' of problem solving and how to get information about anything. I would like to thank my 2nd floor neighbors, the infinitely goofy Al-Ray and Ged, for destroying serious moments when necessary (and often when unnecessary), all of the Hogs (including The Big Cheese) and Barb Burger for coffee-break company, and dinner treats. Barb you are *my* heroine.

Pixie (aka Miriam Zietlow), bless her heart, welcomed me with open arms into the Gray group and in addition to being my best bench-buddy ever, has left me with many fond memories of life off campus. Thanks Miriam, for bowling (and breakfast), Claro's, Santa Anita, Wednesday lunches, euchre (and dinners), for late-night visits to the Saw Mill, and for being such a considerate and thoughtful friend.

I would like to thank Tad Fox, David Smith, Jay Winkler, I-Jy Chang, and Vinny Miskowski for helpful discussions, Bob and Erica for sharing their points of view, Wayne, David, and Julia for bizarre moments. I would like to thank Ramy, for all of his help in and out of lab, and for sharing his infinite 'MacVice.' Mark McCleskey has been a good friend, the world's most patient travelling companion, a critical proofreader and a superb ligand-field tutor. Opie (aka Holden Thorp) has been a faithful friend, roommate, and

colleague. His scientific input has been invaluable and I hope we will have many more fruitful collaborations. Opie, you will soon be able to show me how one lives at the center of the universe.

The Gray group has had a continual stream of visitors who have also contributed to my progress at Caltech. I would like to thank Dave McMillin for interesting discussions, and Pat Sullivan for his boundless enthusiasm for chemistry, his "let's do it" attitude, and for hosting me during my visit to Chapel Hill.

I certainly owe a *great* deal to Harry Gray, who has demonstrated over and over again that it is possible to be a great scientist and a great person at the same time. Everyone who has had the privilege of working with him has been touched by his generosity and fun-loving approach to life. I am very grateful to have had many, many stimulating discussions with Harry (both with and without Old Weller). Thanks Harry, for all of the support, fun times, dinner treats, care and encouragement you have bestowed upon me. I promise I will keep an eye out for 'that truck.'

The support staff at Caltech deserve a special thanks: Dana , Paul, Jess, Larry , Kirby, and Dave Malerba shared their talents with me and helped my research move forward. Catherine, Fran, Virginia, Pat, and Beth have provided friendly assistance on a daily basis. I would like to thank Rhonda, Lori, John, Bruce, and especially Jeannette for considerate and sympathetic attention when I needed it.

Some of the best friendships evolve from sharing mealtime with others; I would thank Barry for breakfast, Jim for lunch, and Andy for dinner company and for being my close friends.

I was lucky to have had the opportunity to experience chemistry *en France* with Michèle and Yves Dartiguenave. I would like to thank them and the Dartiguenave group, especially Marie Alvarez, Eric Deydier, and Marie-Jöelle Menu (et Jean-François), for being wonderful hosts and for tolerating my rusty French. Madame LeClous provided all kinds of assistance and tasty treats on Sunday mornings. André and Philip were great

apartment mates during my stay; I sorely miss the late-evening trips to the Oxford Pub and Place du Capitol.

Scott, Todd and David were the best roommates one could possibly hope for. Scotty has been great company the last five years and I will miss him a great deal. Todd (with his 'kick-ass' drinks) and Val were always there to make sure I 'lightened-up' when I needed to.

I would like to thank Liz for all of the butt-bumping good times in the USA and Italy. Liz, the nine hours of hell in Milano Centrale were well worth it!

As my best friend, Marion defines perfection. I am indebted to her for many fond memories and for the continual support, love and encouragement she has unselfishly given me. She has been my family away from home.

I would like to thank my mom for all of her cheerful phone calls, her faithful letter writing (I figure at this point I am behind by about 52x5 responses), her love and her thoughtful surprises. My father is entirely responsible for nurturing my early scientific interests. Thanks Dad, for your unwavering patience as my childhood lab partner, from building ant farms, and short-wave radios, to climbing the 20-foot television mast to install weather instruments. I would like to thank my brother and sister for their love and concern throughout the years.

Of course, none of this would have been possible without financial support. I would like to thank Caltech for giving me a Blanche A. Mowrer fellowship during my first year, NATO for an exchange grant, and B. P. America for graduate fellowships.

to Mom, Dad, and Marion

Abstract

The synthesis, electronic structure and reactivity of *trans*-dioxorhenium(V) and -(VI) complexes have been examined in detail. An improved general synthesis of *trans*-$[ReO_2(L)_4]X$ complexes is presented. The amine complex $[ReO_2(en)_2]I$ can be made in 90% yield from $ReO_2(PPh_3)_2I$ and ethylenediamine in less than 15 minutes at room temperature. Refluxing methanol suspensions of $ReO_2(PPh_3)_2I$ with 12-50 equivalents of electron-rich pyridines results in the formation of $[ReO_2L_4]I$ compounds in 50 to 85% yield.

Systematic substituent studies reveal the influence of ancillary ligands on the physical properties of *trans*-$[ReO_2(L)_4][PF_6]$ compounds. The Re(VI)/Re(V) redox couple is a linear function of pyridine ligand ΔpK_a: $E_{1/2}$ (ReVI/ReV) = (0.96 + 0.21ΔpKa) V vs. Fc^+/Fc. The $d_{xy}/d_{xz},d_{yz}$ energy gap is also a linear function of pyridine ΔpK_a; increasing the pyridine basicity lowers the energy of the $d_{xy} \rightarrow d_{xz},d_{yz}$ transition and the energy of the ^3E_g $(d_{xy})^1(d_{xz},d_{yz})^1$ excited state. The excited-state properties of *trans*-$[ReO_2(L)_4][PF_6]$ pyridine complexes follow a trend consistent with the energy-gap law.

Strongly basic 4-dialkylaminopyridine ligands stabilize d^1 *trans*-dioxorhenium(VI) complexes. Analysis of the X-ray structure of *trans*-$[ReO_2(dmap)_4]^{2+}$ shows that there is considerable shortening (0.04 Å) in the Re-N bond lengths relative to Re(V) analogues, but the Re-oxo bond lengths are virtually the same in both oxidation states. The EPR spectrum of the d^1 ion *trans*-$[ReO_2(dmap)_4]^{2+}$ (dmap = 4-dimethylaminopyridine) has been measured in a 50% DMSO/H_2O glass at 7 K. Analysis of the spectrum gives $g_\perp = 1.91$, $A_\perp = 0.031$ cm^{-1}, $g_{||} = 1.83$, $A_{||} = 0.060$ cm^{-1}, and $Q_z = 0.0075$ cm^{-1}. Because of the large quadrupole coupling, the forbidden ($\Delta M_I = \pm1, \pm2$) transitions are quite intense and some are stronger than the allowed ($\Delta M_I = 0$) transitions. Comparison of Q_z values and $d_{xy} \rightarrow d_{xz}$, d_{yz} transition energies for *trans*-$[ReO_2(dmap)_4]^{2+}$ and related monooxo and mononitrido complexes confirms that the ligand-field splitting associated with the multiply bonded units increases in the order $ReO^{4+} < ReN^{3+} < ReO_2^{2+}$.

Table of Contents

List of Figures

Chapter 1

Chapter 2

Chapter 3

List of Tables

Chapter 3

Chapter 4

List of Abbreviations

A	associative (mechanism)
Å	angstrom
anal.	analysis
assign.	assignment (NMR spectra)
asym	asymmetric
atm	atmosphere
bpy	2,2'-bipyridine
br	broad
Bu	butyl
C	Celsius, coulomb
ca.	approximately (circa; about)
cal	calorie
calcd	calculated
cb	conjugate (counter) base
cf.	compare
cm^{-1}	wavenumber(s)
concd	concentrated
cont'd	continued
cor	corrected
CT	charge transfer
CV	cyclic voltammetry
D	dissociative (mechanism)
d	doublet (spectral)
δ	parts per million (NMR scale)
Δ O.D.	optical density change
diphos	1,2-bis(diphenylphosphino)ethane

dmap	4-dimethylaminopyridine
DMSO	dimethyl sulfoxide
DNA	deoxyribonucleic acid
dppen	1,2-bis(diphenylphosphino)ethene
Dq, Ds, Dt	cyrstal field splittings
e^-	electron
ε	molar absorptivity
$E_{1/2}$	half-wave potential
$E_{(0\text{-}0)}$	electronic transition energy between two n = 0 vibrational levels
e $Å^{-3}$	electrons per cublic angstrom
ed.	edition
Ed., Eds.	editor, editors
e.g.	for example
E_{em}	emission energy maximum
en	ethylenediamine
EPR	electron paramagnetic resonance
eq	equation
equiv	equivalent
ESR	electron spin resonance
Et	ethyl
et al.	and others
etc.	and so forth
eV	electron volt
exp	exponential
Φ_{em}	emission quantum yield
FTIR	Fourier transform infrared spectroscopy
g	gram

G	Gauss, giga
GOF	goodness-of-fit
h	hour
hν	UV-visible radiation
HOMO	highest occupied molecular orbital
Hz	Hertz (s^{-1})
I	electric current, intimate mechanism
I_a	intimate-associative mechanism
I_d	intimate-dissociative mechanism
i.e.	that is
int.	integration results (NMR spectra)
inten	intensity
IR	infrared
k	kilo, rate constant
k_r	radiative decay rate constant
k_{nr}	non-radiative decay rate constant
K	Kelvin
l	liquid
L	litre, ligand
λ	wavelength
λ_{max}	band maximum
LF	ligand field
LMCT	ligand-to-metal charge transfer
ln	natural logarithm
LUMO	lowest unoccupied molecular orbital
3,5-lut	3,5-lutidine
m	meter, milli, multiplet (spectra)

μ	micro
μ_B	Bohr magneton
M	mega (10^6), metal, mol dm^{-3} or mol L^{-1} (molar)
max	maximum
Me	methyl
4-MeOpy	4-methoxypyridine
3-Medmap	3-methyl-4-(dimethylamino)pyridine
min	minute, minimum
mg	milligram
MLCT	metal-to-ligand charge transfer
mmHg	millimetres of mercury (measure of pressure)
MO	molecular orbital
mol	mole
mult.	multiplicity (NMR spectra)
MV^{2+}	methylviologen
n	nano
n	normal (as in *n*-butyl, *n*-Bu)
ν	frequency (wavenumber)
ν_{asym}	frequency of asymmetric stretch
ν_{sym}	frequency of symmetric stretch
NHE	normal hydrogen electrode
nm	nanometer
μ_N	nuclear magneton
NMR	nuclear magnetic resonance
no.	number
obsd	observed
ORTEP	Oak Ridge Thermal Ellipsoid Peak Program

p	page, negative logarithm of (as in pH, pKa)
PAR	Princeton Applied Research
Ph	phenyl
4-Phpy	4-phenylpyridine
phen	1,10-phenanthroline
4-pic	4-picoline (4-methylpyridine)
pKa	negative logarithm of acid dissociation constant
pp	pages
PPh_3	triphenylphosphine
ppm	parts per million
Pr	propyl
py	pyridine
4-pyrrpy	4-pyrrolidinopyridine
q	quartet (spectra)
ρ_{calc}	calculated density
ref	reference
rel	relative
RT	room temperature
s	second, singlet (NMR), strong (IR spectra)
SCE	standard calomel electrode
sec	secondary (as in *sec*-butyl, *sec*-Bu)
sh	shoulder (spectral)
SSCE	saturated sodium choride electrode
sym	symmetrical
t	triplet (spectra)
t	tertiary (as in *t*-Bu; but *tert*-butyl)
τ_o	excited-state lifetime

TBABr	tetra-*n*-butylammonium bromide
TBAH	tetra-*n*-butylammonium hexafluorophosphate
THF	tetrahydrofuran
tmc	1,4,8,11-tetramethyl-1,4,8,11-tetraazacyclotetradecane
TMPD	tetramethyparaphenylenediamine
TPP	*meso*-tetraphenylporphyrin
trans. coeff.	transmission coefficient
uncor	uncorrected
UV	ultraviolet
UV-vis	ultraviolet-visible
V	Volt
vol	volume
vs	very strong (UV-vis, IR spectra)
vs.	versus
v/v	volume-to-volume ratio
vw	very weak
w	weak
W	watt
X	halide

Chapter 1.

Introduction and Background.

INTRODUCTION

Metal-oxo complexes are an important class of oxidizing agents.[1,2] For this reason, there have been numerous studies to obtain a detailed understanding of their electronic structure and reactivity patterns.[3-5] These species also have biological relevance; the reactive intermediate in the cytochrome P-450 cycle has been postulated to be an iron(IV) terminal oxo porphyrin complex.[6] In an attempt to develop a detailed understanding of this last species, several groups have studied the generation and reactivity of metal-oxo porphyrin complexes of the transition metals.[7,8]

Metal-oxo porphyrin complexes are often very thermally reactive and can only be generated as reactive transients from a metal porphyrin halide and some source of oxygen atoms such as hydrogen peroxide or iodosylbenzene. Addition of an oxygen atom formally results in a two-electron metal-centered oxidation. In this manner, metal oxo complexes have been made with metals in a variety of oxidation states and different d-electron configurations. Examples include O=Mn(TPP), O=Cr(X)(TPP), and O=Fe(X)(TPP) with d-electron configurations of 2, 1, and 4, respectively.

Although metal porphyrin complexes have certainly dominated the metal-oxo area for the last decade, they are not the only species which have been studied in mechanistic detail. Meyer and coworkers have published a very informative series of mechanistic studies concerning the oxidation chemistry associated with $[(bpy)_2(py)Ru(O)]^{2+}$ and related complexes.[9-17] This ruthenium(IV) oxo complex epoxidizes olefins, and can oxidize aldehydes, alcohols[17] and unsaturated hydrocarbons.[15]

Che and coworkers have also developed oxoruthenium complexes that are effective oxidants. This group has made use of oxidation resistant saturated amine ligands and nitrogen heterocycles as successful ancillary ligands.[18]

What is the origin of metal-oxo reactivity, and how does oxygen atom transfer proceed at the molecular level? To begin to address these questions, it is essential to examine in detail, the electronic structure associated with these compounds.

BACKGROUND

The MO diagram developed by Ballhausen and Gray[19] to explain the EPR, magnetic, and optical properties of the vanadyl ion, $[VO(H_2O)_5]^{2+}$, is a good starting point for understanding the electronic structure of metal-(di)oxo complexes with square-pyramidal (point group C_{4v}) and octahedral (point group D_{4h}) geometries. This MO diagram is provided in Figure 1.1. The presence of the oxo ligand, with its strong σ– and π-donor properties, partially resolves the degeneracy in the e_g and t_{2g} manifolds of the d-orbitals in an octahedral environment. Taking the z-axis as lying along the M-O axis, the d_{xz} and d_{yz} orbitals are used to form π-bonds with the oxo ligand(s), leaving the d_{xy} orbital non-bonding in nature. In monooxo complexes, the bond M-O bond order would formally be 3 (one σ– and two π-bonds); in the case of a dioxo complex, each oxygen ligand forms one π-bond with one $d\pi$ orbital and the net bond order for each M-O bond is 2.

The MO diagram in Figure 1.1 readily explains the empirical observation that stable oxo complexes with these coordination geometries exist only for d configurations of 4 or less.[1,4] This is a result of the requirement that at least one $d\pi$ orbital must be vacant (or two half-occupied) to accept an electron pair from an oxygen p-orbital. In the case of dioxo complexes, a limit of 2 electrons exists, as both d_{xz} and d_{yz} must be vacant to allow each oxygen atom to form one π-bond with the metal center.

When one considers the metal-oxo complexes that are known to be effective oxidants, the following observation is noted: All are either good electron-transfer oxidants and/or have the d_{xz},d_{yz} orbitals populated. The first property ensures that the compound is capable of extracting an electron from the substrate, thereby activating it towards further redox or acid-base reactions. The second property primes the oxo group to become extremely reactive upon electron addition; M-O π-antibonding levels become populated causing an M-O π-bond to rupture, increasing the oxo ligand's basicity. The oxo ligand becomes susceptible to protonation or electrophilic attack by an electron poor substrate.

Figure 1.1. MO diagram for octahedral and square-pyramidal metal-oxo complexes. The diagram is valid for a *trans*-dioxo complex with D_{4h} symmetry. For monooxo complexes of C_{4v} symmetry, remove the subscripts u and g on the orbital labels.

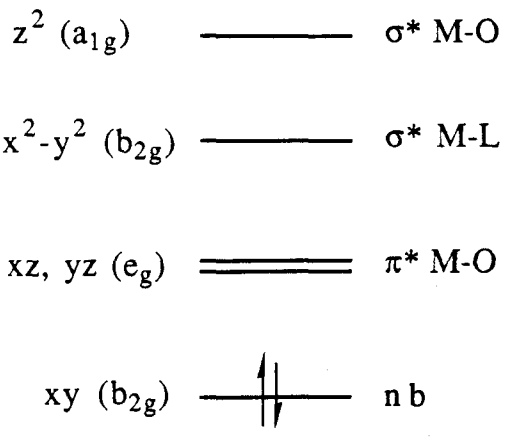
z^2 (a_{1g})
σ* M-O
x^2-y^2 (b_{2g})
σ* M-L
xz, yz (e_g)
π* M-O
xy (b_{2g})
n b

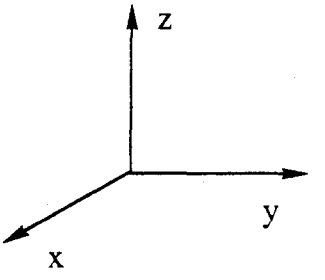
z
y
x

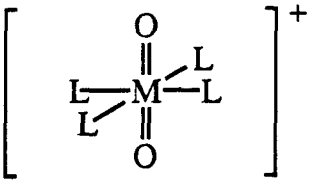
O
L
L
M
L
L
O
+

The above information can be put to use in the design of new metal-oxo reagents. The ideal complex would be strongly oxidizing with as high a d-electron population as possible. This is exactly what nature has accomplished with Fe(IV)-oxo reagents. This ion is highly oxidizing in virtually all[20] coordination environments and has a metal-oxo bond order of two. Upon transfer of a single electron to this entity, the metal-oxo π-bond would be ruptured, and the oxo group would become more nucleophilic. The design of such species has been difficult because of the inherently high activity associated with these d-configurations. Meyer's complex, $[(bpy)_2(py)Ru(O)]^{2+}$, probably represents the best example to date of this approach.

If one considers the MO diagram of Figure 1.1, an alternative approach becomes evident: One could attempt to activate thermally inert species photochemically. Excitation of a non-bonding (d_{xy}) electron to the d_{xz},d_{yz} level will have two consequences: it will make the compound a stronger (electron-transfer) oxidant by virtue of the hole created in d_{xy}, and it will weaken the M-O bond because of π^* orbital population.

To explore this approach, Winkler and Gray began a detailed study[21] of the electronic structure and excited-state properties of the two possible cases, d^1 and d^2. In the first case, molybdenum(V) oxohalide species, $[MoOX_4]^-$, were considered. These species were deemed to be unpromising because of their short-lived excited states.[21] In order for bimolecular photochemistry to compete with other deactivation processes, the excited state must live for at least 50 ns,[21] and these compounds did not fulfill this requirement.

It was thought that d^2 complexes might have inherently longer-lived excited states because of the potential spin-barrier that could exist for relaxation back to the ground state (*i.e.*, triplet-singlet conversion).[21] Indeed, this is the case for the rhenium(V) complex *trans*-$[ReO_2(py)_4]^+$. Detailed single-crystal absorption and emission studies[22] revealed that the lowest excited state was a triplet with a $(d_{xy})^1(d_{xz},d_{yz})^1$ configuration, as was expected. In fluid solution, this excited state had a mean radiative lifetime of 10 μs in the absence of protic solvents.[22,23] A Franck-Condon analysis of the vibronic structure present in the low

temperature emission spectrum revealed that there was a 0.07 Å elongation along Re-O in the excited state, indicative of the bond weakening expected from (d_{xz},d_{yz}) population.[22] In light of doing photochemcially induced oxo transfer, these results were quite encouraging. This flicker of hope was rapidly extinguished, however, by the fact that the oxo groups of *trans*-$[ReO_2(py)_4]^+$ were found to be photo-inert towards transfer to even the most obliging of acceptors, triphenylphosphine.[21,24]

In contrast to the lack of success that had been observed in the rhenium systems, Che and coworkers found some reactivity in related osmium systems. Photo-induced oxo transfer to triphenylphosphine was accomplished as shown in the following reaction:[25]

$$[OsO_2(tmc)]^{2+} + 2PPh_3 \xrightarrow[CH_3CN]{h\nu,\ \lambda > 300\ nm} [Os(NCCH_3)_2(tmc)]^{2+} + 2\ O{=}PPh_3 \quad (1)$$

Photochemical alcohol oxidation could also be effected as shown below:[26]

$$[OsO_2(CN)_4]^{2-} + 2\ PhCH_2OH \xrightarrow[MeCN]{h\nu,\ \lambda > 300\ nm} [Os(NCMe)_2(CN)_4]^{2-} + 2\ PhCHO + 2\ H_2O \quad (2)$$

84%

Even alkene substrates could be functionalized:[26]

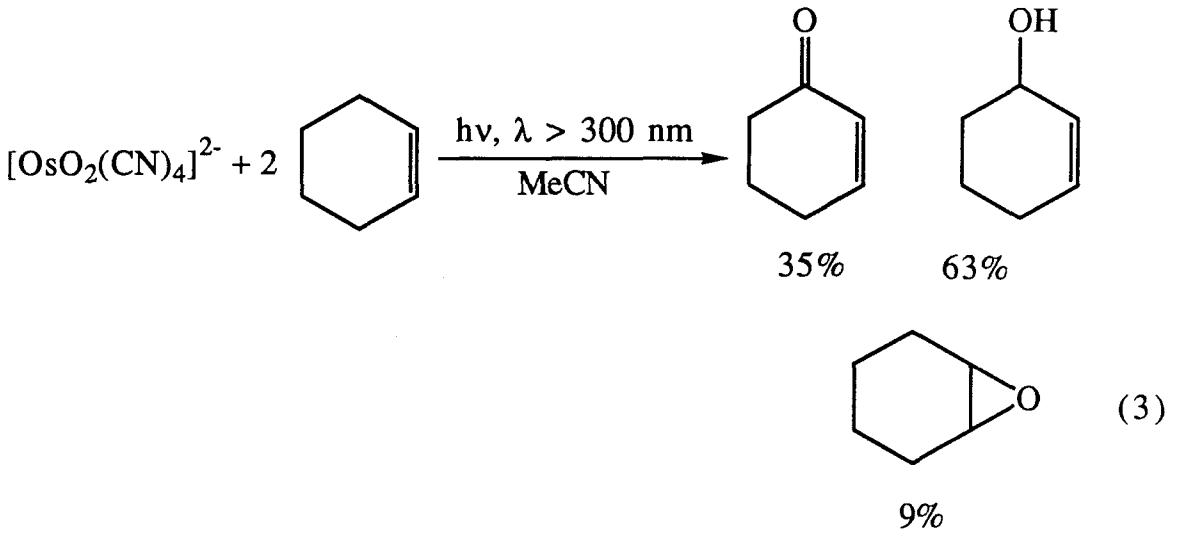

(3)

Trans-$[ReO_2(py)_4]^+$, *trans*-$[OsO_2(tmc)]^{2+}$, and *trans*-$[OsO_2(CN)_4]^{2-}$ are isoelectronic systems with the same lowest-energy excited states.[25] What then, is the source of the drastic difference in excited-state reactivity between the rhenium and osmium systems?

Recall that metal-oxo bond weakening was only one component of the effect expected from electronic excitation. The other, which has not been examined so far, is the redox character of the excited state.

Using thermodynamic cycles, excited-state potentials can be estimated from a knowledge of ground state electrochemistry and excited state energy as shown in the equations below:[27]

$$E^o(M^+/M^*) = E^o(M^+/M) - E_{(0,0)}[M \rightarrow M^*] \quad (4)$$

$$E^o(M^*/M^-) = E^o(M/M^-) + E_{(0,0)}[M \rightarrow M^*] \quad (5)$$

As indicated by the above equations, excited complexes are both stronger oxidants and reductants than when in their ground states.[27]

Che and coworkers found that the osmium complexes could be reduced electrochemically as shown below:[25]

trans-$[OsO_2(tmc)]^{2+} + e^- \rightarrow$ *trans*-$[OsO_2(tmc)]^+$ $E_{1/2}$ = -0.31 V vs. SSCE (6)

trans-$[OsO_2(CN)_4]^{2-} + e^- \rightarrow$ *trans*-$[OsO_2(CN)_4]^{3-}$ $E_{1/2}$ = -1.1 V vs. SSCE (7)

Using the above formal potentials and an estimated $E_{0\text{-}0}$ value of ~2 eV (~16,000 cm^{-1} or 620 nm emission), it is possible to predict that the above complexes will behave as excited-state oxidants with potentials of 1.7 and 0.9 V (vs. SSCE) respectively.[25] It is significant that no oxidative chemistry is observed in these systems within the anodic limits of the solvent (2.5 V vs. SCE in CH_3CN), suggesting that the excited states of these complexes can be no more reducing than 0.5 V. That the osimium complexes behave as excited-state oxidants was verified experimentally by electron-transfer quenching experiments,[25] such as the one shown below:

$$[OsO_2(tmc)]^{2+} + TMPD \xrightarrow[MeCN]{h\nu,\ \lambda > 300\ nm} [OsO_2(tmc)]^{+} + TMPD^{+\bullet} \quad (8)$$

Using the known reduction potential of 0.12 for the radical cation of tetramethylparaphenylenediamine, $(TMPD)^{+\bullet}$, the above reaction is determined to be exergonic by 0.8 V.

From these results, it is believed that substrate oxidation is initiated via electron abstraction by the excited osmium complex. This is followed by a nucleophilic attack on the substrate by the oxo ligand. The net result is the ultimate transfer of both oxo ligands to substrate molecules by a complex cascade of reactions after these initial steps.[28]

Pipes and Meyer[29] first studied the aqueous electrochemistry of *trans*-$[ReO_2(py)_4]^+$ and this was followed by work in non-aqueous solvents by Thorp *et al*[30]. In contrast to what was observed in the osmium systems, *trans*-$[ReO_2(py)_4]^+$ could be reversibly *oxidized* at ~1.3 V vs. SSCE. Considering an excited-state energy of ~2.0 V, the Re(VI)/Re^*(V) potential was estimated to be -0.7 V vs. SSCE. In its excited state, *trans*-

$[ReO_2(py)_4]^+$ was therefore expected to behave as a reductant. This was verified by excited-state electron-transfer quenching reactions,[30] such as that shown below in Equation 9.

$$[ReO_2(py)_4]^+ + MV^{2+} \xrightarrow[MeCN]{h\nu,\ \lambda > 300\ nm} [ReO_2(py)_4]^{2+} + MV^{+\bullet} \quad (9)$$

The reaction depicted in Equation 9 is predicted to be exergonic by ~0.25 V vs. SSCE.

The thermodynamics relevant to the osmium and rhenium systems are summarized in the modified Latimer diagrams presented in Figure 1.2. Note the complimentary behavior that exists between the two systems. A molecular orbital view of the consequences of these thermodynamic properties is presented in Figure 1.3. *Trans*-$[ReO_2(py)_4]^+$ behaves as an excited state reductant and is converted into a d^1 species by electron transfer. In contrast, *trans*-$[OsO_2(CN)_4]^{2-}$ and *trans*-$[OsO_2(tmc)_4]^{2+}$ behave as excited-state oxidants and are converted into reactive d^3 species.

Although the oxo groups in *trans*-$[ReO_2(py)_4]^+$ were found to be photo-inert, the oxidized rhenium center generated by photo-induced electron transfer appeared to be reactive. When the reaction represented in Equation 9 was carried out by bulk photolysis in CH_2Cl_2 solvent, the radical cation $MV^{+\bullet}$ accumulated, indicating consumption of the rhenium(VI) species. Electrochemically generated *trans*-$[ReO_2(py)_4]^{2+}$ was observed to react with silanes and secondary alchohols. Bulk electrolysis of *sec*-phenethylalcohol was effected in the presence of *trans*-$[ReO_2(py)_4]^{2+}$ with 90% current efficiency and three 'turn-overs' of rhenium complex base on the coulometry.[30] No detailed mechanistic information could be obtained nor could the structure of the active oxidant be studied because of the short-lived character of *trans*-$[ReO_2(py)_4]^{2+}$.

The results obtained for the d^2 osmium complexes clearly show that the original idea of photo-induced oxo transfer can be realized under appropriate conditions. It is clear that the

Figure 1.2. Modified Latimer diagrams for *trans*-$[ReO_2(py)_4]^+$ and *trans*-$[OsO_2(tmc)]^{2+}$.

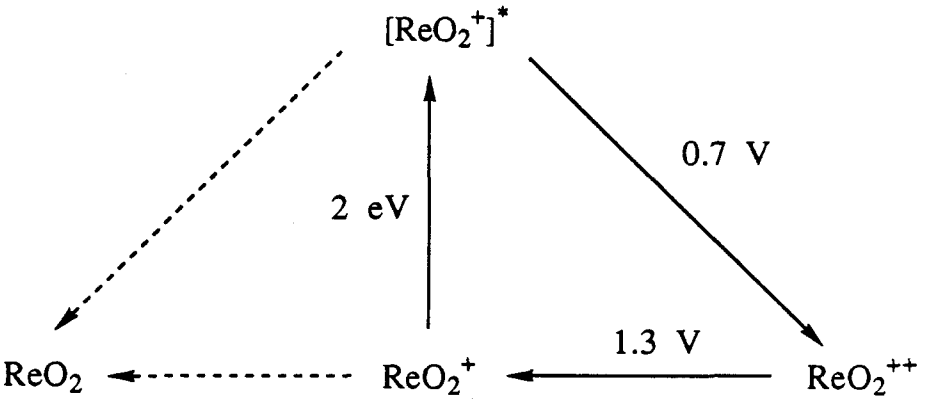
[ReO2+]*
0.7 V
2 eV
1.3 V
ReO2
ReO2+
ReO2++

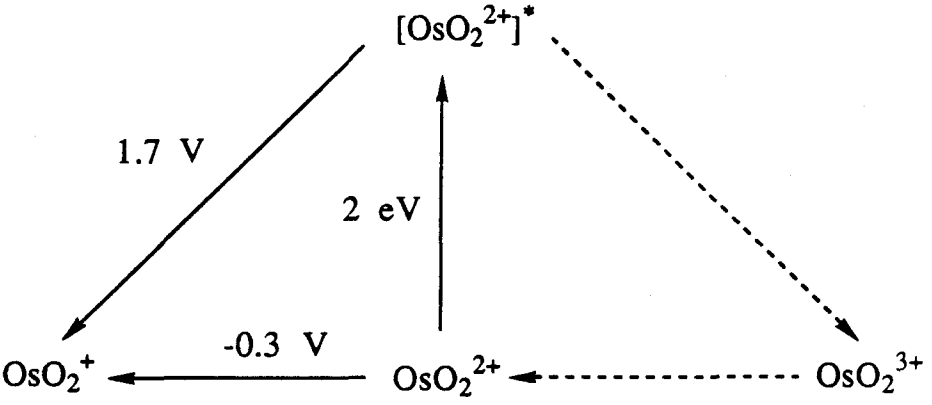
[OsO2 2+]*
1.7 V
2 eV
-0.3 V
OsO2+
OsO2 2+
OsO2 3+
d3
d2
d1

Figure 1.3. MO description of the excited-state reaction course for *trans*-$[ReO_2(py)_4]^+$ and *trans*-$[OsO_2(tmc)]^{2+}$.

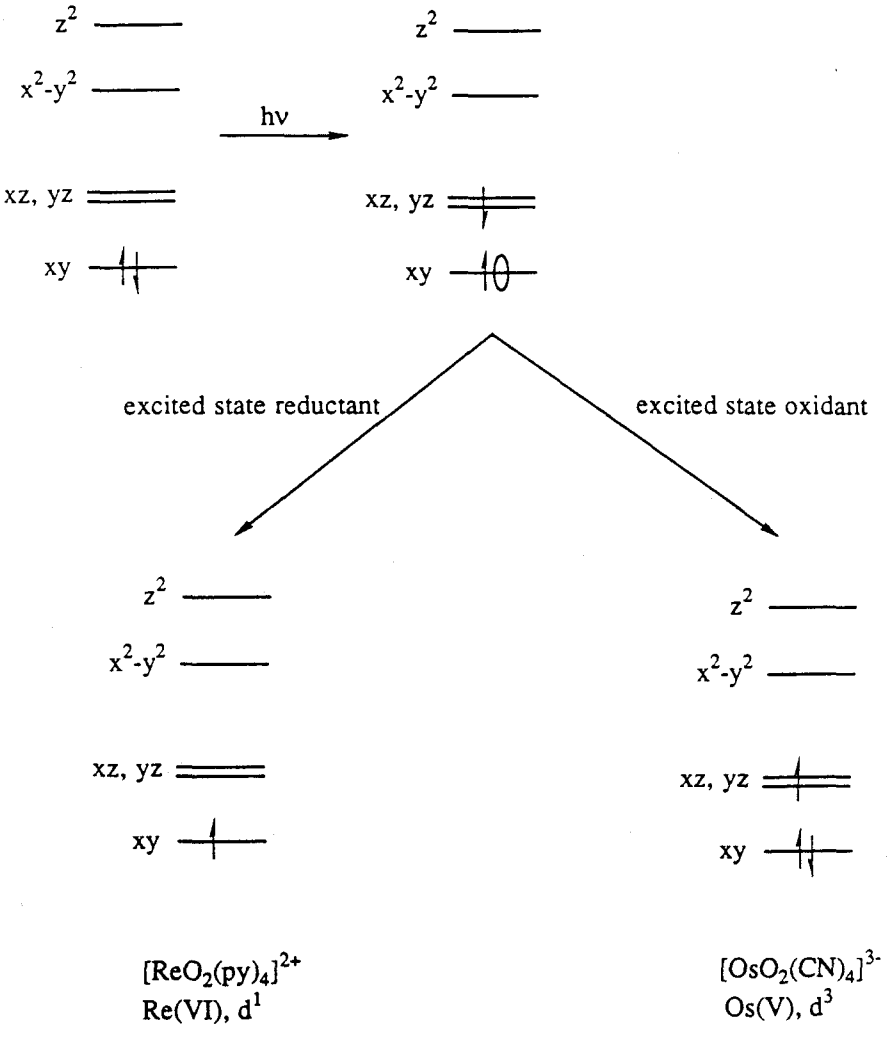
z²
x²-y²
xz, yz
xy
hν
z²
x²-y²
xz, yz
xy
excited state reductant
excited state oxidant
z²
x²-y²
xz, yz
xy
z²
x²-y²
xz, yz
xy
[ReO2(py)4]2+
Re(VI), d1
[OsO2(CN)4]3-
Os(V), d3

ground-state redox properties are crucial and set the stage for excited-state behavior. The natural direction of this research is to explore to what extent the ground and excited-state properties of metal-oxo units can be modified by changes in ancillary ligand identity. Can the environment around ReO_2^+ be modified to make it behave in an analogous fashion to osmium complexes? There is also the question of the nature and reactivity of the d^1 species, *trans*-$[ReO_2(py)_4]^{2+}$. It is the purpose of this thesis to begin walking down the long path to answering these questions.

In Chapter 2, we will discuss the first problem encountered in this endeavor: The insertion of the *trans*-ReO_2^+ unit into a variety of coordination environments. In order to modify the ancillary ligands at will, it is essential to have efficient synthetic methods for making the complexes. A new, general synthetic method for insertion of the *trans*-ReO_2^+ unit will be presented along with a brief discussion of the reaction mechanism.

In Chapter 3, the electronic structure, excited-state properties and redox behavior of a family of pyridine complexes and some phosphine compounds are examined in detail. From these studies, it will become clear how systematic changes in ancillary ligand affect the physical properties of *trans*-$[ReO_2(L)_4]^+$ complexes.

Chapter 4 is devoted to the synthesis, characterization and reactivity of some stabilized *trans*-dioxorhenium(VI) compounds that provide insight into the mechanism of *trans*-$[ReO_2(py)_4]^{2+}$ alcohol oxidation. Optical, EPR, and X-ray structural information are used to gain a better understanding of *trans*-$[ReO_2(L)_4]^{2+}$ electronic structures. This information is valuable for the design of new complexes containing high-valent O=Re=O units.

REFERENCES AND NOTES

(1) Nugent, W. A.; Mayer, J. M. *Metal-Ligand Multiple Bonds*; John Wiley and Sons: New York, 1988.

(2) Sheldon, R. A.; Kochi, J. K. *Metal-Catalyzed Oxidations of Organic Compounds*; Academic: New York, 1981.

(3) Griffith, W. P. *Coord. Chem. Rev.* **1970**, *5*, 459-517.

(4) Holm, R. H. *Chem. Rev.* **1987**, *87*, 1401-1449.

(5) Yamaguchi, K.; Takahara, Y.; Fueno, T. In *Applied Quantum Chemistry, Proceedings of Nobel Laureate Symposium, Meeting Date 1984*; Smith, V. H.; Schaefer, H. F., Ed.; 1986; pp 155-184.

(6) Guengerich, F. P.; MacDonald, T. L. *Acc. Chem. Res.* **1984**, *17*, 9-16.

(7) Bruice, T. C. *Aldrichimica Acta* **1988**, *21*, 87-94.

(8) Groves, J. T.; Nemo, T. E. *NATO Adv. Study Int. Ser., Ser. C.,(Coord. Chem. Metalloenzymes)* **1983**, *100*, 329-341.

(9) Dobson, J. C.; Meyer, T. J. *Inorg. Chem.* **1988**, *27*, 3283-3291.

(10) Gilbert, J.; Roecher, L.; Meyer, T. J. *Inorg. Chem.* **1987**, *26*, 1126-1132.

(11) Meyer, T. J. *J. Electrochem. Soc.* **1984**, *131*, 221C-228C.

(12) Meyer, T. J. In *Metal Oxo Complexes and Oxygen Activation*; Martell, A. E., Ed.; Plenum: New York, 1988; pp 33-47.

(13) Moyer, B. A.; Thompson, M. S.; Meyer, T. J. *J. Am. Chem. Soc.* **1980**, *102*, 2310-2312.

(14) Roecher, L.; Dobson, J. C.; Vining, W. J.; Meyer, T. J. *Inorg. Chem.* **1987**, *26*, 779-781.

(15) Seok, W. K.; Dobson, J. C.; Meyer, T. J. *Inorg. Chem.* **1988**, *27*, 5-8.

(16) Seok, W. K.; Meyer, T. J. *J. Am. Chem. Soc.* **1988**, *110*, 7358-7367.

(17) Thompson, M. S.; Meyer, T. J. *J. Am. Chem. Soc.* **1982**, *104*, 4106-4115.

(18) Che, C.; Ho, C.; Lee, W.; Lau, T. In *PREPRINTS, Division of Petroleum Chemistry*; Haines, W. E., Ed.; American Chemical Society: Washington, D. C., 1990; Vol. 35, pp 179-186.

(19) Ballhausen, C. J.; Gray, H. B. *Inorg. Chem.* **1962**, *1*, 111-122.

(20) For an exceptional example of stabilized, five-coordinate Fe(IV), see: Collins, T. J.; Kostka, K. L.; Münck, E.; Uffelman, E. S. *J. Am. Chem. Soc.* **1990**, *112*, 5637-5639.

(21) Winkler, J. R.; Ph.D. Thesis, August 1983, California Institute of Technology.

(22) Winkler, J. R.; Gray, H. B. *Inorg. Chem.* **1985**, *24*, 346-355.

(23) Winkler, J. R.; Gray, H. B. *J. Am. Chem. Soc.* **1983**, *105*, 1373-1374.

(24) Nocera, D. G.; Maverick, A. W.; Winkler, J. R.; Che, C. M.; Gray, H. B. *ACS Symp. Ser.* **1983**, *211*, 21-33.

(25) Che, C. M.; Yam, V. W. W.; Cho, K. C.; Gray, H. B. *J. Chem. Soc., Chem. Commun.* **1987**, 948-949.

(26) Yam, V. W. W.; Che, C. M.; Tang, W. T. *J. Chem. Soc., Chem. Commun.* **1988**, 100-102.

(27) Balzani, V.; Bolletta, F.; Gandolfi, M. T.; Maestri, M. *Top. Current. Chem.* **1978**, *75*, 1-64.

(28) Che, C. -M., personal communcation, 1988.

(29) Pipes, D. W.; Meyer, T. J. *Inorg. Chem.* **1986**, *25*, 3256-3262.

(30) Thorp, H. H.; Van Houten, J.; Gray, H. B. *Inorg. Chem.* **1989**, *28*, 889-892.

Chapter 2.

Synthetic Routes to *trans*-Dioxorhenium(V) Complexes.*

*A portion of this chapter has been previously published: Brewer, J. C.; Gray, H. B. *Inorg. Chem.* **1989**, *28*, 3334-3336.

INTRODUCTION

Before exploring the effects of ancillary ligand identity on the ground and excited-state properties of *trans*-dioxorhenium(V) complexes, it is necessary to develop a facile method for inserting the *trans*-ReO_2^+ unit into a variety of ligand environments. The ideal starting material would (1) be synthesized in high yield from $K[ReO_4]$ (commercially available), (2) contain ligands that could be easily substituted without complicating product work-up, and (3) require only stoichiometric amounts of ligands in substitution reactions.

The Re(IV) compound, $K_2[ReCl_6]$, is the common starting material for the syntheses of coordination complexes containing the *trans*-ReO_2^+ unit. For example, the compound *trans*-$[ReO_2(py)_4]Cl$ is obtained (in 34 to 60% yield) by bubbling O_2 through an aqueous pyridine solution of $K_2[ReCl_6]$.[1]

$$2K_2[ReCl_6] + 14\ py + 1/2\ O_2 \rightarrow 2[ReO_2(py)_4]Cl{\cdot}2H_2O + 6(pyH)Cl + 4KCl \quad (1)$$

In a similar fashion, the ethylenediamine complex *trans*-$[ReO_2(en)_2]Cl$ is synthesized by reacting $K_2[ReCl_6]$ in aerated 90% ethylenediamine for a 12 h period.[2]

$$4\ K_2[ReCl_6] + 8\ C_2H_4(NH_2)_2 + O_2 + 6\ H_2O \rightarrow 4\ [ReO_2(en)_2]Cl + 8\ KCl + 12\ HCl \quad (2)$$

The three major drawbacks of methods employing this material are: (1) long reaction times, (2) the use of aqueous solvents (because of the solubility properties of $K_2[ReCl_6]$), and (3) moderate to poor yields of desired product. Rhenium(IV) has a d^3 configuration and would therefore be expected to be substitutionally inert.[3,4] Because the target molecules contain Re(V), both an oxidant *and* an oxygen source must be present under the

reaction conditions. For all of the above reasons, $K_2[ReCl_6]$ is a poor choice of starting material for *trans*-$[ReO_2(L)_4]^Z$ compounds.

A literature search (CAS on-line) was conducted in order to locate all varieties of known complexes containing an ReO_2^+ framework. The compound $ReO_2(PPh_3)_2I$ stood out as exceptional; it has a *cis* disposition of oxo groups (rare for a d^2 dioxometal configuration) and is coordinatively unsaturated.[5] Substitution of the phosphine ligands for 'harder' amine donors was expected because Re(V) is a hard acid.[6] These characteristics and the fact that the complex could be synthesized[5] in two (high yield) steps from $K[ReO_4]$ lead us to believe that $ReO_2(PPh_3)_2I$ might be an ideal synthon for the ReO_2^+ unit.

Earlier work lent support to this hypothesis. In 1969, Freni[7] first prepared and studied the reactivity of $ReO_2(PPh_3)_2I$. Noteworthy was the observation that *trans*-$[ReO_2(py)_4]I$ could be obtained in 91% yield from boiling $ReO_2(PPh_3)_2I$ in neat pyridine for 15 minutes.

Chakravorti[8-14] had commented on the lability of the pyridine ligands in *trans*-$[ReO_2(py)_4]^+$. Hence, the use of this material as an ReO_2^+ synthon is also briefly explored in this chapter.

EXPERIMENTAL

Materials. All chemicals were either of reagent grade or the best grade commercially available and used as received. The ligand 4-methoxypyridine was prepared from the commercially available N-oxide using the method of Ochiai,[15] as described below. The sample of 3-methyl-4-dimethylaminopyridine used was a generous gift from Dr. Eric Scriven of Reilly Tar and Chemicals.

Physical Measurements. ^1H NMR spectra were recorded at 90 MHz on a Varian EM-390 spectrometer or at 89.93 MHz on a JEOL FX90-Q spectrometer. ^1H chemical shifts are reported in ppm (δ) using the solvent ($CHCl_3$ δ7.24, $CHDCl_2$ δ5.32, CD_3SOCD_2H δ2.49, CD_2HCN δ1.93, or CD_3COCHD_2 δ2.04) as an internal standard,

unless noted otherwise. $^{31}P\{^{1}H\}$ NMR spectra were recorded at 36.27 MHz on a JEOL FX90-Q spectrometer and referenced to external 85% aqueous phosphoric acid. By established convention, peaks appearing upfield from this standard are assigned *negative* shift values. Infrared spectra were recorded as Nujol mulls on a Beckman IR 4240 spectrometer or on a Perkin-Elmer 1600 series FTIR. Background-corrected electronic absorption spectra were obtained using a Shimadzu UV-260 recording spectrometer or on a Cary Model 14 Spectrophotometer that had been rebuilt by On-Line Instruments Service (OLIS). Quartz cells of 1-cm pathlength were used in all cases. Elemental analyses were obtained at the Caltech analytical facility or from Galbraith Laboratories Inc.

Syntheses. The purple-violet compound $ReO_2(PPh_3)_2I$, **1**, was prepared by hydrolysis of $ReO(OEt)(PPh_3)_2I_2$ using the literature method[7] except that $KReO_4$ was used in place of $H[ReO_4]$. The complex $ReO_2(PPh_3)_2I$ is soluble in benzene, chloroform, dichloromethane and nitromethane. It is insoluble in water, alcohols, acetone, diethyl ether and hydrocarbons. Except where noted, all manipulations were carried out in air.

4-methoxypyridine. Approximately 25 mL of 6 N NaOH solution was prepared by dissolving 6 grams of NaOH in 25 mL of distilled water. After mixing, this solution was set aside to cool to room temperature. 4-Methoxypyridine-*N*-oxide (1.32 g, 10.5 mmol) was placed in a 100-mL round-bottomed flask and dissolved in ~11 mL of chloroform. The solution, which contained a small amount of undissolved solid, was immersed in an ice water bath and allowed to cool for 5 min. With rapid stirring, PCl_3 (2 mL, 23 mmol) was added dropwise over a 10 min period. The first drop caused a violent fizzing in the solution that was *not* observed with subsequent additions. After the addition of PCl_3, the solution was homogeneous and pale yellow in color. The cooling bath was removed, and the solution was allowed to warm to room temperature. After standing for 5 min, it developed an opaque, milky appearance. The mixture was brought to and maintained at reflux for 35 min. After this heating period, the solution was still opaque and a small number of pale orange crystals had formed. Heating was discontinued and the solution

cooled to room temperature. The flask was immersed in an ice bath and allowed to cool for 5 min. Distilled water (15 mL) was then *slowly* added from an addition funnel over a 10 min period, while stirring vigorously. (CAUTION: This hydrolysis reaction is very exothermic.) After the addition was complete, the solution was left to stir 5 min and then the aqueous and organic layers were separated. The clear aqueous layer was made alkaline (pH ~11 by litmus paper) by *slow* addition of ~15 mL of 6 N NaOH solution. The approach of the correct pH was signalled by the development of an opaque appearance to the solution. The alkaline aqueous layer was extracted with 3 X 40 mL of diethyl ether. These extracts were combined and dried over K_2CO_3 for 10 min. The suspension was filtered by gravity (Whatman #1 filter paper) and the diethyl ether removed by rotary evaporation. Yield: 960 mg, 83%. ^{1}H NMR (δ, $CDCl_3$ *rel* to Me_4Si) shift (mult., int., assign.): (1) 4-methoxypyridine: 8.45 (d; J = 7 Hz, 2H, *o*-H); 6.80 (d; J = 7 Hz, 2H, *m*-H); 3.85 (s, 3H, OCH_3); (2) 4-methoxypyridine-*N*-oxide: 8.14 (d; J = 9 Hz, 2H, *o*-H); 6.81 (d; J = 9 Hz, 2H, *m*-H); 3.84 (s, 3H, OCH_3). UV-vis, λ_{max} in nm (CH_3CN solution): 216, 240sh.

***trans*-[$ReO_2(py)_4$]I, and *trans*-[$ReO_2(py)_4$][PF_6] (py = pyridine).** **1** (2.01 g, 2.31 mmol) was added in small portions, over a 5 min period, to 50 mL of pyridine. The pyridine was brought to its boiling point. After 10 min, small orange crystals began to precipitate. Heating was discontinued 5 min later and the solution was allowed to cool to room temperature on the hot plate. The reaction mixture was placed in a refrigerator (4 °C) and left standing for 3 h. The product was collected on a medium-porosity sintered-glass frit and washed successively with 2 X 30 mL of toluene, 2 X 30 mL of diethyl ether, and 30 mL of pentane. The material was aspirated to dryness (4 h). Yield: 1.52 g, 91%. UV-vis, λ_{max} in nm (CH_3OH solution): 345, 427.

Conversion to the hexafluorophosphate salt was accomplished as follows. *Trans*-[$ReO_2(py)_4$]I (700 mg, 1.06 mmol) was dissolved in 12 mL of chloroform in a 125-mL Erlenmeyer flask. Approximately 1.0 g (2.6 mmol) [Bu_4N][PF_6] was dissolved in 5 mL

of chloroform and added to the first solution. An orange precipitate formed immediately upon mixing. The slurry was stirred for an additional 10 min and the product was collected on a medium-porosity sintered-glass frit and washed successively with 5 mL of chloroform, 2 X 10 mL of ethanol, 2 X 10 mL of diethyl ether and 2 X 10 mL of pentane. After aspirating to dryness (1 h) the yield was 490 mg, 68%. Anal. Calcd for $C_{20}H_{20}N_4F_6O_2PRe$: C, 35.35; H, 2.97; N, 8.24. Found: C, 34.96; H, 2.92; N, 8.25. ^1H NMR (δ, CD_3CN) shift (mult., int., assign.): 9.03 (d; J = 7 Hz, 2H, *o*-H); 7.77 (m, 1H, *p*-H); 7.47 (m, 2H, *m*-H). UV-vis, λ_{max} in nm (ε, M^{-1} cm^{-1}), CH_3CN solution: 248 (17,000); 279 (4,200); 352 (22,000); 418 (2,000). IR (ν_{asym} ReO_2): 816 cm^{-1}.

***trans*-[ReO_2(4-Phpy)$_4$]I, and *trans*-[ReO_2(4-Phpy)$_4$][PF_6] (4-Phpy = 4-phenylpyridine).** **1** (200 mg, 0.23 mmol) and 4-phenylpyridine (710 mg, 4.57 mmol) were placed in a 25-mL round-bottomed flask. About 5 mL of methanol was added and the pale orange suspension was stirred. As the solution was heated to reflux, a deep orange color developed and an orange solid began to precipitate. The mixture was refluxed for 15 min, cooled to room temperature and then placed in a refrigerator for 4 h. The orange solid was collected on a medium-porosity sintered-glass frit and washed successively with 3 X 10 mL of diethyl ether, 10 mL of toluene, 2 X 10 mL of pentane, and then aspirated to dryness. Yield : 120 mg, 54 %. Anal. Calcd for $C_{44}H_{36}N_4IO_2Re$: C, 54.71; H, 3.76; N, 5.80. Found: C, 54.96; H, 4.15; N, 5.05. ^1H NMR (δ, $CDCl_3$) shift (mult., int., assign.): 9.21 (d; J = 7 Hz, 2H, *o*-H); 7.59 (m, 7H, *m*-H and C_6H_5). UV-vis, λ_{max} in nm (ε, M^{-1} cm^{-1}), CH_3OH solution: 269 (62,000); 371 (41,000).

Metathesis to the hexafluorophosphate salt was accomplished as follows. The iodide salt (105 mg) was dissolved in 100 mL of methanol and filtered by gravity (Whatman #1 filter paper). To this yellow-orange solution, 100 mg of [NH_4][PF_6] was added and the solution was vigorously stirred. Within 2 min, a precipitate began forming. The mixture was placed in a refrigerator for 4 h to encourage further precipitation. The product was collected, washed successively with 2 X 15 mL of cold (4 °C) methanol, 2 X 15 mL of

toluene, 2 X 15 mL of diethyl ether, 2 X 15 mL of pentane, and then aspirated to dryness. Yield: 55 mg, 51 %. Anal. Calcd for $C_{44}H_{36}N_4F_6O_2PRe$: C, 53.71; H, 3.69; N, 5.69. Found: C, 51.47; H, 3.77; N, 5.44. ^1H NMR (δ, CD_3CN) shift (mult., int., assign.): 9.12 (d; J = 7 Hz, 2H, *o*-H); 7.66 (m, 7H, *m*-H and C_6H_5). UV-vis, λ_{max} in nm (ε, M^{-1} cm^{-1}), CH_3CN solution: 266 (56,000); 383 (37,000).

***trans*-[ReO_2(4-pic)$_4$]I, and *trans*-[ReO_2(4-pic)$_4$][PF_6] (4-pic = 4-methylpyridine).** **1** (410 mg, 0.47 mmol) was combined with 4-picoline (4-methylpyridine) in a 25-mL round-bottomed flask fitted with a reflux condensor. Approximately 5 mL of methanol was added. A deep orange solution developed immediately upon mixing. The mixture was refluxed for 30 min. A small sample was examined by UV-visible spectroscopy; absorption band energies indicated the reaction had gone to completion. To ensure complete conversion, the mixture was refluxed for an additional 30 min and then allowed to cool to room temperature. Toluene (10 mL) was added and the solution volume reduced (rotary evaporation) until precipitate began forming (*ca.* 5 mL total volume). The reaction mixture was placed in a freezer (-10 °C) and allowed to stand overnight. The following morning, the mother liquor was separated from the precipitate using a Pasteur pipette. The residue was washed successively with 2 X 15 mL of toluene, 2 X 15 mL of diethyl ether, and 2 X 15 mL of pentane. The solid was dried on a rotary evaporator for 30 min at 50 °C (aspirator vacuum). Yield: 275 mg, 82%. UV-vis, λ_{max} in nm (CH_3OH solution): 339, 433.

Conversion to the hexafluorophosphate salt was accomplished as follows. *Trans*-[ReO_2(4-pic)$_4$]I (150 mg, 0.21 mmol) was dissolved in 10 mL of methanol and filtered by gravity (Whatman #1 filter paper). [NH_4][PF_6] (360 mg, 2.2 mmol) was dissolved in 5 mL of methanol and filtered by gravity into the first solution. Beautiful orange microcrystals began forming within 5 min of mixing. Approximately 4 drops of free 4-picoline were added to the solution. The flask was then covered with aluminum foil and allowed to stand undisturbed in a fumehood. After waiting 4.5 h, the orange microcrystals

were filtered off (Büchner funnel) and washed briefly with small portions (*ca.* 5 mL) of diethyl ether, and pentane. After aspirating to dryness, the yield was 100 mg, 65%. Anal. Calcd for $C_{24}H_{28}N_4F_6O_2PRe$: C, 39.18; H, 3.84; N, 7.62. Found: C, 39.17; H, 3.93; N, 7.53. ^1H NMR (δ, acetone-d6) shift (mult., int., assign.): 8.95 (d; J = 7 Hz, 2H, *o*-H); 7.42 (d; J = 7 Hz, 2H, *m*-H); 2.58 (s, 3H, *p*-CH_3). UV-vis, λ_{max} in nm (ε, M^{-1} cm^{-1}), CH_3CN solution: 247 (16,000); 277 (4,400); 353 (32,000); 429 (2,000). IR (ν_{asym} ReO_2): 820 cm^{-1}.

***trans*-[ReO_2(3,5-lut)$_4$]I, and *trans*-[ReO_2(3,5-lut)$_4$][PF_6] (3,5-lut = 3,5-dimethylpyridine).** **1** (210 mg, 0.24 mmol) and 2 mL of methanol were combined in a 25-mL round-bottomed flask. 3,5-lutidine (3,5-dimethylpyridine) (710 mg, 6.6 mmol) was added and rinsed into the above mixture with an additional 3 mL of methanol. An orange color developed immediately upon mixing, becoming a lighter yellow-orange color after stirring for *ca.* 3 min. The reaction mixture was refluxed for 12 h and then allowed to cool to room temperature. Approximately 10 mL of toluene was added and the solution volume reduced (rotary evaporation) until a yellow-orange solid had precipitated (the total volume of solution was about 10 mL). The pale yellow mother liquor was removed by Pasteur pipette and the residue washed (in the flask) successively with 10 mL of toluene (this wash was also pale yellow), 2 X 10 mL of diethyl ether (colorless), and 2 X 10 mL of pentane. The solid was then aspirated to dryness on a rotary evaporator (30 min). Yield: 165 mg, 91%. UV-vis, λ_{max} in nm (CH_3OH solution): 346, 426.

Conversion to the hexafluorophosphate salt was accomplished as follows. *Trans*-[ReO_2(3,5-lut)$_4$]I (150 mg, 0.19) was dissolved in 5 mL of methanol and filtered by gravity (Whatman #1 filter paper). [NH_4][PF_6] (410 mg, 2.5 mmol) was dissolved in 5 mL of methanol and filtered into the first solution. Upon mixing a small amount of orange precipitate began forming. Approximately 5 drops of free 3,5-lutidine were added, and the mixture was covered with aluminum foil and then allowed to stand undisturbed in a fumehood for two days. The yellow-orange crystals that had formed were collected on a

Büchner funnel and washed with small amounts (*ca.* 5 mL) of diethyl ether and pentane. After aspirating to dryness (1 h) the yield was 80 mg, 52%. Anal. Calcd for $C_{28}H_{36}N_4F_6O_2PRe$: C, 42.47; H, 4.58; N, 7.08. Found: C, 42.16; H, 4.60; N, 7.11. ^1H NMR (δ, CD_3CN) shift (mult., int., assign.): 8.70 (s, 2H, *o*-H); 7.37 (s, 1H, *p*-H); 2.20 (s, 6H, *m*-CH_3). UV-vis, λ_{max} in nm (ε, M^{-1} cm^{-1}), CH_3CN solution: 258 (24,000); 275 (5,700); 356 (29,000); 416 (2,100). IR (ν_{asym} ReO_2): 820 cm^{-1}.

***trans*-[ReO_2(4-MeOpy)$_4$]I, and *trans*-[ReO_2(4-MeOpy)$_4$][PF_6] (4-MeOpy = 4-methoxypyridine).** **1** (420 mg, 0.48 mmol) was combined with 4-methoxypyridine (890 mg, 8.2 mmol) in 5 mL of methanol. A dark orange solution formed initially and this became lighter orange after stirring for 5 min. This solution was refluxed for 2 h and then allowed to cool to room temperature. Toluene (10 mL) was added and the solution volume reduced by rotary evaporation until an orange product precipitated (the solution volume was about 5 mL at this point). The mixture was placed in a refrigerator to stand overnight. The solid was collected on a medium-porosity sintered-glass frit, then washed successively with 3 X 15 mL of toluene, 3 X 15 mL of diethyl ether, and 3 X 15 mL of pentane. The material was aspirated to dryness (1 h). Yield : 290 mg, 75%. UV-vis, λ_{max} in nm (CH_3OH solution): 334, 452.

Conversion to the hexafluorophosphate salt was accomplished as follows. *Trans*-[ReO_2(4-MeOpy)$_4$]I (160 mg, 0.2 mole) was dissolved in 20 mL of 50% aqueous methanol and filtered by gravity. The filter paper was rinsed with 2 mL of distilled water. [NH_4][PF_6] (190 mg, 1.2 mmol) was added to the filtrate and a bright yellow solid immediately precipitated. The mixture was left to stand for 10 min to ensure complete precipitation. The solid was collected on a medium-porosity sintered-glass frit, washed successively with 2 X 15 mL of distilled water, 3 X 15 mL of toluene, 3 X 15 mL of diethyl ether, 3 X 15 mL of pentane, and then aspirated to dryness. Recrystallization from acetone-hexane mixtures gave yellow-orange needles. These were dried at room temperature *in vacuo* (<10^{-3} torr) overnight. Yield :115 mg, 70%. Anal. Calcd for

$C_{24}H_{28}N_4F_6O_6PRe$: C, 36.05; H, 3.53; N, 7.01. Found: C, 35.66; H, 3.44; N, 6.96. ^1H NMR (δ, $CDCl_3$) shift (mult., int., assign.): 8.74 (d; J = 7 Hz, 2H, *o*-H); 6.99 (d; J = 7 Hz, 2H, *m*-H); 3.94 (s, 3H, OCH_3). UV-vis, λ_{max} in nm (ε, M^{-1} cm^{-1}), in CH_3CN solution: 227 (33,000); 281 (6,800); 347 (27,000); 438 (1,500). IR (ν_{asym} ReO_2): 810 cm^{-1}.

***trans*-[ReO_2(3-Medmap)$_4$]I, and *trans*-[ReO_2(3-Medmap)$_4$][PF_6] (3-Medmap= 3-methyl-4-dimethylaminopyridine).** **1** (420 mg, 0.48) was rinsed into a 25-mL round-bottomed flask with 2 mL of methanol. 3-methyl-4-dimethylaminopyridne (960 mg, 7.1 mmol) was added, followed by an additional 8 mL of methanol. In less than 1 min, all of the starting complex dissolved and a deep orange solution formed. The mixture was refluxed for 90 min and then allowed to cool to room temperature. Toluene (10 mL) was added and the total solution volume reduced to 3 mL, at which point a large amount of rust-colored precipitate had formed. Toluene (10 mL) was again added and the slurry allowed to stand for 1 h. The product was collected on a medium-porosity sintered-glass frit and washed successively with 4 X 10 mL of toluene, 5 X 10 mL of diethyl ether, 2 X 10 mL of pentane and then aspirated to dryness (30 min). Yield: 385 mg, 94%. UV-vis, λ_{max} in nm (CH_3OH solution): 342, 473.

Conversion to the hexafluorophosphate salt was accomplished as follows. *Trans*-[ReO_2(3-Medmap)$_4$]I (240 mg, 0.27 mmol) was dissolved in 8 mL of methanol and filtered by gravity (Whatman #1 filter paper). [NH_4][PF_6] (660 mg, 4.0 mmol) was dissolved in 5 mL of methanol and filtered into the first solution. Immediately upon mixing a large amount of powdery rust-colored precipitate began forming. Free 3-Medmap (*ca.* 3 drops) was added and the reaction mixture covered with foil. After standing undisturbed in a fumehood for 2 days, the product was collected on a medium-porosity sintered-glass frit and washed with small amounts (*ca.* 5 mL) of diethyl ether and pentane; it was then aspirated to dryness (1 h). Yield: 155 mg, 63%. Anal. Calcd for $C_{32}H_{48}N_8F_6O_2PRe$: C, 42.33; H, 5.33: N, 12.34. Found: C, 42.78; H, 5.30; N, 12.71. ^1H NMR (δ, $CDCl_3$)

shift (mult., int., assign.): 8.36 (d; J = 7 Hz, 1H, *o*-H); 8.28 (s, 1H, *o*-H); 6.63 (d; J = 7 Hz, 1H, *m*-H); 2.98 (s, 6H, $N(CH_3)_2$); 2.20 (s, 3H, *m*-CH_3). UV-vis, λ_{max} in nm (ε, M^{-1} cm^{-1}), CH_3CN solution: 280 (38,000); 363 (42,000); 455 (2,600). IR (ν_{asym}, ReO_2): 810 cm^{-1}.

***trans*-[ReO_2(dmap)$_4$]I (dmap = 4-dimethylaminopyridine).** **1** (0.5 g, 0.57 mmol) and 4-dimethylaminopyridine (860 mg, 7.0 mmol) were placed in a 50-mL round-bottomed flask. Approximately 10 mL of methanol was added; stirring gave a deep yellow-brown solution. This was brought to reflux. After heating for 10 min, the color changed to a deep red-brown color and a small amount of precipitate appeared. A sample of the crude reaction mixture was examined by UV-visible spectroscopy; the positions of the absorption bands in the spectrum suggested the reaction was complete. Refluxing was continued an additional 25 min to ensure that a complete reaction had occurred. The heating was stopped and the reaction mixture allowed to cool to room temperature. The product was collected on a coarse-porosity sintered-glass frit and washed successively with 3 X 15 mL of toluene, 3 X 15 mL of diethyl ether, 2 X 15 mL of pentane and then aspirated to dryness (1 h). Yield: 290 mg. Toluene (10 mL) was added to the filtrate and solution taken to near dryness by rotary evaporation; another portion of toluene (10 mL) was then added. The mother liquor was removed by Pasteur pipette and the solid washed as before. Yield: 120 mg. The combined yield of product was 410 mg, 86%. UV-vis, λ_{max} in nm (MeOH solution): 332, 483.

***trans*-[ReO_2(dmap)$_4$][PF_6].** This compound was prepared directly from **1**, without isolation of the intermediate iodide salt, as described below. **1** (410 mg, 0.47 mmol) was combined with 4-dimethylaminopyridine (820 mg, 6.7 mmol) in 30 mL of methanol. A dirty orange solution formed upon mixing and this was refluxed for 12 h. The reaction mixture was cooled and filtered by gravity (Whatman #1 filter paper). [NH_4][PF_6] (230 mg, 1.4 mmol) was added to the filtrate. Immediately after addition of the [NH_4][PF_6], a rust colored precipitate began forming. The rust colored slurry was

placed in a refrigerator (4 °C) for 2 hours to ensure complete precipitation. The product was collected, washed successively with 2 X 10 mL of cold (4 °C) methanol, 3 X 30 mL of diethyl ether, 2 X 20 mL of pentane and then aspirated to dryness (1 h). The solid was transferred to a vial and dried *in vacuo* at 90 °C for 4 hours. Yield 325 mg, 81%. Anal. Calcd for $C_{28}H_{40}N_8F_6O_2PRe$: C, 39.48; H, 4.73; N, 13.15. Found: C, 39.53; H, 4.70; N, 12.78. ^1H NMR (δ, DMSO-d^6) shift (mult., int., assign.): 8.24 (d; J = 7 Hz, 2H, *o*-H); 6.68 (d; J = 7Hz; 2H, *m*-H); 3.30 (s, 6H, $N(CH_3)_2$). UV-vis, λ_{max} in nm (ε, M^{-1} cm^{-1}), CH_3CN solution: 272 (47,000); 358 (37,000); 462 (2,300). IR (ν_{asym} ReO_2): 800 cm^{-1}.

***trans*-[ReO_2(4-pyrrpy)$_4$]I, and *trans*-[ReO_2(4-pyrrpy)$_4$][PF_6] (4-pyrrpy = 4-pyrrolidinopyridine).** **1** (1.00 g, 1.15 mmol) and 4-pyrrolidinopyridine (2.20 g, 14.8 mmol) were combined with 10 mL of methanol. Immediately upon mixing, a deep orange-brown solution was obtained. After stirring about 10 min, an orange-brown solid began precipitating. The reaction slurry was then refluxed for about 1 hr, cooled to room temperature and placed in a refrigerator to stand overnight. The precipitate was collected on a medium-porosity sintered-glass frit and washed successively with 3 X 15 mL of toluene, 3 X 15 mL of diethyl ether and 2 X 15 mL of pentane. The product was then aspirated to dryness. Yield: 920 mg, 85%. UV-vis, λ_{max} in nm (MeOH solution): 335, 490.

Conversion to the hexafluorophosphate salt was accomplished as follows. *Trans*-[ReO_2(4-pyrrpy)$_4$]I was dissolved in a minimum volume of 2:1 (v/v) methanol/acetone and then 2-3 equivalents of [NH_4][PF_6] were added. The material obtained was then washed successively with 2 X 7 mL of cold (4° C) methanol, 2 X 15 mL of toluene, 2 X 15 mL of diethyl ether and 2 X 15 mL of pentane. The product was aspirated to dryness. Yields were typically 50% or greater. Anal. Calcd for $C_{36}H_{48}N_8F_6O_2PRe$: C, 45.23; H, 5.06; N, 11.72. Found: C, 45.02; H, 5.24:; N, 11.59. ^1H NMR (δ, CD_2Cl_2) shift (mult., int., assign.): 8.31 (d; J = 7 Hz, 2H, *o*-H); 6.34 (d; J = 7 Hz, 2H, *m*-H); 3.36 (m, 4H,

$N(CH_2CH_2)$; 2.00 (m, 4H, $N(CH_2CH_2)$. UV-vis, λ_{max} in nm (ε, M^{-1} cm^{-1}), CH_3CN solution: 273 (52,000); 353 (42,000); 465 (2,600). IR (ν_{asym} ReO_2): 798 cm^{-1}.

***trans*-[$ReO_2(en)_2$]I.** **1** (210 mg, 0.24 mmol) and 10 mL of methanol were combined in a 50-mL round-bottomed flask. To this purple slurry, 340 mg (5.7 mmol, 24 equiv) of ethylenediamine and another 10 mL of methanol were added. In less than 2 min, all of the purple solid disappeared and *trans*-[$ReO_2(en)_2$]I began to settle out. The pale yellow slurry was stirred for 15 min to ensure complete reaction. The precipitate was collected on a coarse-porosity sintered-glass frit, washed with 3 X 15 mL of diethyl ether, and aspirated to dryness. Yield: 90 mg, 80%. UV-vis, λ_{max} in nm (*rel inten*), H_2O solution: 254(vs); 280(sh); 440(w). IR (ν_{asym} ReO_2): 815 cm^{-1}.

***trans*-[$ReO_2(en)_2$][PF_6].** This compound could not be obtained from metathesis of the iodide salt. Therefore a route using a complex containing the PF_6^- counterion was developed.

Trans-[$ReO_2(py)_4$][PF_6] (440 mg, 0.65 mmol) was dissolved in 50 mL of methanol in a 125-mL Erlenmeyer flask. Ethylenediamine (2.25 g, 37.3 mmol, 57 equiv) was added and the mixture then brought to reflux. After 40 min, a large amount of pale yellow precipitate formed and the solution developed a purple color. Toluene (30 mL) was added to induce precipitation. The solid was collected on a medium-porosity sintered-glass frit and washed successively with 3 X 30 mL of diethyl ether, 2 X 15 mL of pentane and then aspirated to dryness (15 min). Yield: 130 mg, 42%. UV-vis, λ_{max} in nm (*rel inten*), H_2O solution: 254(vs); 275(sh); 439(w).

***trans*-[$ReO_2(py)_3(PPh_3)$]I.** This complex was prepared using *trans*-[$ReO_2(py)_4$]I according to the literature procedure.[7] Yield based upon 105 mg of *trans*-[$ReO_2(py)_4$]I: 60 mg, 60%. Anal. Calcd for $C_{33}H_{30}N_3IO_2PRe$: C, 46.92; H, 3.58; N, 4.97. Found: C, 46.75; H, 3.70; N, 5.01. ^1H NMR (δ $CDCl_3$, zero ref 1% Me_4Si) shift (mult., int., assign.): δ9.00 (d; J = 7 Hz; 2H, *o*-H on py *trans* to PPh_3); δ 8.75 (d; J = 7 Hz, 4H, *o*-H on py *cis* to PPh_3); δ 7.00 - 8.00 (m, 24H, all remaining H). $^{31}P\{^1H\}$ NMR: δ -1.7 (s).

UV-vis, λ_{max} in nm: 335 (CH_3CH_2OH solution); 341 (CH_2Cl_2 solution). IR (ν_{asym} ReO_2): 815 cm^{-1}.

***trans*-[ReO_2(diphos)$_2$]I (diphos = 1,2-bis(diphenylphosphino)ethane).** There are four possible routes to this compound. The first two were developed by Freni in 1969 and are fully documented elsewhere.[7,16] Two alternative routes are described below.

Method 1. **1** (330mg, 0.35 mmol) and diphos (330 mg, 0.75 mmol) were placed in 10 mL of methanol. Neither reagent dissolved in this medium. The suspension was brought to reflux. After heating for 45 min, the solution was a rosé-red and a cream colored solid had precipitated. This mixture was refluxed overnight (12 h). After cooling to room temperature, the solid was collected by filtration on a medium-porosity sintered-glass frit and washed successively with 3 X 15 mL of diethyl ether, 2 X 15 mL of pentane and then aspirated to dryness (1 h). Yield: 175 mg, 44%. (The yield is limited by the formation of an unidentified red side product.)

Method 2. *Trans*-[$ReO_2(py)_4$]I (105 mg, 0.16 mmol) and diphos (105 mg, 0.16 mmol) were placed in 10 mL of acetone. The mixture was brought to reflux. After heating for 1.75 h, a light yellow solid began to precipitate and the heating was discontinued. The solution was left to cool overnight. The following morning, the light yellow solid was collected by filtration on a medium-porosity sintered-glass frit and washed successively with 3 X 10 mL of diethyl ether, 10 mL of pentane and then aspirated to dryness. Yield: 105 mg, 76%.

***trans*-[ReO_2(diphos)$_2$][PF_6].** A reflux condensor, with attached gas inlet, was fitted to a 50-mL three-necked round-bottomed flask. The apparatus was thoroughly flushed with argon and then diphos (920 mg, 2.3 mmol) and *trans*-[$ReO_2(py)_4$]PF_6 (150 mg, 0.22 mmol) were added. Deoxygenated acetone (10 mL) was added by syringe. The reaction assembly was momentarily swept out with argon gas and then kept under a slight positive pressure of argon. The white and orange slurry was refluxed overnight. The following morning (10 h later) the bright yellow solution was cooled to room temperature.

A white solid had precipitated (excess diphos) and was removed by filtration through a coarse-porosity sintered-glass frit; it was washed with 2 X 10 mL of acetone and the washings added to the filtrate. Toluene (20 mL) was added and the solution volume reduced by rotary evaporation until a yellow solid began forming. The mother liquor (colorless) was removed by Pasteur pipette and the residue washed successively with 2 X 15 mL of toluene, 2 X 15 mL of diethyl ether, 2 X 15 mL of pentane and then taken to dryness by rotary evaporation (aspirator vacuum, 30 min). Yield: 200 mg (mono-toluene adduct), 72%. Anal. Calcd for $C_{59}H_{56}F_6P_5O_2Re$: C, 56.59; H, 4.51. Found: C, 56.77; H, 4.55. ^1H NMR (δ, CD_3CN) shift (mult., int., assign.): 7.04 (m, 20H, 4 X C_6H_5); 2.60 (t; $^2J_{PH} + {}^3J_{PH}$ = 7 Hz, 4H, CH_2CH_2).[17] UV-vis, λ_{max} in nm, CH_3CN solution; 220sh, 257. IR (ν_{asym} ReO_2): 780 cm^{-1}.

***trans*-[ReO_2(dppen)$_2$][PF_6] (dppen = 1,2-bis(diphenylphosphino)ethene).** A reflux condensor with attached gas inlet was fitted to a 25-mL three-necked round-bottomed flask. This was charged with dppen (900 mg, 2.3 mmol) and *trans*-[$ReO_2(py)_4$]PF_6 (150 mg, 0.22 mmol). The assembly was flushed with argon gas and then 10 mL of deoxygenated acetone was introduced by syringe. After warming for 10 min, the white-orange slurry became a homogeneous orange solution. The mixture was refluxed under argon for 4.5 h and then cooled to room temperature. The green-yellow solid that had precipitated was collected on a medium-porosity sintered-glass frit and washed successively with 2 X 10 mL of acetone (this dissolved some colorless crystals that had co-precipitated), 2 X 15 mL of diethyl ether, 2 X 15 mL of pentane and then aspirated to dryness (40 min). Yield: 155 mg, 61%. Anal. Calcd for $C_{52}H_{44}F_6P_5O_2Re$: C, 54.03; H, 3.84. Found: C, 54.54; H, 3.84. ^1H NMR (δ, $CD_3CN/CDCl_3$) 7.24 (m) (zero ref Me_4Si). UV-vis, λ_{max} in nm, CH_3CN solution; 228sh, 267sh. IR (ν_{asym} ReO_2): 790 cm^{-1}.

RESULTS

The complex $ReO_2(PPh_3)_2I$ is an ideal starting material for the synthesis of pyridine and amine complexes of the ReO_2^+ unit. Upon addition of ligating agents, the methanol-insoluble $ReO_2(PPh_3)_2I$ dissolved, and orange solutions rapidly developed. Reaction mixtures were stirred at room temperature or brought to reflux to drive the reaction

$$[ReO_2(PPh_3)_2I] + 4\,L \rightarrow [ReO_2L_4]I + 2\,PPh_3 \qquad (3)$$

to completion. Reaction progress was monitored by UV-visible spectroscopy. The energies of the MLCT and LF transitions were used to estimate the extent of the reaction; refluxes were terminated when the LF band ceased to move to lower energy. In general, the more basic pyridines required fewer excess equivalents of ligand and shorter reflux times.

The iodide salts of the complexes could be isolated by concentrating methanolic solutions or by addition of toluene and subsequent removal of the more volatile methanol solvent. Metatheses to hexafluorophosphate salts were accomplished using $[NH_4][PF_6]$ in methanol, aqueous methanol, or methanol/acetone mixtures. Complexes of the form *trans*-$[ReO_2L_4]^+$ could be made from the following pyridines: 4-dimethylaminopyridine (dmap), 3-methyl-4-dimethylaminopyridine (3-Medmap), 4-pyrrolidinopyridine (4-pyrrpy), 4-methoxypyridine (4-MeOpy), 3,5-lutidine (3,5-lut), 4-picoline (4-pic), and 4-phenylpyridine (4-Phpy). For pyridine and less basic derivatives, the method was not successful. Solvolysis reactions and competition for coordination sites from the displaced triphenylphosphine became significant side reactions.

All of the tetrapyridine complexes synthesized were unstable in solution with respect to ligand loss. This occurred over hours (pyridine) or several days (dmap) and was readily evident from the appearance of multiple signals in the region δ8.2 to δ9.2 of the ^1H NMR spectra. In general, this instability became more pronounced (1) in polar coordinating

solvents (*e.g.*, DMSO), (2) in the presence of coordinating anions (Cl^-, I^-), and (3) as the basicity of the ligand decreased. To suppress this reaction, traces of free ligand were added to solutions left standing for extended periods.

Complexes of saturated amines could also be obtained from $ReO_2(PPh_3)_2I$. The compound *trans*-$[ReO_2(en)_2]I$ could be prepared in 80% yield in less than 15 minutes at room temperature:

$$[ReO_2(PPh_3)_2I] + 2\ en \rightarrow [ReO_2(en)_2]I\downarrow + 2\ PPh_3 \qquad (4)$$

As had been noted previously,[7,16] $ReO_2(PPh_3)_2I$ could also be used to synthesize phosphine complexes.

$ReO_2(PPh_3)_2I$ was not always the starting material of choice. Reactions with ligands that did not have appreciable solubility in methanol did not proceed efficiently. In preparations that were exposed to air, the reaction[7,18]

$$4\ ReO_2(PPh_3)_2I + 7/2\ O_2 \rightarrow ReO(PPh_3)_2I_2(OReO_3) + ReO(PPh_3)(OPPh_3)I_2(OReO_3) + 4\ OPPh_3 \qquad (5)$$

was likely competitive. The above reaction also became relevant for reactions conducted in solvents that appreciably dissolved $ReO_2(PPh_3)_2I$. For these reasons, *trans*-$[ReO_2(py)_4]I$ was a superior starting material to prepare the complexes *trans*-$[ReO_2(py)_3(PPh_3)]I$ and *trans*-$[ReO_2(diphos)_2]I$.

There were also occasional difficulties in metathesizing the iodide salts of some complexes to their hexafluorophosphate analogs. In these cases, it was desirable to use *trans*-$[ReO_2(py)_4][PF_6]$ as the starting material. Here solvent identity was not crucial and was chosen on the basis of ease of product work-up. By substitution reactions on *trans*-

$[ReO_2(py)_4][PF_6]$, the compounds *trans*-$[ReO_2(en)_2][PF_6]$, *trans*-$[ReO_2(diphos)_2][PF_6]$, and *trans*-$[ReO_2(dppen)_2][PF_6]$ were obtained.

DISCUSSION

Reaction Mechanisms Relevant to the Synthetic Strategy. The planning and execution of successful inorganic syntheses requires a thorough understanding of substitution mechanisms. A brief summary of mechanisms relevant to octahedral systems is presented below. For a more complete description, the reader should consult one of the many books[4,19,20] or monographs[3] on this topic.

From the wealth of information that has been collected on substitution reactions of octahedral centers, four mechanistic schemes have emerged. The fundemental criterion for classification is whether or not a discreet intermediate is encountered at any point along the reaction coordinate. If an intermediate of higher coordination number is involved, the mechanism is classified as associative (A); similarly, a dissociative (D) mechanism implies an intermediate with a lower coordination number. If no intermediate is detectable, the classification is intimate (I). The 'I' category is further qualified based upon the effects of the incoming ligand on substitution rate. If the rate of substitution is dependent upon the identity of the incoming ligand, this is labelled intimate-associative (I_a); if independent, it is intimate-dissociative (I_d).

To date there are few examples of octahedral substitutions that occur via an 'A' mechanism.[20] This result is not surprising on steric or electronic grounds. Formation of a seven coordinate intermediate would increase ligand congestion (*e.g.*, a bicapped pentagon would have ligands only 72° apart instead of 90° as in the octahedron). Electronically, addition of an electron pair from the incoming ligand requires a vacant, low-energy orbital. In *trans*-$[ReO_2(L)_4]^Z$ complexes the LUMO is the degenerate pair of d_{xz},d_{yz} orbitals, which are O=Re=O π-antibonding (see Figure 1.1). This level lies to considerably higher

energy than the d_{xy} HOMO; $[ReO_2(L)_4]^Z$ complexes can only be reduced at very negative potentials.[21,22]

There have been several investigations of both oxo[23-25] and ancillary ligand[26] substitutions in $[ReO_2(L)_4]^Z$ complexes. These studies suggest that a D mechanism may be operative. For $[ReO_2(amine)_4]^+$, the rate of amine exchange is described by the following rate expression:[26]

$$R = k_o[complex] + k_1[OH^-][complex] \qquad (6)$$

The first term is due to loss of ligand from the complex; the second term is the result of a conjugate base mechanism (S_N1-cb) and is absent when no ionizable protons are available on the amine (*e.g.*, pyridine). The role of hydroxide ion is to deprotonate the amine group to form a coordinated amide. The strong *trans*-effect of this ligand results in expulsion of the *trans*-NH_2 group and the formation of a five coordinate species.

The existence of $ReO_2(PPh_3)_2I$ as a stable solid[5] suggests that five coordinate $[ReO_2(L)_3]^Z$ complexes are reasonable to propose. A complex with the formulation $ReO_2(py)_2I$ has been reported[7] but has not been completely characterized. Additional support for this intermediate has recently appeared from the results of synthetic methods developed by Hupp and co-workers.[27,28] This group found that mixed ligand complexes *trans*-$[ReO_2(py\text{-}X)_2(py\text{-}Y)_2]^+$ could be obtained from reactions of pyridine ligands with $Re(OEt)(py)_2I_2$ in wet alcohol. These workers propose[27,28] the intermediacy of $ReO_2(py)_2I$, formed from the hydrolysis of $Re(OEt)(py)_2I_2$. Experimental results suggest that $ReO_2(py)_2I$ may also have a *cis* disposition of oxo ligands, implying that upon ligand loss, the *trans* -ReO_2^+ core isomerizes to yield a *cis*-ReO_2^+ unit. For this to occur prior to ligand attack, the five coordinate intermediate would have to have a considerable lifetime.

From the above analyses, it is clear why both $ReO_2(PPh_3)_2I$ and *trans*-$[ReO_2(py)_4]^+$ are good starting materials for the synthesis of $[ReO_2(L)_4]^Z$ complexes. Substitutions with $ReO_2(PPh_3)_2I$ likely proceed stepwise as shown in Figure 2.1.

$ReO_2(PPh_3)_2I$ is completely insoluble in methanol. When a potentially ligating species, L, is added, the solid is consumed in seconds, suggesting steps 1, 2 and 3 in Figure 2.1 are very fast. The orange color of the solutions, early in the course of the reaction, also suggest that steps 4 and 5 are rapid; *trans*-$[ReO_2(py)_2(PPh_3)_2]^+$ is yellow while *trans*-$[ReO_2(py)_3(PPh_3)]^+$ is orange-yellow in color. Substitution of the last triphenylphosphine ligand appears to be much slower than the previous steps.

Substitution reactions of *trans*-$[ReO_2(py)_4]^+$ could occur by a related mechanism. For example, the generation of *trans*-$[ReO_2(diphos)_2]^+$ might proceed as in Figure 2.2. Upon substitution of one pyridine ligand by one arm of diphos, a second substitution of pyridine would rapidly follow due to the chelate effect. The rate-limiting step would be the introduction of the first PPh_2 group into the coordination sphere. The lability of the pyridine ligands in *trans*-$[ReO_2(py)_4]^+$ has be noted previously[8-14] and alkylating agents such as CH_3I or Me_2SO_4 have been used to make the loss of pyridine irreversible.[10]

Syntheses employing $ReO_2(PPh_3)_2I$ work well for very basic or chelating ligands. Complexes containing electron-poor pyridines cannot be isolated in pure form using $ReO_2(PPh_3)_2I$ for two reasons: (1) As the pyridine ligand becomes less basic, PPh_3 competes more effectively for a coordination position, that is, the equilibria

$$[ReO_2(PPh_3)_2(L)_2]I + L \rightleftharpoons [ReO_2(PPh_3)(L)_3]I + PPh_3 \quad (7)$$

$$[ReO_2(PPh_3)(L)_3]I + L \rightleftharpoons [ReO_2(L)_4]I + PPh_3 \quad (8)$$

Figure 2.1. Reaction mechanism likely for substitution reactions employing $ReO_2(PPh_3)_2I$.

$$ReO_2(PPh_3)_2I + L \xrightarrow{fast} ReO_2(PPh_3)_2(L)I \quad (1)$$

$$ReO_2(PPh_3)_2(L)I \xrightarrow{fast} [ReO_2(PPh_3)_2(L)]I \quad (2)$$

$$[ReO_2(PPh_3)_2(L)]I + L \xrightarrow{fast} [ReO_2(PPh_3)_2(L)_2]I \quad (3)$$

$$[ReO_2(PPh_3)_2(L)_2]I \xrightarrow{fast} [ReO_2(PPh_3)(L)_2]I + PPh_3 \quad (4)$$

$$[ReO_2(PPh_3)(L)_2]I + L \xrightarrow{fast} [ReO_2(PPh_3)(L)_3]I \quad (5)$$

$$[ReO_2(PPh_3)(L)_3]I \xrightarrow{slow} [ReO_2(L)_3]I + PPh_3 \quad (6)$$

$$[ReO_2(L)_3]I + L \xrightarrow{fast} [ReO_2(L)_4]I \quad (7)$$

Figure 2.2. Reaction mechanism likely for substitution reactions employing *trans*-$[ReO_2(py)_4]^+$.

$$[ReO_2(py)_4]^+ \xrightarrow{\text{slow}} [ReO_2(py)_3]^+ + py \quad (1)$$

$$[ReO_2(py)_3]^+ + diphos \xrightarrow{\text{fast}} [ReO_2(py)_3(\eta^1\text{-diphos})]^+ \quad (2)$$

$$[ReO_2(py)_3(\eta^1\text{-diphos})]^+ \xrightarrow{\text{fast}} [ReO_2(py)_2(diphos)]^+ + py \quad (3)$$

$$[ReO_2(py)_2(diphos)]^+ \xrightarrow{\text{slow}} [ReO_2(py)(diphos)]^+ + py \quad (4)$$

$$[ReO_2(py)(diphos)]^+ + diphos \xrightarrow{\text{fast}} [ReO_2(py)(diphos)(\eta^1\text{-diphos})]^+ \quad (5)$$

$$[ReO_2(py)(diphos)(\eta^1\text{-diphos})]^+ \xrightarrow{\text{fast}} [ReO_2(diphos)_2]^+ + py \quad (6)$$

$$[ReO_2(L)_4]I + S \rightleftharpoons [ReO_2(L)_3(S)]I + L \qquad (9)$$

In aqueous solutions of *trans*-$[ReO_2(py)_4]Cl$, this reaction is known to proceed (25 °C) with a half-life of several days.[24] Thus, *trans*-$[ReO_2(py)_4]I$ can be cleanly synthesized from neat pyridine but not from methanol solutions containing up to 40 equivalents of pyridine.

CONCLUSIONS

The complex $ReO_2(PPh_3)_2I$ can be used to insert the *trans*-ReO_2^+ unit into coordination environments containing pyridine or saturated amine ligands. The complex *trans*-$[ReO_2(py)_4]^+$ is an alternative material that is useful when the former does not give satisfactory results. Our results and the studies of others[28,29] suggest these substitution reactions proceed via a series of dissociative steps involving reactive five-coordinate intermediates. Recent research completed on analagous technetium complexes is consistent with this hypothesis.[30-32]

REFERENCES AND NOTES

(1) Chakravorti, M. C. *Inorg. Syn.* **1982**, *21*, 116-118.

(2) Murmann, R. K. *Inorg. Syn.* **1966**, *8*, 173-177.

(3) Taube, H. *Chem. Rev.* **1952**, *50*, 69-126.

(4) Basolo, F.; Pearson, R. G. *Mechanisms of Inorganic Reactions; A Study of Metal Complexes in Solution*; 1st ed.; John Wiley and Sons: New York, 1967; pp 141-158.

(5) Ciani, G.; D'Alfonso, G.; Romiti, P.; Sironi, A.; Freni, M. *Inorg. Chim. Acta* **1983**, *72*, 29-37.

(6) Bertolasi, V.; Ferretti, V.; Gilli, G.; Duatti, A.; Marchi, A.; Magon, L. *J. Chem. Soc. Dalton Trans.* **1987**, 613-617.

(7) Freni, M.; Giusto, D.; Romiti, P.; Minghetti, G. *Gazz. Chim. Ital.* **1969**, *99*, 286-299.

(8) Chakravorti, M. C. *J. Ind. Chem. Soc.* **1969**, *46*, 383-385.

(9) Chakravorti, M. C. *J. Ind. Chem. Soc.* **1970**, *47*, 844-850.

(10) Chakravorti, M. C. *J. Ind. Chem. Soc.* **1970**, *47*, 827-833.

(11) Chakravorti, M. C. *J. Ind. Chem. Soc.* **1970**, *47*, 838-843.

(12) Chakravorti, M. C. *J. Inorg. Nuc. Chem.* **1972**, *34*, 893-900.

(13) Chakravorti, M. C.; Chaudhuri, M. K. *J. Inorg. Nuc. Chem.* **1972**, *34*, 3479-3484.

(14) Chakravorti, M. C.; Chaudhuri, M. K. *J. Inorg. Nuc. Chem.* **1974**, *36*, 757-761.

(15) Ochiai, E. *Aromatic Amine Oxides*; Elsevier: New York, 1967; p 195.

(16) Freni, M.; Giusto, D.; Romiti, P. *Gazz. Chim. Ital.* **1967**, *97*, 833-844.

(17) Carty, A. J.; Harris, R. K. *J. Chem. Soc., Chem. Commun.* **1967**, 234-236.

(18) Ciani, G.; Sironi, A.; Beringhelli, T.; D'Alfonso, G.; Freni, M. *Inorg. Chim. Acta* **1986**, *113*, 61-65.

(19) Langford, C. H.; Gray, H. B. *Ligand Substitution Processes*; 2nd ed.; W. A. Benjamin: Reading, Massachusetts, 1974; Chapter 3, pp 79-89.

(20) Tobe, M. L. *Inorganic Reaction Mechanisms*; Nelson: Don Mills, Ontario, Canada, 1972; Chapters 3 and 7.

(21) Lawrance, G. A.; Sangster, D. F. *J. Chem. Soc. Chem. Comm.* **1984**, 1706-1707.

(22) Pipes, D. W.; Meyer, T. J. *Inorg. Chem.* **1986**, *25*, 3256-3262.

(23) Saito, K.; Sasaki, Y. In *Advances in Inorganic and Bioinorganic Mechanisms*; Sykes, A. G., Ed.; Academic: New York, 1982; Vol. 1, pp 179-216.

(24) Kashani, F. F.; Murmann, R. K. *Int. J. Chem. Kinet.* **1985**, *17*, 1007-1015.

(25) Gamsjäger, H.; Murmann, R. K. In *Advances in Inorganic and Bioinorganic Mechanisms*; Sykes, A. G., Ed.; Academic: New York, 1983; Vol. 2, pp 317-380.

(26) Beard, J. H.; Calhoun, C.; Casey, J.; Murmann, R. K. *J. Am. Chem. Soc.* **1968**, *90*, 3389-3394.

(27) Ram, M. S.; Jones, L. M.; Ward, H. J.; Wong, Y.; Johnson, C. J.; Subramanian, P.; Hupp, J. T. manuscript in preparation.

(28) Ram, M. S.; Hupp, J. T. *Inorg. Chem.*, submitted May 1990.

(29) Ram, M. S.; Johnson, C. S.; Blackbourn, R. L.; Hupp, J. T. *Inorg. Chem.* **1990**, *29*, 238-244.

(30) Lu, J.; Clark, M. J. *Inorg. Chem.* **1989**, *28*, 2315-2319.

(31) Kastner, M. E.; Lindsay, M. J.; Clarke, M. J. *Inorg. Chem.* **1982**, *21*, 2037-2040.

(32) Kastner, M. E.; Fackler, P. H.; Clarke, M. L.; Deutsch, E. *Inorg. Chem.* **1984**, *23*, 4683-4688.

Chapter 3.

Ground and Excited-State Properties of *trans*-Dioxorhenium(V) Complexes as a Function of Ancillary Ligand Identity.*

*A portion of this chapter has been previously published: Brewer, J. C.; Gray, H. B. In *PREPRINTS, Division of Petroleum Chemistry*; Haines, W. E., Ed.; American Chemical Society: Washington, D. C., 1990; Vol. 35, pp 187-191.

INTRODUCTION

Organic chemists have frequently used systematic substituent studies to elucidate the mechanism of organic reactions. Linear free-energy relationships, such as the Hammett correlation, often characterize the nature of the transition state in both redox[1] and acid-base transformations.[2,3] Using the large amount of experimental data available from organic studies, substituent effects can be resolved into σ and π contributions. These organic chemistry concepts can be readily applied to inorganic systems,[4] and in many cases, a more thorough understanding of the electronic structure and bonding in coordination compounds can be obtained.

In this chapter, the effects of ancillary ligand identity on the ground and excited-state properties of *trans*-$[ReO_2(L)_4]^+$ complexes are examined. The focus is on a series of substituted pyridine compounds, because electronic modulation of this ligand family is facile. The studies presented in this chapter use ligand basicity as a measure of donor strength towards metal centers. For heterocycles, the pKa of the corresponding conjugate acid is the operative parameter. Differences in pKa values between ligands can arise from variations in solvent and temperature for independent determinations. For this reason, most correlations in this section have been made with the parameter ΔpKa, as defined below:[5]

$$\Delta pKa = pKa(py) - pKa(py\text{–}X) \qquad (1)$$

In each case, the pKa of both pyridine itself[6] and the derivative in question, have been determined independently in the same medium under identical conditions.

The estimation of ligand donating strength from basicity values has received some critisism by others.[7] The results in this chapter will demonstrate, however, that this approximation is valid when comparisons are made among ligands in the same heterocycle family.

Substitutions *ortho* to the ring nitrogen would be expected to alter drastically binding properties because of steric interactions with the oxo groups of *trans*-ReO_2^+. Thus, in order to study the effects due to electronic changes only, pyridine ligands substituted in the 3, 4 or 5 position were employed. This still permits extensive electronic tuning; the tabulation of ΔpKa values compiled by Swada *et al.*[5] shows that pyridine basicity can be varied over 9 orders of magnitude, from the very electron-poor 3,5-dichloropyridine (ΔpKa = 4.44) to the electron-rich 4-dimethylaminopyridine (ΔpKa = -4.36).

By examining the series of pyridine complexes using classical physical methods, we will obtain a more complete description of the electronic structure and bonding present in *trans*-$[ReO_2(L)_4]^+$ compounds. In order to determine the effects of changing the nature of the ligating atom, we will also briefly examine the properties of some related phosphine complexes.

EXPERIMENTAL

Materials. All chemicals were either of reagent grade or the best grade commercially available and used as received. Tetra-*n*-butylammonium hexafluorophosphate, TBAH, was prepared as described below. Methylviologen hexafluorophosphate,[8] $[MV][PF_6]_2$, and *tris*-(bipyridyl)ruthenium(II) hexafluorophosphate,[9] $[Ru(bipy)_3][PF_6]_2$, were generous gifts of Dr. M. Heinrichs-Zietlow. For electrochemical experiments, dichloromethane and acetonitrile (EM, OMNISOLV) were freshly distilled from calcium hydride before use. Acetonitrile (Burdick and Jackson) was used as received for UV-vis experiments; for emission measurements this solvent was degassed with five freeze-pump-thaw cycles on a high-vacuum line ($<10^{-3}$ torr), dried, and stored under vacuum over activated[10-12] 3 Å sieves (Strem Chemicals).

Syntheses. ***Trans*-$[ReO_2(L)_4]PF_6$.** The syntheses of these complexes are described in the previous chapter.

Tetra-*n*-butylammonium hexafluorophosphate (TBAH). Sixty milliliters of concd HPF_6 (60-65%) was carefully diluted with 80 mL of distilled water and set aside. A 5% $NaHCO_3$ solution was prepared by dissolving 25 g of $NaHCO_3$ in 500 mL of distilled water. Sixty grams of tetra-*n*-butylammonium bromide, TBABr, was dissolved in 200 mL of distilled water, and the solution was filtered by gravity (Whatman #1 filter paper) into a 500-mL Erlenmeyer flask. The 140-mL HPF_6 solution was placed in a 250-mL addition funnel and added slowly, with rapid stirring, to the TBABr solution. After the addition was complete, a heavy white precipitate formed; this was difficult to stir magnetically. Water (80 mL) was added, and the mixture was stirred manually with a glass rod. Due to the large volume of material produced, the product was collected in several portions on a coarse-porosity sintered-glass frit. Each portion was washed with 3 X 100 mL of distilled water followed by 75 mL portions of 5% $NaHCO_3$ until the washings were neutral to litmus paper. The product was then washed with an additional 5 X 100 mL of distilled water. (All waste solutions in this preparation were neutralized with solid $NaHCO_3$ before disposal.) The resulting paste was aspirated on the frit for at least 1 h and then spread out on a watch glass, covered with a large piece of filter paper (Whatman #1), and left to dry overnight in an efficient fumehood. The following morning, the crude product was twice recrystallized (in smaller batches) from absolute alcohol. The large needles obtained were crushed and dried *in vacuo* ($<10^{-3}$ torr) at 80 °C for 6 h. In a typical recrystallization step, 30 g of crude TBAH yielded 25 g of purified product (after drying) from 300 mL of hot absolute alcohol.

Physical Measurements. Cyclic voltammetry measurements were made using a Princeton Applied Research (PAR) 173 potentiostat and a PAR 175 universal programmer. Platinum button working electrodes were prepared by polishing with 5 μm alumina, washing with water, and sonicating in 1:1 MeOH/water. Solutions were deoxygenated with argon purging and kept under an argon blanket during the experiment. A saturated sodium chloride calomel (SSCE) reference electrode was used in each experiment. A

platinum wire/glass joint was used to prevent water leakage from the SSCE into the cell. A platinum wire was used as the auxiliary electrode. In cyclic voltammetry experiments, solutions were 0.1 M in TBAH and approximately 1-2 mM in Re compound. The iR drop across the cell was electronically compensated by positive feedback. Ferrocene (Fc), decamethylferrocene (*Fc), or methylviologen (MV^{2+}) was used as an internal redox standard in these experiments. Under the given experimental conditions, the ferricenium/ferrocene couple (Fc^+/Fc) occurred at 0.42 V and 0.51 V (vs. SSCE) in acetonitrile and dichloromethane, respectively. The decamethylferricenium/decamethyl-ferrocene couple ($*Fc^+/*Fc$) was at -0.55 V vs. Fc^+/Fc in 0.1 M TBAH CH_2Cl_2 solution. The two reduction waves for $[MV][PF_6]_2$ were found at -0.83 and -1.25 V vs. Fc^+/Fc in 0.1 M TBAH CH_3CN solution.

Bulk electrolysis experiments were conducted at a Pt gauze working electrode using the PAR 173 potentiostat equipped with a digital coulometer. The bulk electrolysis cell was a two-compartment cell fitted with an argon inlet and a Pt wire/glass joint for holding the SSCE reference electrode. Argon flow and stirring were continual throughout the experiment. The digital coulometry was not corrected for solvent electrolysis because of the short duration of the experiments and the moderate potentials involved.

Spectroscopy. Background-corrected electronic absorption spectra were obtained using a Shimadzu UV-260 recording spectrometer or a Cary Model 14 Spectrophotometer that had been rebuilt by On-Line Instruments Service (OLIS). Quartz cells of 1-cm pathlength were used in all cases. Extinction coefficients of the ligand-field (LF) transitions were determined from solutions that were 0.2-0.5 mM in Re complex; these were diluted by 1/25 to examine the more intense MLCT transitions. Free-ligand absorption spectra were measured on solutions that had absorbances < 2.5. The concentrations of these solutions were not determined. Luminescence spectra were recorded on an instrument constructed at Caltech that has been described previously.[13] The spectrometer response was determined with a calibrated tungsten filament lamp, and spectra

were corrected for this response by the method of Drushel, Sommers, and Cox.[14] The corrected spectrum of $[Ru(bipy)_3]Cl_2$ agreed with that reported in the literature,[15,16] verifying that the correction routine was being properly applied. Solution samples were prepared under vacuum in a 10-mL round-bottomed flask equipped with a side-arm 1-cm fluorescence cuvette[17] and were rigorously degassed with no fewer than five freeze-pump-thaw cycles. Unless noted otherwise, all measurements were conducted at room temperature. An excitation wavelength of 436 nm was used for the tetrapyridine complexes and *trans*-$[ReO_2(py)_3(PPh_3)]I$. The emission spectra of *trans*-$[ReO_2(diphos)_2]PF_6$ and *trans*-$[ReO_2(dppen)_2]PF_6$ were measured in the solid state using 366-nm excitation. The absolute luminescence quantum yield for *trans*-$[ReO_2(py)_3(PPh_3)]I$ was determined by the method of Demas and Crosby.[18] The absorbance of the solution was less than 0.1 (1-cm pathlength cell) at the 436-nm excitation wavelength used. The quantum yield standard was $[Ru(bipy)_3]Cl_2$ (Aldrich Chemical Co.) in water (NANOpure), which has a reported quantum yield of 0.042 using a 436-nm exictation wavelength.[16] Luminescence lifetimes were measured with a Quanta Ray DCR Nd-YAG laser system.[19] Solution samples were prepared in a cell[17] identical to that used for collecting luminescence spectra.

Transient-absorption spectra (TA) of *trans*-$[ReO_2(4\text{-}Phpy)_4]PF_6$, *trans*-$[ReO_2(4\text{-}MeOpy)_4]PF_6$, *trans*-$[ReO_2(3\text{-}Medmap)_4]PF_6$ and *trans*-$[ReO_2(dmap)_4]PF_6$ were kindly measured by Dr. I-Jy Chang at Brookhaven National Laboratory using an apparatus that has been previously described.[20] Data were collected from dry, degassed acetonitrile solutions of the complexes. Samples were excited at 355 nm. Excited-state lifetimes were determined by monitoring the recovery of the ground-state MLCT bleach and/or the decay of new absorptions (both for at least 4 half-lives). Transient spectra were recorded point-by-point and correspond to optical density changes (Δ O.D.) at time zero relative to the excitation pulse.

Infrared spectra were recorded as Nujol mulls on a Beckman IR 4240 spectrometer with internal calibration or on a Perkin-Elmer 1600 Series FTIR spectrometer.

RESULTS

Electrochemistry. All *trans*-$[ReO_2(L)_4]PF_6$ pyridine complexes exhibit a single reversible oxidation wave within the limits of the solvent. The square-root dependence of anodic peak current on scan rate (varied from 20 – 500 mV s^{-1}) suggested that in addition to being reversible, the oxidative processes observed were under diffusion control.[21,22] Two representative cyclic voltammograms are given in Figures 3.1 and 3.2. The $E_{1/2}$ values measured for each complex are summarized in Table 3.1.

Table 3.1. Formal potentials of the Re(VI)/Re(V) couple for *trans*-$[ReO_2(L)_4]PF_6$ pyridine complexes in 0.1 M TBAH CH_3CN solution.

L=	ΔpK_a[b]	$E_{1/2}$, V vs. Fc^+/Fc
py	0.00	0.95
4-Phpy	-0.14	0.87
4-pic	-0.82	0.83
3,5-lut	-0.93	0.83
4-MeOpy	-1.37	0.65
3-Medmap	-3.45	0.18
dmap	-4.36	0.10[a]
4-pyrrpy	-4.36[c]	0.05[a]

[a]0.1 M TBAH CH_2Cl_2 solution

[b]$\Delta pK_a = pK_a(py) - pK_a(py\text{-}X)$ for the conjugate acids of the pyridine ligands.

[c]The pKa of this ligand is not known. Due to the small difference in structure between 4-pyrrpy and dmap, the pKa's of these two ligands were assumed to be identical.

Figure 3.1. Cyclic voltammogram of *trans*-$[ReO_2(4\text{-Phpy})_4]PF_6$ in 0.1 M TBAH CH_3CN solution. The peak at approximately 0.45 V is due to the internal redox standard ferrocene.

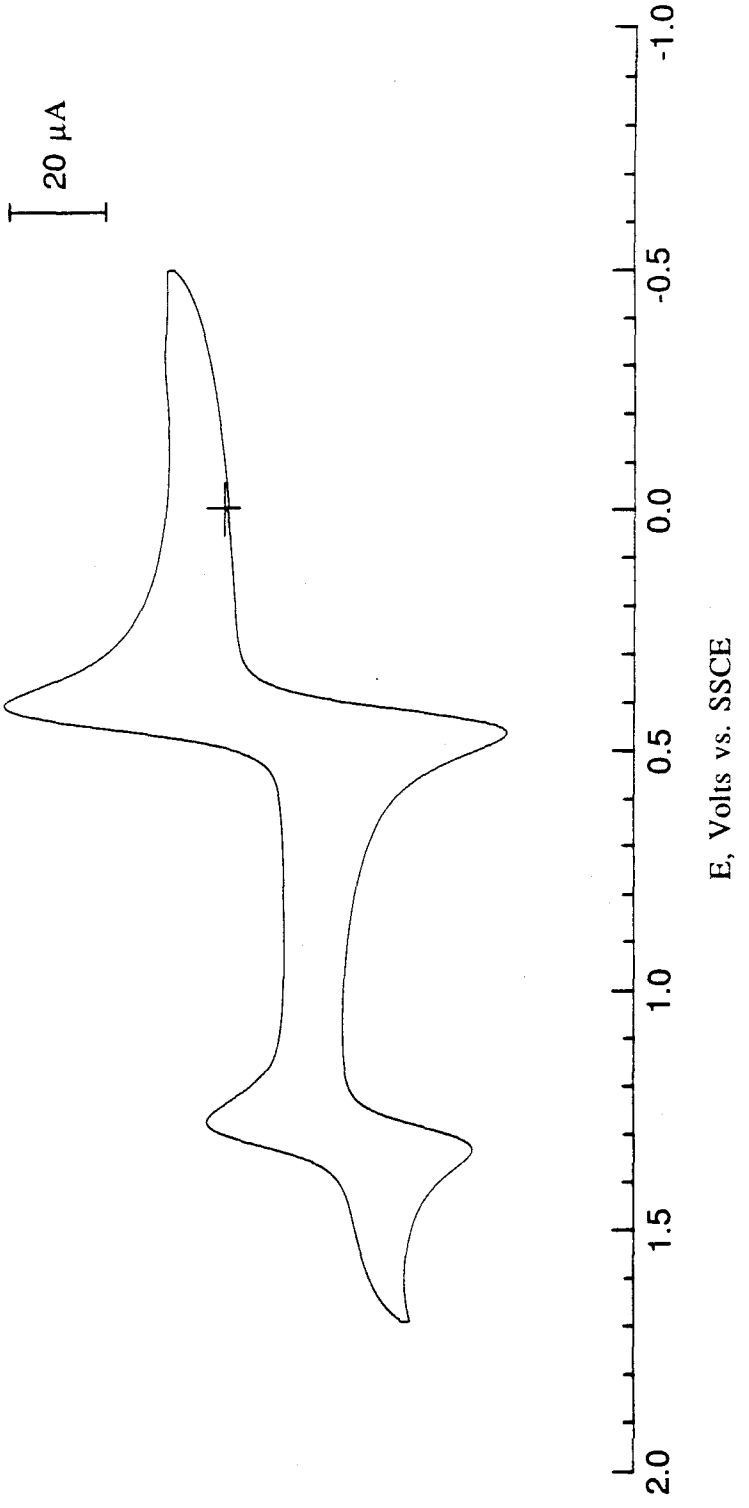
20 μA
2.0
1.5
1.0
0.5
0.0
-0.5
-1.0
E, Volts vs. SSCE

Figure 3.2. Cyclic voltammogram of *trans*-[ReO_2(3-Medmap)$_4$]PF_6 in 0.1 M TBAH CH_3CN solution. The peaks at approximately -0.4 and -0.8 V are due to the internal redox standard [MV][PF_6]$_2$.

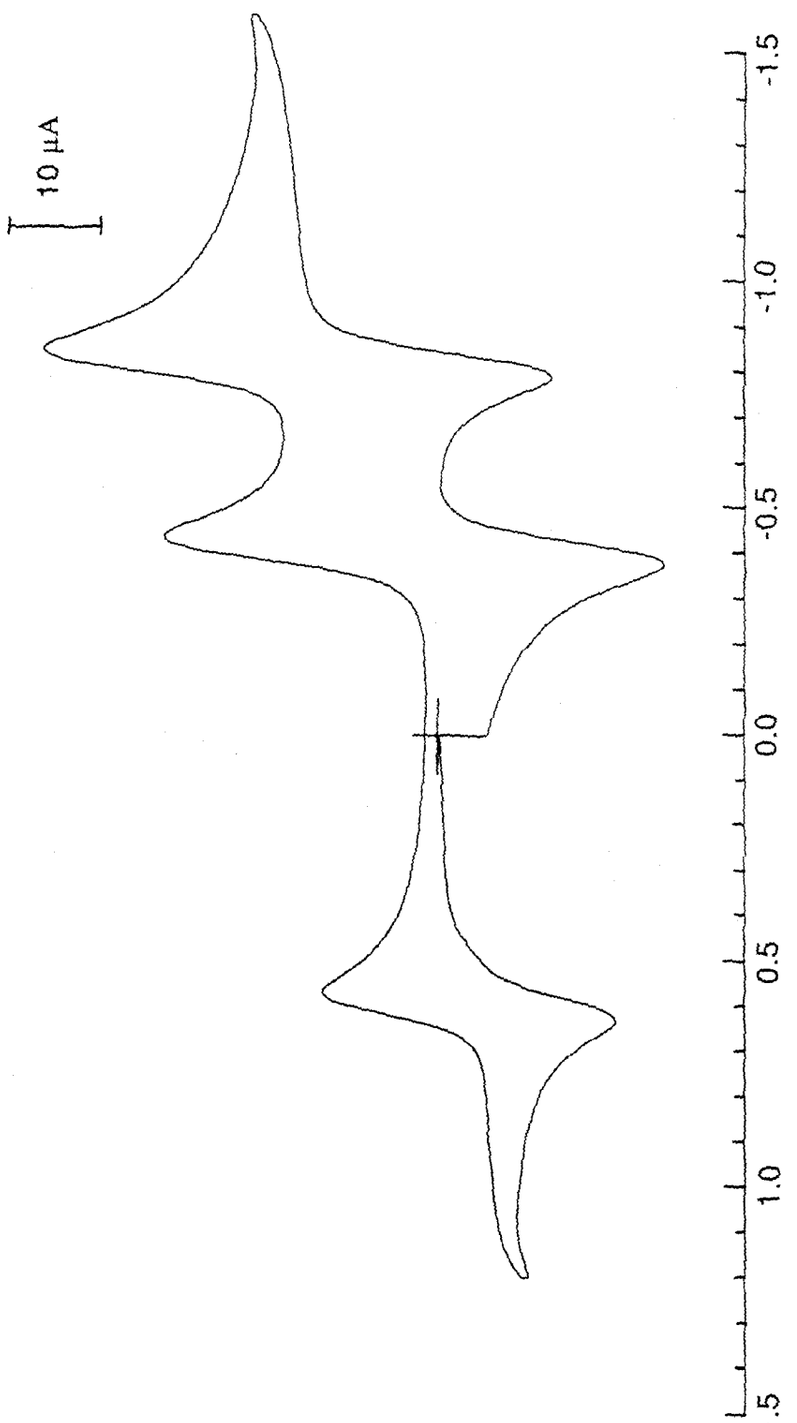
10 µA
1.5
1.0
0.5
0.0
-0.5
-1.0
-1.5
E, Volts vs. SSCE

The complexes *trans*-[ReO_2(dmap)$_4$][PF_6] and *trans*-[ReO_2(4-pyrrpy)$_4$][PF_6] also exhibited additional, irreversible oxidations at 1.07 and 0.97 V vs. Fc^+/Fc. The assignment of these couples was not determined. The current associated with these anodic waves suggested 1-e^- processes.

The complex *trans*-[ReO_2(diphos)$_2$][PF_6] was electro-inactive in the potential range accessible (-1.5 to 1.8 V vs. SSCE) under the experimental conditions (0.1 M TBAH CH_3CN). The complex *trans*-[ReO_2(dppen)$_2$][PF_6] had insufficient solubility (in both 0.1 M TBAH CH_2Cl_2 and CH_3CN solutions) to be examined by cyclic voltammetry. *Trans*-[ReO_2(py)$_3PPh_3$]$^+$ was not examined by cyclic voltammetry because only the iodide salt of the complex was available and the I_2/I^- couple complicated the measurement.

Three complexes were subjected to bulk (oxidative) electrolysis: *trans*-[ReO_2(4-pyrrpy)$_4$][PF_6], *trans*-[ReO_2(3-Medmap)$_4$][PF_6] and *trans*-[ReO_2(4-MeOpy)$_4$][PF_6]. These three complexes were chosen because their low Re(VI)/Re(V) potentials suggested they might yield stable rhenium(VI) products.

Within minutes after initiating the bulk electrolysis of a solution of *trans*-[ReO_2(4-pyrrpy)$_4$][PF_6] (at 0.9 V vs. SSCE; 0.1 M TBAH CH_2Cl_2) the orange solution became deep green (orange + blue). After current ceased to flow, the solution was deep blue. The amount of charged passed at this point was within 10% of that calculated for a 1-e^- oxidation of *trans*-[Re_2(4-pyrrpy)$_4$][PF_6]. Bulk reduction of this solution (at 0.3 V vs. SSCE) appeared to quantitatively regenerate the starting material, based on the charge passed and the cyclic voltammograms taken after the oxidation/reduction cycle. Similar behavior was observed for *trans*-[ReO_2(3-Medmap)$_4$][PF_6].

In contrast to the former two cases, *trans*-[ReO_2(4-MeOpy)$_4$][PF_6] was not stable to oxidation on the bulk electrolysis time scale. The current decreased substantially after 1 equivalent of charge had been passed but did not go to zero. After 1.4 equivalents of charge had been passed, a cyclic voltammogram was taken. In addition to a reversible wave at 1.05 V (vs. SSCE), indicative of starting material, there was an irreversible

reduction wave at approximately -0.7 V. Subsequently, a reducing potential was applied, but only 0.2 equivalents of charge was passed. Estimated $i_{p,a}$ from the cyclic voltammogram taken after the cycle of oxidation/reduction suggested that 60% of the original material had decomposed. In addition, the broad irreversible reduction wave was still present between -0.6 and -0.9 V.

Three pyridine derivatives were also examined by cyclic voltammetry: 4-methoxypyridine (4-MeOpy), 3-methyl-4-dimethylaminopyridine (3-Medmap), and 4-dimethylaminopyridine (dmap). No reversible electrochemistry was seen for any of these; broad anodic waves were observed in all cases. The position of the anodic waves varied with scan rate. In each case the wave shape was similar to that shown in Figure 3.3 for 4-dimethylaminopyridine. At a scan rate of 200 mV s^{-1}, the anodic peak potentials (vs. Fc^+/Fc) were 1.1, 0.9 and 1.2 V for dmap, 3-Medmap and 4-MeOpy, respectively.

Infrared Spectra. The IR spectra of the pyridine complexes of *trans*-$[ReO_2(L)_4][PF_6]$ are provided in an appendix of this thesis. In addition to bands resulting from the coordinated pyridine ligands, medium to strong absorptions were observed at 845 cm^1 and ~800 cm^{-1} arising from $[PF_6]^-$ and the *trans*-ReO_2^+ asymmetric stretch, respectively. Band positions of the asymmetric *trans*-ReO_2^+ stretch for several *trans*-$[ReO_2(L)_4]^+$ complexes are summarized in Table 3.2.

The IR spectra of *trans*-$[ReO_2(py)_3(PPh_3)]I$, *trans*-$[ReO_2(diphos)_2][PF_6]$ and *trans*-$[ReO_2(dppen)_2][PF_6]$ are also provided in an appendix of this thesis along with the corresponding free-ligand spectra. In addition to ligand vibrations, absorptions due to the *trans*-ReO_2^+ asymmetric stretch occur in the vicinity of 800 cm^{-1} along with additional bands at 845 cm^{-1} due to $[PF_6]^-$ (if present). The assignment of the metal-oxo vibration is dubious for the diphos and dppen complexes because of the presence of bands with similar energies in the corresponding free ligands. Oxygen-18 labelling of the rhenium complexes would be necessary to make this band assignment with certainty.

Table 3.2. Position of the asymmetric O=Re=O stretch for *trans*-$[ReO_2(L)_4]^+$ pyridine and phosphine complexes.

L=	ν_{asym} for ReO_2^+ (cm^{-1})
py	816
4-Phpy	810
4-pic	820
3,5-lut	820
4-MeOpy	810
3-Medmap	810
dmap	800
4-pyrrpy	798
$(py)_3(PPh_3)$	815
1/2 diphos	780
1/2 dppen	790

Figure 3.3. Cyclic voltammogram of free 4-dimethylaminopyridine in 0.1 M TBAH CH_3CN solution.

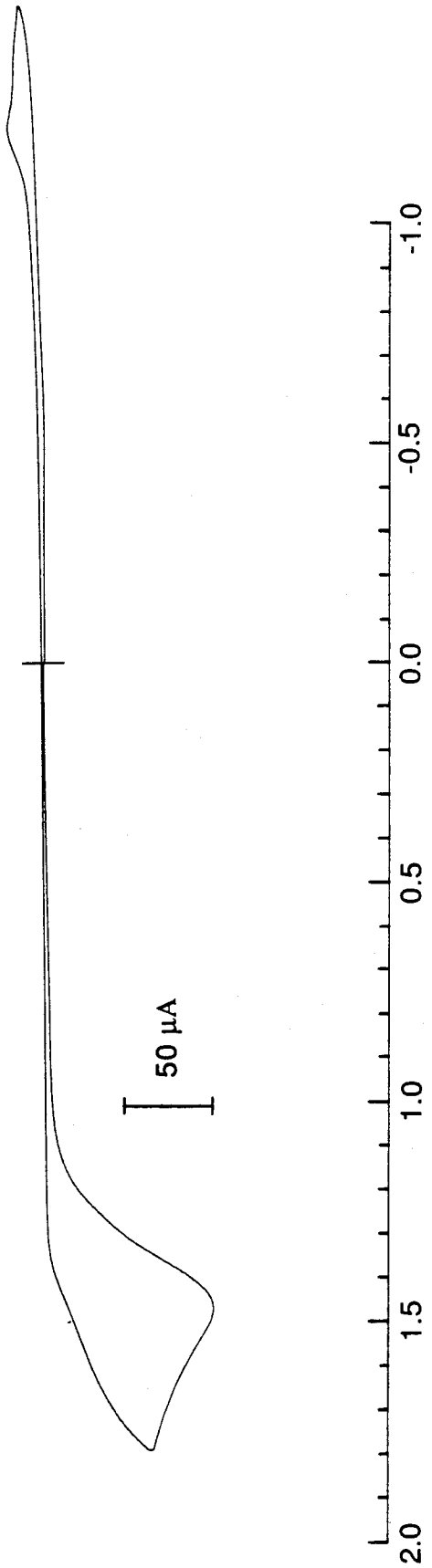
50 µA
2.0
1.5
1.0
0.5
0.0
-0.5
-1.0
E, Volts vs. SSCE

Spectroscopy. The *trans*-$[ReO_2(L)_4]^+$ complexes of pyridine and its derivatives exhibit several prominent absorptions in their electronic spectra. The two lowest energy transitions exhibit a marked solvent dependence: the band occurring in the region 400 - 500 nm shifts to lower energy in Lewis acidic solvents, while the band in the region 340 - 370 nm shifts to higher energy. This dependence has been previously noted[23] and is attributed to the interaction of lone-pair electrons on the oxo ligands with vacant low-energy orbitals in the solvent molecules. Because of this behavior, all UV-vis data were collected using the same solvent (CH_3CN).

In order to aid in the assignment of the electronic transitions, the UV-vis spectra of the corresponding free pyridine ligands were measured in CH_3CN solution. These spectra are dominated by a single strong absorption ($\varepsilon \sim 5{,}000$) in the region 200 – 260 nm; in some cases vibrational fine structure is present in these bands. The UV-vis spectrum of each *trans*-$[ReO_2(L)_4]^+$ pyridine complex and the corresponding free ligand are provided in Figures 3.4 – 3.11.

The compounds *trans*-$[ReO_2(L)_4]PF_6$ with L= py, 4-Phpy, 4-pic, 3,5-lut, and 4-MeOpy all exhibit red emission upon excitation with 436-nm light. For solid samples, emission bands showed vibrational fine structure that became more pronounced upon cooling to 77 K. The solution luminescence properties are summarized in Table 3.3. The emission spectrum displayed in Figure 3.12 for *trans*-$[ReO_2(3,5\text{-lut})_4][PF_6]$ is representative of those observed for the other luminescent tetrapyridine complexes. Excited-state lifetimes of the above complexes were determined by monitoring the rate of luminescence decay. Incident laser power was between 0.2 - 0.4 mJ/pulse and emission decays were monitored between 640 - 660 nm. All decay curves could be fit to single exponentials for at least 4 half-lives.

Figure 3.4. UV-vis absorption spectra of *trans*-$[ReO_2(py)_4]PF_6$ (top) and free pyridine (bottom) in CH_3CN solution. The ordinate scale is in arbitrary absorbance units.

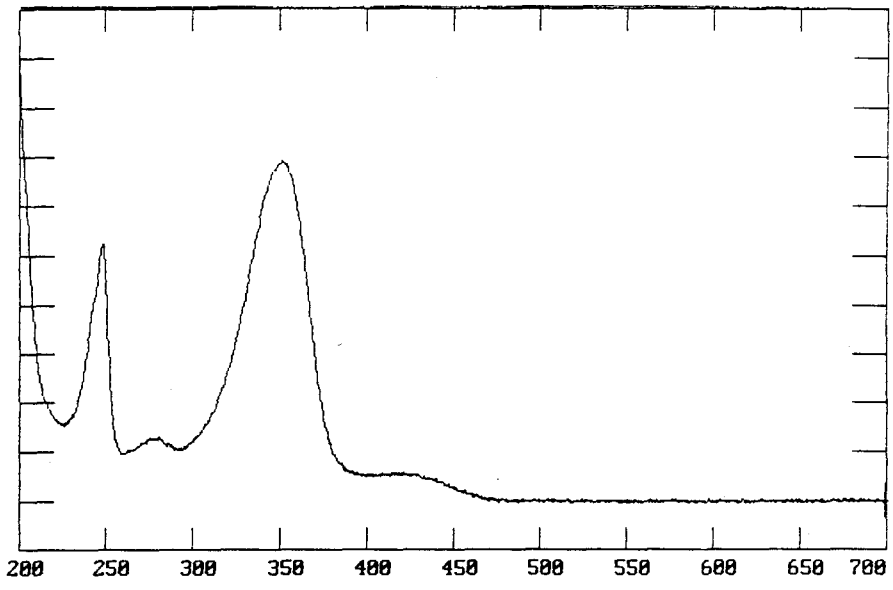
200 250 300 350 400 450 500 550 600 650 700
WAVELENGTH

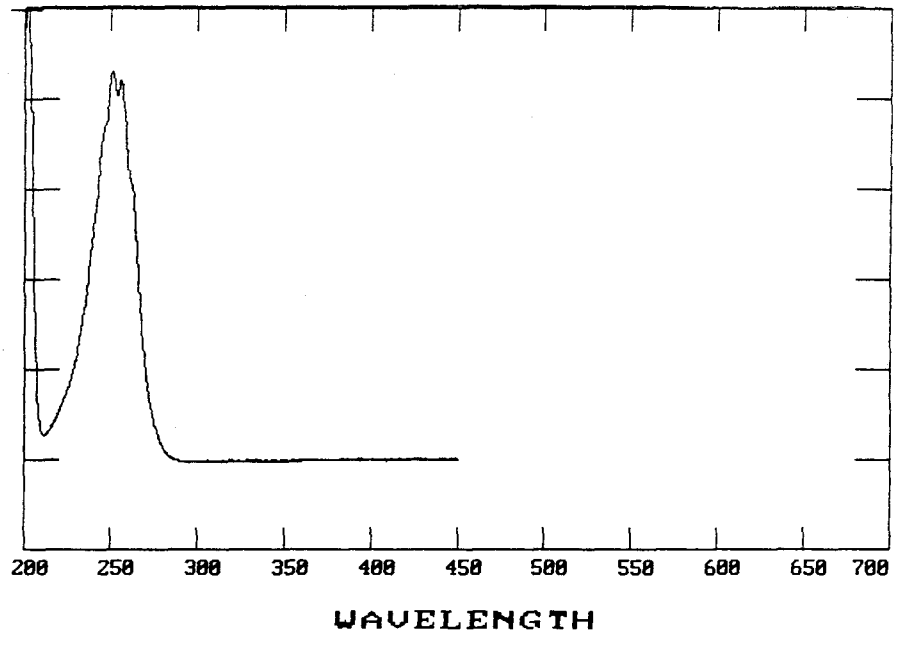
200 250 300 350 400 450 500 550 600 650 700
WAVELENGTH

Figure 3.5. UV-vis absorption spectra of *trans*-[ReO_2(4-Phpy)$_4$]PF_6 (top) and free 4-phenylpyridine (bottom) in CH_3CN solution. The ordinate scale is in arbitrary absorbance units.

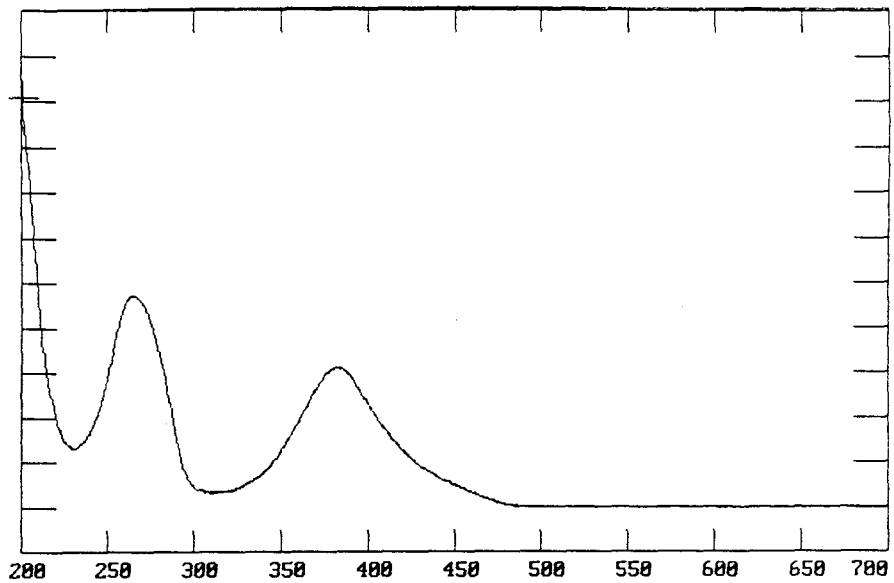
200
250
300
350
400
450
500
550
600
650
700
WAVELENGTH

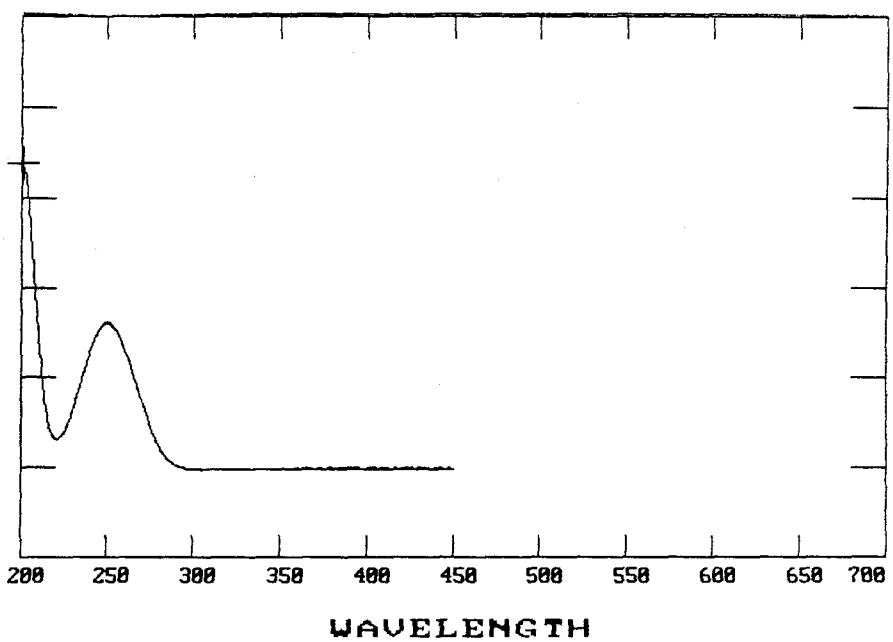
200
250
300
350
400
450
500
550
600
650
700
WAVELENGTH

Figure 3.6. UV-vis absorption spectra of *trans*-$[ReO_2(4\text{-pic})_4]PF_6$ (top) and free 4-picoline (bottom) in CH_3CN solution. The ordinate scale is in arbitrary absorbance units.

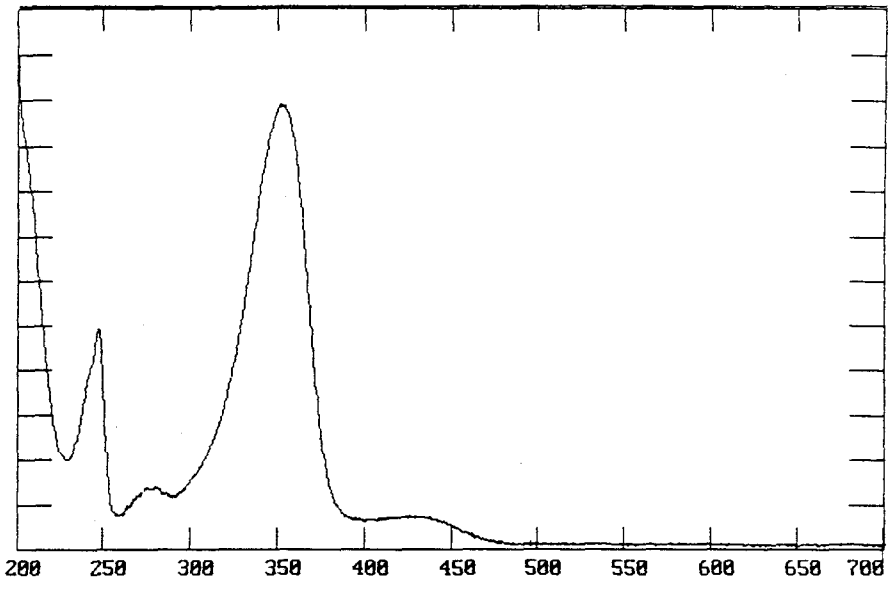
200
250
300
350
400
450
500
550
600
650
700
WAVELENGTH

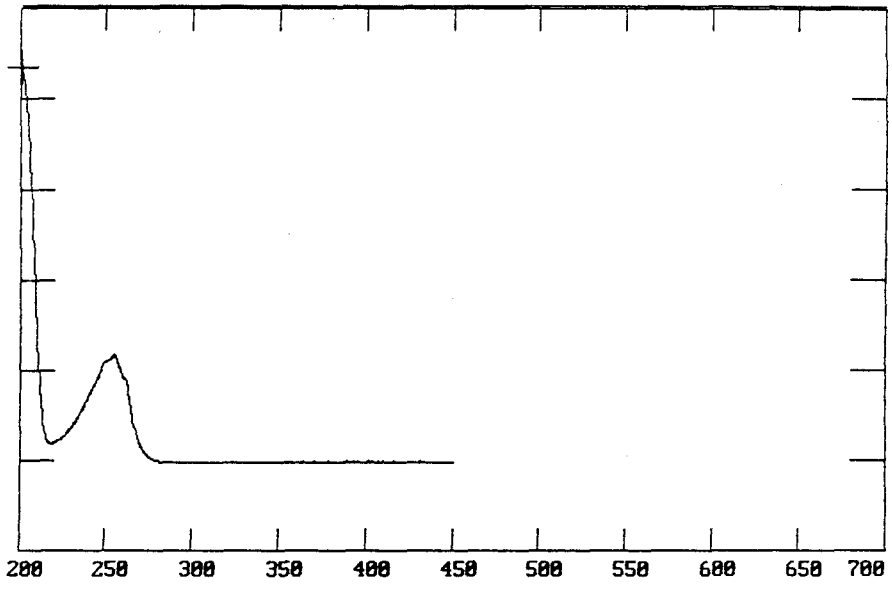
200
250
300
350
400
450
500
550
600
650
700
WAVELENGTH

Figure 3.7. UV-vis absorption spectra of *trans*-$[ReO_2(3,5\text{-lut})_4]PF_6$ (top) and free 3,5-lutidine (bottom) in CH_3CN solution. The ordinate scale is in arbitrary absorbance units.

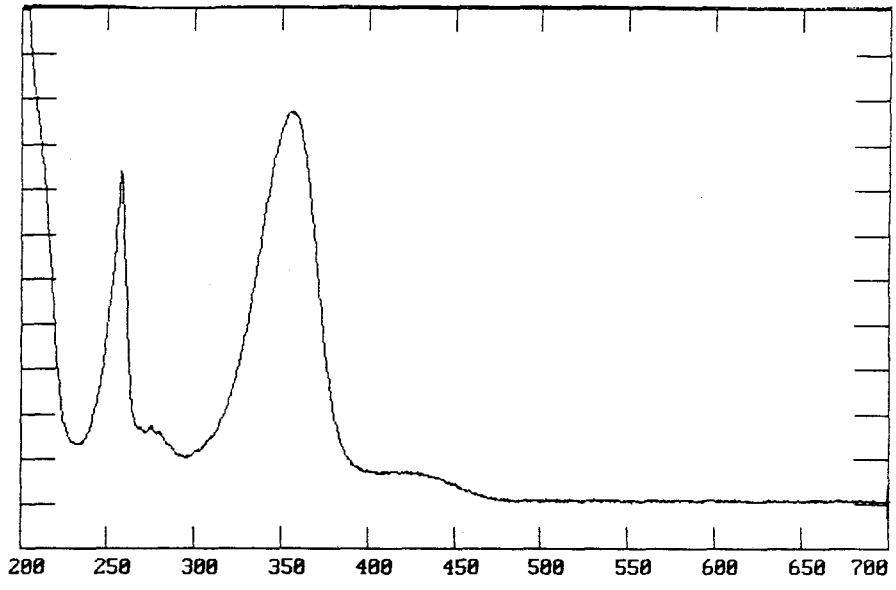
200 250 300 350 400 450 500 550 600 650 700
WAVELENGTH

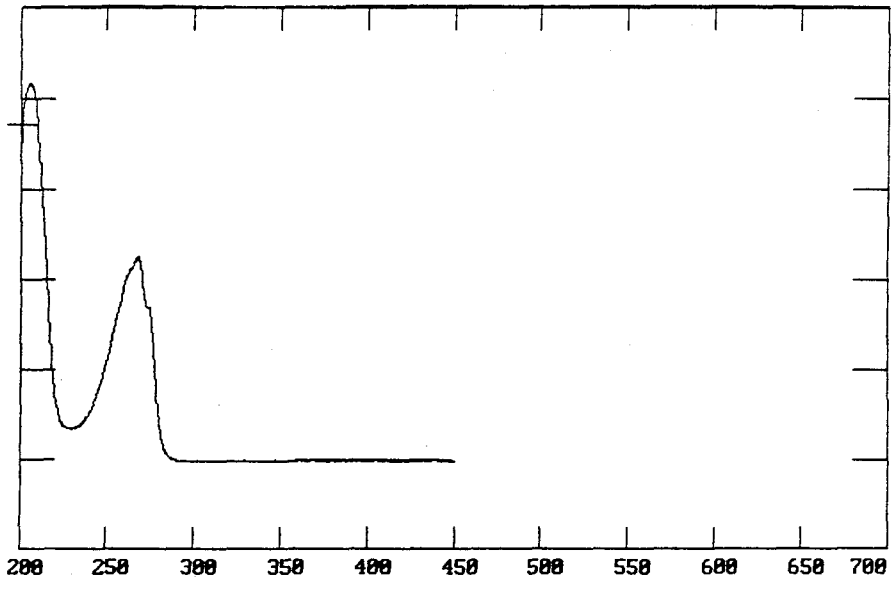
200 250 300 350 400 450 500 550 600 650 700
WAVELENGTH

Figure 3.8. UV-vis absorption spectra of *trans*-[ReO_2(4-MeOpy)$_4$]PF_6 (top) and free 4-methoxypyridine (bottom) in CH_3CN solution. The ordinate scale is in arbitrary absorbance units.

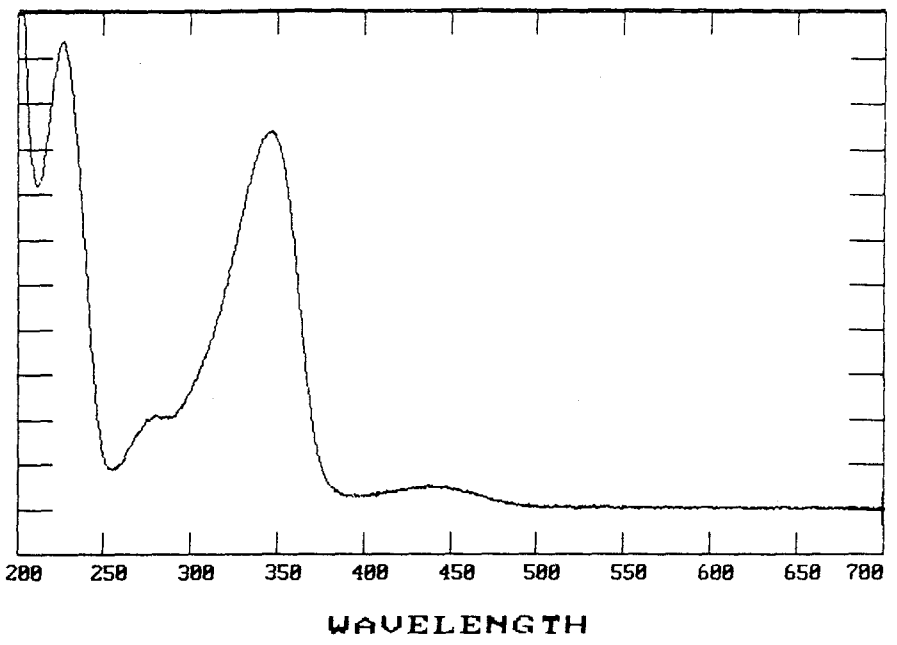
200
250
300
350
400
450
500
550
600
650
700
WAVELENGTH

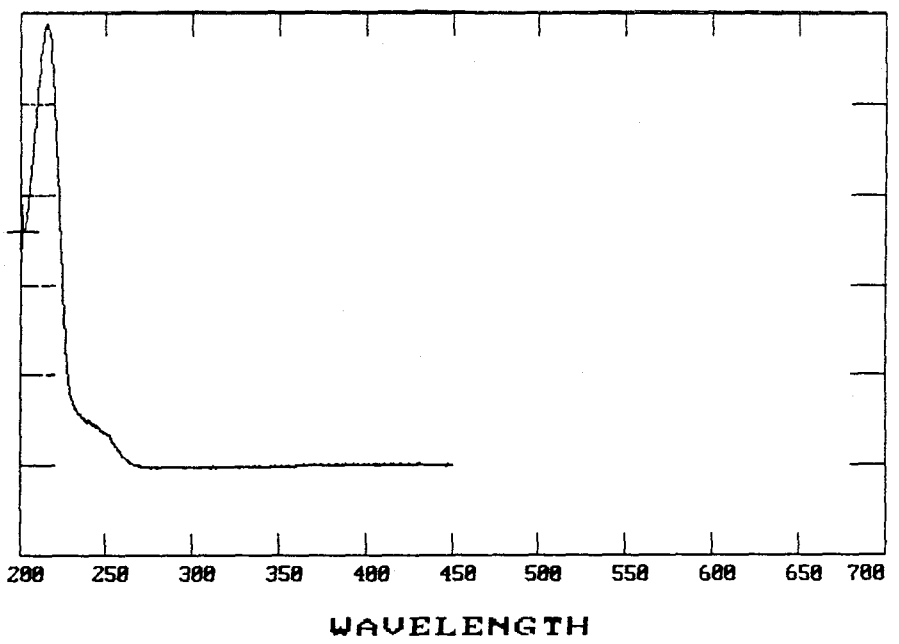
200
250
300
350
400
450
500
550
600
650
700
WAVELENGTH

Figure 3.9. UV-vis absorption spectra of *trans*-[ReO_2(3-Medmap)$_4$]PF_6 (top) and free 3-methyl-4-dimethylaminopyridine (bottom) in CH_3CN solution. The ordinate scale is in arbitrary absorbance units.

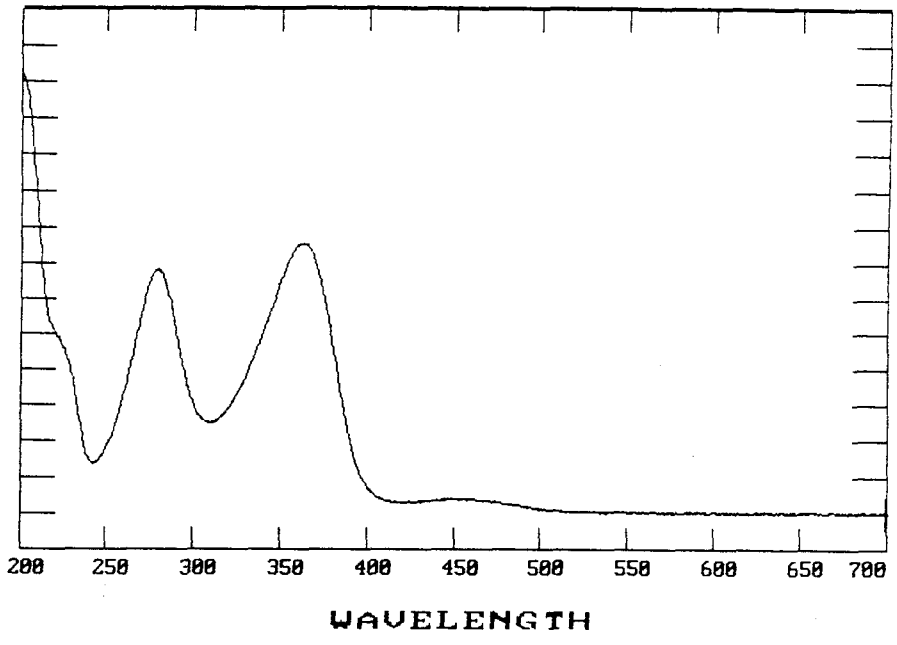
200
250
300
350
400
450
500
550
600
650
700
WAVELENGTH

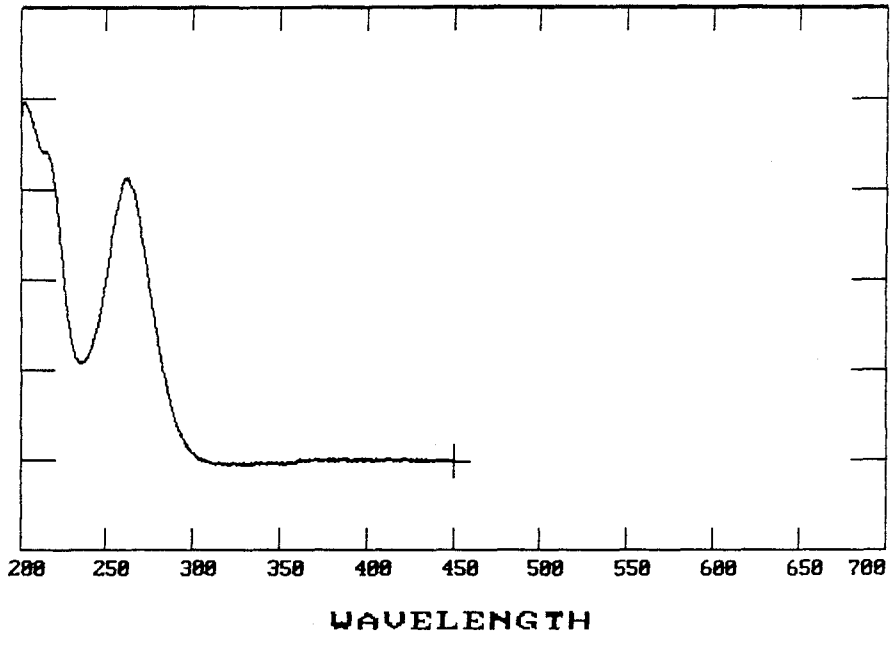
200
250
300
350
400
450
500
550
600
650
700
WAVELENGTH

Figure 3.10. UV-vis absorption spectra of *trans*-$[ReO_2(dmap)_4]PF_6$ (top) and free 4-dimethylaminopyridine (bottom) in CH_3CN solution. The ordinate scale is in arbitrary absorbance units.

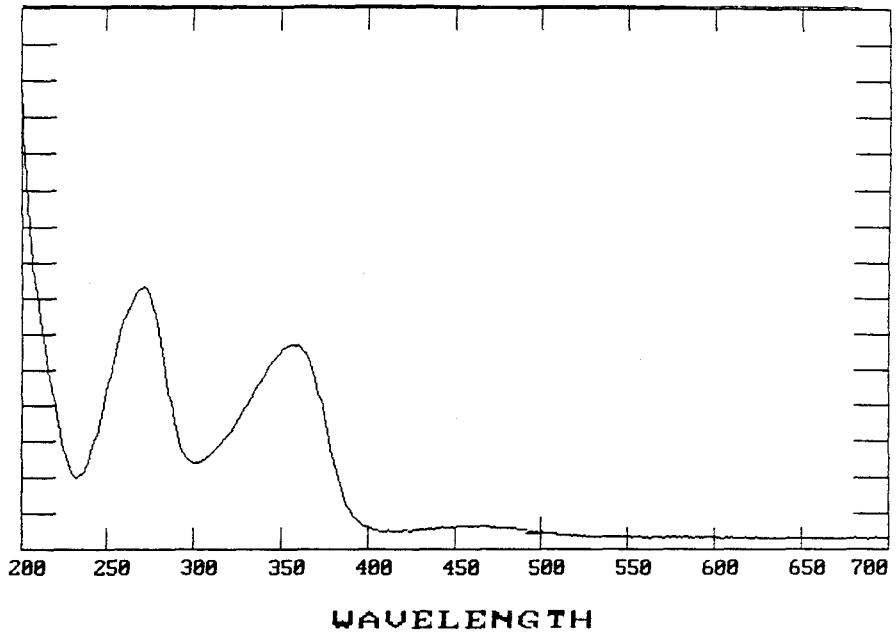
200 250 300 350 400 450 500 550 600 650 700
WAVELENGTH

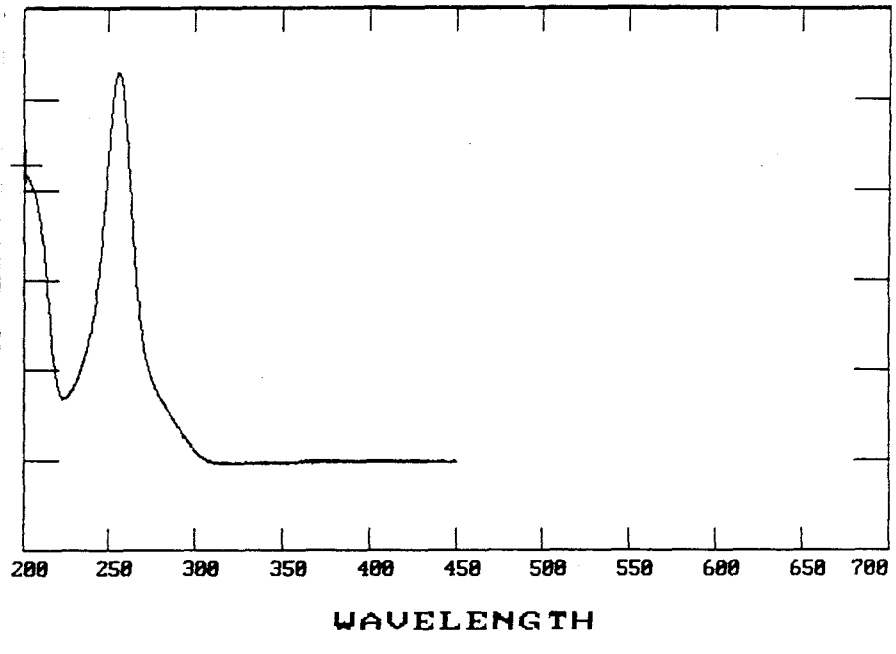
200 250 300 350 400 450 500 550 600 650 700
WAVELENGTH

Figure 3.11. UV-vis absorption spectra of *trans*-[ReO_2(4-pyrrpy)$_4$]PF_6 (top) and free 4-pyrrolidinopyridine (bottom) in CH_3CN solution. The ordinate scale is in arbitrary absorbance units.

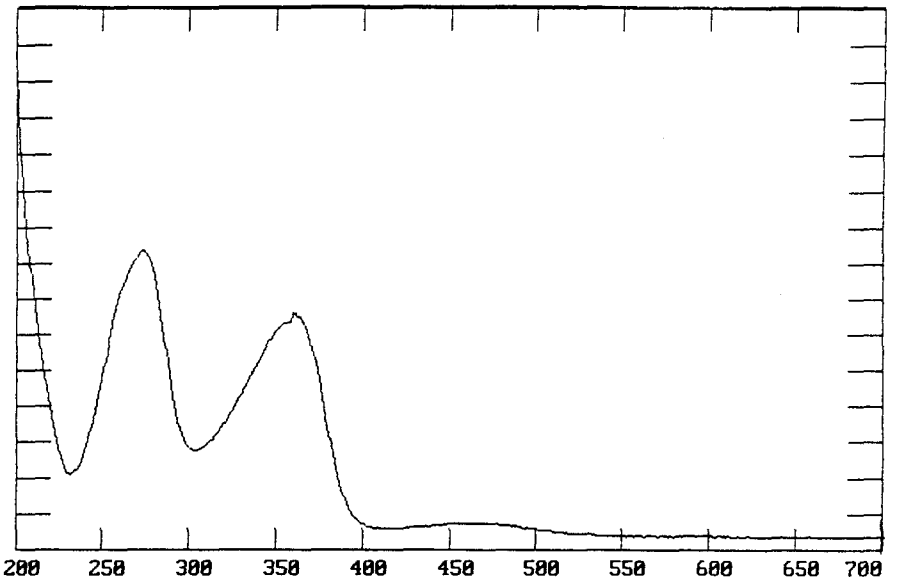
200 250 300 350 400 450 500 550 600 650 700
WAVELENGTH

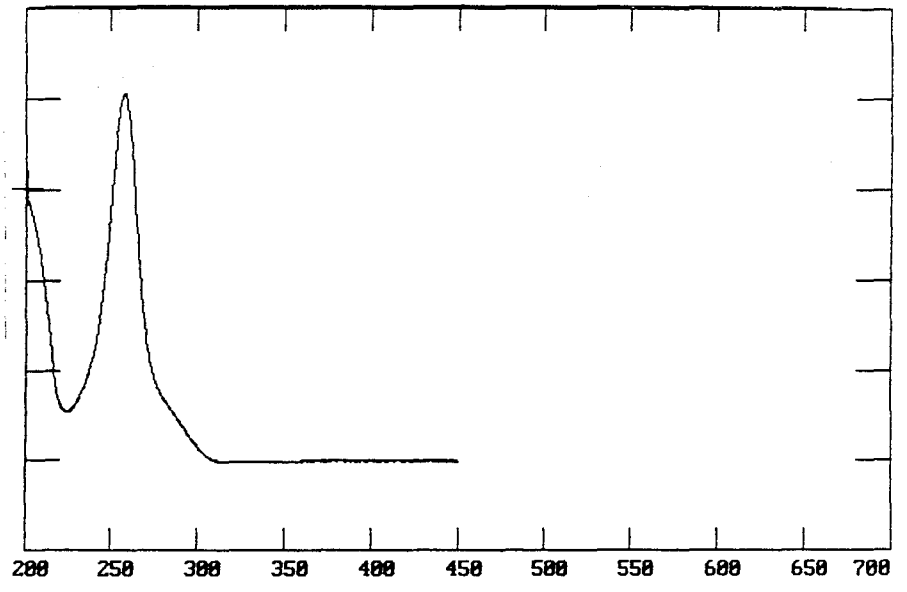
200 250 300 350 400 450 500 550 600 650 700
WAVELENGTH

Figure 3.12. Room temperature emission spectrum *trans*-[ReO_2(3,5-lut)$_4$][PF_6] in CH_3CN solution. The spectrum has been corrected for spectrometer response.

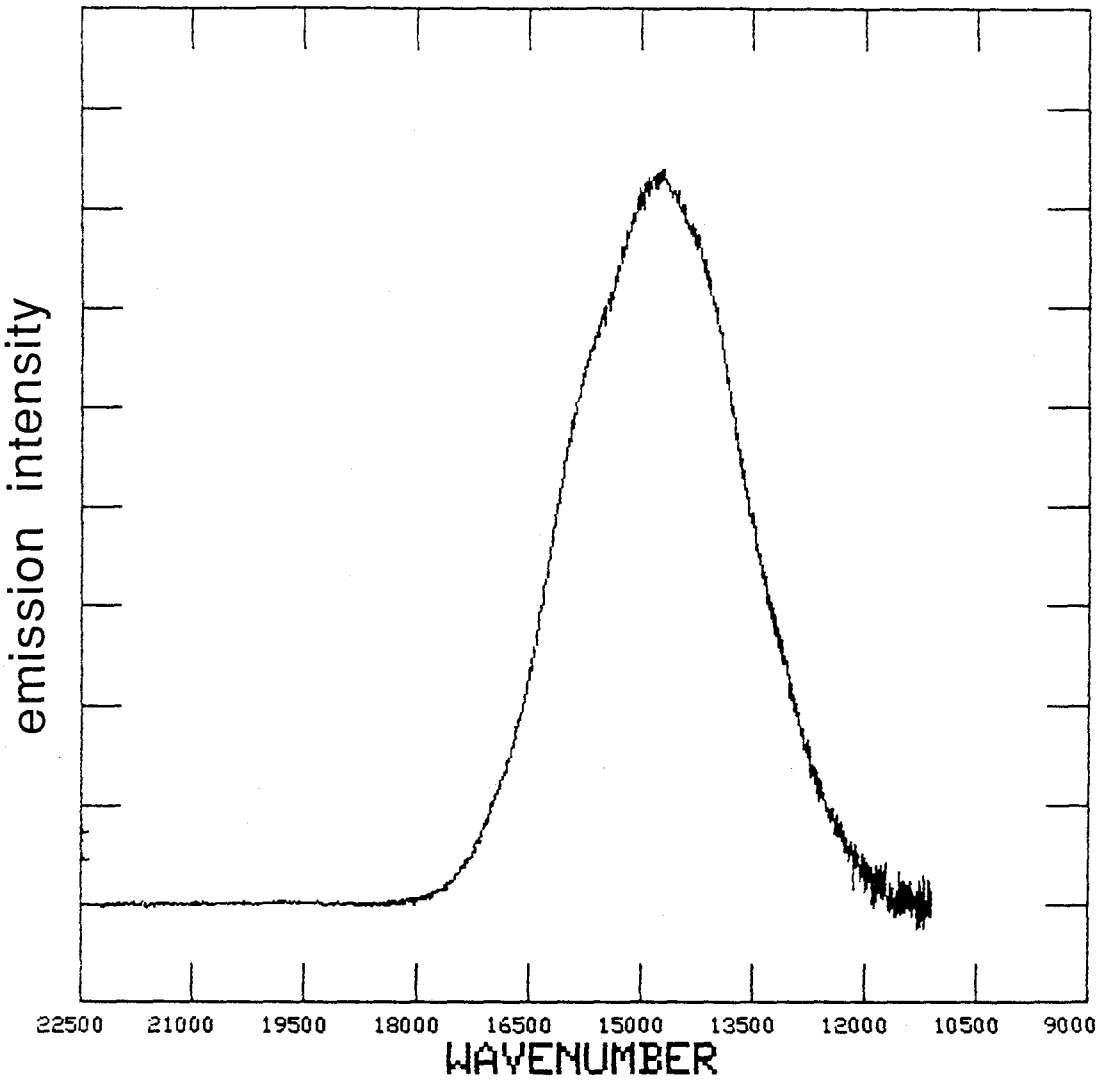
emission intensity
22500
21000
19500
18000
16500
15000
13500
12000
10500
9000
WAVENUMBER

Table 3.3. Luminescence properties of *trans*-$[ReO_2(L)_4][PF_6]$ pyridine complexes in CH_3CN solution at room temperature. All values reported have been corrected for spectrometer response.

L=	E_{max} (cm^{-1})	τ_o (μs)
py	14,920	14
4-Phpy	14,720	14
4-Mepy	14,580	12
3,5-lut	14,760	13
4-MeOpy	13,790	2.8

The UV-visible spectrum of *trans*-$[ReO_2(py)_3(PPh_3)]I$ is similar to that of the tetrapyridine complex, except that the far UV region is dominated by the intense π-π^* transitions of the phenyl rings. The spectrum is shown in Figure 3.13 along with the spectrum of free PPh_3 for comparison.

The compound *trans*-$[ReO_2(py)_3(PPh_3)]I$ was luminescent in CH_2Cl_2 solution (E_{max} = 15,150 cm^{-1}, τ = 1.5 μs). The emission quantum yield was found to be 0.003, an order of magnitude smaller than that of *trans*-$[ReO_2(py)_4]PF_6$. The solid-state emission spectrum (τ = 33 μs at RT) of *trans*-$[ReO_2(py)_3(PPh_3)]I$ exhibited vibrational fine structure (Figure 3.14) which became well resolved at 77 K (Figure 3.15). The peak positions (uncorrected) are summarized in Table 3.4. At low temperature, two progressions were clearly evident: a major progression of ~800 cm^{-1} and a minor progression of ~190 cm^{-1}. From analogy with the low temperature emission spectrum of *trans*-$[ReO_2(py)_4][BPh_4]$, the vibrational modes causing these progressions are probably the symmetric O=Re=O stretch and a Re-py stretch, respectively.[28]

Table 3.4. Summary of emission peak maxima for the 77 K spectrum of *trans*-$[ReO_2(py)_3(PPh_3)][PF_6]$ (uncorrected for spectrometer response).

peak position, nm (cm^{-1})	minor progression (cm^{-1})	major progression(cm^{-1})
560.25 (17,849)		
566.25 (17,660)	189	
589.50 (16,964)		885
621.75 (16,084)	193	
629.25 (15,892)		880
657.75 (15,203)	192	
666.75 (14,998)		881
698.25 (14,322)	205	
708.00 (14,124)		881

In contrast to the pyridine complexes, the UV-vis spectra of the phosphine complexes *trans*-$[ReO_2(diphos)_2][PF_6]$ and *trans*-$[ReO_2(dppen)_2][PF_6]$ are essentially featureless, exhibiting only broad absorptions with intense transitions at ~ 266 nm extending out into the near-visible region. Poor solubility precluded accurate extinction measurements; however, an $\varepsilon \sim 30{,}000\ M^{-1}\ cm^{-1}$ can be estimated. The spectra of these complexes, accompanied by those of the free ligand, are provided in Figures 3.16 and 3.17.

Both *trans*-$[ReO_2(diphos)_4][PF_6]$ and *trans*-$[ReO_2(dppen)_4][PF_6]$ exhibit emission *only* in frozen dichloromethane solutions and in the solid state (λ_{max} = 15,100 and 16,170 cm^{-1} for the diphos and dppen complexes, respectively). The bands were Gaussian in shape, and no fine structure was evident down to temperatures as low as 77 K.

Figure 3.13. UV-vis absorption spectra of *trans*-[$ReO_2(py)_3(PPh_3)$]I (top) and free PPh_3 (bottom) in CH_3CN solution. The ordinate scale is in arbitrary absorbance units.

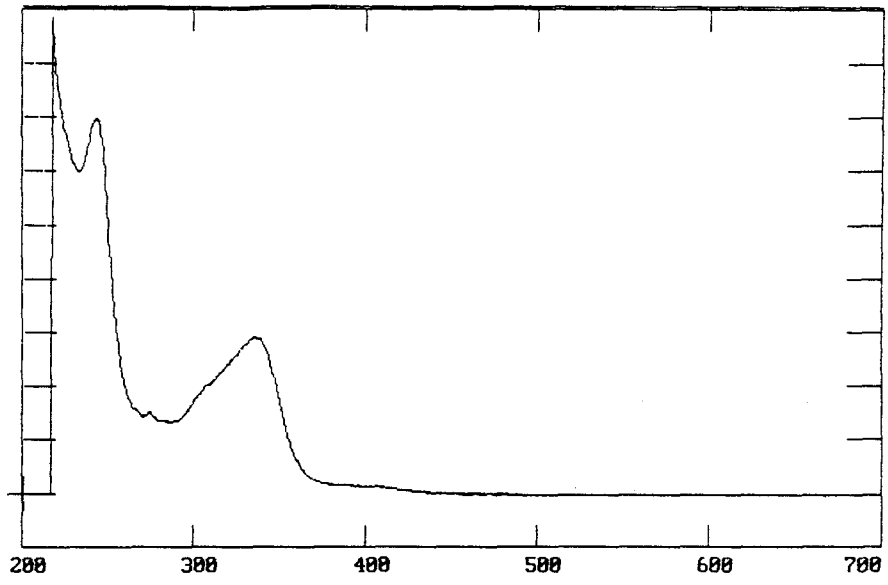
200
300
400
500
600
700
WAVELENGTH

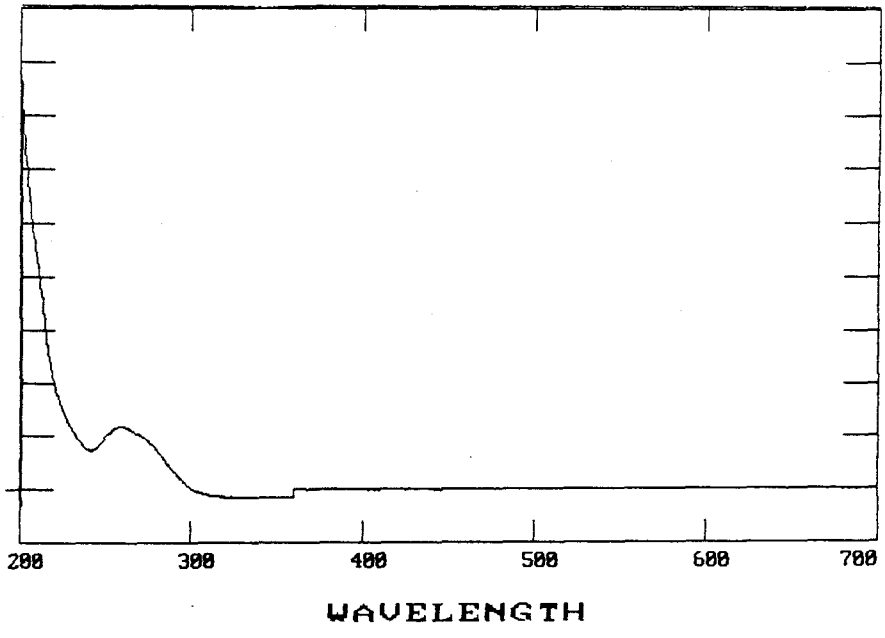
200
300
400
500
600
700
WAVELENGTH

Figure 3.14. Room temperature emission spectrum of a solid sample of *trans*-$[ReO_2(py)_3PPh_3]I$ (not corrected for spectrometer reponse). The band shape is due to incompletely resolved metal-oxo vibrational fine structure.

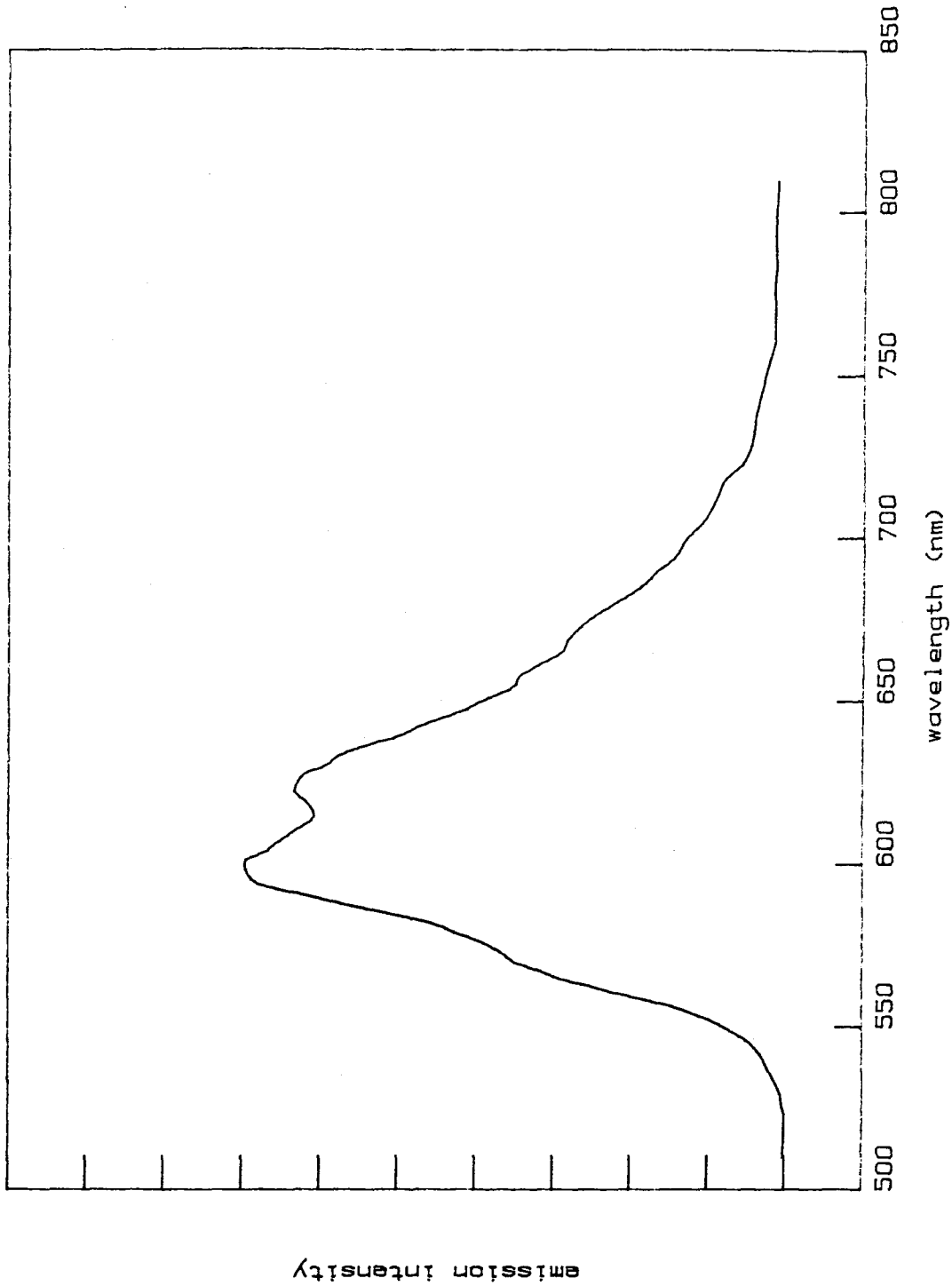
500
550
600
650
700
750
800
850
wavelength (nm)
emission intensity

Figure 3.15. Low temperature (77 K) emission spectrum of a solid sample of *trans*-$[ReO_2(py)_3PPh_3]I$. The spectrum has not been corrected for spectrometer response.

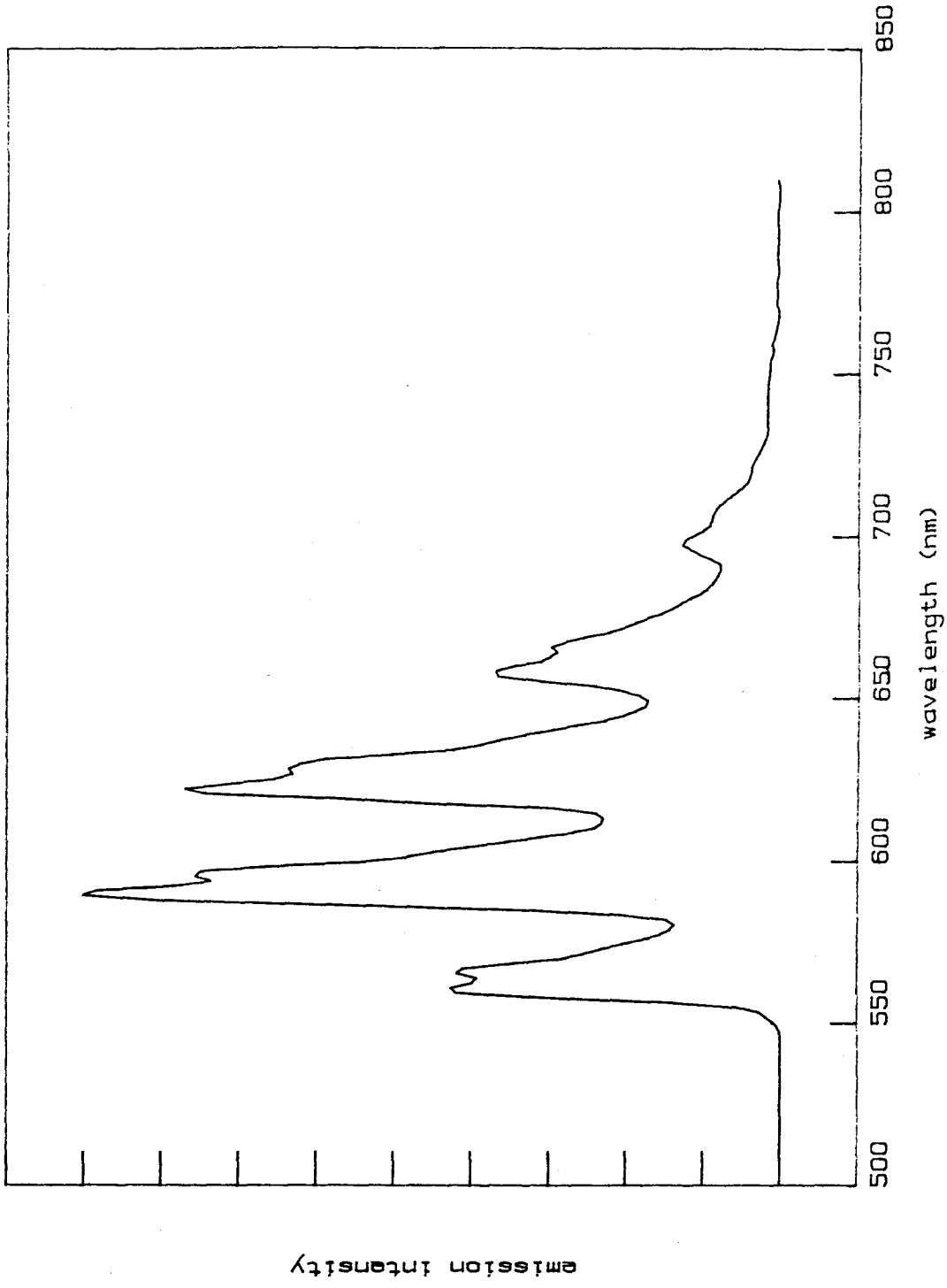
500
550
600
650
700
750
800
850
wavelength (nm)
emission intensity

Figure 3.16. UV-vis absorption spectra of *trans*-[$ReO_2(diphos)_2$][PF_6] (top) and free diphos (bottom) in CH_3CN solution.

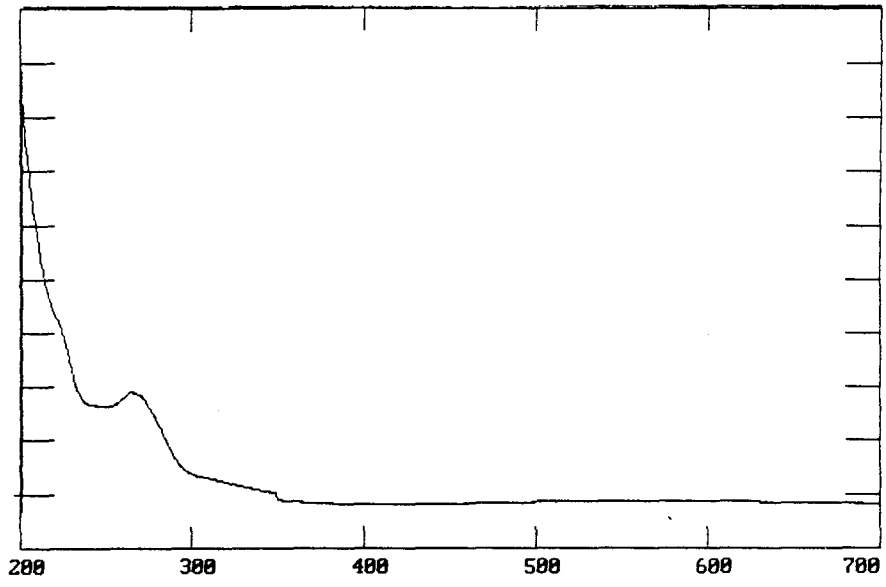
200
300
400
500
600
700
WAVELENGTH

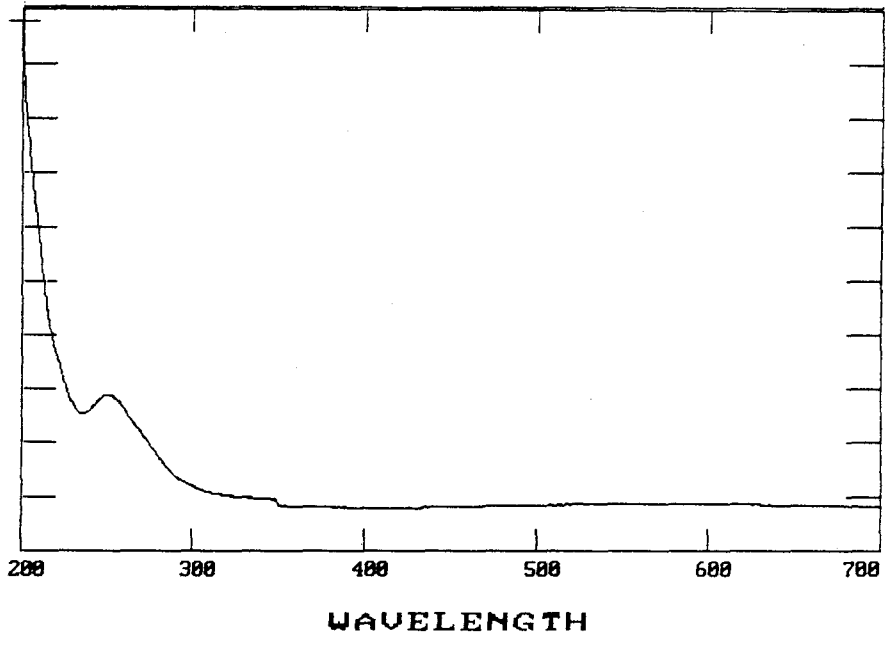
200
300
400
500
600
700
WAVELENGTH

Figure 3.17. UV-vis absorption spectra of *trans*-[$ReO_2(dppen)_2$][PF_6] (top) and free dppen (bottom) in CH_3CN solution.

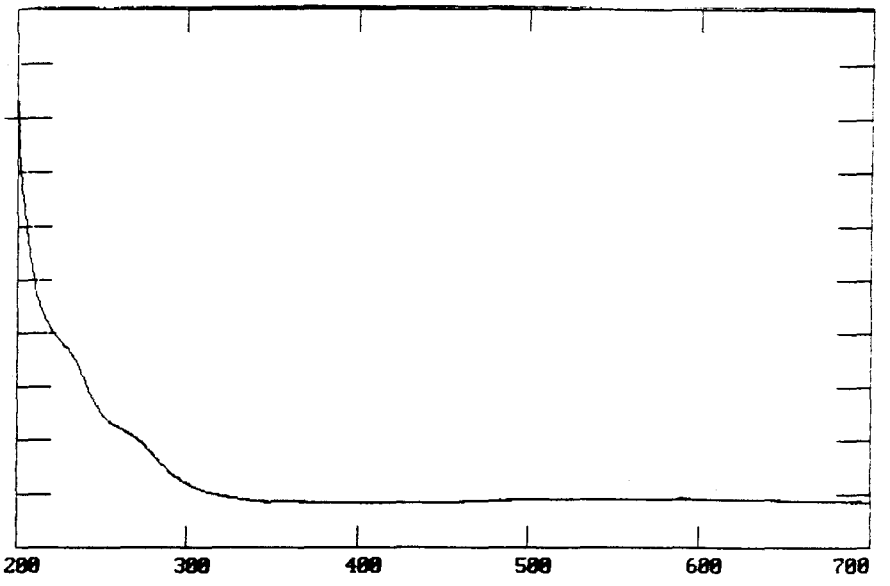
200
300
400
500
600
700
WAVELENGTH

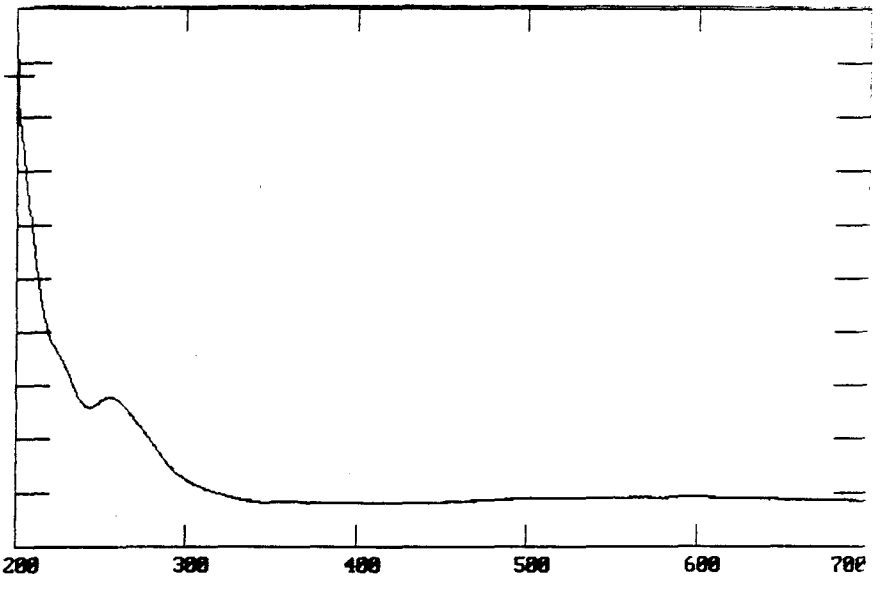
200
300
400
500
600
700
WAVELENGTH

Curiously, no emission could be detected for the following complexes under any conditions: *trans*-[ReO_2(3-Medmap)$_4$][PF_6], *trans*-[ReO_2(dmap)$_4$][PF_6], and *trans*-[ReO_2(4-pyrrpy)$_4$][PF_6].

The transient-absorption (TA) spectra of *trans*-[ReO_2(4-Phpy)$_4$]PF_6, *trans*-[ReO_2(4-MeOpy)$_4$]PF_6, *trans*-[ReO_2(3-Medmap)$_4$]PF_6, and *trans*-[ReO_2(dmap)$_4$]PF_6 are shown in Figures 3.18 to 3.21. All TA spectra are dominated by a pronounced bleach in the region 350 – 400 nm. In the case of *trans*-[ReO_2(4-Phpy)$_4$]PF_6, there is a weak band at approximately 500 nm which is also seen for *trans*-[ReO_2(4-MeOpy)$_4$]PF_6. The latter complex exhibits an additional absorption at ~380 nm. The spectra of *trans*-[ReO_2(3-Medmap)$_4$]PF_6 and *trans*-[ReO_2(dmap)$_4$]PF_6 exhibit intense absorptions with maxima at 510 and 450 nm, respectively. The excited-state lifetime data determined from TA experiments are summarized in Table 3.5.

Table 3.5. Excited-state lifetime data for some *trans*-[$ReO_2(L)_4$]PF_6 pyridine complexes determined from TA measurements.

complex	τ_o (μs)
trans-[ReO_2(4-Phpy)$_4$]PF_6	11.5
trans-[ReO_2(4-MeOpy)$_4$]PF_6	2.5
trans-[ReO_2(3-Medmap)$_4$]PF_6	0.36
trans-[ReO_2(dmap)$_4$]PF_6	0.15

Figure 3.18. TA spectrum of *trans*-[ReO_2(4-Phpy)$_4$][PF_6] in CH_3CN solution. Data were collected point-by-point at time zero with respect to the excitation pulse.

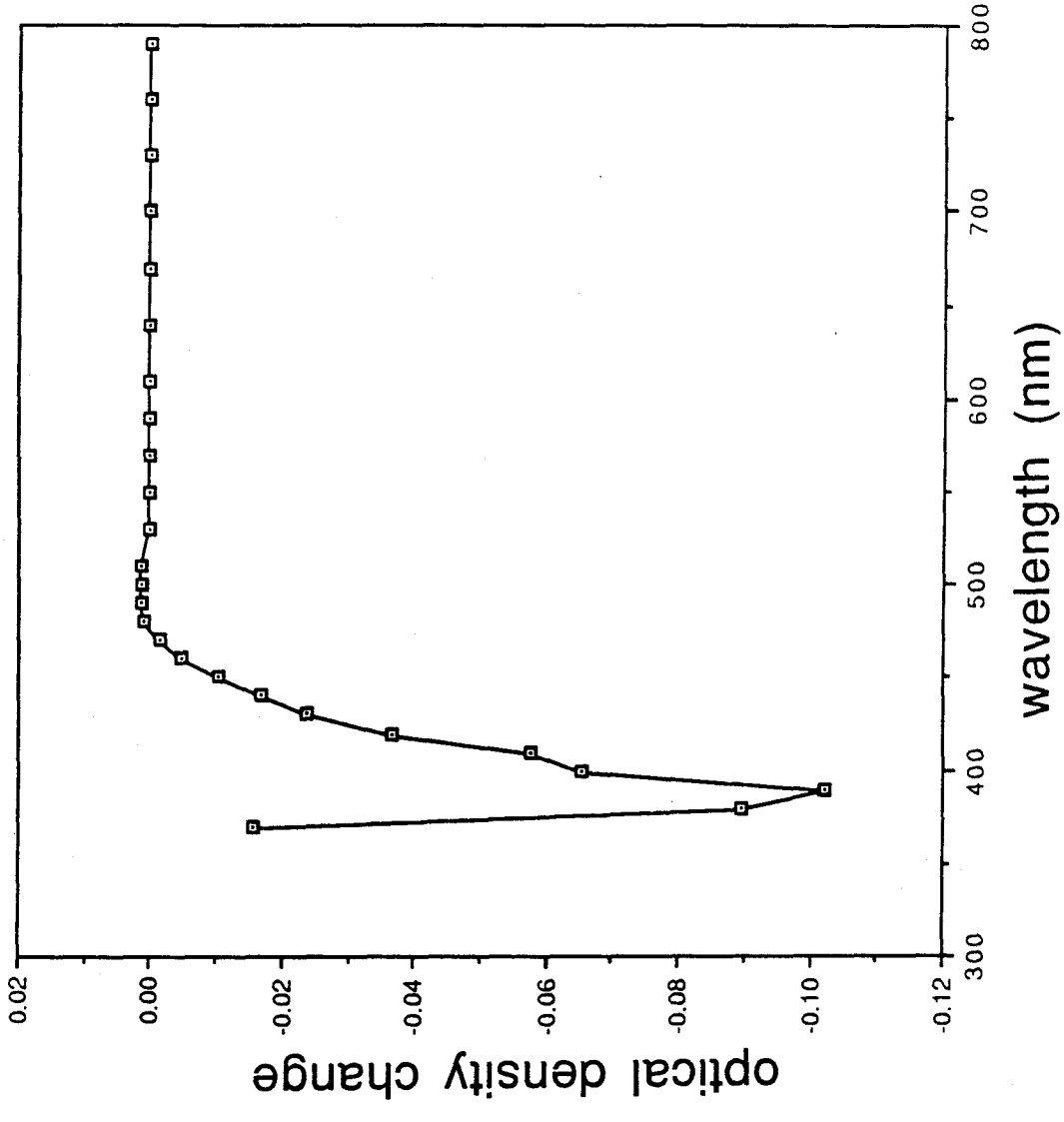
optical density change
0.02
0.00
-0.02
-0.04
-0.06
-0.08
-0.10
-0.12
300
400
500
600
700
800
wavelength (nm)

Figure 3.19. TA spectrum of *trans*-[ReO_2(4-MeOpy)$_4$][PF_6] in CH_3CN solution. Data were collected point-by-point at time zero with respect to the excitation pulse.

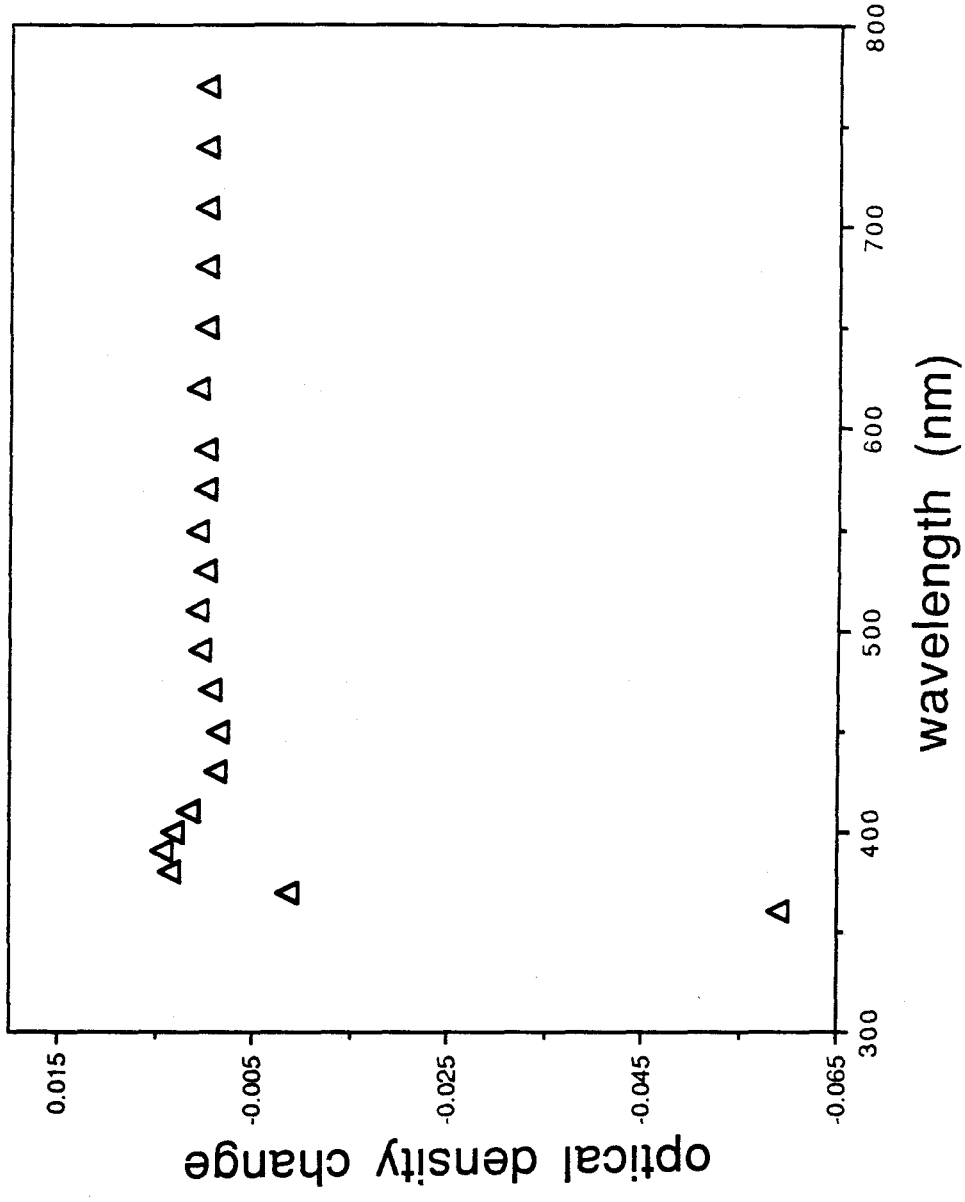
optical density change
0.015
-0.005
-0.025
-0.045
-0.065
300
400
500
600
700
800
wavelength (nm)

Figure 3.20. TA spectrum of *trans*-[ReO_2(3-Medmap)$_4$][PF_6] in CH_3CN solution. Data were collected point-by-point at time zero with respect to the excitation pulse.

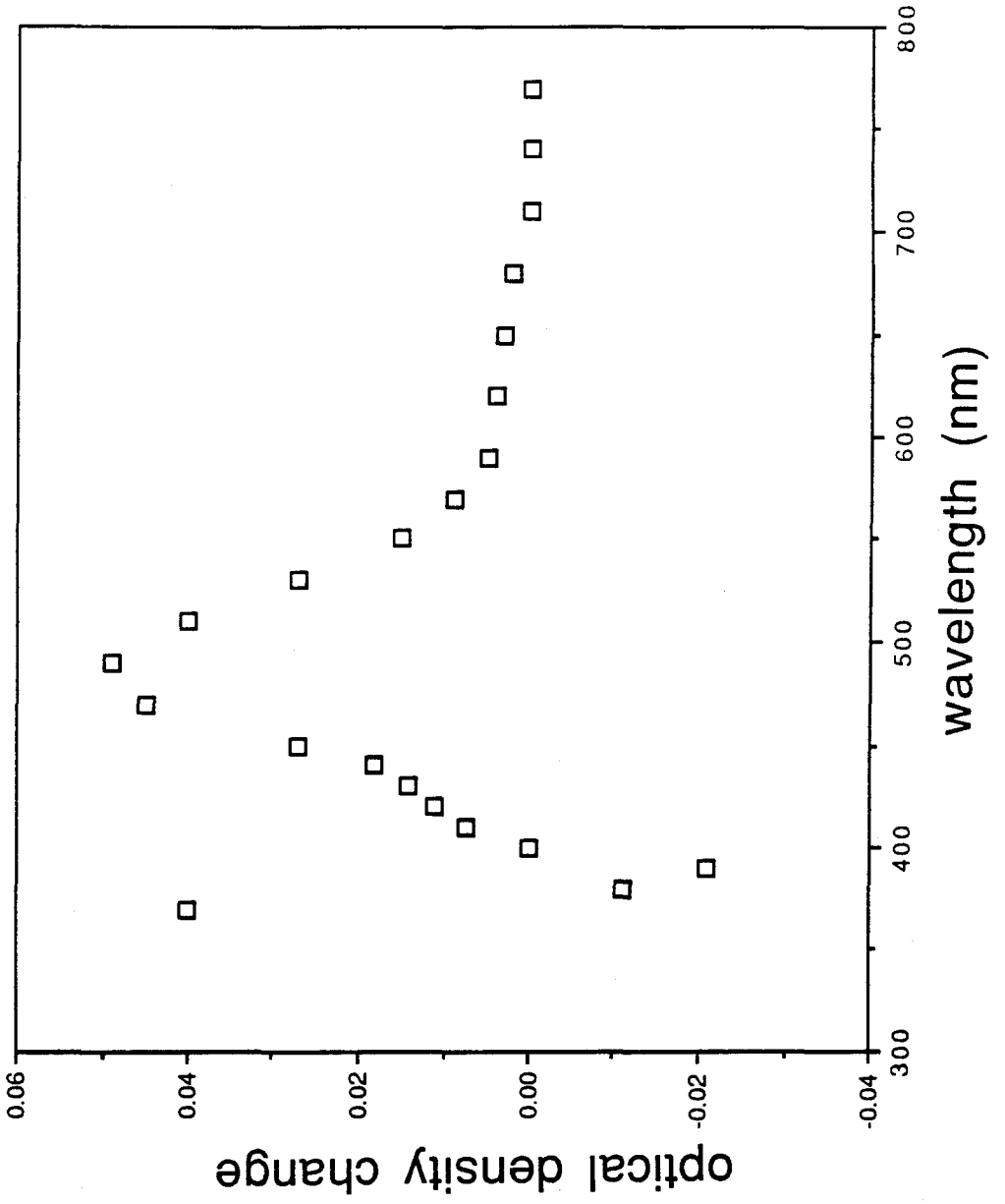
optical density change
0.06
0.04
0.02
0.00
-0.02
-0.04
300
400
500
600
700
800
wavelength (nm)

Figure 3.21. TA spectrum of *trans*-[$ReO_2(dmap)_4$][PF_6] in CH_3CN solution. Data were collected point-by-point at time zero with respect to the excitation pulse.

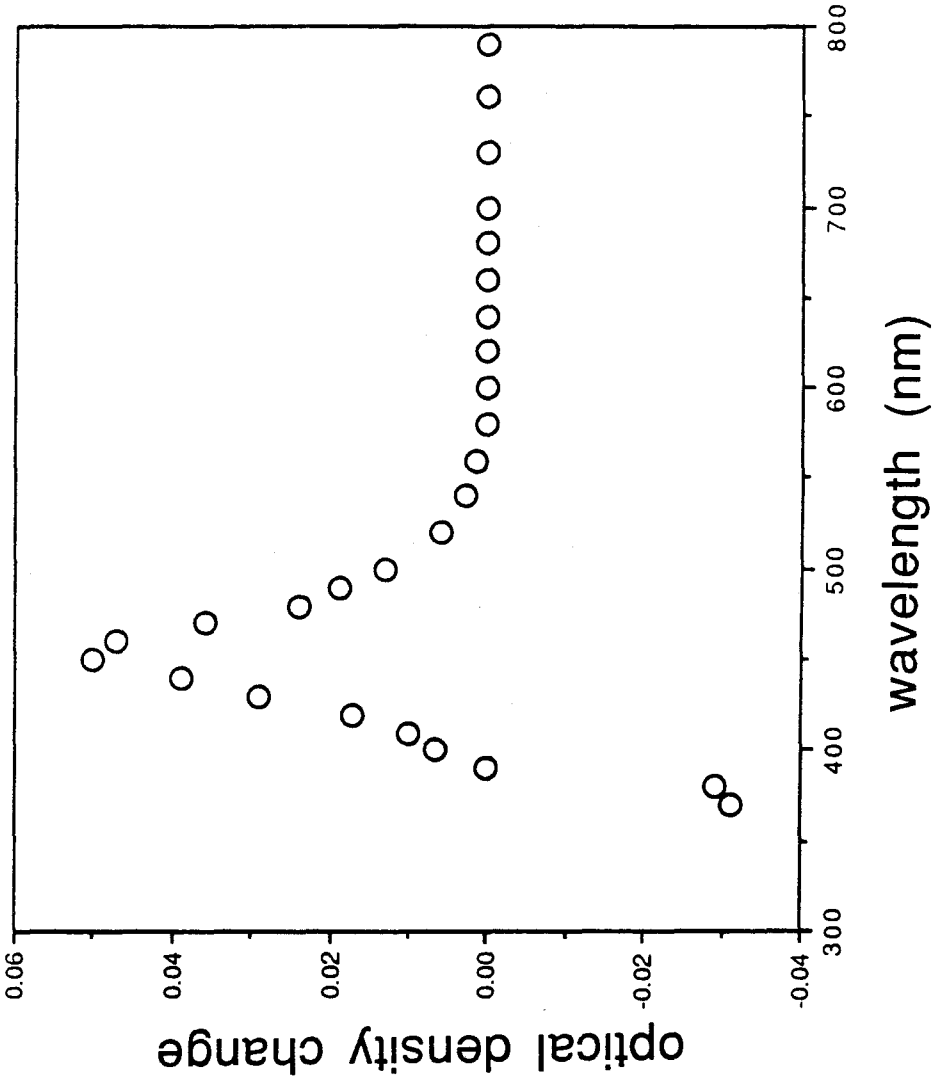
optical density change
0.06
0.04
0.02
0.00
-0.02
-0.04
300
400
500
600
700
800
wavelength (nm)

Figure 3.22. Plot of $E_{1/2}$ Re(VI)/Re(V) for *trans*-$[ReO_2(L)_4]PF_6$ pyridine complexes vs. ΔpK_a of free ligand L.

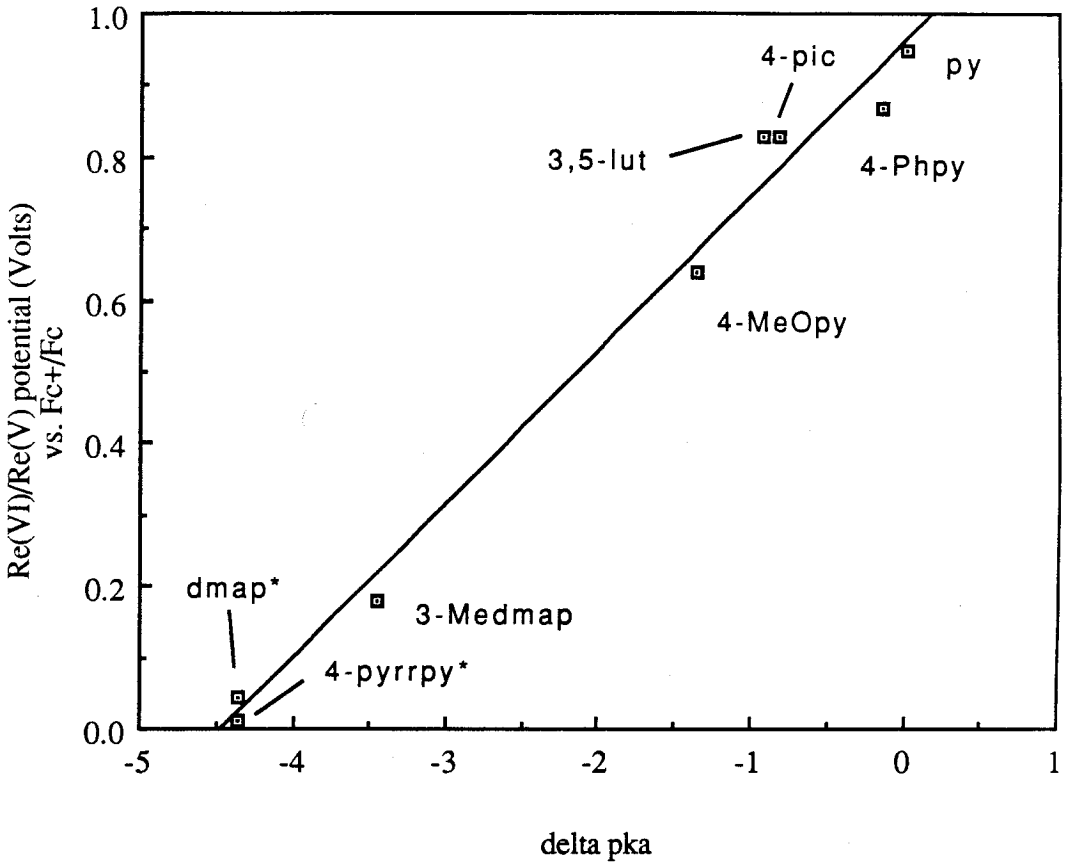
1.0
0.8
0.6
0.4
0.2
0.0
-5
-4
-3
-2
-1
0
1
Re(VI)/Re(V) potential (Volts) vs. Fc+/Fc
delta pka
4-pic
py
3,5-lut
4-Phpy
4-MeOpy
dmap*
3-Medmap
4-pyrrpy*

DISCUSSION

Electrochemistry. Cyclic voltammetry measurements reveal a most striking relationship between ligand donor strengths and the corresponding oxidation potential of the *trans*-$[ReO_2(L)_4][PF_6]$ pyridine complexes. A plot of $E_{1/2}$[Re(VI)/Re(V)] vs. ΔpK_a of the free pyridine (see Figure 3.22) yields a straight line with a slope of 0.21 and an intercept of 0.95 (R = 0.99). This linear dependence permits tuning of the Re(VI)/Re(V) couple by almost 1 V. The result is a family of Re(VI) complexes spanning a wide range of oxidizing power. The pyridine complex is about as oxidizing as Ce(IV). The 4-pyrrolidinopyridine complex is as mild as the ferricenium ion. The low oxidizing potential of this last complex suggested that isolation and full characterization of *trans*-$[ReO_2(4\text{-pyrrpy})_4][PF_6]_2$ might be possible. Bulk electrolysis experiments supported this hypothesis; *trans*-$[ReO_2(4\text{-pyrrpy})_4][PF_6]$ can be oxidized and re-reduced several times without suffering any decomposition. The complex *trans*-$[ReO_2(3\text{-Medmap})_4][PF_6]_2$ is also stable on the bulk electrolysis time scale. These compounds provide insight into the nature of *trans*-$[ReO_2(L)_4]^{2+}$ species and are discussed in further detail in Chapter 4.

The Re(VI)/Re(V) couple of *trans*-$[ReO_2(4\text{-MeOpy})_4][PF_6]$ is 600 mV more oxidizing than that of *trans*-$[ReO_2(4\text{-pyrrpy})_4][PF_6]$. Thus it is not surprising that *trans*-$[ReO_2(4\text{-MeOpy})_4][PF_6]$ is *not* stable to oxidation on the bulk electrolysis time scale. After one equivalent of charge was passed, current continued to flow at a measurable rate. When a reducing potential was applied, only 0.2 equivalents of charge was passed, but cyclic voltammetry indicated that 40% of the original material was present. A slow reaction converting the Re(VI) product back to the Re(V) starting material must occur concurrently with the oxidation process. The identity of the reductant is unknown. Evidence of the slow back reaction can be obtained from UV-vis spectra recorded at the end of the electrolysis. Apparently the additional products generated by the decomposition do not absorb in the UV-vis region since two well-defined isosbestic points were clearly evident

(Figure 3.23). Some possible reactions accounting for this behavior are presented in Chapter 4.

In order to determine whether the *trans*-$[ReO_2(L)_4]^{2+}$ complexes contained stabilized ligand radicals or oxidized metal centers, the redox properties of some substituted pyridines were examined.

Cyclic voltammograms of 4-MeOpy, 3-Medmap and dmap exhibit only irreversible oxidations that are well above the potentials measured (> 600 mV) for the corresponding *trans*-$[ReO_2(L)_4][PF_6]$ complexes. This is good evidence that the oxidations observed in each case are metal-centered. Further support for this hypothesis is evident from literature data.

The electrochemistry of pyridine itself has been studied. Turner and Elving[24] reported that pyridine is oxidized irreversibly at 1.49 V vs. SCE in 0.1 M $Li[ClO_4]$ solution. Bulk electrolysis at 1.69 V produces the 2-pyridyl pyridinium ion. The reversible oxidation of *trans*-$[ReO_2(py)_4][PF_6]$ at a potential more than 200 mV *lower* than for free pyridine argues strongly for a metal-centered oxidation. Studies completed by Pipes and Meyer[25] on the aqueous electrochemistry are also consistent with a 1-e^- metal-centered oxidation. The bulk electrolyses of *trans*-$[ReO_2(4\text{-pyrrpy})_4][PF_6]$ and *trans*-$[ReO_2(3Medmap)_4][PF_6]$ also suggest 1-e^- metal-centered processes.

Infrared Spectroscopy. Previous work has confirmed that the absorption at ~800 cm^{-1} is due to the asymmetric O=Re=O stretch.[26] Noteworthy is the fact that this vibration does not vary considerably with changes in pyridine ligand basicity, implying that changes in the σ-properties of equatorial ligands do not perturb Re-O bond strengths.

The asymmetric metal-oxo stretch of *trans*-$[ReO_2(py)_3(PPh_3)]I$ occurs at essentially the same energy as that of the tetrapyridine complex, indicating no significant change in metal-oxo bonding between the two complexes. For *trans*-$[ReO_2(diphos)_2][PF_6]$ and *trans*-$[ReO_2(dppen)_2][PF_6]$, the metal-oxo stretch occurs at a considerably lower energy, (780 and 790 cm^{-1}, respectively) which suggests weaker O=Re=O bonding. This result is rather

surprising. Phosphorous ligands are typically poorer σ-donor ligands than heterocycles, and the Re-O bond strength might be expected to increase as a form of electronic compensation. Perhaps there is some steric interaction between the PPh_3 phenyl groups and the oxo ligands that causes a net bond weakening.

Absorption Spectroscopy and Electronic Stucture. In order to interpret the UV-vis spectra of *trans*-$[ReO_2(L)_4]^+$ complexes, it is necessary to consider the generalized MO scheme[27,28] in Figure 3.24. The lowest energy band common to all *trans*-$[ReO_2(L)_4]^+$ complexes has been assigned to a singlet LF transition, $^1A_{1g}[(b_{2g})^2] \rightarrow {}^1E_g[(b_{2g})^1(e_g)^1]$. The single-crystal polarized absorption and emission studies on the compounds *trans*-$[ReO_2(py)_4][BPh_4]$, *trans*-$[ReO_2(en)_2]Cl$, and *trans*-$K_3[ReO_2(CN)_4]$ strongly support this assignment.[28] The positions and extinctions of the $^1A_{1g} \rightarrow {}^1E_g$ bands for several previously studied[23,26,28-31] *trans*-$[ReO_2(L)_4]^+$ complexes are summarized in Table 3.6. The low extinction coefficients arise because these transitions are Laporte-forbidden and must acquire intensity by vibronic coupling. In the pyridine complex, the absorption is appreciably stronger due to intensity stealing from an adjacent charge-transfer transition. The corresponding triplet absorptions are very weak and acquire intensity through spin-orbit coupling mechanisms.[28]

Table 3.6. Band positions for the $^1A_{1g}[(b_{2g})^2] \rightarrow {}^1E_g[(b_{2g})^1(e_g)^1]$ transition for several *trans*-$[ReO_2(L)_4]^+$ complexes in aqueous solution.

compound	band position, nm (ε)
trans-$[ReO_2(py)_4]Cl$[a]	445 (1240)
trans-$[ReO_2(en)_2]Cl$[b]	439 (27.5), 550sh (6)[d]
trans-$[ReO_2(CH_3NH_2)_4]Cl$[a]	445, 550sh[d]
trans-$K_3[ReO_2(CN)_4]$[c]	420 (30), 505(4)[d]

[a]ref 29 [b]ref 31 [c]ref 30 [d]corresponding triplet absorption

Figure 3.23. Time-lapse UV-vis absorption spectrum of the decomposition of *trans*-$[ReO_2(4\text{-}MeOpy)_4]^{2+}$ back to *trans*-$[ReO_2(4\text{-}MeOpy)_4]^{+}$, 0.1 M TBAH CH_3CN solution. Scan intervals were 2, 2, 2, 13, and 22 min respectively. The last scan represents the absorption spectrum of *trans*-$[ReO_2(4\text{-}MeOpy)_4]^{+}$.

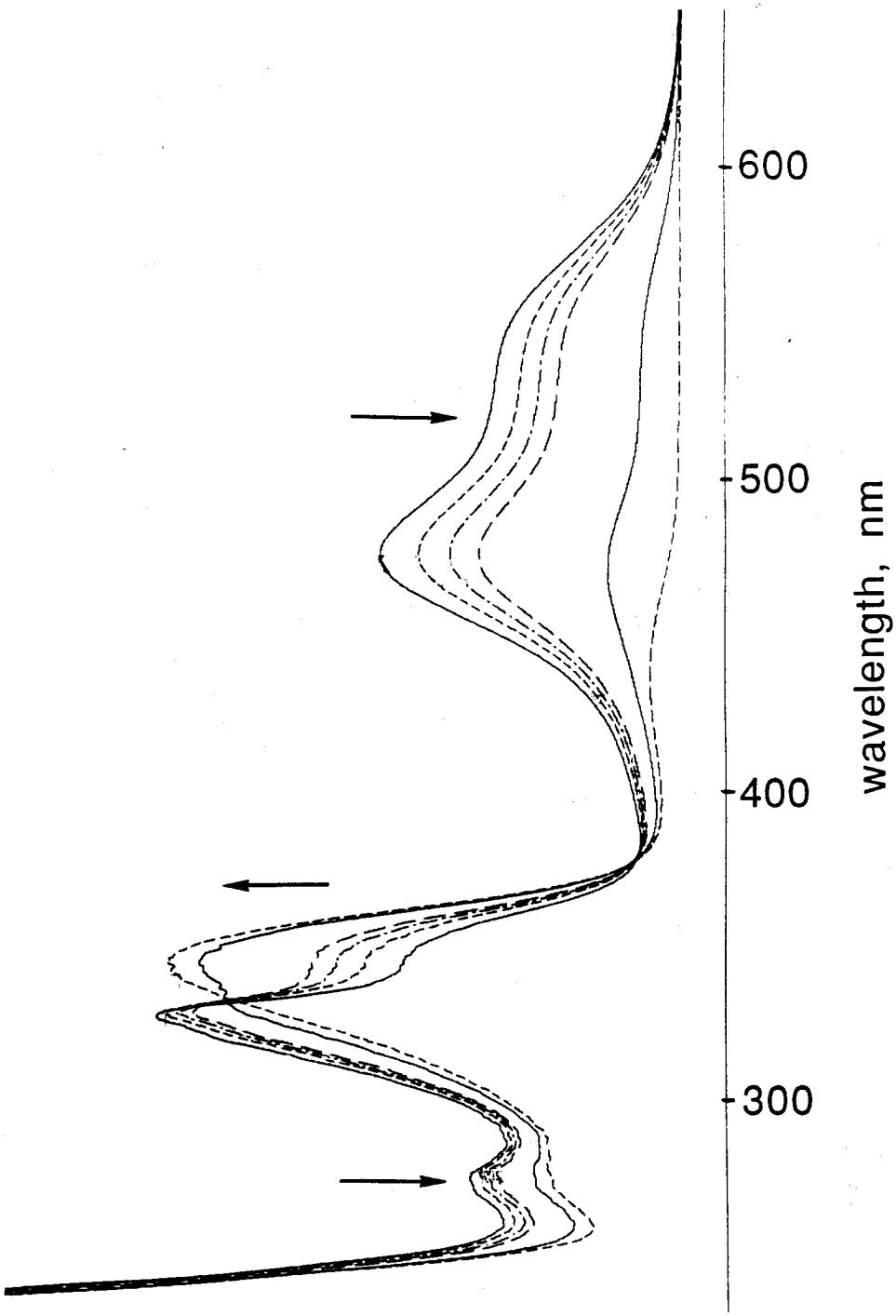
600
500
400
300
wavelength, nm

Figure 3.24. MO diagram for *trans*-$[ReO_2(L)_4]^+$ complexes. The absolute positions of the energy levels are *not* shown. The a_{2g} and b_{2g} pyridine π (π^*) levels have been omitted for clarity.

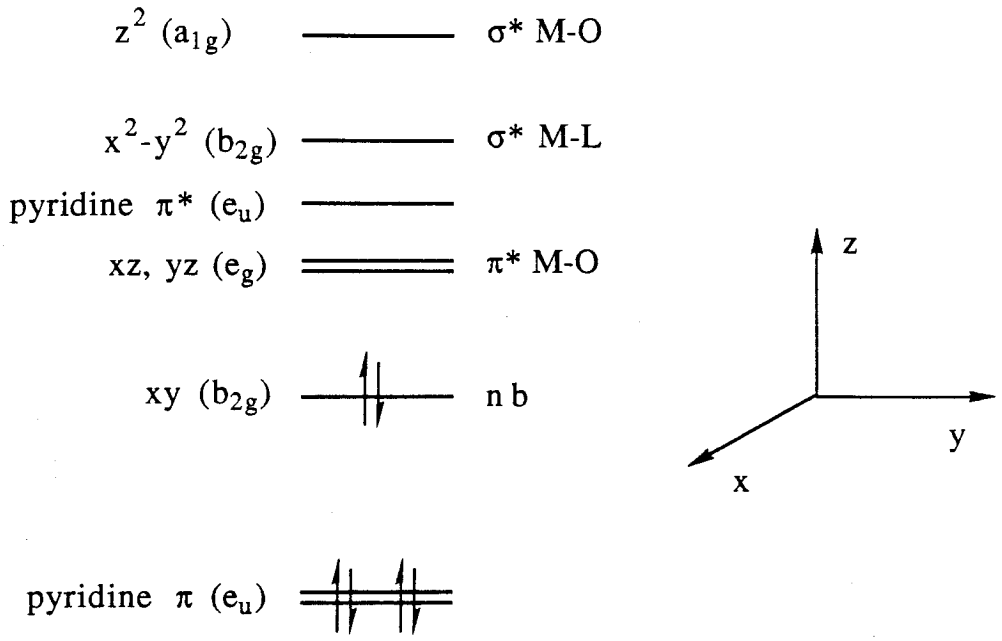
z^2 (a_{1g})
σ* M-O
x^2-y^2 (b_{2g})
σ* M-L
pyridine π* (e_u)
xz, yz (e_g)
π* M-O
xy (b_{2g})
n b
pyridine π (e_u)
z
y
x

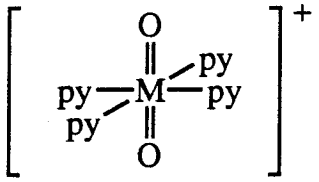
O
py
py
M
py
py
O
+

The energy of the $^1A_{1g}[(b_{2g})^2] \rightarrow {}^1E_g[(b_{2g})^1(e_g)^1]$ transition for each member of the tetrapyridine family is plotted against ΔpKa of the free pyridine ligand[5] in Figure 3.25. Note that there is a linear relationship between the ΔpKa of the pyridine ligand and the band energy. The linear least-squares fit gives $E_{LF} = (23{,}960 + 555\ \Delta pKa)\ cm^{-1}$ (R = 0.96). This demonstrates that the rhenium center is directly influenced by the σ-donor strength of the pyridine ligand. The d_{xy} orbital is raised in energy as the pyridine ligand basicity increases. The absolute energy of the e_g (d_{xz}, d_{yz}) level is primarily determined by the amount of mixing between the rhenium d_{xz}, d_{yz} and the 2 p_x,p_y orbitals of the oxo ligand, and, therefore, this level does not vary appreciably with changes in the σ-properties of the equatorial ligands. As a result, the $d_{xy}/d_{xz},d_{yz}$ energy gap is reduced, and the LF transition moves to the red as the pyridine ligand becomes more basic.

All *trans*-$[ReO_2(L)_4]^+$ pyridine complexes exhibit an intense band ($\varepsilon > 19{,}000\ M^{-1}\ cm^{-1}$) to slightly higher energy of the LF transition described above. This absorption has been assigned to either LMCT[32] (oxo to rhenium) or MLCT[23] (d_{xy} to pyridine π*). The rationale for the former has been that the high oxidation state of rhenium should promote reductive charge transfer. Others have argued MLCT on the basis of the blue shift in band energy that occurs upon oxo protonation.[25] Several arguments exist in favor of the MLCT assignment. These will be considered sequentially below.

Strong evidence comes from the observations of pyridine substituent effects on band energies and intensities. It is instructive to compare the UV-vis spectra of *trans*-$[ReO_2(py)_4]^+$ and *trans*-$[ReO_2(4\text{-}Phpy)_4]^+$. In the 4-phenylpyridine complex, the CT band is more intense ($\varepsilon \sim 37{,}000$ vs. $\varepsilon \sim 22{,}000\ M^{-1}\ cm^{-1}$) and occurs at a lower energy than for the pyridine complex (λ_{max} = 383 nm vs. 352 nm). Analogous behavior has been observed in the pair of complexes $[Ru(NH_3)_5(py)]^{2+}$ and $[Ru(NH_3)_5(4\text{-}Phpy)]^{2+}$, where the intense absorption in the visible region has also been assigned to MLCT (Ru $t_{2g} \rightarrow$ pyridine π*).[33] The band positions in the Ru complexes are seen at 408 and 446 nm, respectively. The differences in CT energies between the pyridine and 4-phenylpyridine

Figure 3.25. Plot of $^1A_{1g}[(b_{2g})^2] \rightarrow {}^1E_g[(b_{2g})^1(e_g)^1]$ and MLCT transitions for *trans*-$[ReO_2(L)_4]^+$ pyridine complexes as a function of ΔpK_a of free L. Lines drawn are the results of linear least-squares fitting. Note the lack of correlation for MLCT data: $E_{MLCT} = (27{,}840 - 27.6\ \Delta pK_a)\ cm^{-1}$ (R = 0.06).

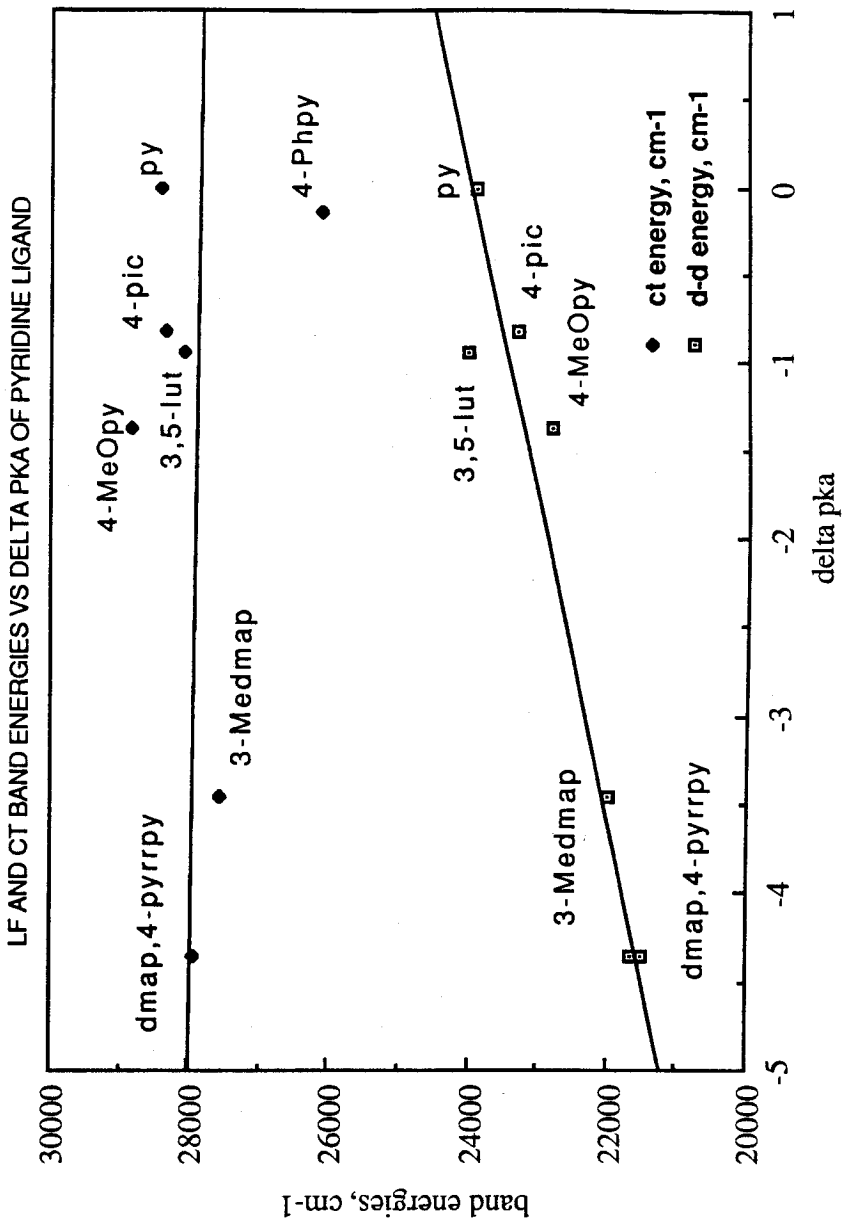
LF AND CT BAND ENERGIES VS DELTA PKA OF PYRIDINE LIGAND
band energies, cm-1
30000
28000
26000
24000
22000
20000
-5
-4
-3
-2
-1
0
1
delta pka
dmap,4-pyrrpy
3-Medmap
4-MeOpy
3,5-lut
4-pic
py
4-Phpy
ct energy, cm-1
d-d energy, cm-1

complexes are almost identical for both the Ru and Re systems: 2100 cm^{-1} and 2300 cm^{-1}, respectively. The red shift can be attributed to the lowering of the pyridine π^* orbital energy due to phenyl ring conjugation, which also increases the intensity. Both of these effects, the lowering in energy and increase in intensity of MLCT bands, have been observed[34] in *o*-phenanthroline complexes of Cu(I). In this case, it has been argued that the higher intensity results from an increase in transition-moment dipole length.

The results of the electrochemical measurements also support a MLCT assignment. All pyridine complexes exhibit a 1-e^- oxidation between 0.4 and 1.3 V (SSCE) indicating the electron richness of the Re center. No reversible reductive waves are apparent in any of the complexes. Empirically, it has been found that the direction of charge transfer in coordination complexes is consistent with the observed redox chemistry of the metal center: Where CT transitions occur, complexes containing metal centers that are easily reduced exhibit LMCT bands, while easily oxidizable centers participate in MLCT behavior. The redox behavior of Re in *trans*-$[ReO_2(L)_4]^+$ complexes is consistent with an MLCT assignment.

In order to account for the intensity of this transition, the metal and ligand orbitals involved must be examined in more detail. It is inaccurate to view the MLCT transition as occurring from d_{xy} to a single pyridine π^* level, since there are four pyridine ligands present in the complex. The energetically proximal orbitals of the pyridine ligand[35] are shown in Figure 3.26. From this diagram, it is clear that the π^* orbital relevant to the problem is $3B_1$, as it has orbital density on the nitrogen atom. The $4B_1$ (π^*) orbital also satisfies this criterion, but it is too high in energy to be important. The appropriate linear combinations for equatorial π^* orbitals in D_{4h} symmetry have been previously derived.[36,37] The four pyridine π^* orbitals transform as a_{2g}, b_{2g}, and e_u, as shown schematically in Figure 3.27. Thus, instead of one MLCT transition in *trans*-$[ReO_2(L)_4]^+$, there are actually three: $A_{2g}[(b_{2g})^2] \rightarrow B_{1g}\ [(b_{2g})^1(a_{2g})^1]$, $A_{2g}[(b_{2g})^2] \rightarrow A_{1g}\ [(b_{2g})^1(b_{2g})^1]$ and $A_{2g}[(b_{2g})^2] \rightarrow E_u\ [(b_{2g})^1(e_u)^1]$. The first two transitions are Laporte-

forbidden (g → g) and would be expected to be weak in intensity; the last should be fully allowed (g → u) in D_{4h}. A favorable spatial overlap also accounts for the large intensity of the $A_{2g}[(b_{2g})^2] \rightarrow E_u\ [(b_{2g})^1(e_u)^1]$ transition.

Finally, it should be noted that there are now several examples of MLCT transitions occurring from electron-rich metal complexes to vacant π* levels of pyridine ligands. A metal → pyridine π* transition has been identified in the following complexes:[33,38-46] $[Ir(NH_3)_5(py)]^{3+}$, $[Ru(NH_3)_5(py)]^{2+}$, $[Os(NH_3)_5(py)]^{2+}$, $[Fe(CN)_5(py)]^{3-}$, $[Ru(CN)_5(py)]^{3-}$ and $W(CO)_5(py)$.

There are two observations that can be used to rule out a LMCT assignment. If the CT transition was associated with the oxo functionality, then this band should occur in the same region for all *trans*-$[ReO_2(L)_4]^+$ complexes exhibiting similar reduction potentials. An intense band in the vicinity of 350 nm is conspicuously absent from the UV-vis spectra of the complexes *trans*-$[ReO_2(en)_2]Cl$ and *trans*-$K_3[ReO_2(CN)_4]$ (see Table 3.7), which are reduced at potentials similar to that of *trans*-$[ReO_2(py)_4]^+$.[25]

Table 3.7. UV-visible data for *trans*-$[ReO_2(en)_2]Cl$, and *trans*-$K_3[ReO_2(CN)_4]$ in aqueous solution. Band positions are given in nm and their associated extinctions are enclosed in parentheses.

complex	band positions	ref
trans-$[ReO_2(en)_2]Cl$	205(18,500); 255(1070); 276sh(630); 439(27.5); 550sh(6.0)	31
trans-$K_3[ReO_2(CN)_4]$	223(12,300); 272(1300); 298(380); 420(30); 505(4)	30

Figure 3.26. Energetically proximal π- and π*-orbitals of the pyridine ligand (reproduced from ref 35).

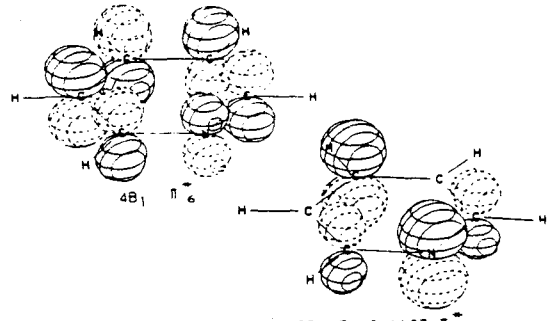
4B1 π6
3B1 E= 0.1107 π5

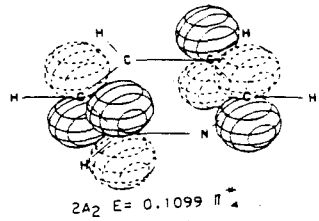
2A2 E= 0.1099 π4

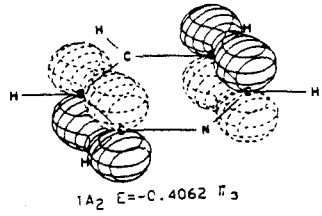
1A2 E=-0.4062 π3

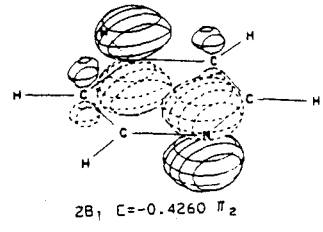
2B1 E=-0.4260 π2

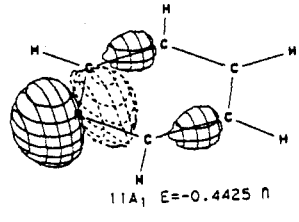
11A1 E=-0.4425 n

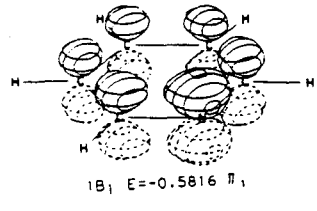
1B1 E=-0.5816 π1

Figure 3.27. Linear combinations of the pyridine π^*-orbitals relevant to the $d_{xy} \rightarrow \pi^*$ MLCT transition in *trans*-$[ReO_2(L)_4][PF_6]$ compounds.

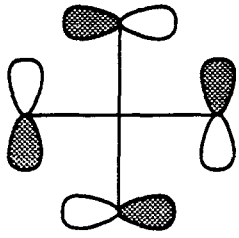

a_{2g}

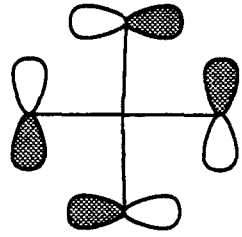

b_{2g}

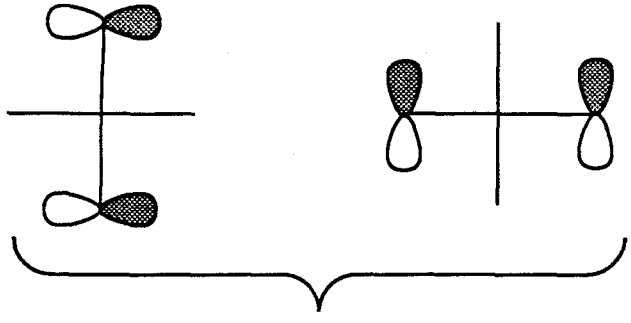

e_u

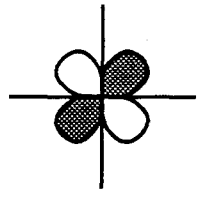

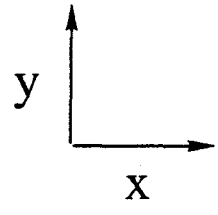

Re d_{xy}

It is also significant that reduction in non-aqueous solution is only observed at very negative potentials (~-1.8 V vs. SSCE). This makes reductive charge-transfer unlikely in these systems.

Technetium analogues of some of the *trans*-$[ReO_2(L)_4]^+$ pyridine complexes have been prepared and their UV-vis spectra reported.[47-49] The strong band in the vicinity of 310 nm has been assigned to oxo-to-metal charge transfer based upon the observation that the band energies were insensitive to changes in ancillary ligands. This same observation in the Re complexes can be explained by considering the two phenomena that occur on proceeding from pyridine to more electron-rich pyridines. As the donor strength of the ligand increases, the π^* levels in the pyridine ligands also rise in energy.[45] The Re d_{xy} orbital also rises in energy due the increase in electron density at the Re center from stronger pyridine σ-donation. These two effects operate in the same direction so that the net change in $d_{xy}/d_{yz},d_{xz}$ gap is near zero. As a result, the MLCT transitions vary little in energy from complex to complex.

Recall that the biggest shift in MLCT energy was between pyridine and 4-phenylpyridine complexes. The pKa's of the free ligands, the emission maxima of the corresponding *trans*-dioxorhenium complexes, and the potentials of the Re(VI)/Re(V) couples indicate that the σ properties of the two ligands are essentially identical. If the transition was LMCT, a dramatic change in transition energy would not be expected. The large red shift that *does* occur (34 nm) allows us to dismiss forever the possibility of low energy oxo-to-metal charge transfer in these systems.

In four of the *trans*-$[ReO_2(L)_4]^+$ pyridine complexes (L = py, 4-pic, 3,5-lut , and 4-MeO), there is a medium intensity band to slightly higher energy (~280 nm) of the MLCT transition. This band lies to lower energy than anything observed in the spectra of the associated free ligands and must therefore involve the rhenium center. Some information on the nature of this band can be obtained from the UV-vis spectrum of a frozen 5:1

methanol/ethanol glass solution of *trans*-$[ReO_2(py)_4]I$ (Figure 3.28). Note that like the low energy LF transition, the 280 nm band exhibits vibrational progressions similar in energy to the symmetric O=Re=O stretch of the $^3E_g[(b_{2g})^1(e_g)^1]$ excited state (~800 cm^{-1}). This indicates that the excited state created by the transition induces a large displacement along the O=Re=O coordinate. The LF transition $^1A_{1g}[(b_{2g})^2] \rightarrow {}^1B_{2g}[(b_{2g})^1(a_{1g})^1]$ ($d_{xy} \rightarrow d_z^2$), would be expected to induce a large distortion in the O=Re=O unit because of population of a formally Re-O σ-antibonding level (see Figure 3.24). A similar band is seen in the complexes *trans*-$K_3[ReO_2(CN)_4]$ and *trans*-$[ReO_2(en)_2]Cl$ at about 300 and 275 nm respectively (Table 3.7). The associated progressions are 770 cm^{-1} and 800 cm^{-1}. These bands have also been tentatively assigned to the $^1A_{1g}[(b_{2g})^2] \rightarrow {}^1B_{2g}[(b_{2g})^1(a_{1g})^1]$ ($d_{xy} \rightarrow d_z^2$) transition.

It should be noted, however, that this assignment is in contrast to that predicted by Szterenberg *et al.*[30] Using the SCCC MO method, these workers have calculated the orbital energies of *trans*-$[ReO_2(CN)_4]^{3-}$ which indicate that the $d_{xy} \rightarrow d_z^2$ transition would be located in the vacuum UV at about 196 nm. The 300 nm band of *trans*-$[ReO_2(CN)_4]^{3-}$ is assigned to a lower energy LF transition, $^1A_{1g}[(b_{2g})^2] \rightarrow {}^1A_{2g}[(b_{2g})^1(b_{1g})^1]$ ($d_{xy} \rightarrow d_{x^2-y^2}$). According to LF theory,[50,51] the difference in the one-electron orbital energies of the b_{1g} and b_{2g} levels is 10 Dq (Δ). Since both pyridine and ethylenediamine have approximately the same ligand field strengths,[52] the $d_{xy} \rightarrow d_{x^2-y^2}$ transition would be expected to occur at similar energies for *trans*-$[ReO_2(en)_2]^+$ and *trans*-$[ReO_2(py)_4]^+$. Note that the band in question occurs at ~280 nm in *both* complexes. Furthermore, in the ethylenediamine and cyanide complexes, bands to slightly higher energy (255 and 272 nm, respectively) could be due to the $d_{xy} \rightarrow d_z^2$ transition (see Figure 3.29). The problem with assigning the 280 nm band to the $d_{xy} \rightarrow d_{x^2-y^2}$ transition is that it is difficult to rationalize why the transition would lead to distortion in the Re-oxo bonds. Population of the $d_{x^2-y^2}$ orbital should result in a significant lengthening in Re-py bonds, because it is formally Re-py σ-antibonding. Perhaps this does occur and as a result, the oxo-ligands move in closer

to compensate for the loss of electron density. Thus, oxo distortion could result indirectly from changes in electronic density at the Re center. That the extinctions of these LF bands are higher than expected ($\varepsilon \sim 500$ - 5,000) could be the result of intensity stealing from higher energy CT transitions. Until further studies are completed, however, the exact location of these higher lying ligand field transitions will remain in question. One way to attempt to locate the $d_{xy} \rightarrow d_{x^2-y^2}$ transition in *trans*-$[ReO_2(py)_4]^+$ might be to photolyze the complex at different wavelengths and measure the amount of ligand exchange between pyridine and d_5-pyridine. Population of the $d_{x^2-y^2}$ would be expected to enhance the rate of this exchange relative to the corresponding dark reaction.

The remaining absorption band common to all of the pyridine complexes is found in the UV between 245 - 280 nm and varies with the identity of the pyridine ligand. Based upon comparisons with the free ligand spectra, this peak is assigned to an intraligand π-π^* transition. Similar assignments have been made for other pyridine metal complexes such as $[Ru(NH_3)_5(py)]^{2+}$. The π-π^* transition energy of pyridine has been found[45] to be invariant among pyH^+, $[(NH_3)_5Ru(py)]^{2+}$, $[(NH_3)_5Ru(py)]^{3+}$, $[(NH_3)_5Os(py)]^{2+}$, $[(CN)_5Fe(py)]^{3-}$, and $[(CN)_5Fe(py)]^{2-}$.

All of the arguments put forth above were used to arrive at the assignments summarized in Table 3.8.

Table 3.8. UV-vis data and assignments for *trans*-$[ReO_2(L)_4]PF_6$ pyridine complexes in CH_3CN solution. Band positions are given in nm with their associated extinctions enclosed in parentheses.

L=	$\pi \rightarrow \pi^*$ pyridine	LF, $d_{xy} \rightarrow$ $d_{x^2-y^2}$ (d_{z^2})	MLCT, $d_{xy} \rightarrow$ π^* pyridine	LF, $d_{xy} \rightarrow$ d_{xz},d_{yz}
py	248 (17,000)	279 (4,200)	352 (22,000)	418 (2,000)
4-Ph	266 (56,000)	obscured	383 (37,000)	obscured
4-pic	247 (16,000)	277 (4,400)	353 (32,000)	429 (2,000)
3,5-lut	258 (24,000)	275 (5,700)	356 (29,000)	416 (2,100)
4-MeOpy	227 (33,000)	281 (6,800)	347 (27,000)	438 (1,500)
3-Medmap	280 (38,000)	obscured	363 (42,000)	455 (2,600)
dmap	272 (47,000)	obscured	358 (37,000)	464 (2,300)
4-pyrrpy	273 (52,000)	obscured	353 (42,000)	465 (2,600)

The final point to be addressed in the electronic structure of the *trans*-$[ReO_2(L)_4]^+$ complexes is the lack of importance of π-backbonding in the Re-py bonding. There are several examples of this type of interaction in other metal systems.[45,53,54] The common features to these examples are that they contain very electron-rich metal centers (formal oxidation states of 2^+ or lower) and/or pyridine ligands with very electron-withdrawing substituents. Neither one of these conditions exist for the Re complexes. While the Re center is considerably electron-rich, there are only two d-electrons, and any back-bonding interaction would be attenuated by distribution among four pyridine ligands. Furthermore, electron-rich pyridines are poor π-acceptors, as indicated by the high MLCT transition energy known for $[Fe(CN)_5(4\text{-}NH_2py)]^{2-}$ (320 nm as compared to 362 nm for the pyridine complex).[44]

Figure 3.28. UV-vis spectrum of *trans*-[$ReO_2(py)_4$]I in 5:1 CH_3OH/CH_3CH_2OH glass at 77 K. Peak positions in nm: (452, 438, 424, 410, 398); 352; (288, 282, 276). The two peaks at high energy are associated with the pyridine π-π^* transition.

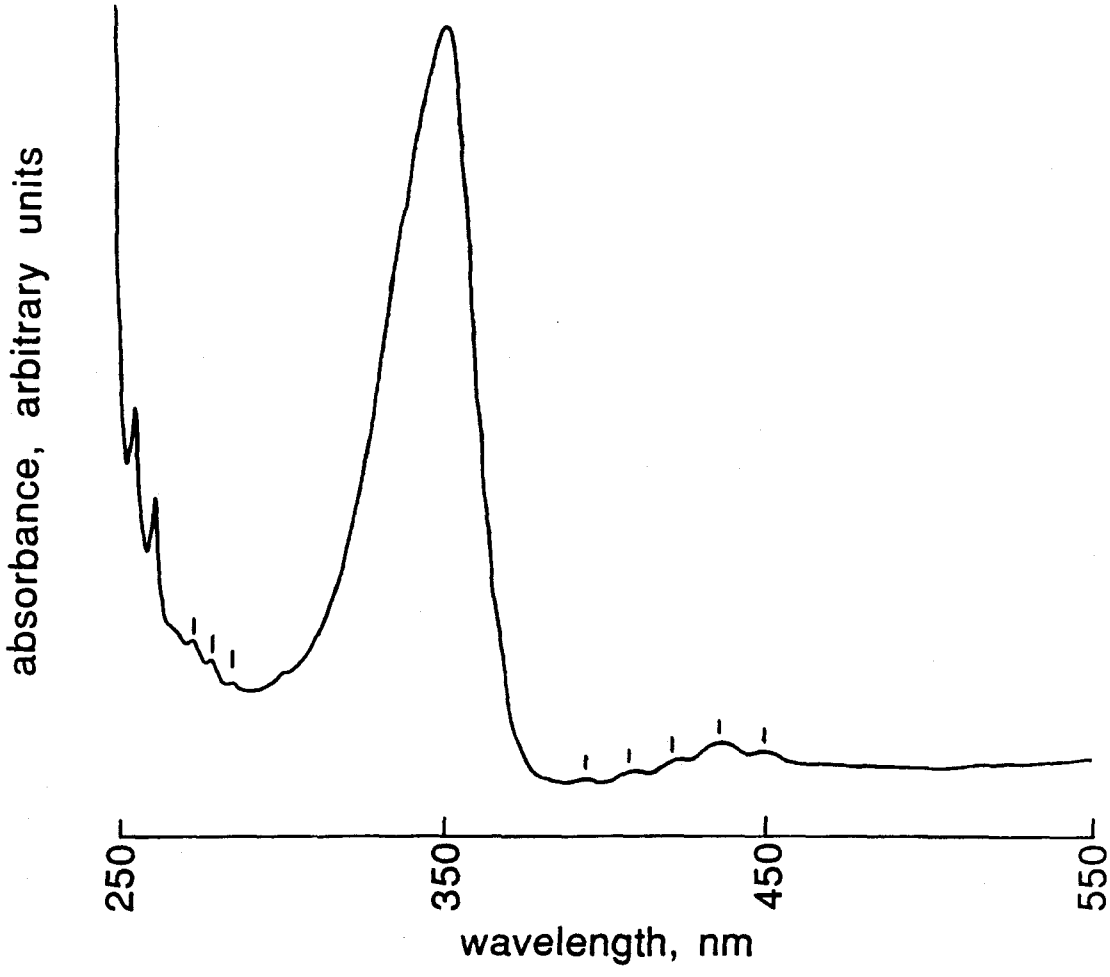
absorbance, arbitrary units
250
350
450
550
wavelength, nm

Figure 3.29. Ultraviolet spectra of *trans*-$[ReO_2(en)_2]PF_6$ (top) and *trans*-$K_3[ReO_2(CN)_4]$ (bottom) in dilute aqueous solution.

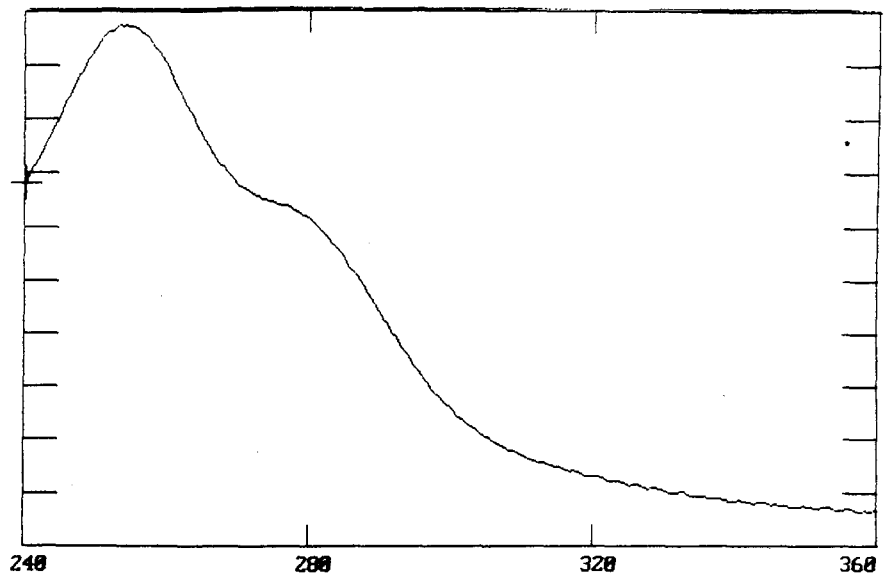
240
280
320
360

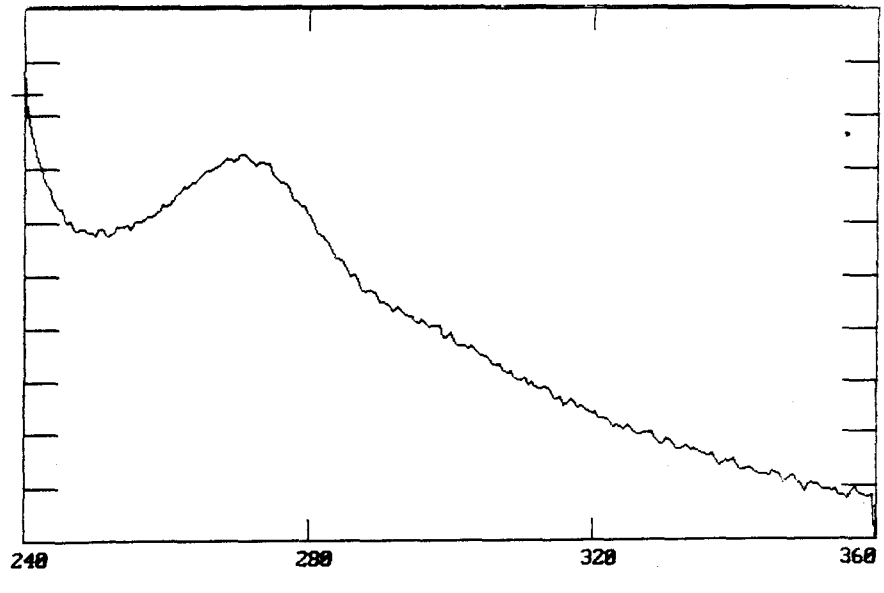
240
280
320
360
WAVELENGTH

Any substantial π-interaction would be expected to perturb the π* levels of the pyridine ligands as shown by the MO diagram in Figure 3.30. This in turn would result in a blue shift in the intra-ligand π-π* transition. In fact, just the opposite effect is observed; complexes containing the electron-rich pyridines exhibit intraligand transitions that are red-shifted (see Table 3.9). It is therefore unlikely that the Re-py bonds in *trans*-$[ReO_2(L)_4]^+$ complexes contain any significant π-component. The observed red shifts of ligand π-π* transitions could be due to the repulsion of the filled π levels of pyridine by the pair of electrons in d_{xy}, resulting in a reduction of the π-π* energy gap.

Table 3.9. UV data for pyridine and some pyridine derivatives (CH_3CN solution). The shifts of the π-π* transition energy upon metal coordination are given in the last column.

ligand	λ_{max} in nm	λ_{max} free – λ_{max} complexed (nm)
py	247sh, 251, 256, 262	–5
4-Phpy	250	16
4-pic	250sh, 255, 262sh	-8
3,5-lut	264sh, 268, 274sh	-10
4-MeOpy	216, 240sh	18
3-Medmap	203, 216sh, 262	18
dmap	256	16
4-pyrrpy	258	15

The UV-vis spectrum of *trans*-$[ReO_2(py)_3(PPh_3)]^+$ is qualitatively similar to that of *trans*-$[ReO_2(py)_4]^+$. The $^1A_{1g}[(b_{2g})^2] \rightarrow {}^1E_g[(b_{2g})^1(e_g)^1]$ transition cannot be resolved from the shoulder of the $d_{xy} \rightarrow$ pyridine (π*) transition and therefore must be located somewhere < 400 nm. The MLCT transition occurs at 336 nm, which is ~1350 cm^{-1}

higher in energy than the corresponding transition in the tetrapyridine complex. The blue shifts observed for both the MLCT and LF transitions reflect the lower energy of the d_{xy} orbital which results from a decrease in electron density at Re brought about by the replacement of one pyridine ligand by PPh_3. The remaining band present at 244 nm is assigned to the π-π^* transition of the pyridine ligand.

The absorption spectra of *trans*-$[ReO_2(diphos)_2][PF_6]$ and *trans*-$[ReO_2(dppen)_2][PF_6]$ are not informative. The diphos complex consists of a shoulder at 220 nm and a strong absorption at 257 nm that extends out into the visible region. In the spectrum of the dppen complex no band maxima are evident but two shoulders in the ultraviolet region (228, 267 nm) can be resolved. These bands are likely due to intraligand π-π^* transitions of the phenyl groups and $d_{xy} \rightarrow$ phosphine (π^*) transitions.[55-60]

Excited-State Properties. The lowest-energy emitting state of *trans*-$[ReO_2(L)_4]^+$ has been unambiguously assigned as ^3E_g $[(b_2g)^1(e_g)^1]$ by Winkler and Gray.[28,61] The emission spectra of this family of complexes are often highly structured in Re-oxo vibrational modes because of the large distortion that occurs along this coordinate upon relaxing to the more bonding ground state ($^1A_{1g}$ $[(b_{2g})^2]$).

The excited-state lifetime of *trans*-$[ReO_2(py)_4]^+$ is markedly affected by the deuteration of the pyridine rings, increasing from 14 to 64 μs in acetonitrile solution (NOTE: These data were erroneously reported in a previous publication).[28] This result demonstrates that the excited-state of *trans*-$[ReO_2(py)_4]^+$ is weakly coupled to the ground state. Under these conditions, the excited-state decay rate is sensitive to the highest-energy vibrational modes present in the molecule.[62] The non-radiative decay rate constant, k_{nr} , exhibits an exponential dependence on the ratio of the transition energy to the energy of the highest frequency vibrational mode. As a result, it can be shown that $\ln(k_{nr}) \propto E_{em}$. This relationship is commonly referred to as the energy-gap law.[63,64]

Figure 3.30. MO diagram describing the interaction of the rhenium d_{xy} orbital with the π^* levels on the pyridine ligand (after ref 45).

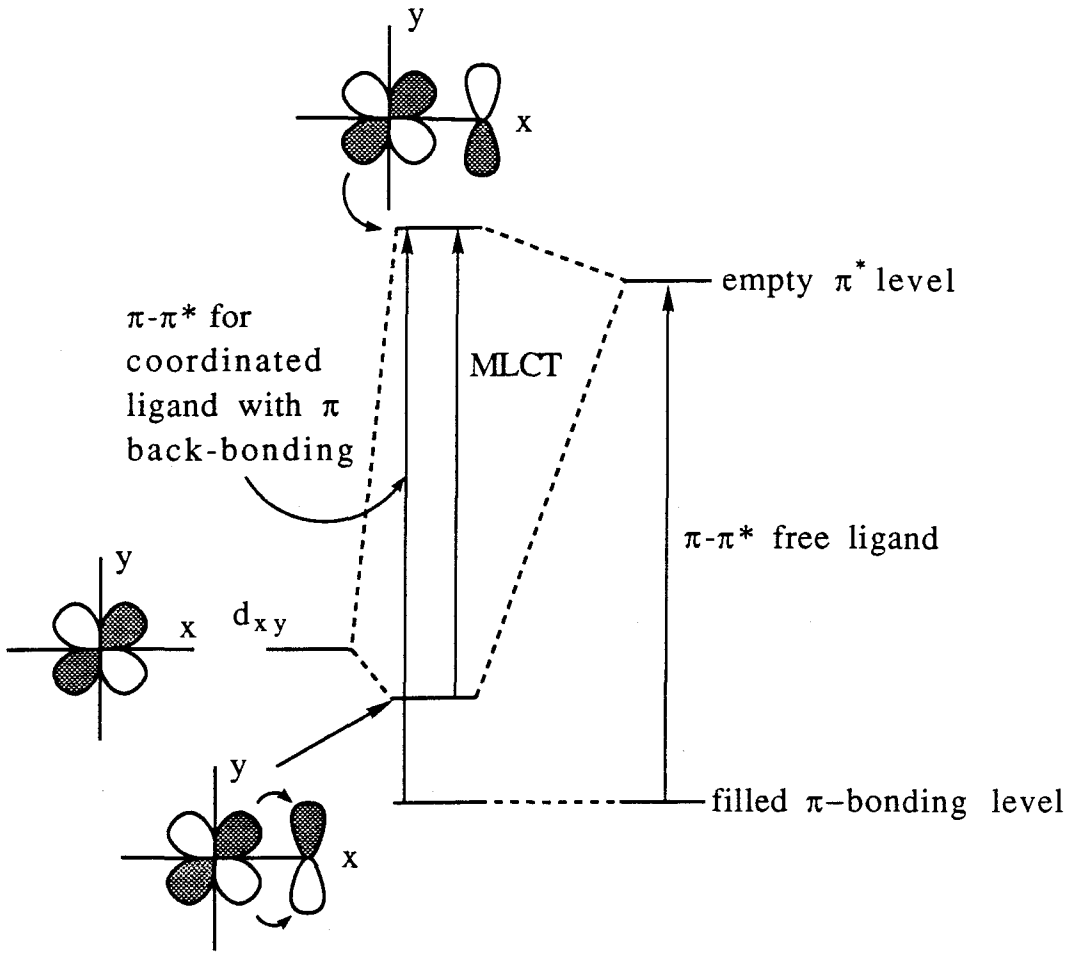

Re(V) center

free pyridine

In order to determine k_{nr}, it is necessary to know both the lifetime and emission quantum yield of the lowest energy excited state. If the emitting state is formed with unit efficiency, Equations 2 and 3 can be used to determine k_r and k_{nr}:[63]

$$\tau_o = (k_r + k_{nr})^{-1} \quad (2)$$

$$\Phi_{em} = k_r \tau_o \quad (3)$$

Unfortunately, the emission quantum yields for all of the *trans*-$[ReO_2(L)_4][PF_6]$ pyridine complexes are not known, so the energy gap law cannot be rigorously tested. For *trans*-$[ReO_2(py)_4][PF_6]$, k_{nr} and k_r are 69,000 and 2,100 s^{-1} (*vide infra*) indicating that the excited-state decay process is dominated by k_{nr}. Thus, $k_{nr} \sim 1/\tau_o$ and a plot of $\ln(1/\tau_o)$ for the pyridine complexes should exhibit a linear dependence on emission energy (see Figure 3.31). A linear least-squares analysis of the data yields a line with slope of 0.1537 and an intercept of 33,920 cm^{-1} (R = -0.97738). Because of the lack of well distributed data points, it can only be concluded that the observed trend is consisted with that expected if *trans*-$[ReO_2(L)_4][PF_6]$ pyridine complexes rigorously obey the energy-gap law. The important point is that as the pyridine basicity increases, the lifetime and energy of the LF excited-state diminishes.

The fluid solution emission spectrum of *trans*-$[ReO_2(py)_3(PPh_3)]^+$ is similar to that of the tetrapyridine complex with a maximum at slightly higher energy (15,150 vs. 14,920 cm^{-1}). The most striking feature is that unlike the tetrapyridine complex, the 77 K emission spectrum is highly structured in *both* metal-oxo and metal-pyridine vibrations. Resolution of this degree is only observed in *trans*-$[ReO_2(py)_4]^+$ at 5 K.[28] The reason for this difference is unknown. It is curious that the metal-oxo mode present in the low temperature spectrum is 100 cm^{-1} higher in energy than that of the tetrapyridine complex. Infrared measurements indicated that the asymmetric O=Re=O mode is almost identical in

Figure 3.31. Plot of $\ln(1/\tau_o)$ vs. E_{em} for luminescent *trans*-$[ReO_2(L)_4]^+$ pyridine complexes.

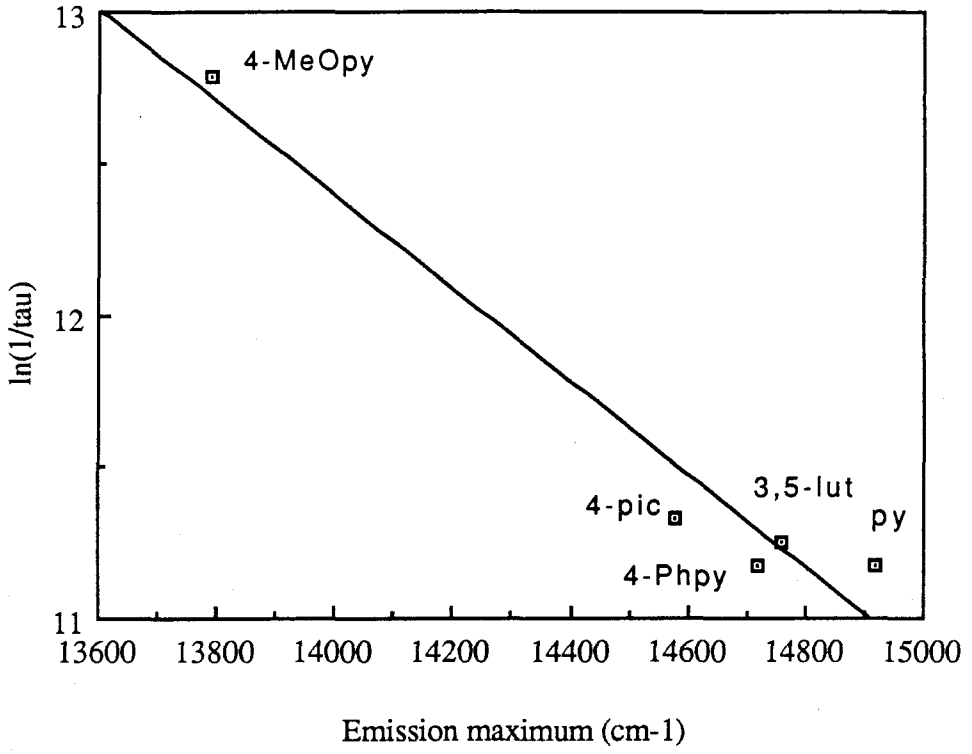
13
12
11
ln(1/tau)
4-MeOpy
4-pic
3,5-lut
py
4-Phpy
13600
13800
14000
14200
14400
14600
14800
15000
Emission maximum (cm-1)

energy for the two complexes; it is not clear why the symmetric mode should occur at a higher energy in *trans*-$[ReO_2(py)_3(PPh_3)]^+$.

Finally, it should be noted that the excited state lifetime of *trans*-$[ReO_2(py)_3(PPh_3)]^+$ is an order of magnitude shorter than that of *trans*-$[ReO_2(py)_4]^+$. The origin of this change can be determined by calculating the radiative and non-radiative rate constants using Equations (2) and (3). For *trans*-$[ReO_2(py)_4]^+$ (τ_o = 14 μs and Φ = 0.03), $k_{nr} = 6.9 \times 10^4$ s^{-1} and $k_r = 2.1 \times 10^3$ s^{-1}. For *trans*-$[ReO_2(py)_3(PPh_3)]^+$ (τ_o = 1.5 μs and Φ = 0.003), $k_{nr} = 6.6 \times 10^5$ s^{-1} and $k_r = 2 \times 10^3$ s^{-1}. Thus, the changes in excited state lifetime result from an dramatic increase in the rate of non-radiative processes. This is likely due to the increase in the number of accepting vibrational modes provided by the phosphine ligand.

The excited-state properties of *trans*-$[ReO_2(diphos)_2][PF_6]$ and *trans*-$[ReO_2(dppen)_2][PF_6]$ are disappointing. These complexes show emission in the solid state and in rigid media but not in fluid solution. Presumably, this behavior is due to several extremely efficient deactivation processes. The energy of the emission for the complexes (15,100 cm^{-1} and 16,170 cm^{-1}) is higher than that observed for the pyridine complexes, as expected from the replacement of pyridine ligands with a more poorly donating set of equatorial ligands. The reduction in electron density at Re should lower the energy of the d_{xy} orbital, and thus increase the $d_{xy}/d_{xz},d_{yz}$ gap. The lack of significant emission in fliud solution was disappointing as it was hoped that lowering the energy of the d_{xy} orbital might render these excited states highly oxidizing.

Transient Absorption (TA) Spectra. In order to gain further insight into the electronic structures of *trans*-$[ReO_2(L)_4][PF_6]$ pyridine complexes and to determine excited-state lifetimes for non-emissive complexes, the absorption spectra of the excited states of *trans*-$[ReO_2(4\text{-}Phpy)_4][PF_6]$, *trans*-$[ReO_2(4\text{-}MeOpy)_4][PF_6]$, *trans*-$[ReO_2(3\text{-}Medamp)_4][PF_6]$ and *trans*-$[ReO_2(dmap)_4][PF_6]$ were measured (Figures 3.18 - 3.21).

The TA spectrum of *trans*-$[ReO_2(py)_4][PF_6]$ has been previously measured.[65] The weak absorption feature observed at 500 nm was assigned to the LF transition $(d_{xy})^1(d_{xz},$

$d_{yz})^1 \rightarrow (d_{xz}, d_{yz})^2$ based upon the observed energy of the band. The absorption and emission spectra of *trans*-$[ReO_2(4\text{-}Phpy)_4][PF_6]$ and *trans*-$[ReO_2(4\text{-}MeOpy)_4][PF_6]$ are similar to those observed for the pyridine complex, implying that the energy gap between the d_{xy} and d_{xz},d_{yz} levels is similar for all three complexes. Thus, the weak features observed at ~ 500 nm in the TA spectra of the 4-phenylpyridine and 4-methoxypyridine complexes are also assigned to the $(d_{xy})^1(d_{xz},d_{yz})^1 \rightarrow (d_{xz}, d_{yz})^2$ transition. The additional band present in the 4-methoxypyridine complex at ~400 nm could be the result of concomitant occurance of an LMCT absorption (*vide infra*) and the MCLT ground-state bleach. The excited-state lifetimes of these two complexes determined from recovery of the MLCT ground-state bleach were within experimental error of those determined by luminescence decay methods.

The TA spectra of *trans*-$[ReO_2(3\text{-}Medamp)_4][PF_6]$ and *trans*-$[ReO_2(dmap)_4][PF_6]$ show strong absorptions in the visible region that are comparable in Δ O.D. to those observed for the MLCT ground-state bleaches. Their intensities and conspicuous absences from the TA spectra of the 4-phenylpyridine and 4-methoxypyridine complexes strongly suggest that they are LMCT in origin. LMCT transitions from 4-aminopyridine ligands to electron-deficient metal centers have literature precedence.[44,66,67] Sutton and Taube[67] have observed this behavior for $[Ru(NH_3)_5(4\text{-}NH_2py)]^{3+}$, and Hrepic and Malin[44] made similar observations for $[Fe(CN)_5(4\text{-}NH_2py)]^{2-}$. Both groups noted that LMCT is not observed for analogous complexes of pyridine, alkylpyridines or electron-poor pyridines. This band is expected to be intense in *trans*-$[ReO_2(L)_4]^+$ complexes based upon the same arguments put forth earlier to explain the MLCT transition intensities (in this case the transition would be $[(e_u)^4(b_{2g})^1(e_g)^1] \rightarrow [(e_u)^3(b_{2g})^2(e_g)^1]$, which is also $g \rightarrow u$). Additional support for this assignment will be presented in Chapter 4, where the spectra of the d^1 rhenium(VI) complexes *trans*-$[ReO_2(3\text{-}Medmap)_4][PF_6]_2$ and *trans*-$[ReO_2(dmap)_4][PF_6]_2$ are presented. The latter complexes exhibit strong absorptions (ε ~ 30,000) at 752 and 699 nm, respectively, that have been assigned to LMCT transitions.

CONCLUSIONS

Through systematic variation of the ancillary ligands in *trans*-$[ReO_2(L)_4][PF_6]$, we have gained a detailed understanding of the electronic structure of this compound family and the role of ancillary ligands in defining their properties. The conclusions drawn from these studies are enumerated below.

1. The Re(VI)/Re(V) redox couple is a linear function of pyridine pK_a. As the donor strength of the pyridine ligand increases, the Re(V) complexes become easier to oxidize. Oxidants as potent as Ce(IV) and as mild as the ferricenium ion are accessible via tuning of the ancillary ligands.

2. The $d_{xy}/d_{xz,yz}$ energy gap is also a linear function of pyridine pK_a; increasing the pyridine basicity lowers the energy of the $d_{xy} \rightarrow d_{xz}$, d_{yz} transition.

3. The excited-state properties of *trans*-$[ReO_2(L)_4][PF_6]$ pyridine complexes follow trends consistent with the energy-gap law. As pyridine basicity increases, the excited-state energies and lifetimes decrease.

4. The energy of the asymmetric O=Re=O stretch is relatively insensitive to the σ-properties of the pyridine ligands, suggesting that the Re-O bond strengths are insensitive to electronic changes in the pyridine ligands. Phosphorous donor ligands (diphos and dppen) weaken Re-O bonds, but this could be due to steric and *not* electronic effects.

5. Pyridine complexes of *trans*-$[ReO_2(L)_4][PF_6]$ have pronounced MLCT transitions, verifying that they are electron-rich systems.

6. Phosphorous donor ligands result in a larger $d_{xy}/d_{xz},d_{yz}$ gap, that is desirable for creating more energetic excited states. Unfortunately, these complexes also have larger non-radiative decay constants, resulting in excited states that are too short-lived to be useful as photochemical reagents.[68]

7. Through use of the strongly basic 4-dialkylaminopyridine ligands, we have shown that it is possible to stablize the corresponding d^1 complexes of *trans*-dioxorhenium(VI).

In the following chapter, we will examine the electronic structures and reactivities of these species in greater detail.

REFERENCES AND NOTES

(1) Bunting, J. W.; Brewer, J. C. *Can. J. Chem.* **1985**, *63*, 1245-1249.

(2) Johnson, C. D. *The Hammett Equation*; University Press: Cambridge, 1973.

(3) Lowry, T. H.; Richardson, K. S. *Mechanism and Theory in Organic Chemistry*; Harper and Row: New York, 1981; pp 130-145.

(4) Anson, F. C.; Collins, T. J.; Gipson, S. L.; Keech, J. T.; Kraft, T. E.; Peake, G. T. *J. Am. Chem. Soc.* **1986**, *108*, 6593-6605.

(5) Swada, M.; Ichihara, M.; Yukawa, Y.; Nakashi, T. *Bull. Chem. Soc. Jpn.* **1980**, *53*, 2055-2060.

(6) Perrin, D. D. *Dissociation Constants of Organic Bases in Aqueous Solution*; 1st ed.; Butterworths: London, 1965; pp 141, 162-163.

(7) Reedijk, J. In *Comprehensive Coordination Chemistry*; Wilkinson, G., Ed.; Pergamon: New York, 1987; Vol. 2, Chapter 13.2, p 74.

(8) Heinrichs-Zietlow, M.; Ph.D. thesis, August 1988, California Institute of Technology; Chapter 2, pp 24-25.

(9) Broomhead, J. A.; Young, C. G. *Inorg. Syn.* **1982**, *21*, 127-128.

(10) Burfield, D. R.; Lee, K. H.; Smithers, R. H. *J. Org. Chem.* **1977**, *42*, 3060-3065.

(11) Burfield, D. R.; Smithers, R. H. *J. Org. Chem.* **1978**, *43*, 3966-3968.

(12) Burfield, D. R.; Gan, G. H.; Smithers, R. H. *J. Appl. Chem. Biotechnol.* **1978**, *28*, 23-30.

(13) Rice, S. F.; Gray, H. B. *J. Am. Chem. Soc.* **1983**, *105*, 4571-4575.

(14) Drushel, H. V.; Sommers, A. L.; Cox, R. C. *Anal. Chem.* **1963**, *35*, 2166-2172.

(15) Caspar, J. V.; Meyer, T. J. *J. Am. Chem. Soc.* **1983**, *105*, 5583-5590.

(16) Van Houten, J.; Watts, R. J. *J. Am. Chem. Soc.* **1976**, *98*, 4853-4858.

(17) Marshall, J. L.; Hopkins, M. D.; Gray, H. B. *ACS Symp. Ser.* **1987**, *357*, 254-256.

(18) Demas, J. N.; Crosby, G. A. *J. Phys. Chem.* **1971**, *75*, 991-1024.

(19) Nocera, D. G.; Winkler, J. R.; Yocum, K. M.; Bordignon, E.; Gray, H. B. *J. Am. Chem. Soc.* **1984**, *106*, 5145-5150.

(20) Winkler, J. R.; Netzel, T. L.; Creutz, C.; Sutin, N. *J. Am. Chem. Soc.* **1987**, *109*, 2381-2392.

(21) Bard, A. J.; Faulkner, L. R. *Electrochemical Methods. Fundementals and Applications*; John Wiley and Sons: New York, 1980; Chapter 6, p 219.

(22) Evans, D. H.; O'Connell, K. M.; Peterson, R. A.; Kelly, M. J. *J. Chem. Ed.* **1983**, *60*, 290-293.

(23) Beard, J. H.; Murmann, R. K. *J. Inorg. Nuc. Chem.* **1968**, *30*, 2467-2474.

(24) Turner, W. R.; Elving, P. J. *Anal. Chem.* **1965**, *37*, 467-469.

(25) Pipes, D. W.; Meyer, T. J. *Inorg. Chem.* **1986**, *25*, 3256-3262.

(26) Beard, J. H.; Casey, J.; Murmann, R. K. *Inorg. Chem.* **1965**, *4*, 797-803.

(27) Winkler, J. R.; Gray, H. B. *Comments Inorg. Chem.* **1981**, *1*, 257-263.

(28) Winkler, J. R.; Gray, H. B. *Inorg. Chem.* **1985**, *24*, 346-355.

(29) Beard, J. H.; Calhoun, C.; Casey, J.; Murmann, R. K. *J. Am. Chem. Soc.* **1968**, *90*, 3389-3394.

(30) Szterenberg, L.; Natkanied, L.; Jezowska-Trzebiatowska, B. *Bull. Acad. Pol. Sci.*, *Ser. Sci. Chim.* **1976**, *24*, 805-810.

(31) Lawrance, G. A.; Sangster, D. F. *Polyhedron* **1986**, *5*, 1553-1558.

(32) Newsham, M. D.; Giannelis, E. P.; Pinnavaia, T. J.; Nocera, D. G. *J. Am. Chem. Soc.* **1988**, *110*, 3885-3891.

(33) Malouf, G.; Ford, P. C. *J. Am. Chem. Soc.* **1974**, *96*, 601-603.

(34) Phifer, C. C.; McMillin, D. R. *Inorg. Chem.* **1986**, *25*, 1329-1333.

(35) Jorgensen, W. L.; Salem, L. *The Organic Chemist's Book of Orbitals*; Academic: New York, 1973; pp 263-265.

(36) Ballhausen, C. J.; Gray, H. B. *Molecular Orbital Theory*; Benjamin/Cummings: London, 1978.

(37) Gray, H. B.; Ballhausen, C. J. *J. Am. Chem. Soc.* **1963**, *85*, 260-265.

(38) Jørgensen, C. K. *Acta Chem. Scand.* **1957**, *11*, 151-165.

(39) Ford, P. C.; Rudd, D. F. P.; Gaunder, R.; Taube, H. *J. Am. Chem. Soc.* **1968**, *90*, 1187-1194.

(40) Sen, J.; Taube, H. *Acta Chem. Scand. Ser. A.* **1979**, *A33*, 125-135.

(41) Figard, J. E.; Petersen, J. D. *Inorg. Chem.* **1978**, *17*, 1059-1063.

(42) Toma, H. E.; Malin, J. M. *Inorg. Chem.* **1973**, *12*, 1039-1045.

(43) Toma, H. E.; Malin, J. M. *J. Am. Chem. Soc.* **1975**, *97*, 288-293.

(44) Hrepic, N. V.; Malin, J. M. *Inorg. Chem.* **1979**, *18*, 409-413.

(45) Johnson, C. R.; Shepherd, R. E. *Inorg. Chem.* **1983**, *22*, 2439-2444.

(46) Wrighton, M. S.; Abrahamson, H. B.; Morse, D. L. *J. Am. Chem. Soc.* **1976**, *98*, 4105-4109.

(47) Kastner, M. E.; Fackler, P. H.; Clarke, M. L.; Deutsch, E. *Inorg. Chem.* **1984**, *23*, 4683-4688.

(48) Kastner, M. E.; Lindsay, M. J.; Clarke, M. J. *Inorg. Chem.* **1982**, *21*, 2037-2040.

(49) Kashani, F. F.; Murmann, R. K. *Int. J. Chem. Kinet.* **1985**, *17*, 1007-1015.

(50) Ballhausen, C. J.; Gray, H. B. *Inorg. Chem.* **1962**, *1*, 111-122.

(51) Jezowska-Trzebiatowska, B.; Natkanei, L. *Zh. Struk. Khim.* **1967**, *8*, 524-527.

(52) Figgis, B. N. *Introduction to Ligand Fields*; Interscience: New York, 1966; p 66.

(53) Barszez, B.; Gabryszewski, M.; Kulig, J.; Lenarcik, B. *J. Chem. Soc. Dalton Trans.* **1986**, 2025-2028.

(54) Sun, M. S.; Brewer, D. G. *Can. J. Chem.* **1967**, *45*, 2729-2739.

(55) Fife, D. J.; Moore, W. M.; Morse, K. W. *Inorg. Chem.* **1984**, *23*, 1545-1549.

(56) Fife, D. J.; Morse, K. W.; Moore, W. M. *J. Photochem.* **1984**, *24,* 249-263.

(57) Marynick, D. S. *J. Am. Chem. Soc.* **1984**, *106,* 4064-4065.

(58) Marynick, D. S.; Askari, S.; Nickerson, D. F. *Inorg. Chem.* **1985**, *24,* 868-870.

(59) Orpen, G. A.; Connelly, N. G. *J. Chem. Soc., Chem. Commun.* **1985**, 1310-1311.

(60) Tossell, J. A.; Moore, J. H.; Giordan, J. C. *Inorg. Chem.* **1985**, *24,* 1100-1103.

(61) Winkler, J. R.; Gray, H. B. *J. Am. Chem. Soc.* **1983**, *105,* 1373-1374.

(62) Thomas, T. R.; Watts, R. J.; Crosby, G. A. *J. Chem. Phys.* **1973**, *59,* 2123-2131.

(63) Caspar, J. V.; Meyer, T. J. *J. Phys. Chem.* **1983**, *87,* 952-957.

(64) Englman, R.; Jortner, J. *Molecular Phys.* **1970**, *18,* 145-164.

(65) Thorp, H. H.; Van Houten, J.; Gray, H. B. *Inorg. Chem.* **1989**, *28,* 889-892.

(66) Warner, L. W.; Hoq, M. F.; Myser, T. K.; Henderson, W. W.; Shepherd, R. E. *Inorg. Chem.* **1986**, *25,* 1911-1914.

(67) Sutton, J. E.; Taube, H. *Inorg. Chem.* **1981**, *20,* 4021-4023.

(68) *Note in proof.* The complex *trans*-$[ReO_2(PMe_3)_4]^+$ has been reported but no spectroscopic data was presented (Edwards, P. G.; Skapski, A. C.; Slawin, A. M. Z.; Wilkinson, G. *Polyhedron* **1984**, *3,* 1083-1085.). The complex has long Re–O bonds (1.79 Å) and a reported ν_{asym} O=Re=O of 778 cm^{-1}. It would be interesting to examine the complex's excited-state properties.

Chapter 4.

Syntheses, Characterization, and Electronic Structure of *trans*-Dioxorhenium(VI) Complexes.

INTRODUCTION

As discussed in Chapter 3, *trans*-$[ReO_2(L)_4]^+$ complexes exhibit reversible oxidations on the cyclic voltammetry time scale. In the absence of a proton source, no facile reduction chemistry is evident. *Trans*-$[ReO_2(L)_4]^+$ pyridine complexes are electron-rich species, and thus, the important redox partners to these systems are their oxidized counterparts.

Earlier results indicated that the Re(VI) complex *trans*-$[ReO_2(py)_4]^{2+}$ was a potent oxidant towards silanes, halocarbons, secondary alcohols, and calf thymus DNA. Thorp *et al.* proposed that this activity resulted from the radical nature imparted to the oxo ligand upon metal oxidation.[1,2] *Trans*-$[ReO_2(py)_4]^{2+}$ was so reactive that it had but a fleeting existence, and the fate of the Re after substrate oxidation was unknown. As a result, the nature of the Re(VI) species and the mechanism of its action remained obscure.

The systematic ancillary ligand changes discussed in Chapter 3 revealed that stabilization of Re(VI) was possible through the use of strongly basic pyridine ligands. Bulk electrolysis on *trans*-$[ReO_2(4\text{-pyrrpy})_4][PF_6]$, a more soluble relative of *trans*-$[ReO_2(dmap)_4][PF_6]$, indicated that the corresponding Re(VI) complex was stable for long periods. Therefore, chemical methods of oxidation were sought in order to isolate the Re(VI) species.

In this chapter the synthesis, electronic structure, X-ray structure, EPR analysis, and chemical reactivity of the complex *trans*-$[ReO_2(dmap)_4][PF_6]_2$ are presented. This compound represents the first[3] isolated d^1 *trans*-dioxo species.

EXPERIMENTAL

Materials. All chemicals were either of reagent grade or the best grade commercially available and used as received. Acetonitrile (Burdick and Jackson) was used as received for UV-vis experiments. Ferricenium hexafluorophosphate was synthesized as described below, using a modified version of the method reported by Jolly.[4]

Physical Measurements. *X-ray Structure Determination.* Ms. Kirby M. Slagle performed the X-ray structure determination as described below.

A prismatic crystal was mounted and centered on a CAD-4 diffractometer. Unit cell parameters and an orientation matrix were obtained by a least-squares calculation from the setting angles of 24 reflections with $18° < 2\theta < 40°$. Two equivalent data sets out to a 2θ of 50° were collected and corrected for absorption and a slight decay. An average background as a function of 2θ was used. Lorentz and polarization factors were applied, and the two data sets were then merged to yield the final data set.

Primary Weissenberg photographs indicated triclinic symmetry. The structure was successfully refined in space group $P\bar{1}$ (#2) in which the sole Re atom must lie on a center of symmetry. Locations of the other non-hydrogen atoms were determined from a structure factor-Fourier calculation. Difference maps showed that the methyl groups were staggered with respect to the adjacent aromatic-ring hydrogen atom. Thus, calculated positions were used for the methyl hydrogen atoms as well as the aromatic-ring hydrogen atoms. All hydrogen atoms were given isotropic B values 20% greater than that of the attached carbon atom. No hydrogen parameters were refined. The complete least-squares matrix, consisting of coordinates and anisotropic thermal parameters for the non-hydrogen atoms and a scale factor, contained 241 parameters. A final difference Fourier map showed deviations ranging from -0.71 to +1.41 eÅ^{-3}. The largest peaks are due to absorption by the Re atom or disorder of the anion. The refinement converged with an *R*-factor of 0.0389 (0.0385 for $F_o^2 > 3\sigma(F_o^2)$) and a GOF of 2.77 for all 3499 reflections.

Calculations were done with programs of the CRYM Crystallographic Computing System and ORTEP. Scattering factors and corrections for anomalous scattering were taken from a standard reference.[5] $R = \Sigma\left|F_o - |F_c|\right| / \Sigma F_o$, for only $F_o^2 > 0$, and goodness of fit $= \left[\Sigma w\left(F_o^2 - F_c^2\right)^2 / (n-p)\right]^{1/2}$, where n is the number of data and p the number of parameters refined. The function minimized in least-squares was $\Sigma w\left(F_o^2 - F_c^2\right)^2$, where $w = 1/\sigma^2\left(F_o^2\right)$. Variances of the individual reflections were assigned based on counting statistics plus an additional term, 0.014I. Variances of the merged reflections were

determined by standard propagation of error plus another additional term, 0.014 $\langle I \rangle^2$. The absorption correction was done by Gaussian integration over an 8 X 8 X 8 grid. Transmission factors varied from 0.51 to 0.64.

EPR Measurements. Preliminary EPR measurements on solid samples of oxidized Re complexes were performed on a Varian E-line Century Series spectrometer (X-band, ~9.514 GHz) at 0.05 - 1 mW power. Solid samples were packed in Kimax-51 (no. 34505) capillary tubes and placed inside standard quartz EPR tubes for placement into the instrument cavity. Low temperature measurements were conducted by Dr. H. H. Thorp at Yale University. Reagent grade dimethyl sulfoxide (DMSO) and Millipore water were used. Dilute (~10 μM) solutions in glassing solvents or mixtures were required for resolution of the hyperfine lines. More concentrated solutions gave a single derivative signal at g ~ 1.91. EPR spectra were recorded on a home-built EPR spectrometer equipped with an Oxford Instruments ESR-900 liquid-helium cryostat. This instrument has been described in detail elsewhere.[6] Simulation of EPR spectra was performed using PROGRAM QPOW, written by R.L. Belford, A.M. Maurice, and M.J. Nilges.[7]

Syntheses. All *trans*-dioxorhenium(V) pyridine complexes used were synthesized according to the methods described in Chapter 2.

Ferricenium Hexafluorophosphate, [Fc][PF_6]. Ferrocene (0.51 g, 2.7 mmol) was placed in a 50-mL Erlenmeyer flask. Concentrated H_2SO_4 (10 mL) was measured out in a dry graduated cylinder and added to the above. After stirring the suspension for 15 min, it became a homogeneous deep red-violet solution. After stirring for an additional 20 min, the solution was *slowly* poured into 150 mL of distilled water. After agitating for 15 min, the deep red-purple solution was passed through a 15-mL medium-porosity sintered-glass frit. This failed to remove the small amount of sulfur present, so the filtration was repeated using a 15-mL fine-porosity sintered-glass frit. The filtration was conducted over a 20 min period. KPF_6 (1.0 g, 5.4 mmol) was added to the filtrate with vigorous stirring. The opaque mixture was placed in a refrigerator (4 °C) and left to stand for 1.5 h. After

this period, 215 mg of a dark purple microcrystalline solid was collected on a medium-porosity sintered-glass frit. It was washed with 5 X 15 mL of diethyl ether, 2 X 15 mL of pentane and aspirated to dryness (1 h). Additional KPF_6 (5.0 g, 27 mmol) was added to the mother liquor. The flask was sealed and left to stand in a refrigerator (4 °C) overnight. The following morning, the additional product that had formed was collected, washed with 3 X 15 mL of toluene, 6 X 15 mL of diethyl ether, and 2 X 15 mL of pentane, and aspirated to dryness (1 h). Combined yield of material: 630 mg, 69%. The compound was characterized by UV-vis spectroscopy (aqueous solution).[8,9]

***trans*-[ReO_2(dmap)$_4$][PF_6]$_2$.** Approximately 150 mL of CH_2Cl_2 was added to *trans*-[ReO_2(dmap)$_4$]I (1.125 g, 1.3 mmol) in a 250-mL Erlenmeyer flask; a small amount of solid remained undissolved. Addition of Br_2 (0.5 mL, 5.2 mmol) resulted in the immediate formation of a deep green slurry. This was stirred for 10 min and then filtered through a coarse-porosity sintered-glass frit. The blue-green solid was washed with toluene (3 X 40 mL), diethyl ether (3 X 40 mL), and pentane (2 X 40 mL), and aspirated to dryness (10 min). The yield of crude product was 1.11 g, 95%.

The above material was placed in a 1000-mL Erlenmeyer flask and 600 mL of methanol was added. After vigorous stirring for 10 min, the deep blue solution was filtered by gravity (Whatman #1 filter paper) to remove a dark green-black residue. [NH_4][PF_6] (4.15 g, 25 mmol) was dissolved in 50 mL of methanol and filtered into the above solution. Upon contact, a microcrystalline, blue solid began to precipitate. After standing for 15 min, the solid was collected on a medium-porosity sintered-glass frit and washed successively with ethanol (3 X 15 mL), diethyl ether (3 X 15 mL), pentane (2 X 15 mL), and aspirated to dryness (1 h). The yield was 250 mg, 19%, based upon *trans*-[ReO_2(dmap)$_4$]I. Work-up of the remaining residues yielded another 100 mg of product.

Recrystallization was effected as follows. *Trans*-[ReO_2(dmap)$_4$](PF_6)$_2$ (250 mg, 0.25 mmol) was dissolved in 60 mL CH_2Cl_2 and filtered (Whatman #1 filter paper) by gravity. Ethanol (25 ml) was added to the filtrate. The solvent volume was reduced on a rotary

evaporator until the solution was colorless and a blue precipitate had formed. This was collected on a Büchner funnel and washed with 2 X 5 mL of ethanol, 2 X 5 mL of diethyl ether, and 2 X 5 mL pentane. After aspirating to dryness (1 h) the yield was 70 mg, 28%. Approximately 40 mg of this material was dissolved in 5 mL of CH_3CN. One millilitre of this solution was placed in a 1-dram vial, and this was placed inside a 4-dram vial containing 2 mL of diethyl ether. The large vial was then sealed with a Teflon-lined cap. The assembly was allowed to stand in a dark cupboard for 1 week, after which time several rectangular-shaped crystals had formed. One of these was selected for X-ray structure analysis. *Trans*-$[ReO_2(dmap)_4](PF_6)_2$ is very soluble in CH_3CN, moderately soluble in CH_3OH, acetone, and CH_2Cl_2, slightly soluble in ethanol, and insoluble in diethyl ether, THF, and hydrocarbons. Anal. Calcd for $C_{28}H_{40}N_8F_{12}O_2P_2Re$: C, 33.74%; H, 4.04%; N, 11.24%. Found: C, 33.41%; H, 4.01%; N, 10.94%. UV-vis, λ_{max} in nm (ε, M^{-1} cm^{-1}), CH_3CN solution: 273 (59,000); 364 sh (28,000); 372 (35,000); 699 (27,000). IR (ν_{asym} ReO_2): 820sh cm^{-1}.

RESULTS AND DISCUSSION

Chemical Oxidations of *trans*-$[ReO_2(dmap)_4]^+$ and *trans*-$[ReO_2(4\text{-}pyrrpy)_4]^+$. Electrochemical measurements indicated that *trans*-$[ReO_2(dmap)_4][PF_6]$ and *trans*-$[ReO_2(4\text{-}pyrrpy)_4][PF_6]$ were oxidized at 0.10 and 0.05 V vs. Fc^+/Fc, respectively. Using the value of 0.66 V vs. NHE for the Fc^+/Fc couple,[10] the potentials for the Re complexes are ~ 0.76 and ~ 0.71 V vs. NHE. This rough calculation was used to search for promising chemical oxidants by examining tables of standard reduction potentials.[10] Both substituted pyridine complexes were used in exploratory oxidation reactions as their redox properties were essentially identical. The 4-pyrrpy complex is more soluble than the dmap complex for the Re(V) state; the inverse is true for the corresponding Re(VI) compounds.

The first oxidant examined in detail was I_2 ($E_{1/2}$ ~ 0.534 V vs. NHE). Although this appears to be a weaker oxidant than *trans*-$[ReO_2(4\text{-pyrrpy})_4]^{2+}$, it was explored because of its mild nature. Of all the halogens, it would be least likely to react with the pyridine ring. This side reaction was of concern during early stages of this research. The oxidation potentials calculated for the Re complexes are also only estimates and could likely differ substantially from actual values due to solvation effects.

Several attempts were made to oxidize *trans*-$[ReO_2(4\text{-pyrrpy})_4]^+$ with I_2 in CH_2Cl_2 solution. Each attempt was frustrated by erratic behavior of the resulting product. Upon addition of solid I_2 to a CH_2Cl_2 solution of *trans*-$[ReO_2(4\text{-pyrrpy})_4][PF_6]$, a dark green slurry was obtained. A blue-green solid was isolated and its UV-vis spectrum in CH_2Cl_2 solution was identical to that obtained after bulk electrochemical oxidations (see Chapter 3). Unfortunately, the complex was not stable in solution for long time periods. UV-vis spectroscopy revealed decreases in product band intensity with time in all organic solvents examined: acetone, THF, CH_2Cl_2, CH_3CN, and ethanol. The time for total decomposition varied from experiment to experiment. It is possible that this erratic behavior was due to the proximity of the redox couple I_2/I^- to that of the $ReO_2^{2+/+}$. When half-cell potentials differ by 100 mV or less, a redox buffering effect can occur. The oxidized complex was stable in the presence of excess oxidant, but upon isolation, reverted back to the Re(V) starting material. The infrared spectrum of the product obtained indicated that no PF_6^- was present. The elemental analysis suggested the composition *trans*-$[ReO_2(4\text{-pyrrpy})_4][I_9]$ (Anal. Calcd for $C_{36}H_{48}N_8I_9O_2Re$: C, 22.14%; H, 2.48%; N, 5.74%. Found: C, 22.02%; H, 2.55%; N, 6.00%). The counterion could consist of two triodide anions along with an iodine molecule of crystallization. Thus, a possible sequence of reactions that may have occurred is as follows:

$$[ReO_2(4\text{-pyrrpy})_4]PF_6 + \text{xs } I_2 \xrightarrow{CH_2Cl_2} [ReO_2(4\text{-pyrrpy})_4][I_9]\downarrow \quad (1)$$

$$[ReO_2(4\text{-pyrrpy})_4][I_9] \xrightarrow{\text{dissolve}} [ReO_2(4\text{-pyrrpy})_4][I_3] + 3\ I_2 \quad (2)$$

The combination of excess I_2 and product insolubility would drive reaction (1) to the right. Upon redissolving the complex, comparatively little excess I_2 is present and the reaction reverses, *i. e.*, the Re(VI) complex oxidizes the I^- counterions back to I_2 and regenerates the Re(V) species.

It was also speculated that the instability might originate from the nucleophilicity of the I^- counterion. To test this hypothesis, oxidations were attempted with [Fc][PF_6], which has a reduction potential similar to that of I_2 (0.548 V vs. NHE). The PF_6^- anion is a non-nucleophilic species and, hence, was not expected to initiate any decomposition reactions. Unfortunately, reactions with [Fc][PF_6] were equally troublesome; the instability of this oxidant in organic solvents has been noted by others.[11-13] Based upon these results, it was concluded that a much stronger oxidant was required, one with a reduction potential well removed from that of the Re(VI) complexes.

Bromine ($E_{1/2}$ ~ 1.1 V vs. NHE) was the next oxidant to be explored. When excess Br_2 was added to a CH_2Cl_2 solution of *trans*-[ReO_2(dmap)$_4$]I, a blue-green solid precipitated. In this case, bromine was expected to oxidize both the complex and the iodide anion:

$$[ReO_2(4\text{-pyrrpy})_4]I + Br_2 \xrightarrow{CH_2Cl_2} [ReO_2(4\text{-pyrrpy})_4][Br]_2\downarrow + 1/2\ I_2 \quad (3)$$

The material obtained was very soluble in CH_3CN, alcohols and CH_3NO_2. It dissolved with reaction in acetone, THF, DMSO, butyronitrile, and CH_2Cl_2. A UV-vis spectrum of the crude material appeared similar to that of *trans*-$[ReO_2(4\text{-pyrrpy})_4]^{2+}$ synthesized by bulk electrolysis. Samples sent for elemental analysis gave results suggesting the

molecular formula was *trans*-$[ReO_2(dmap)_4][Br_x]$ where x = 7-9. This material was difficult to handle and often (unpredictably) decomposed to what appeared to be the Re(V) complex. For this reason, it was metathesized to the corresponding $[PF_6]^-$ salt. During this process ~ 20% of the *trans*-$[ReO_2(dmap)_4]Br_x$ complex could not be dissolved. The identity of this material and the reason for its recalcitrant behavior are unknown.

Curiously, the $[PF_6]^-$ salt of *trans*-$[ReO_2(dmap)_4]^{2+}$ was stable in organic solvents such as acetone and dichloromethane; the polyhalide salts decomposed in less than 5 min under identical conditions. When TBABr was added to an acetone solution of *trans*-$[ReO_2(dmap)_4][PF_6]_2$, decomposition began immediately. The complex was also unstable to bases (OH^-, amines, K_2CO_3, $KHCO_3$) and to excess free ligand. Stability was greatest in methanol free of halides and basic agents.

After successful metathesis, *trans*-$[ReO_2(dmap)_4][PF_6]_2$ was recrystallized from CH_2Cl_2/EtOH mixtures using a rotary evaporator to slowly remove the more volatile CH_2Cl_2. The material obtained was then used for physical measurements. A single crystal suitable for X-ray structure analysis was grown by slow diffusion of diethyl ether into an CH_3CN solution of the complex.

As discussed in the previous chapter, bulk electrolyses were performed on both *trans*-$[ReO_2(3\text{-Medmap})_4][PF_6]$ and *trans*-$[ReO_2(4\text{-MeOpy})_4][PF_6]$ but only the former was stable on the time scale of the experiment. In the latter case, substantial decomposition was evident from the low yield (~40%) of the Re(V) product upon electrolytic reduction. Fortunately, both materials could be transiently characterized by UV-vis spectroscopy.

Electronic Spectroscopy. The UV-vis spectra of the three Re(VI) complexes *trans*-$[ReO_2(4\text{-pyrrpy})_4]^{2+}$, *trans*-$[ReO_2(dmap)_4]^{2+}$, and *trans*-$[ReO_2(3\text{-Medmap})_4]^{2+}$ are similar. The spectrum of *trans*-$[ReO_2(dmap)_4][PF_6]_2$ presented in Figure 4.1 is representative. The spectrum of *trans*-$[ReO_2(4\text{-MeOpy})_4]^{2+}$ has already been presented in

Figure 4.1. UV-vis absorption spectra of *trans*-$[ReO_2(dmap)_4][PF_6]_2$ (top) and *trans*-$[ReO_2(dmap)_4][PF_6]$ (bottom) in CH_3CN solution. The ordinate scale is in arbitrary absorbance units.

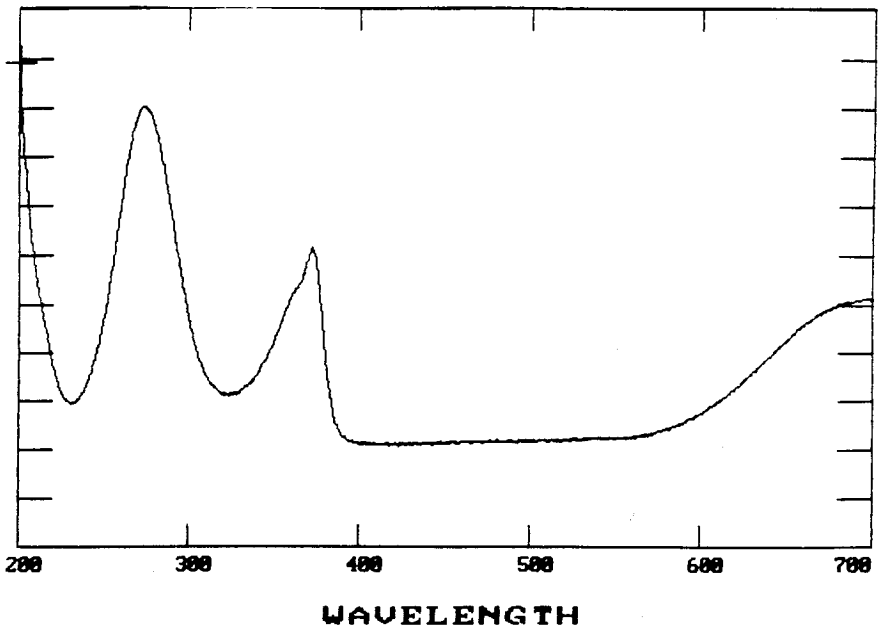
200
300
400
500
600
700
WAVELENGTH

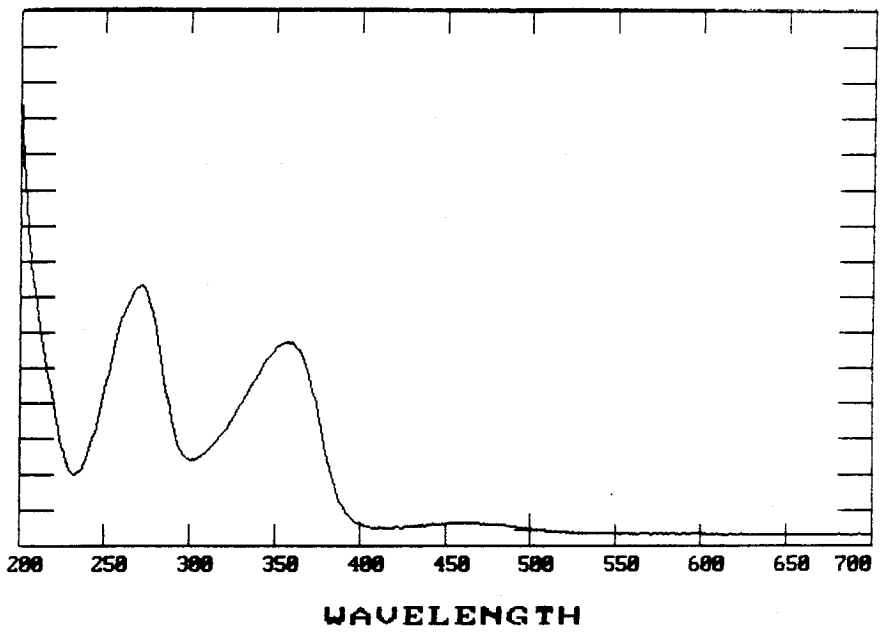
200
250
300
350
400
450
500
550
600
650
700
WAVELENGTH

Figure 3.23 and is likely a composite of both the Re(V) and Re(VI) species. A summary of the data is set out in Table 4.1, along with selected absorption data for the corresponding Re(V) materials (for comparison). The band assignments are discussed below.

Table 4.1. Selected UV-vis absorption data of *trans*-$[ReO_2(L)_4][PF_6]$ and *trans*-$[ReO_2(L)_4][PF_6]_2$ complexes. Except where otherwise indicated, measurements were made in CH_3CN solution. Roman numerals refer to the formal oxidation state of Re in the complexes.

L =	$\pi \rightarrow \pi^*$ py	MLCT, $d_{xy} \rightarrow \pi^*$ py	LMCT, π py $\rightarrow d_{xy}$
4-pyrrpy, (V)	273	353	
(VI)[a]	280	365 sh, 375	720
dmap, (V)	272	358	
(VI)	273	364 sh, 372	699
3-Medmap, (V)	280	363	
(VI)[b]	291	375 sh, 384	752
4-MeOpy (V)	227	347	
(VI)[b]	?	330	478, 530 sh

[a] 0.1 M TBAH CH_2Cl_2 solution. [b] 0.1 M TBAH CH_3CN solution.

All of the *trans*-$[ReO_2(L)_4]^{2+}$ pyridine complexes exhibit strong absorptions in the visible region ($\varepsilon > 10{,}000\ M^{-1}\ cm^{-1}$) that are too intense to be of LF origin. As in the case of the Re(V) complexes, all LF transitions are Laporte-forbidden ($g \rightarrow g$) and therefore are expected to have low extinction coefficients. The most probable origin of these bands is

LMCT from the filled π-levels of the electron-rich pyridine ligands to the hole created in the d_{xy} orbital. The overlap and symmetry arguments put forth in the previous chapter to explain MLCT intensities apply equally here, the only difference being the direction of the charge transfer. Rigorously, the 1-e⁻ transition is e_u (py, π^b) → b_{2g} (d_{xy}). Note again that this is Laporte-allowed (u → g) and hence will be intense. On this basis, the bands appearing at 720, 699, 752 and 478-530 nm for the complexes of 4-pyrrpy, dmap, 3-Medmap and 4-MeOpy, respectively, are assigned to LMCT. (The literature precedence for such an assignment was discussed in the previous chapter. See the section on transient absorption spectra.) The bands occurring in the near-UV have been assigned to MLCT because of their energetic proximity to MLCT bands of the corresponding Re(V) complexes.

Exactly where are the LF transitions? Obviously, they are obscured by one of the CT transitions, but which one? If one assumes that the 1-e⁻ MO energies do not change as a result of Re oxidation (Koopman's Theorem), it is possible to calculate the approximate positions of the LF transitions based upon transition energies known for the corresponding Re(V) compounds. In the Re(V) systems, the energy of a given transition will be equal to the 1-e⁻ MO energy splitting minus the difference in electron-repulsion energy between the two states. The 2-e⁻ transition energies can therefore be expressed in terms of 1-e⁻ energy level differences and repulsion energies. The repulsion energies for states derived from the D_{4h} d^2 case will be identical to those for the d^8 D_{4h} case from the electron pair/hole equivalence principle.[14] These repulsion energies were calculated by Gray[15,16] sometime ago. Using this information and referring to the definitions set out in Figure 4.2, the state energies summarized in Table 4.2 were calculated. From Table 4.2 it appears that the 1-e⁻ transition $d_{xy} \rightarrow d_{xz},d_{yz}$ should appear to the blue of the corresponding transition in the d^2 complex by (3B + C) or half the energy of the singlet-triplet gap in the d^2 complex.

Figure 4.2. MO diagram for *trans*-$[ReO_2(L)_4]^+$ complexes. The 1-e^- orbital energies are given in classical LF notation[17] and in terms of empirical values.

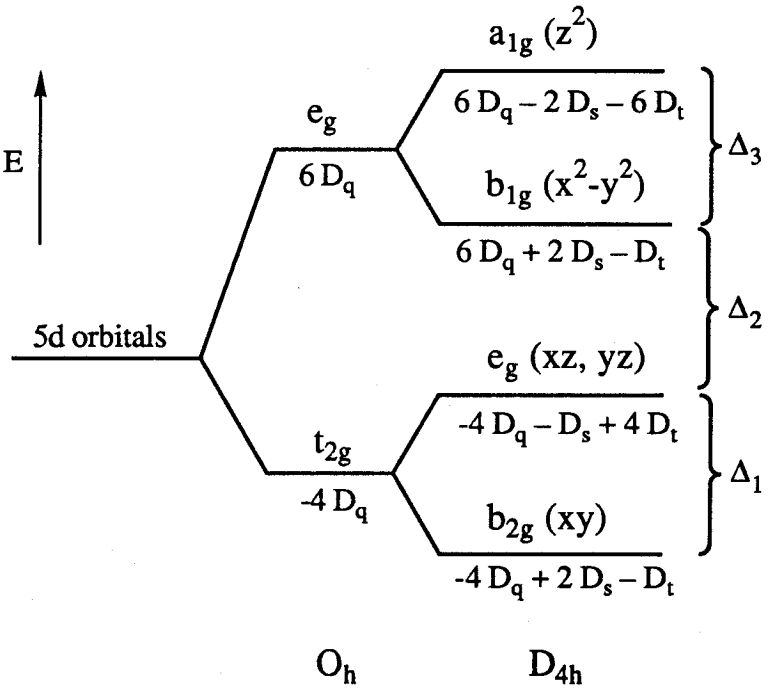
E
5d orbitals
e_g
$6 D_q$
t_{2g}
$-4 D_q$
a_{1g} (z^2)
$6 D_q - 2 D_s - 6 D_t$
b_{1g} (x^2-y^2)
$6 D_q + 2 D_s - D_t$
e_g (xz, yz)
$-4 D_q - D_s + 4 D_t$
b_{2g} (xy)
$-4 D_q + 2 D_s - D_t$
Δ_3
Δ_2
Δ_1
O_h
D_{4h}

Table 4.2. State energies for *trans*-$[ReO_2(L)_4][PF_6]$ complexes in terms of 1-e$^-$ MO energy differences and electron-electron repulsion energies.[16,18]

State	Energy in Racah Parameters	Energy in Slater-Condon Parameters
$^1A_{1g}$	0	0
^3E_g	$\Delta_1 - 3(3B + C)$	$\Delta_1 - 9F_2 - 60F_4$
^1E_g	$\Delta_1 - (3B + C)$	$\Delta_1 - 3F_2 - 20F_4$
$^3A_{2g}$	$\Delta_1 + \Delta_2 - 3C$	$\Delta_1 + \Delta_2 - 105F_4$
$^1A_{2g}$	$\Delta_1 + \Delta_2 - C$	$\Delta_1 + \Delta_2 - 35F_4$
$^3B_{2g}$	$\Delta_1 + \Delta_2 + \Delta_3 - 3(4B + C)$	$\Delta_1 + \Delta_2 + \Delta_3 - 12F_2 - 45F_4$
$^1B_{2g}$	$\Delta_1 + \Delta_2 + \Delta_3 - (4B + C)$	$\Delta_1 + \Delta_2 + \Delta_3 - 4F_2 - 15F_4$

From single-crystal studies completed by Winkler[19] on *trans*-$[ReO_2(py)_4]BPh_4$, the singlet-triplet splitting of the E_g term is known to be 3900 cm^{-1}. Thus, the 1-e$^-$ transition $d_{xy} \rightarrow d_{xz},d_{yz}$ should appear at 22,500 + 1950 = 24,450 cm^{-1} (~400 nm) for the pyridine complex. Based on this analysis, it is likely that all of the LF transitions for the other Re(VI) complexes are obscured by the high energy MLCT and π-π^* pyridine transitions.

What about the $d_{xy} \rightarrow d_{x^2-y^2}$ transition? Examination of the spectra of the ethylenediamine and pyridine *trans*-$[ReO_2(L)_4]^+$ complexes reveals that they both have an absorption in the vicinity of 270-280 nm. The transition energy of interest actually corresponds to the LF parameter 10 Dq. Since pyridine and ethylenediamine have approximately the same ligand field strength,[20] the 10 Dq values for the two complexes should be almost identical. Thus, the $d_{xy} \rightarrow d_{x^2-y^2}$ transition should occur at the same energy for both complexes. The results in Table 4.2 predict that the d^1 complex should

have the corresponding transition to the blue by an amount C. Thus, the $d_{xy} \rightarrow d_{x^2-y^2}$ transition energy is at *least* at 36,000 cm^{-1} (~280 nm) in the Re(VI) complexes.

It is important to remember that the above arguments assume the 1-e^- orbital energies are identical for the Re(V) and Re(VI) complexes. This might have some validity since the electron removed during the oxidation event is from a non-bonding level. Gross changes in bond lengths and angles are therefore not expected; this is born out by the results of an X-ray structure determination of *trans*-$[ReO_2(dmap)_4][PF_6]_2$.

X-ray structure of *trans*-$[ReO_2(dmap)_4][PF_6]_2$. An X-ray structure determination was successfully carried out for *trans*-$[ReO_2(dmap)_4](PF_6)_2$ by Ms. Kirby M. Slagle. The results are summarized in a series of figures and tables. A crystallographic data summary, final non-hydrogen parameters, and a list of selected bond lengths and angles are provided in Tables 4.3, 4.4, and 4.5, respectively. All other data pertaining to this structure have been collected in an appendix at the end of this thesis. An ORTEP diagram showing the gross structural features and the atomic numbering scheme used are given in Figures 4.3 and 4.4, respectively. A view of the structure looking down the O=Re=O axis is provided in Figure 4.5, and finally, the relative orientation of the complex and its counterions is illustrated in the unit cell diagram of Figure 4.6. A brief description of the structure is now presented.

The octahedrally coordinated Re atom lies on a crystallographic center of symmetry (Figure 4.6); the two oxo ligands are axial and the four pyridyl nitrogen atoms are equatorial. The Re-O bond is 1.764(4) Å; the Re-N11 and Re-N21 bonds are 2.108(4) Å and 2.120(5) Å, respectively. The O-Re-N11 and the O-Re-N21 angles are both 90.0(2)°; the N11–Re–N21 angle is 91.9(2)°. The dmap ligands are nearly perpendicular to the equatorial plane (Figure 4.5); the angles between the pyridine rings and the plane defined by the Re and four pyridyl nitrogen atoms are 93.6(3.1)° and 94.3(3.1)°. The amino nitrogen atoms are trigonal planar; the sums of the angles about the nitrogen atom are 359.9°

Table 4.3. Crystallographic data for *trans*-$[ReO_2(dmap)_4][PF_6]_2$.

Formula: $ReO_2C_{28}N_8P_2F_{12}H_{40}$	Formula weight: 996.813
a = 8.307(3) Å	Space Group: $P\bar{1}$ (#2)
b = 10.911(5) Å	T = 293 K
c = 11.907(11) Å	λ = 0.7107 Å
α = 96.24(6)°	ρ_{calc} = 1.662 g cm^{-3}
β = 108.28(6)°	μ = 34.09 cm^{-1}
γ = 99.42(6)°	trans. coeff. = 0.51 - 0.64
V = 996.1(11) Å^3	$R(F_o)$ = 0.0389
Z = 1	GOF = 2.77

Table 4.4. Final non-hydrogen parameters for *trans*-[$ReO_2(dmap)_4$][PF_6].

x, y, z and $U_{eq}{}^a \times 10^4$

Atom	x	y	z	U_{eq}
Re	0	0	0	479(1)
O	2122(4)	360(4)	1052(3)	575(10)
N11	−985(5)	451(4)	1387(4)	515(11)
C11	34(7)	893(6)	2535(5)	587(15)
C12	−562(7)	1182(6)	3452(5)	651(16)
C13	−2345(8)	1042(6)	3242(5)	649(16)
C14	−3414(7)	569(7)	2033(5)	722(18)
C15	−2706(7)	283(7)	1185(5)	649(17)
N12	−2991(7)	1327(7)	4094(5)	967(21)
C16	−1868(11)	1804(12)	5324(7)	1375(37)
C17	−4859(11)	1124(15)	3831(8)	1705(48)
N21	295(6)	1882(4)	−325(4)	544(11)
C21	−925(8)	2248(6)	−1221(5)	634(16)
C22	−691(9)	3380(7)	−1558(6)	714(17)
C23	868(9)	4281(7)	−1014(6)	719(17)
C24	2075(9)	3926(7)	−34(7)	779(20)
C25	1761(8)	2761(6)	261(6)	665(17)
N22	1189(10)	5351(6)	−1367(7)	675(17)
C26	2829(14)	6226(8)	−843(10)	1233(32)
C27	56(17)	5645(9)	−2392(11)	1365(37)
P	3778(3)	2979(3)	6815(2)	1027(7)
F1	3027(12)	1927(13)	5816(9)	2834(51)
F2	5023(11)	2204(11)	7362(13)	3012(56)

Table 4.4. (Cont'd)

Atom	x	y	z	U_{eq}
F3	5256(13)	3534(12)	6403(10)	2547(46)
F4	4531(14)	3988(13)	7852(10)	3070(54)
F5	2677(18)	3684(11)	6123(15)	3503(72)
F6	2374(13)	2432(14)	7248(12)	3076(58)

[a] $U_{eq} = \frac{1}{3}\sum_i \sum_j [U_{ij}(a_i^* a_j^*)(\vec{a}_i \cdot \vec{a}_j)]$

Table 4.5. Selected distances and angles for *trans*-$[ReO_2(dmap)_4][PF_6]_2$.

Distance(Å)			Angle(°)			
Re	–O	1.764(4)	O	–Re	–N11	90.0(2)
Re	–N11	2.108(4)	O	–Re	–N21	90.0(2)
Re	–N21	2.120(5)	N11	–Re	–N21	91.9(2)
N11	–C11	1.346(7)	C15	–N11	–C11	115.2(5)
N11	–C15	1.351(8)	C12	–C11	–N11	124.5(5)
C11	–C12	1.361(9)	C13	–C12	–C11	120.6(6)
C12	–C13	1.401(9)	C14	–C13	–C12	114.7(6)
C13	–C14	1.419(9)	N12	–C13	–C12	123.1(6)
C13	–N12	1.319(9)	N12	–C13	–C14	122.2(6)
C14	–C15	1.352(9)	C15	–C14	–C13	120.5(6)
N12	–C16	1.451(12)	C14	–C15	–N11	124.4(6)
N12	–C17	1.457(13)	C16	–N12	–C13	121.1(7)
N21	–C21	1.368(8)	C17	–N12	–C13	120.7(7)
N21	–C25	1.352(8)	C17	–N12	–C16	118.1(7)
C21	–C22	1.343(10)	C25	–N21	–C21	115.8(5)
C22	–C23	1.408(10)	C22	–C21	–N21	123.5(6)
C23	–C24	1.418(11)	C23	–C22	–C21	121.7(7)
C23	–N22	1.298(10)	C24	–C23	–C22	114.2(7)
C24	–C25	1.362(10)	N22	–C23	–C22	123.6(7)
N22	–C26	1.438(13)	N22	–C23	–C24	122.2(7)
N22	–C27	1.394(14)	C25	–C24	–C23	121.0(7)
			C24	–C25	–N21	123.5(6)
			C26	–N22	–C23	122.6(8)
			C27	–N22	–C23	121.6(8)
			C27	–N22	–C26	115.2(8)

Figure 4.3. An ORTEP diagram for *trans*-$[ReO_2(dmap)_4][PF_6]_2$.

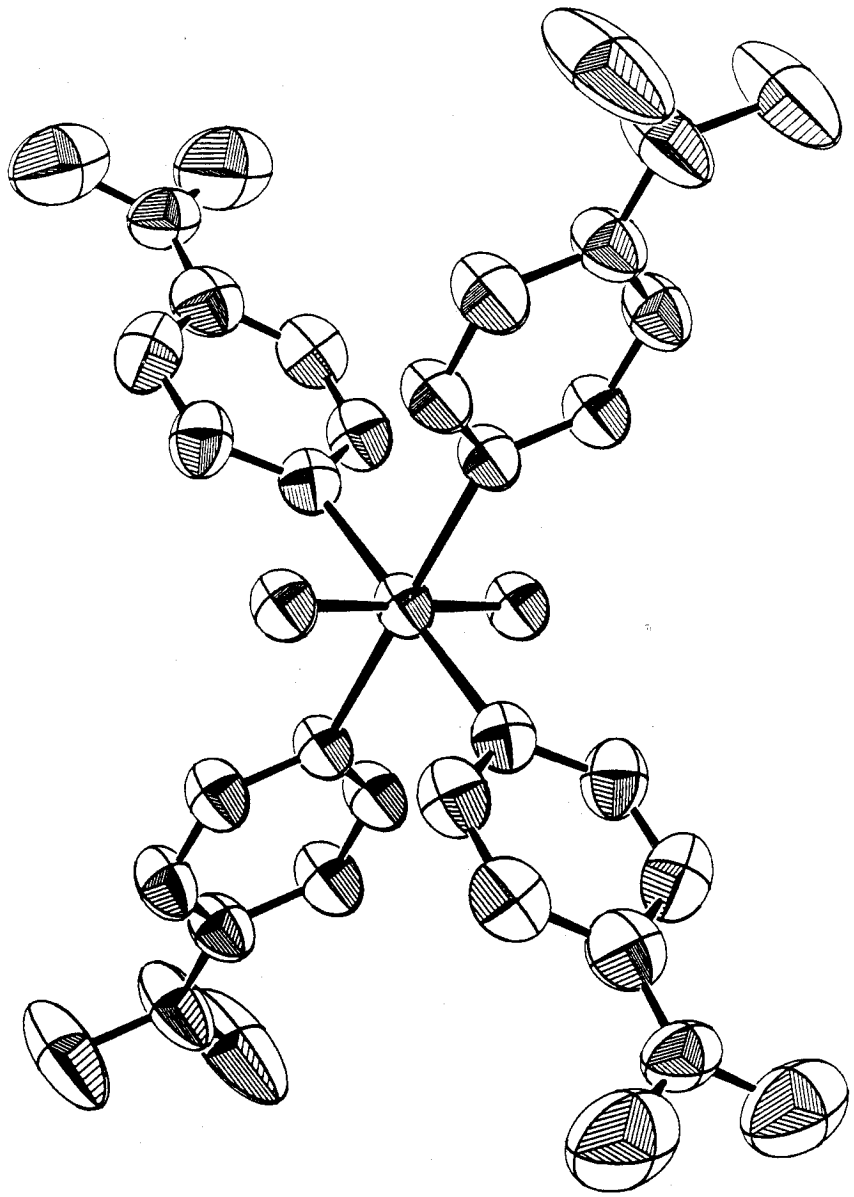

Figure 4.4. Atomic numbering scheme used for the *trans*-$[ReO_2(dmap)_4][PF_6]_2$ structure determination.

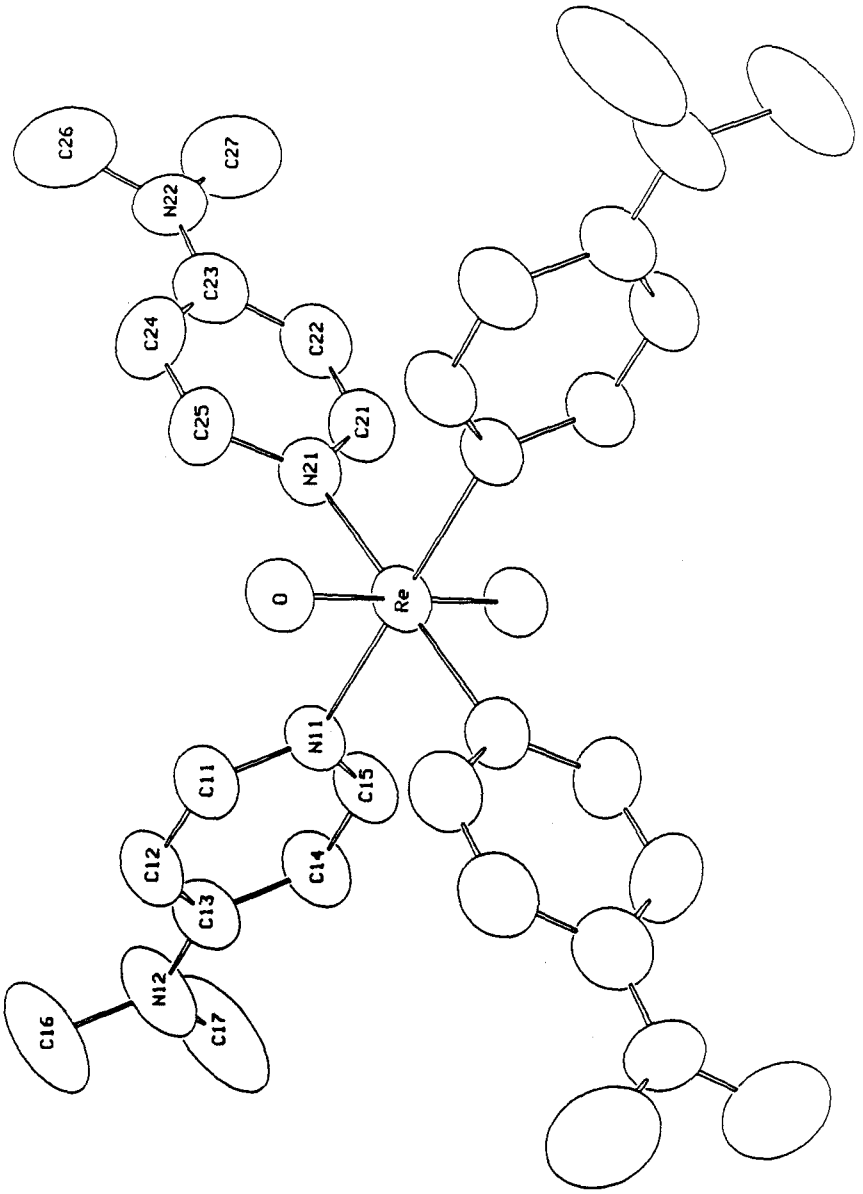
C26
C27
N22
C23
C24
C22
C25
C21
N21
O
Re
N11
C11
C15
C12
C14
C13
N12
C16
C17

Figure 4.5. A view down the O=Re=O axis of the *trans*-$[ReO_2(dmap)_4][PF_6]^{2+}$ molecule.

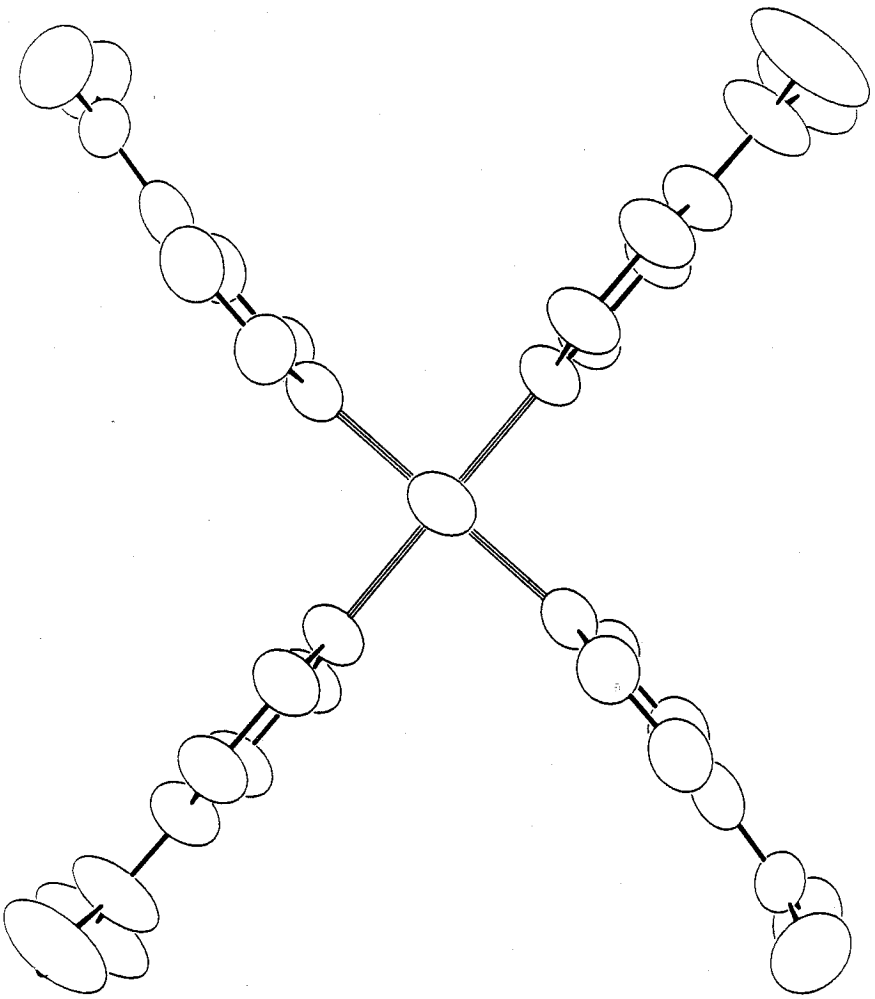

Figure 4.6. The unit cell of *trans*-$[ReO_2(dmap)_4][PF_6]_2$ structure.

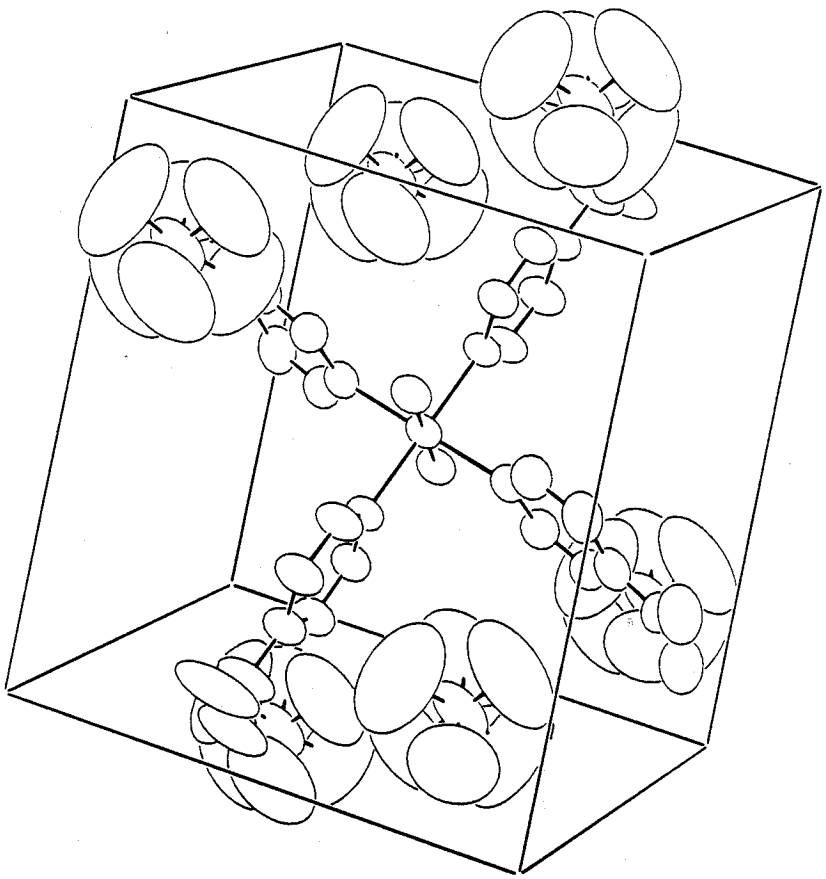

and 359.4°. The amino-ring bond length is very short, only 1.319(9) Å for C13–N12 and 1.298(10) Å for C23–N22, indicating significant double-bond character.[21] The NMe_2 groups are tilted slightly with respect to the pyridine ring; the dihedral angles are 178.5(9.1)° and 168.7(9.5)°. The remaining ligand bond lengths and angles are normal.

The anion is slightly disordered. The P–F bond lengths range from 1.415(15) to 1.521(12) Å (average: 1.469 Å), and the F–P–F angles for adjacent fluorine atoms vary from 81.7(7) to 97.0(7)°.

To determine if any unusual features were present in this structure, a comparison was made with the X-ray structure data gathered on the following materials : dmap,[22] dmap•HCl,[23] 1,1'-methylenebis(4,4'-dimethylaminopyridinium)iodide,[24] *trans*-$[ReO_2(py)_4]Cl•2H_2O$,[25,26] and *trans*-$[ReO_2(4\text{-pic})_4][ReO_4]$.[27]

The Re–O bond length is essentially identical between the three complexes *trans*-$[ReO_2(py)_4]Cl•2H_2O$, *trans*-$[ReO_2(4\text{-pic})_4][ReO_4]$ and *trans*-$[ReO_2(dmap)_4][PF_6]_2$ (1.76, 1.75, 1.76 Å, respectively). The MO description of *trans*-$[ReO_2(L)_4][PF_6]$ (Figure 4.2) shows the highest-lying electron pair to be in the non-bonding orbital Re d_{xy}. Therefore, a 1-e^- oxidation would not be expected to cause a disturbance in any bond lengths or angles. This concurs with what is observed.

There is a slight contraction in the Re–N distance in *trans*-$[ReO_2(dmap)_4][PF_6]_2$ compared to *trans*-$[ReO_2(py)_4]Cl•2H_2O$ and *trans*-$[ReO_2(4\text{-pic})_4][ReO_4]$ (2.11, 2.15 and 2.14 Å, respectively). This could be due to an electrostatic effect (the Re(VI) species has one full unit higher formal charge) or a π-bonding interaction between the filled π-level of dmap and the half-empty d_{xy} orbital on Re. Evidence supporting the last hypothesis is (1) the minimal amount of twisting of the dmap plane with respect to the O=Re=O axis, (2) the short Me_2N-py bond distance, and (3) the shorter Re–N bond length. A pure σ-effect would not require minimal twisting between the pyridine ring plane and the O=Re=O axis. Ring twisting (10 - 20°) has been observed in the X-ray structures of other *trans*-$[ReO_2(L)_4]^+$ pyridine complexes[25-27] and has been attributed to both crystal packing

effects, and the result of steric congestion between the oxo ligands and the *ortho*–H's on pyridine.[26] The latter effect should be even more pronounced as the Re–N distance contracts. Therefore, it is somewhat surprising that the pyridine planes are almost perfectly parallel with the O=Re=O vector.

Structural data that are available for the dmap ligand and a related compound are presented in Table 4.6. The atom numbering scheme used to identify bond distances is provided below the table. Note that the C_4–C_3 and C_4–C_5 bonds are considerably longer (~1.41 Å) than other C-C bonds in the aromatic ring (~1.35 Å). The NMe_2-pyridine ring bond distance is substantially shorter (~1.34 Å) than a single C-N bond (~1.46 Å), indicating double-bond character. These features suggest that there is appreciable quinoidal character to the dmap ring, as depicted by the resonance structures drawn in Figure 4.7. This explains the superior donating ability of this particular pyridine derivative. The lack of significant change in the bond lengths and angles of the *trans*-ReO_2 unit between the Re(V) and Re(VI) complexes suggests that resonance structures resulting in formal reduction of Re(VI) to Re(V) with concomitant development of oxo-radical character are not accurate descriptions of the bonding in *trans*-$[ReO_2(L)_4]^{2+}$ complexes.

EPR spectra of *trans*-$[ReO_2(dmap)_4][PF_6]_2$. Although hexavalent states are rare for rhenium, there have been several studies completed on the EPR of d^1 rhenium compounds.[28-37] There are two naturally occurring isotopes of rhenium. Both of them are spin active (I = 5/2) with almost identical nuclear moments (^{185}Re, 37.07%, 3.143 μ_N ; ^{187}Re, 62.93%, 3.176 μ_N).[28,38] The small difference in moments is not sufficient, however, to generate separate line manifolds in any spectra that have been observed to date.

The EPR spectra of Re(VI) species are often challenging to interpret because of the extremely large Re hyperfine and quadrupole coupling constants associated with tetragonal geometries of this ion.[28,31,32,39,40] As a result, the spectra exhibit (1) variations in band

Table 4.6. Bond length data for dmap and dmap-like molecules obtained from other X-ray structure determinations. The number scheme used to identify bond lengths is illustrated below the table.

compound	N_2–C_4	C_4–C_3	C_3–C_2	C_2–N_1	N_1–M
dmap	1.367(2)	1.404(3)	1.375(3)	1.335(3)	---
dmap•HCl•$2H_2O$	1.340[a]	1.421[a]	1.350[a]	1.343[a]	1.06[a]
1,1'-methylenebis(4,4'dimethylamino pyridinium)iodide •H_2O	1.333(4)	1.419(4)	1.351(4)	1.345(4)	1.468(4)
trans-[ReO_2(dmap)$_4$][PF_6]$_2$	1.309[a]	1.405[a]	1.352[a]	1.357[a]	2.114[a]

[a]In structures where the distances were not uniquely defined, an average value has been determined.

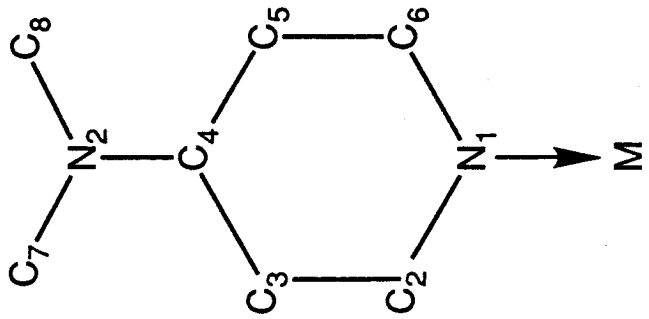

Figure 4.7. Important resonance structures for the dmap ligand. The bottom structure represents the best description of electron density distribution in the dmap ligand.

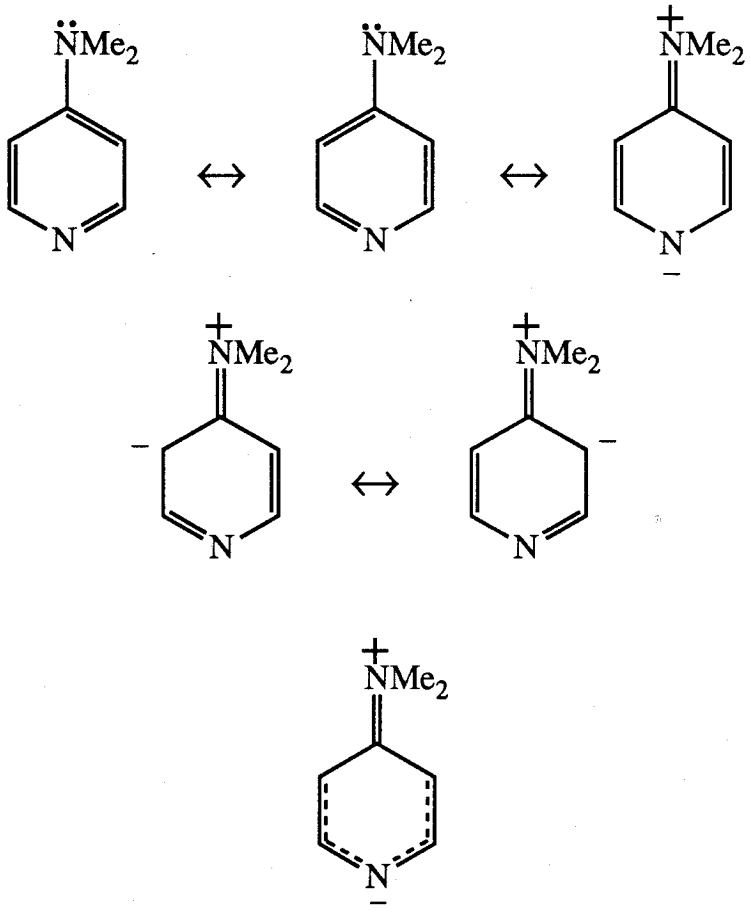
NMe2
N
NMe2
N
NMe2
N
NMe2
N
NMe2
N
NMe2
N

intensities for $\Delta M_I = 0$ transitions, (2) unequal Re hyperfine spacing, (3) the presence of forbidden features due to $\Delta M_I = \pm 1, \pm 2$ transitions, and (4) intense features at off axis turning points.[32] These complications are evident in the spectra of $ReOCl_4$, $[ReOF_5]^-$, $[ReNCl_4]^-$,and *trans*-$[ReO_2(dmap)_4]^{2+}$.

No EPR signal could be detected for *trans*-$[ReO_2(dmap)_4][PF_6]_2$ in CH_3CN, CH_3OH or acetone solutions. The EPR of a solid (powder) sample gave a single line with <g>~1.91. In attempt to obtain a better spectrum, a dilute (~10 μM) 50% aqueous DMSO solution was examined at 7 K (Figure 4.8 (A)). The large $A_{||}$ hyperfine coupling is apparent from the two outermost transitions of the parallel manifold (labelled a). The magnitude of $A_{\perp}$ is somewhat smaller; the outermost transitions of the perpendicular manifold are labelled b. The number of lines is greater than the six parallel and six perpendicular features expected for an axially symmetric system with I = 5/2. The extra features arise from $\Delta M_I = \pm 1$ (*e.g.*, peak c) and $\Delta M_I = \pm 2$ (*e.g.*, peak d) transitions and their off-axis turning points. The strength of these features is indicative of a large quadrupole coupling constant, which increases the probability of the forbidden transitions.[39,40] In some cases, the intensity of the forbidden transitions is even higher than the allowed transitions.

In order to estimate the g and hyperfine coupling values, a simulation was performed using the QPOW program,[7] which calculates a second-order spectrum with quadrupole coupling and forbidden transitions. The simulation that best represents the experimental spectrum is shown in Figure 4.8 (B). It was generated using the following parameters: $g_{\perp} = 1.91$, $A_{\perp} = 0.031\ cm^{-1}$, $g_{||} = 1.83$, $A_{||} = 0.060\ cm^{-1}$, and $Q_z = 0.0075\ cm^{-1}$. Note that the simulation accounts for all of the major transitions and reproduces qualitatively the experimental intensity pattern. Unfortunately, the calculation is complicated by the strong intensity of the forbidden transitions resulting from the large quadrupole coupling. The EPR results of related Re(VI) complexes are collected in Table 4.7.

Figure 4.8. (A) EPR spectrum at 7 K of $[ReO_2(DMAP)_4](PF_6)_2$ (~10 μM) in 50% DMSO. Microwave frequency: 9.0505 GHz. Modulation frequency: 100 kHz. Modulation amplitude: 10 G. Microwave power: 0.05 mW. a: outermost peaks in the parallel manifold. b: outermost peaks in the perpendicular manifold. c: $\Delta M_I = \pm 1$ transition. d: $\Delta M_I = \pm 2$ transition. (B) Simulated spectrum calculated using $g_\perp = 1.91$, $A_\perp = 0.031\ cm^{-1}$, $g_{||} = 1.83$, $A_{||} = 0.060\ cm^{-1}$, and $Q_z = 0.0075\ cm^{-1}$.

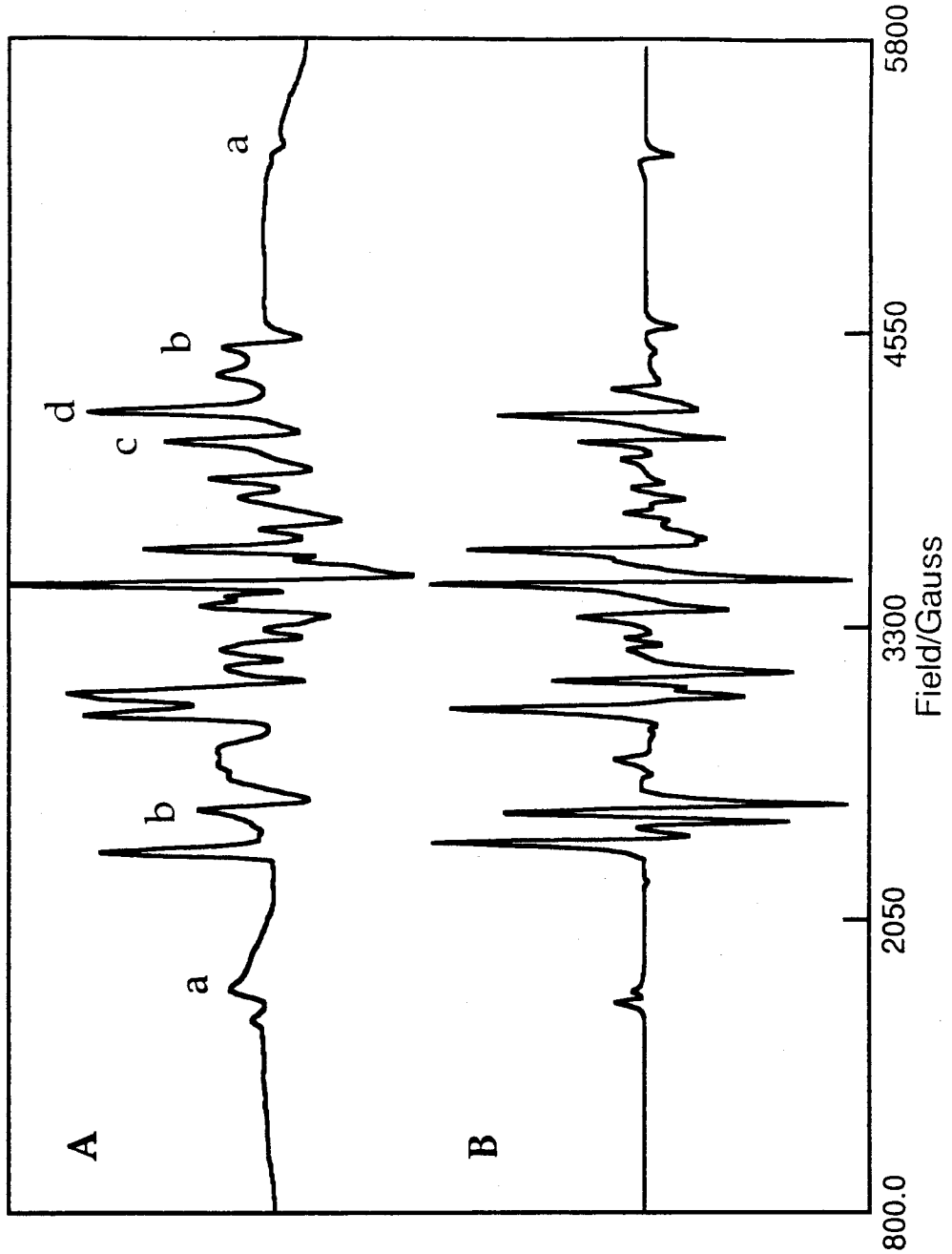
A
B
a
b
c
d
a
b
800.0
2050
3300
4550
5800
Field/Gauss

Table 4.7. EPR data for some Re(VI) complexes also containing π-bonds.

compound	$g_{\perp}$	$A_{\perp}$ (cm^{-1})	$g_{\|\|}$	$A_{\|\|}$ (cm^{-1})	$\|Q_z\|$ (cm^{-1})	Ref
$[ReO_2(dmap)_4][PF_6]_2$[a]	1.91	-0.031	1.83	-0.060	0.0075	this work
$[Ph_4As][ReNCl_4]$[b]	1.934	-0.0382	1.909	-0.077	0.0047	32
$ReOCl_4$[c]	1.720	-0.0320	1.968	-0.0630	0.0020	28
$ReOCl_4(NCCH_3)$[d]	1.732	-0.0315	1.970	-0.0621	0.0020	28
$ReOCl_4(OPCl_3)$[e]	1.734	-0.0308	1.97	-0.0616	0.0019	28
$[Ph_4As][ReOCl_5]$[c]	1.740	-0.0305	1.975	-0.0609	0.0020	28
$[H_3O][ReOF_5]$[f]	1.74	-0.0500	1.72	-0.0960	0.0045	31

[a]frozen 50% aqueous DMSO, 7 K

[b]frozen CH_3CN, 110 K

[c]frozen dioxane, 77 K

[d]frozen CH_3NO_2, 77 K

[e]frozen $OPCl_3$, 77 K

[f]frozen anhydrous HF, 77 K

First order perturbation theory predicts that $g_{||} < g_{\perp} < 2.0023$. Note that this is not the case for nitrido- and oxorhenium(VI) chlorides. In these cases, the order $g_{||} > g_{\perp}$ is attributable to the effect of spin-orbit coupling of a $(Cl)_4$ d_{xy}-symmetry hole associated with in-plane π-bonding between the Re d_{xy} orbital and equitorial ligand π-orbitals.[36]

The low energy LMCT transition of *trans*-$[ReO_2(dmap)_4][PF_6]_2$ indicates the energetic proximity of the filled π-levels of the dmap ligand to the Re d_{xy} orbital. Therefore, in-plane π-bonding between dmap and Re is likely significant in *trans*-$[ReO_2(dmap)_4][PF_6]_2$. This does *not*, however, perturb the g-values because nitrogen has a very small spin-orbit coupling constant ($\xi_N = 70$ cm^{-1}).[41]

In contrast to nitrogen, chlorine has a large spin-orbit coupling constant ($\xi_{Cl} = 587$ cm^{-1})[41] and, therefore, any in-plane π -bonding involving this ligand dramatically affects g-values. The g-values of $[Ph_4As][ReNCl_4(NCCH_3)]$ are not inverted (in contrast to $ReOCl_4$), suggesting in-plane Cl π-bonding is not important in this complex.[32]

Several attempts have been made to evaluate the degree of covalency in Re(VI) complexes using the results obtained from EPR spectra. The analysis is complex and hindered by the lack of good values for both orbital wavefunctions and Re spin-orbit coupling constants.

Gray and Ballhausen[17] employed a semi-empirical MO approach to analyse the electronic structure of the vanadyl ion, $[VO(OH_2)_5]^{2+}$. The molecular orbitals used were of the form

$$\psi^b = c_1\Phi(\text{metal}) + c_2\Phi(\text{ligand}) \qquad (4)$$

$$\psi^* = c_1^*\Phi(\text{metal}) + c_2^*\Phi(\text{ligand}) \qquad (5)$$

for the bonding and antibonding wavefunctions, respectively. The orbitals Φ(metal) and Φ(ligand) refer to the proper combination of metal and ligand orbitals for a given representation. The g values of the complex are related to the d-orbital coefficients and

state energies by the following equations:

$$g_{\perp} = 2(1 - (c_1^*)^2\xi/\Delta E(^2B_{2g} \rightarrow {}^2E_g)) \quad (6)$$

$$g_{||} = 2(1 - (c_1^*)^2 4\xi/\Delta E(^2B_{2g} \rightarrow {}^2B_{1g})) \quad (7)$$

The relevant d-orbitals are (d_{xz}, d_{yz}) and $d_{x^2-y^2}$ respectively and ξ is the metal spin-orbit coupling constant. As discussed earlier, the LF transitions are not observed in *trans*-$[ReO_2(dmap)_4][PF_6]_2$ but can be estimated to be at 25,000 and 36,000 cm^{-1} (for $^2B_{2g} \rightarrow {}^2E_g$ and $^2B_{2g} \rightarrow {}^2B_{1g}$, respectively). The actual value of ξ is unknown and must be estimated. If one plots ξ versus the charge (z) of the free Re ion,[20,42] a linear relationship is obtained: $\xi = (540(z) + 1000)cm^{-1}$. If it is assumed that due to charge neutralization effects, the residual charge on Re will be 2^+, then $\xi = 2080\ cm^{-1}$ would be a good estimate.[28] Using all of the above information, one obtains $c_1^*(d_{xz}, d_{yz}) = 0.735$ and $c_1^*(d_{x^2-y^2}) = 0.606$, indicating appreciable covalency in both the Re-oxo and Re-py bonds. MO coefficients calculated for some other Re(VI) complexes are presented in Table 4.8. These have been obtained by a variety of methods. Note that in *trans*-$[ReO_2(dmap)_4][PF_6]_2$ the Re-oxo bonds are appreciably more covalent than in the oxohalide complexes. There is also appreciable covalency in the equitorial bonds. MO coefficients for the imido complex calculated by the method of Ballhausen and Gray are 0.557 and 0.365 for (d_{xz},d_{yz}) and $d_{x^2-y^2}$, respectively, and these are in good agreement with values obtained by an independent method (Table 4.8).[32]

It should be noted that others have claimed that the semi-empirical treatment overestimates bond covalency,[43] so that one may view the coefficients obtained as lower limits. Another source of error is the fact that no provision has been made for equitorial ligand-d_{xy} π-bonding.

Table 4.8. MO coefficients for d_{xy}, (d_{xz},d_{yz}), and $d_x{}^2{}_{-y}{}^2$ orbitals for some selected Re(VI) complexes.

compound	$c_1{}^*(d_{xy})$	$c_1{}^*(d_{xz},d_{yz})$	$c_1{}^*(d_x{}^2{}_{-y}{}^2)$	Ref
$[ReO_2(dmap)_4][PF_6]_2$	–	0.735	0.606	here
$[Ph_4As][ReNCl_4(NCCH_3)]$	0.811	0.512	0.449	32
$ReOCl_4$	0.820	0.920	0.780	28
$ReOCl_4(NCCH_3)$	0.809	0.907	0.781	28
$ReOCl_4(OPCl_3)$	0.808	0.906	0.781	28
$[Ph_4As][ReOCl_5]$	0.805	0.903	0.780	28
$[H_3O][ReOF_5]$	0.85	0.92	0.78	31

In axially symmetric systems where the unpaired electron is coupled to a nucleus with a high quadrupole moment such as Re ($Q(^{185}Re) = 2.8 \times 10^{24}/cm^2$, $Q(^{187}Re) = 2.6 \times 10^{24}/cm^2$), the magnitude of Q_z reflects the concentration of charge along the z-axis, which induces a large electric-field gradient in the complex.[39,40] As evident in Table 4.7, Q_z generally increases in the order $ReO^{4+} < ReN^{3+} < ReO_2{}^{2+}$. In addition, estimated LF energies ($d_{xy} \rightarrow d_{xz},d_{yz}$) increase with Q_z,[28,31,32] consistent with an increase in π-bonding on going from monooxo to mononitrido to *trans*-dioxo axial units. This combined spectroscopic evidence emphasizes dramatically the strong axially compressed tetragonal ligand field associated with the *trans*-dioxo moiety.

***Trans*-$[ReO_2(L)_4]^{2+}$ reactivity.** As mentioned in the introduction, *trans*-$[ReO_2(py)_4]^{2+}$ behaved as a potent oxidant towards silanes, halocarbons and secondary alcohols.[1,2] Cyclic voltammograms of *trans*-$[ReO_2(py)_4]^+$ were indicative of this reactivity; anodic current enhancement was observed when oxidizable substrates were added to the compound solutions. *Sec*-phenethylalcohol was converted to acetophenone at

1.5 V vs. SSCE with 90 ± 5% current efficiency and three 'turn-overs' of Re complex.[1,2] The term turn-over is used loosely here as no defineable Re species was found at the end of the experiment.

It was thought that the Re(VI) complexes possessing milder oxidizing potentials might be less prone to decomposition reactions and hence, more efficient catalysts. *Trans*-$[ReO_2(4\text{-}MeOpy)_4]^{2+}$ is ~300 mV less oxidizing than *trans*-$[ReO_2(py)_4]^{2+}$ and unlike it, accumulates during bulk electrolysis experiments. Cyclic voltammograms of *trans*-$[ReO_2(4\text{-}MeOpy)_4]^{2+}$ are unperturbed when *sec*-phenethylalcohol is added. Bulk electrolysis at 1.2 V vs. SSCE in the presence of a 100-fold excess of alcohol yields no appreciable ketonic product; after 15 hours only 10 coulombs (3 equivalents of charge based upon Re) are passed, indicating some slow decompostion process. Isolated samples of *trans*-$[ReO_2(dmap)_4]^{2+}$ are also ineffective oxidants. Thus, the oxidation of alcohols with *trans*-$[ReO_2(L)_4]^{2+}$ appears to be limited to the unsubstituted pyridine complex.

Since the series of pyridine complexes are isoelectronic and differ essentially only in redox potential, it is likely that the lack of activity observed is due to the lowering of the Re(VI)/Re(V) couple. The rate-limiting step in the reaction sequence is likely to be the abstraction of one electron from the alcohol, and the efficiency of this step will depend upon the oxidizing strength of the metal complex. Wong and Anson[44] completed a detailed study of electrochemical oxidations of benzylalcohol mediated by oxoruthenium(IV) amine complexes. The compounds studied and the relevant electrochemical couples are set out in Table 4.9. Comparison of results obtained for benzylalcohol to those for *sec*-phenylethylalcohol is valid since the weakest C-H bonds in the two molecules are of identical strength (~85 kcal mol^{-1}).[45]

Table 4.9. Ruthenium(IV) oxo complexes that mediate electrooxidation of benzylalcohol. Potentials are measured in 0.1 M $[Et_4N][BF_4]$ CH_3CN solutions.

complex	$E_{1/2}$, V vs. Fc^+/Fc
trans-[Ru(TMC)O(Cl)][ClO_4]	1.05
trans-[Ru(TMC)O(NCO)][ClO_4]	0.89
trans-[Ru(TMC)O(N_3)][ClO_4]	0.72

The authors noted that benzylalcohol is not oxidized at glassy carbon at potentials less positive than 1.2 V vs. Fc^+/Fc, so the activity observed must have originated from the Ru(V) complexes. Rotating-disk electrode and bulk electrolysis studies suggested the oxidations occurred via the following mechanism:

$$Ru(IV) - e^- \rightleftharpoons Ru(V) \quad (8)$$

$$Ru(V) + PhCH_2OH \xrightarrow{k} Ru(IV) + PhCH\bullet(OH) + H^+ \quad (9)$$

$$Ru(V) + PhCH\bullet(OH) \xrightarrow{fast} Ru(IV) + PhCHO + H^+ \quad (10)$$

Ru = coordinated ruthenium species

The proposed rate-limiting step is a bimolecular electron transfer between the electrochemically generated Ru(V) species and the alcohol substrate. Bimolecular rate constants of 2.1×10^2 and 1.4×10^2 M^{-1} s^{-1} were measured for the Cl^- and NCO^- complexes, respectively. The azide catalyst was too sluggish for reliable kinetic measurements. The general trend observed was a decrease in catalyst efficiency with decreasing oxidation potential of the Ru complexes.

It has been proposed that the oxo ligand receives the proton released from the alcohol upon (a 1 e^-) oxidation.[44] It is more likely that the oxo group assists in the simultaneous

transfer of an electron and a proton (H• transfer). This would not be possible in complexes where the ligands lack basic sites: The Ru(IV) complex *trans*-$[Ru(TMC)Cl_2]^{2+}$ is a potent 1 e^- oxidant ($E_{1/2}$ ~1.15 V vs. Fc^+/Fc) but an extremely poor catalyst for alcohol electrooxidation.

It has long been known that *trans*-$[ReO_2(L)_4]^+$ complexes can be protonated in acidic solutions,[46-53] indicating that the oxo group is capable of acting as a surrogate base. There is also substantial evidence from UV-vis spectroscopy,[19,54,55] ^1H NMR,[1,2,56] emission spectroscopy,[1,2,19,54-56] and luminescence decay data[2,19,55,56] that alcohol complexation occurs with *trans*-$[ReO_2(py)_4]^+$. Thus, the electrooxidation of secondary alcohols by *trans*-$[ReO_2(py)_4]^{2+}$ likely takes place via a H• abstraction mechanism as shown in Figure 4.9. The Re(VI) pyridine complex must represent the lower limit of oxidizing strength required to realize this reaction.

The final issue to be addressed in the properties of the Re(VI) complexes is the instability towards reduction observed in the presence of halides and basic agents. As mentioned in previous sections, the Re(VI) complexes react rapidly under basic conditions to regenerate the corresponding Re(V) species. All absorption bands present in UV-vis spectra could be assigned to the Re(V) complexes. This result was puzzling since the source of reducing equivalents was not obvious; the hydroxide ligand is not a strong reducing agent ($E_{1/2}$ ~1.89 V vs. NHE).[57]

This behavior is remarkably reminiscent of that observed for $[M(bpy)_3]^{3+}$ and $[M(phen)_3]^{3+}$ (M= Fe, Ru, Os) complexes.[58,59] Meyer has also observed metal complex self-reduction in basic solutions of $[(bpy)_2(py)Ru(O)]^{2+}$ and $[(trpy)(phen)Ru(O)]^{2+}$.[60] Each complex has its own manifold of complex reactions. The mechanism presented in Figure 4.10 has been proposed[58,60] for hydroxide-induced, self-reduction of $[Ru(bpy)_3]^{3+}$.

Figure 4.9. Proposed mechanism of alcohol electrooxidation by *trans*-$[ReO_2(py)_4]^{2+}$.

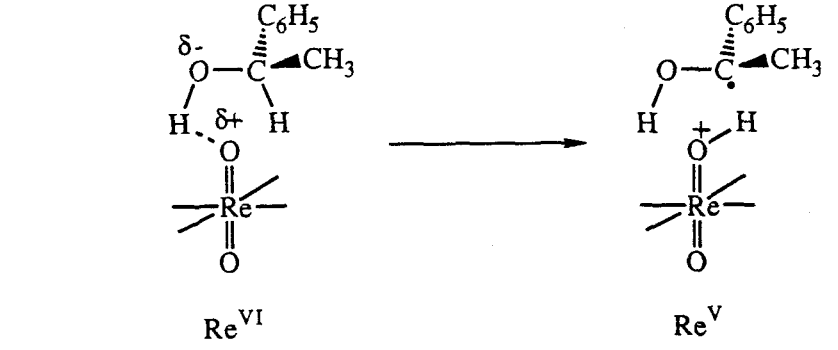
δ-
δ+
Re
Re
Re^VI
Re^V

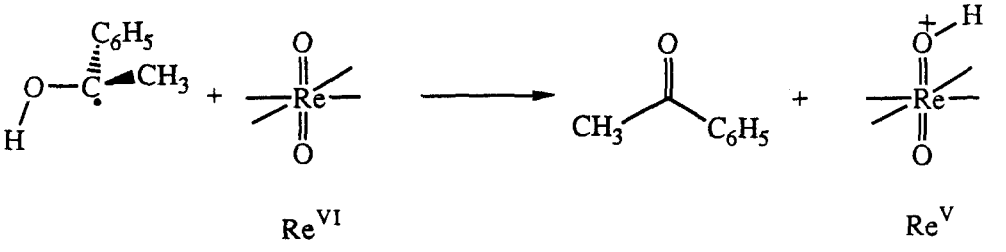
Re
Re
Re
Re^VI
Re^V

Figure 4.10. Proposed mechansim of base-induced self-reduction of $[Ru(bpy)_3]^{3+}$.

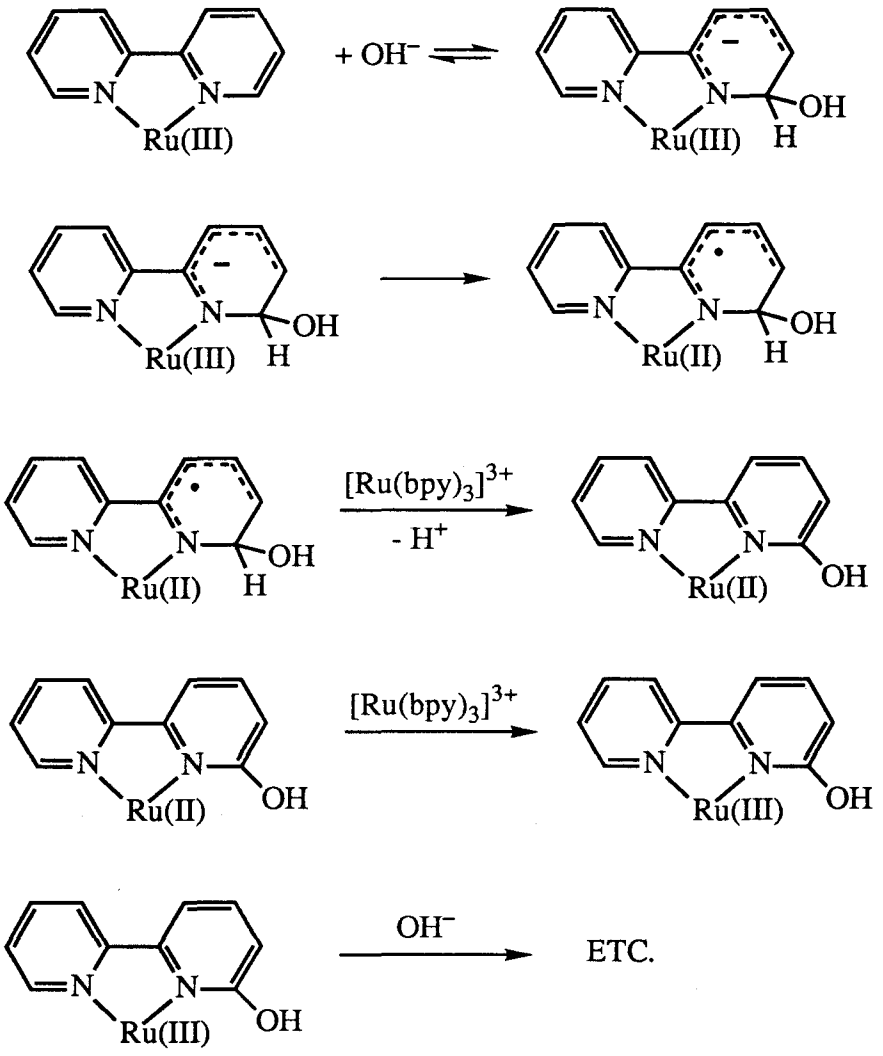

Part of the coordination sphere of ruthenium has been omitted for clarity.

After nucleophilic attack on the bipyridyl ring, an intramolecular electron-transfer event occurs to produce a coordinated hydroxy-bipyridyl radical and ruthenium(II). This species is oxidized by a molecule of $[Ru(bpy)_3]^{3+}$ and loses a proton from the aromatic ring, restoring aromaticity. The resulting complex $[(bpy)_2Ru(bpyOH)]^{2+}$ is oxidized by another $[Ru(bpy)_3]^{3+}$ molecule and the cycle continues, generating ruthenium complexes of bipyridyl ligands with varying degrees of hydroxylation. The net result is that after a given redox cycle, 90% of the original ruthenium(III) complex appears as $[Ru(bpy)_3]^{2+}$. A list of complexes known to undergo self-reduction is provided in Table 4.10 along with the relevant redox potentials.[61-64]

The least oxidizing Re(VI) complex under study has a reduction potential of ~0.5 V vs. SCE. It is therefore possible that analogous reactions take place on the coordinated pyridine ligands in *trans*-$[ReO_2(L)_4]^{2+}$ complexes. The susceptibility towards further hydroxylation (oxidation) results from the effect of hydroxyl groups on pyridine basicity. The pKa's of the conjugate acids of pyridine, 2-hydroxy-, 3-hydroxy- and 4-hydroxypyridine are 5.23, 11.65, 8.75, and 11.12, respectively.[65] From this data, it is clear that as pyridine ligands become hydroxylated in *any* position, they become better σ-donors towards the metal center. This in turn will make the corresponding Re complexes easier to oxidize. The net result will be the reduction of several molecules of *trans*-$[ReO_2(L)_4]^{2+}$ via the degradative hydroxylation of one molecule of $[ReO_2(L-\{OH\}_x)_4]^{+}$.

It is possible that degradation reactions observed in the presence of halides could be inititated in an analogous fashion, but the follow up chemistry is likely to be quite different as halogen substitution makes pyridine ligands *poorer* electron donors.

Table 4.10. Complexes that undergo self-reduction in basic solutions and their associated redox potentials. Potentials were measured in 0.1 M TBAP CH_3CN solution vs. SCE unless noted otherwise.

complex	$E_{1/2}$ for one electron reduction, V vs. SCE	reference source
$[Fe(bpy)_3]^{3+}$	1.03	64
$[Ru(bpy)_3]^{3+}$	1.20	64
$[Os(bpy)_3]^{3+}$	0.81	64
$[Fe(phen)_3]^{3+}$	1.02[a]	63
$[Ru(phen)_3]^{3+}$	1.40[b]	62
$[Os(phen)_3]^{3+}$	0.60[c]	61
$[(bpy)_2(py)Ru(O)]^{2+}$	0.53[d]	60
$[(trpy)(phen)Ru(O)]^{2+}$	0.58[d]	60

[a] 1 M H_2SO_4

[b] 0.1 M $[TBA][BF_4]$ CH_3CN

[c] 0.1 M $NaNO_3$

[d] vs. SSCE, pH = 7.0; μ = 1.0 M

CONCLUSIONS

The reactivity, X-ray structure, electronic structure and EPR studies completed on *trans*-$[ReO_2(dmap)_4][PF_6]_2$ and related compounds provide insight into the nature of *trans*-$[ReO_2(L)_4]^{2+}$. Strongly basic pyridine ligands stablize the *trans*-dioxorhenium(VI) unit due to their favorable σ-properities and their ability to provide π-electron density to the Re d_{xy} hole. The latter interaction is suggested by (1) the small dihedral angle between the O=Re=O vector and the dmap rings in *trans*-$[ReO_2(dmap)_4][PF_6]_2$, and (2) the low energy LMCT transition (dmap $\pi \rightarrow$ Re d_{xy}) present in its UV-vis spectrum. The results of the EPR analysis suggest considerable covalency in Re-oxo and Re-dmap bonds with the unpaired electron being primarily localized in Re d_{xy}. There is no indication of any substantial delocalization of this hole onto the oxo ligands. The high quadrupole splitting observed is consistent with the strong axial field generated by the two *trans* oxo ligands.

The ability of *trans*-$[ReO_2(L)_4]^{2+}$ complexes to effect alcohol oxidation appears to be governed by the Re(VI)/Re(V) redox couple. More oxidizing potentials lead to substrate reactivity but also result in very unstable Re(VI) complexes. Oxidation of Re(V) to Re(VI) makes the pyridine rings susceptible to nucleophilic attack and this is likely responsible for the instablity of highly oxidizing *trans*-$[ReO_2(L)_4]^{2+}$ complexes. Thus, the design of more efficient agents will likely require use of a poorly donating set of equitorial ligands that are robust to both electron abstraction and nucleophilic attack.

REFERENCES AND NOTES

(1) Thorp, H. H.; Van Houten, J.; Gray, H. B. *Inorg. Chem.* **1989**, *28*, 889-892.

(2) Thorp, H. H.; Ph.D. thesis, June 1989, California Institute of Technology.

(3) Nugent, W. A.; Mayer, J. M. *Metal-Ligand Multiple Bonds*; John Wiley and Sons: New York, 1988.

(4) Jolly, W. L. *The Synthesis and Characterization of Inorganic Compounds*; Prentice-Hall: Englewood Cliffs, N. J., 1970; pp 484-488.

(5) International Union of Crystallography *International Tables for X-ray Crystallography*; Kynock: Birmingham, England, 1974; Vol. 4, pp 71, 149.

(6) Beck, W. F.; Innes, J. B.; Lynch, J. B.; Brudvig, G. W. *J. Mag. Res.* **1990**, in press.

(7) The EPR spectrum was simulated using PROGRAM QPOW, written by R.L. Belford, A.M. Maurice, and M.J. Nilges: Nilges, M.J., Ph.D. Thesis, University of Illinois, Urbana, Illinois, 1979. Belford, R.L.; Nilges, M.J. *Computer Simulation of Powder Spectra*; EPR Symposium, 21st Rocky Mountain Conference, Denver, Colorado, 1979. Maurice, A.M., Ph.D. Thesis, University of Illinois, Urbana, Illinois, 1980.

(8) Prins, R. *J. Chem. Soc. Chem. Commun.* **1970**, 280-281.

(9) Sohn, Y. S.; Hendrickson, D. N.; Gray, H. B. *J. Am. Chem. Soc.* **1970**, *92*, 3233-3234.

(10) Bard, A. J.; Faulkner, L. R. *Electrochemical Methods. Fundementals and Applications*; John Wiley and Sons: New York, 1980.

(11) Abakumova, L. G.; Abakumov, G. A.; Razuvaev, G. A. *Dokl. Akad. Nauk. SSSR.* **1975**, *220*, 1317-1320.

(12) Burova, T. V.; Trembovler, V. N.; Yavorsky, B. M.; Fock, N. V.; Materikova, R. B.; Kochetkova, N. S. *J. Organomet. Chem.* **1981**, *217*, 215-219.

(13) Kochetkova, N. S.; Materikova, R. B.; Belousov, Y. A.; Salimov, R. M.; Babin, V. N. *J. Organomet. Chem.* **1982**, *235*, C21-C24.

(14) Cotton, F. A. *Chemical Applications of Group Theory*; 2nd ed.; Wiley-Interscience: New York, 1971; p 264.

(15) Ballhausen, C. J.; Gray, H. B. *Molecular Orbital Theory*; Benjamin/Cummings: London, 1978.

(16) Gray, H. B.; Ballhausen, C. J. *J. Am. Chem. Soc.* **1963**, *85*, 260-265.

(17) Ballhausen, C. J.; Gray, H. B. *Inorg. Chem.* **1962**, *1*, 111-122.

(18) Jezowska-Trzebiatowska, B.; Wajda, S.; Baluka, M. *Zh. Struk. Khim.* **1967**, *8*, 519-523.

(19) Winkler, J. R.; Gray, H. B. *Inorg. Chem.* **1985**, *24*, 346-355.

(20) Figgis, B. N. *Introduction to Ligand Fields*; Interscience: New York, 1966; p 66.

(21) Chao, M.; Schempp, E. *Acta Cryst.* **1977**, *B33*, 1557-1564.

(22) Ohms, U.; Guth, H. *Z. Kristallogr.* **1984**, *166*, 213-217.

(23) Chao, M.; Schempp, E.; Rosenstein, R. D. *Acta Cryst.* **1977**, *B33*, 1820-1823.

(24) Munavalli, J.; Poziomek, E. J.; Day, C. S. *Acta Cryst.* **1988**, *C44*, 272-275.

(25) Lock, C. J. L.; Turner, G. *Acta Cryst.* **1978**, *B34*, 923-927.

(26) Calvo, C.; Krishnamachari, N.; Lock, C. J. L. *J. Cryst. Mol. Struct.* **1971**, *1*, 161-172.

(27) Johnson, J. W.; Brody, J. F.; Ansell, G. B.; Zentz, S. *Inorg. Chem.* **1984**, *23*, 2415-2418.

(28) Al-Mowali, A. H.; Porte, A. L. *J. Chem. Soc., Dalton Trans.* **1975**, 50-55.

(29) Baldas, J.; Boas, J. F.; Bonnyman, J.; Pilbrow, J. R.; Williams, G. A. *J. Am. Chem. Soc.* **1985**, *107*, 1886-1891.

(30) Gibson, J. K.; Lack, G. M.; Mertis, K.; Wilkinson, G. *J. Chem. Soc. Dalton Trans.* **1976**, 1492-1495.

(31) Holloway, J. H.; Raynor, J. B. *J. Chem. Soc., Dalton Trans.* **1975**, 737-741.

(32) Lack, G. M.; Gibson, J. F. *J. Mol. Struct.* **1978**, *46*, 299-306.

(33) Lahiri, G. K.; Goswami, S.; Falvello, L. R.; Chakravorty, A. *Inorg. Chem.* **1987**, *26*, 3365-3370.

(34) Larin, G. M.; Bukharizoda, R. A.; Rakitin, Y. V.; Solozhenkin, P. M. *Dokl. Akad. Nauk. SSSR.* **1980**, *251*, 365-367.

(35) Marov, I. N.; Borisova, L. V.; Ermakov, A. N. *Russ. J. Inorg. Chem.* **1975**, *20*, 415-417.

(36) Marov, I. N.; Dubrov, Y. N.; Belyaeva, V. K.; Ermakov, A. N. *Russ. J. Inorg. Chem.* **1972**, *10,* 1396-1402.

(37) Stravropoulos, P.; Edwards, P. G.; Behling, T.; Wilkinson, G.; Motevalli, M.; Hursthouse, M. B. *J. Chem. Soc. Dalton Trans.* **1987**, 169-175.

(38) Heath, R. L. In *CRC Handbook of Chemistry and Physics*; 60th ed.; Weast, R. C., Ed.; CRC Press: Boca Raton, 1980; p B-289.

(39) Wertz, J. E.; Bolton, J. R. *Electron Spin Resonance: Elementary Theory and Practical Applications*; Chapman and Hall: New York, 1986.

(40) Abragam, A.; Bleaney, B. *Electron Paramagnetic Resonance of Transition Ions*; Clarendon Press: Oxford, 1970.

(41) McClure, D. S. *J. Chem. Phys.* **1949**, *17,* 905-913.

(42) Goodman, B. A.; Raynor, J. B. *Adv. Inorg. Chem. Radiochem.* **1970**, *13,* 135-362.

(43) DeArmond, K.; Garrett, B. B.; Gutowsky, H. S. *J. Chem. Phys.* **1965**, *42,* 1019-1025.

(44) Wong, K. Y.; Che, C. M.; Anson, F. C. *Inorg. Chem.* **1987**, *26,* 737-741.

(45) McMillen, D. F.; Golden, D. M. *Ann. Rev. Phys. Chem.* **1982**, *33,* 493-532.

(46) Beard, J. H.; Casey, J.; Murmann, R. K. *Inorg. Chem.* **1965**, *4,* 797-803.

(47) Beard, J. H.; Murmann, R. K. *J. Inorg. Nuc. Chem.* **1968**, *30,* 2467-2474.

(48) Chakravorti, M. C. *J. Ind. Chem. Soc.* **1967**, *44,* 654-655.

(49) Chakravorti, M. C. *J. Ind. Chem. Soc.* **1970**, *47,* 844-850.

(50) Freni, M.; Giusto, D.; Romiti, P. *Gazz. Chim. Ital.* **1967**, *97,* 833-844.

(51) Lawrance, G. A.; Sangster, D. F. *Polyhedron* **1986**, *5,* 1553-1558.

(52) Murmann, R. K. *Inorg. Syn.* **1966**, *8,* 173-177.

(53) Pipes, D. W.; Meyer, T. J. *Inorg. Chem.* **1986**, *25,* 3256-3262.

(54) Winkler, J. R.; Gray, H. B. *J. Am. Chem. Soc.* **1983**, *105,* 1373-1374.

(55) Winkler, J. R.; Ph.D. thesis, August 1983, California Institute of Technology.

(56) Thorp, H. H.; Kumar, C. V.; Turro, N. J.; Gray, H. B. *J. Am. Chem. Soc.* **1989**, *111*, 4364-4368.

(57) Schwarz, H. A.; Dodson, R. W. *J. Phys. Chem.* **1984**, *88*, 3643-3647.

(58) Ghosh, P. K.; Brunschwig, B. S.; Mei, C.; Creutz, C.; Sutin, N. *J. Am. Chem. Soc.* **1984**, *106*, 4772-4783.

(59) Nord, G.; Pedersen, B.; Bjergbakhe, E. *J. Am. Chem. Soc.* **1983**, *105*, 1913-1919.

(60) Roecker, L.; Kutner, W.; Gilbert, J. A.; Simmons, M.; Murray, R. W.; Meyer, T. J. *Inorg. Chem.* **1985**, *24*, 3784-3791.

(61) Dressick, W. J.; Raney, K. W.; Demas, J. N.; DeGraff, B. A. *Inorg. Chem.* **1984**, *23*, 875-880.

(62) Tokel-Takvoryan, N. E.; Hemingway, R. E.; Bard, A. J. *J. Am. Chem. Soc.* **1973**, *95*, 6582-6589.

(63) (a) Schröder, M.; Stephenson, T. A. In *Comprehensive Coordination Chemistry*; Wilkinson, G., Ed.; Pergamon: New York, 1987; Vol. 4, Chapter 45, pp 277-518.

(b) Lin, C-T.; Böttcher, W.; Chou, M.; Creutz, C.; Sutin, N. *J. Am. Chem. Soc.* **1976**, *98*, 6536-6544.

(64) Saji, T.; Aoyagui, S. J. *Electroanal. Chem. Interf. Electrochem.* **1975**, *60*, 1-10.

(65) Perrin, D. D. *Dissociation Constants of Organic Bases in Aqueous Solution*; 1st ed.; Butterworths: London, 1965; pp 141, 162-163.

Appendix 1. IR spectra of *trans*-dioxorhenium compounds and free ligands. Ordinate scales are in percent transmission and abscissa scales are in wavenumbers. Compound identities are provided at the top of each spectrum.

Figure A1.1. IR spectrum of *trans*-$[ReO_2(py)_4][PF_6]$.

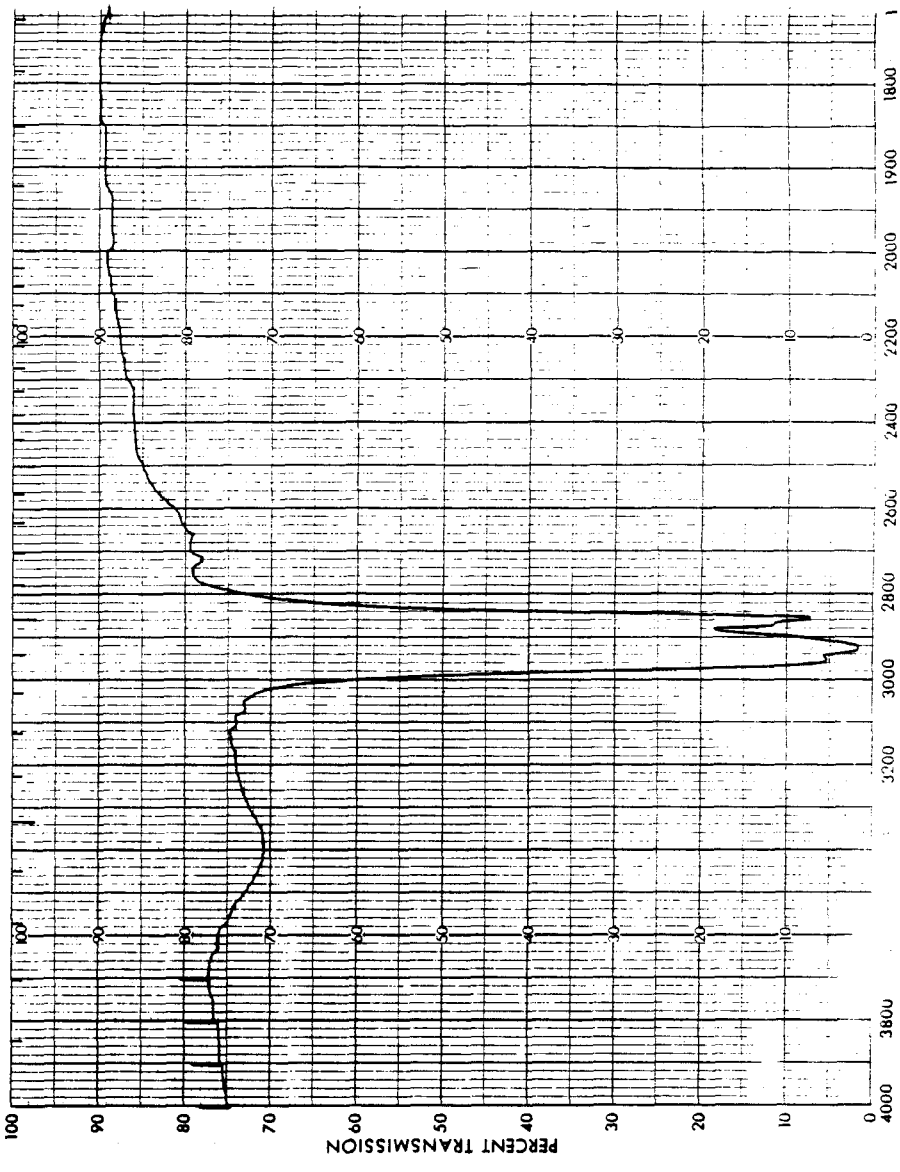

Figure A1.1. (Cont'd)

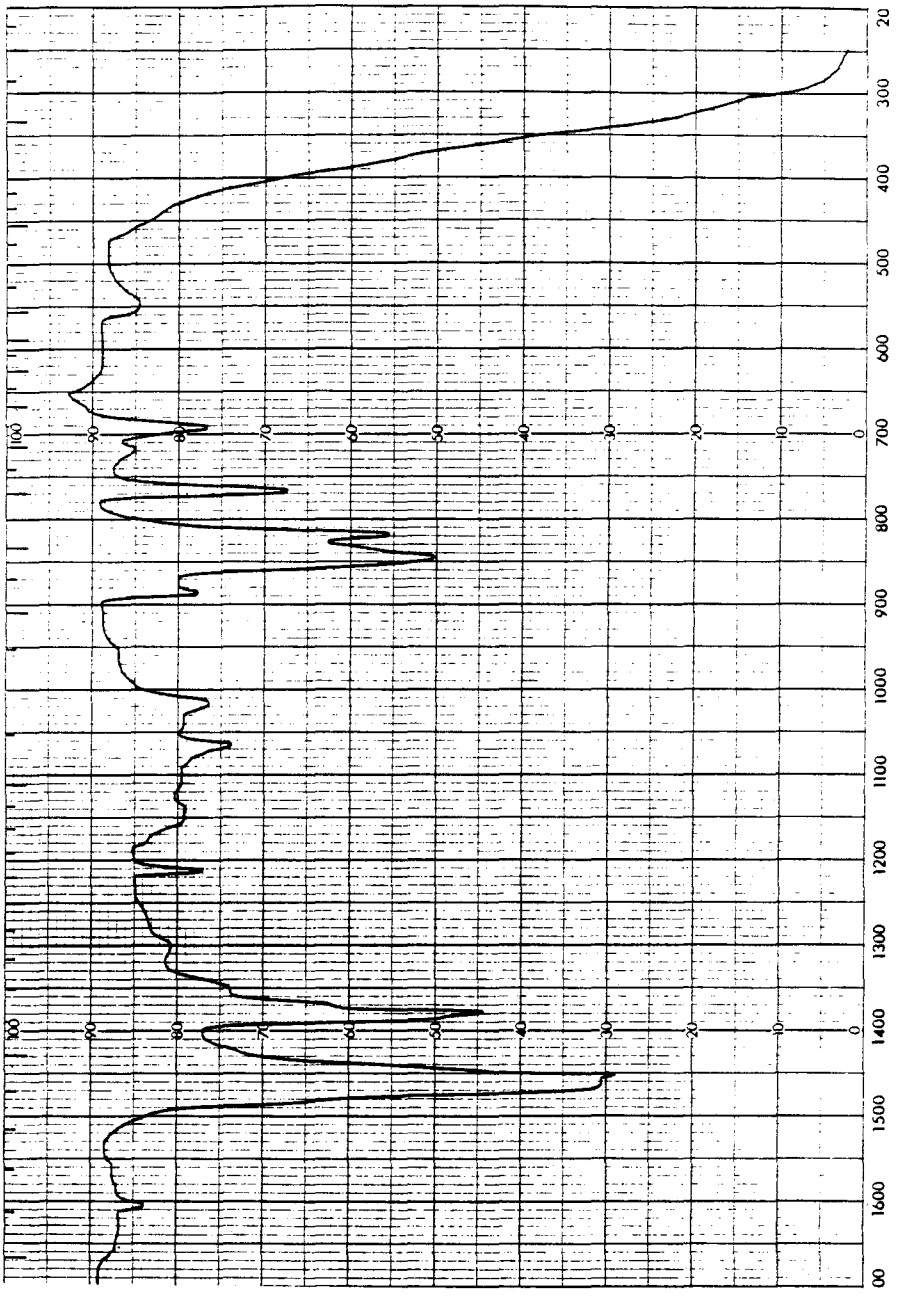

Figure A1.2. IR spectrum of *trans*-$[ReO_2(py)_4]I$.

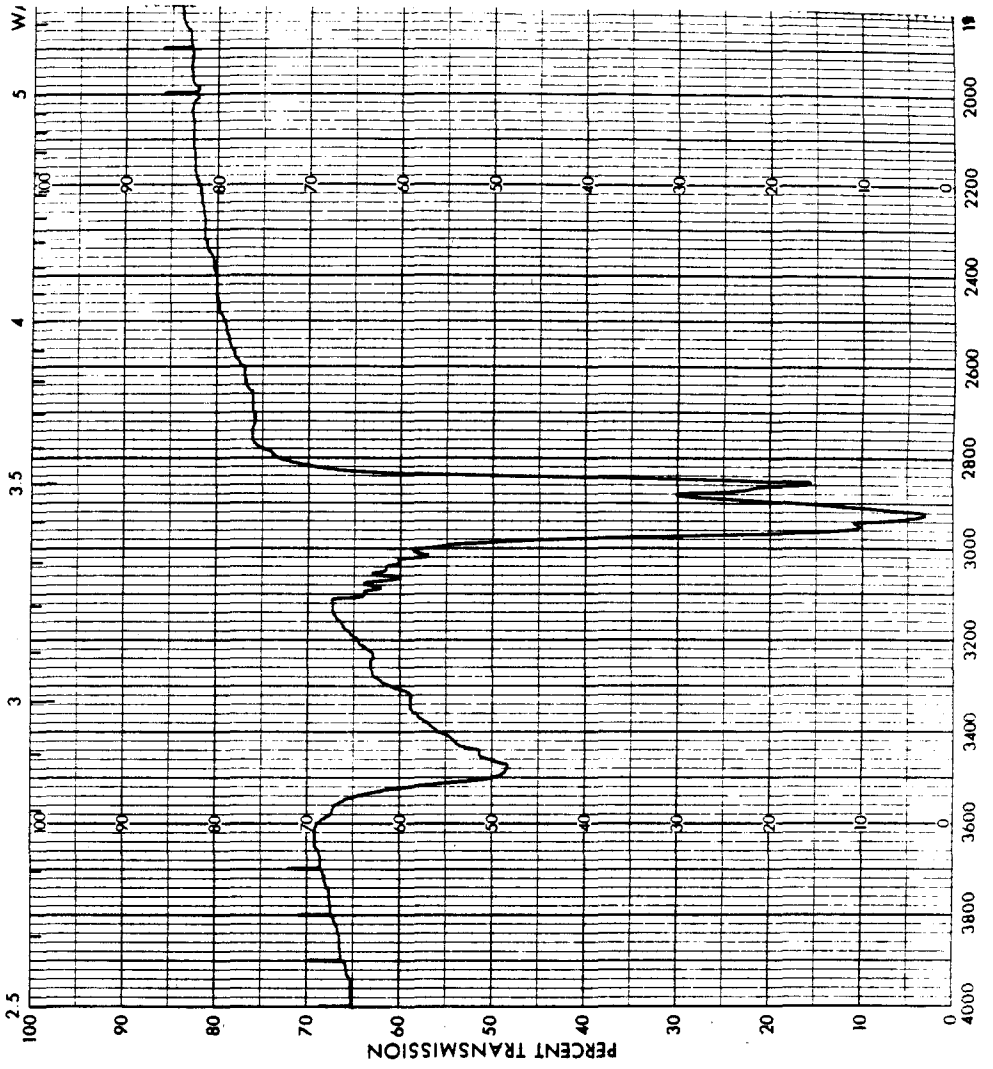

Figure A1.2. (Cont'd)

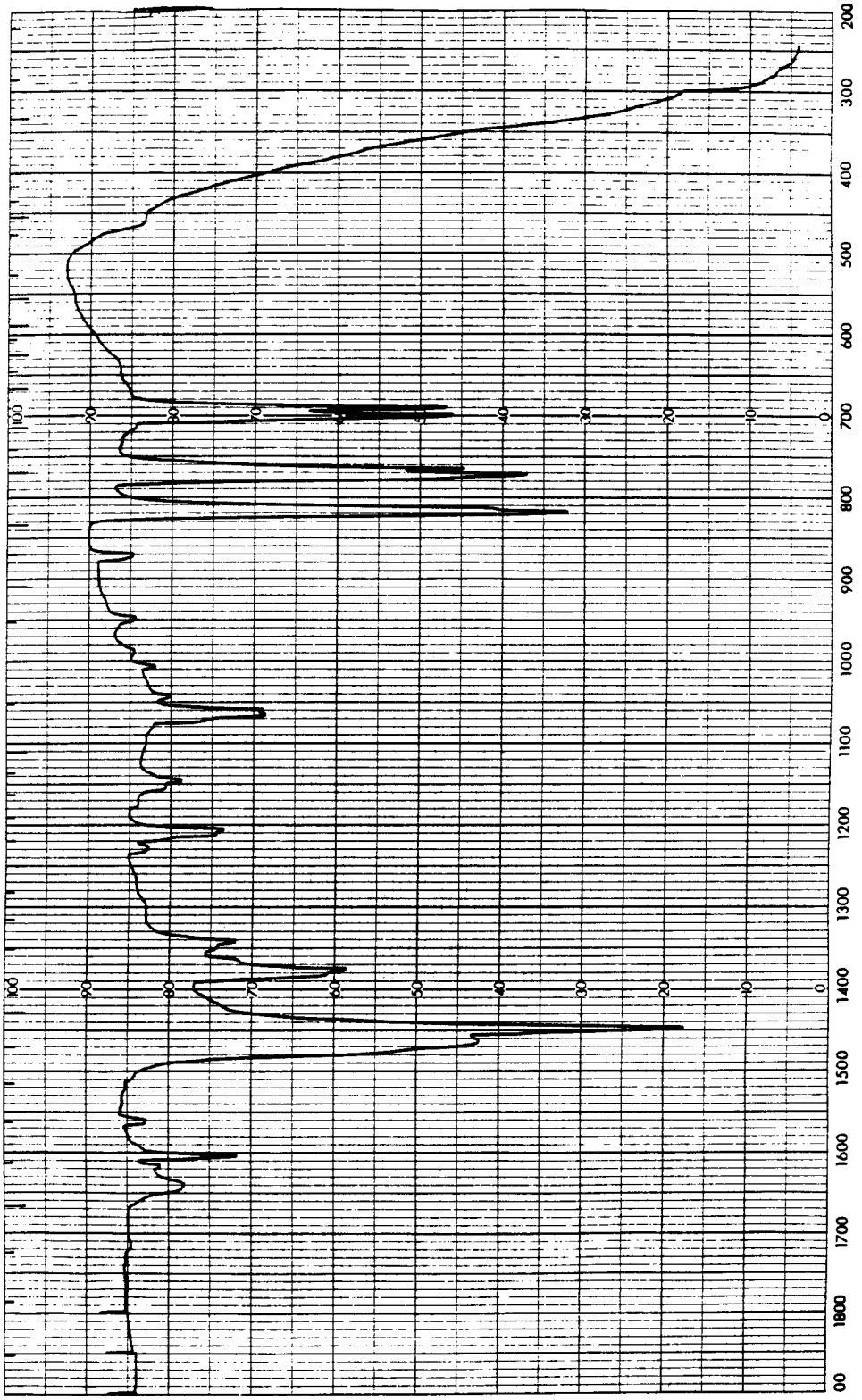

Figure A1.3. IR spectrum of *trans*-[ReO_2(4-Phpy)$_4$][PF_6].

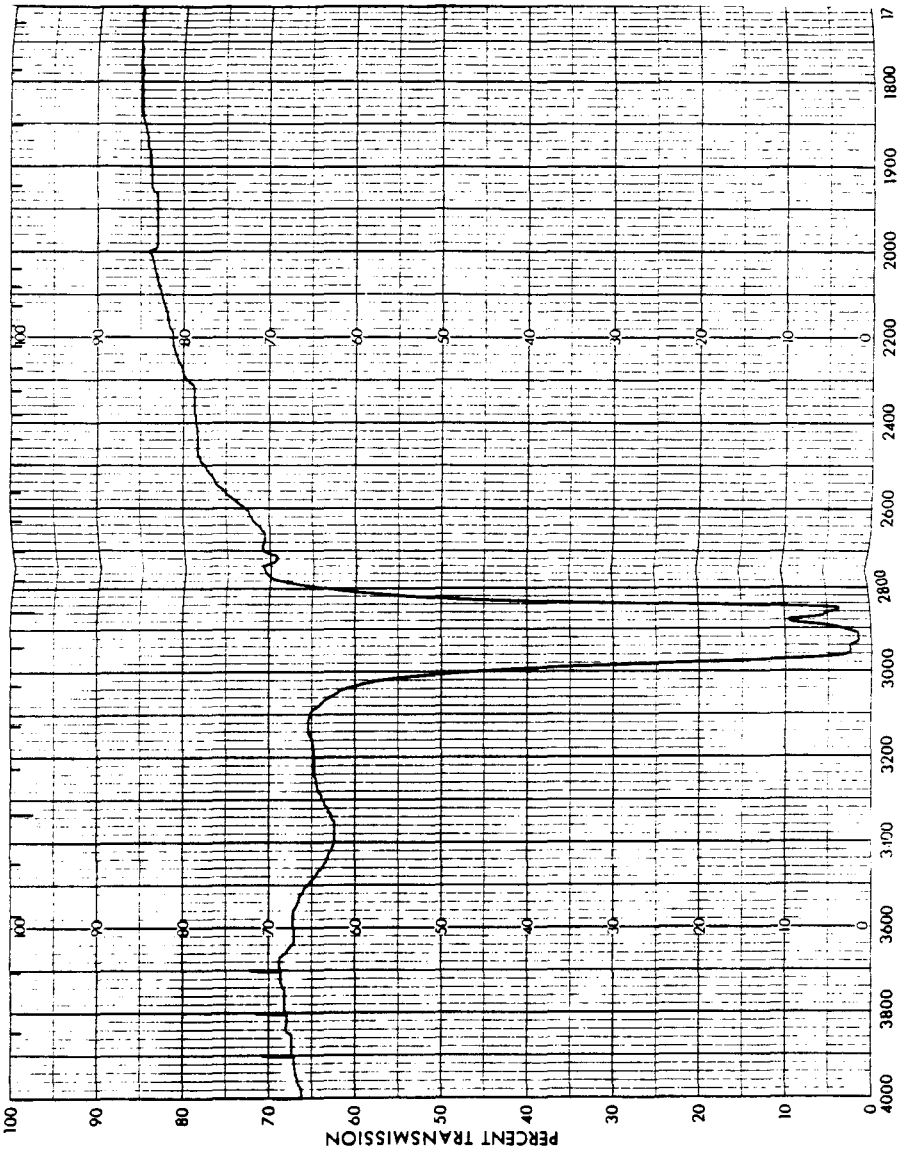

Figure A1.3. (Cont'd)

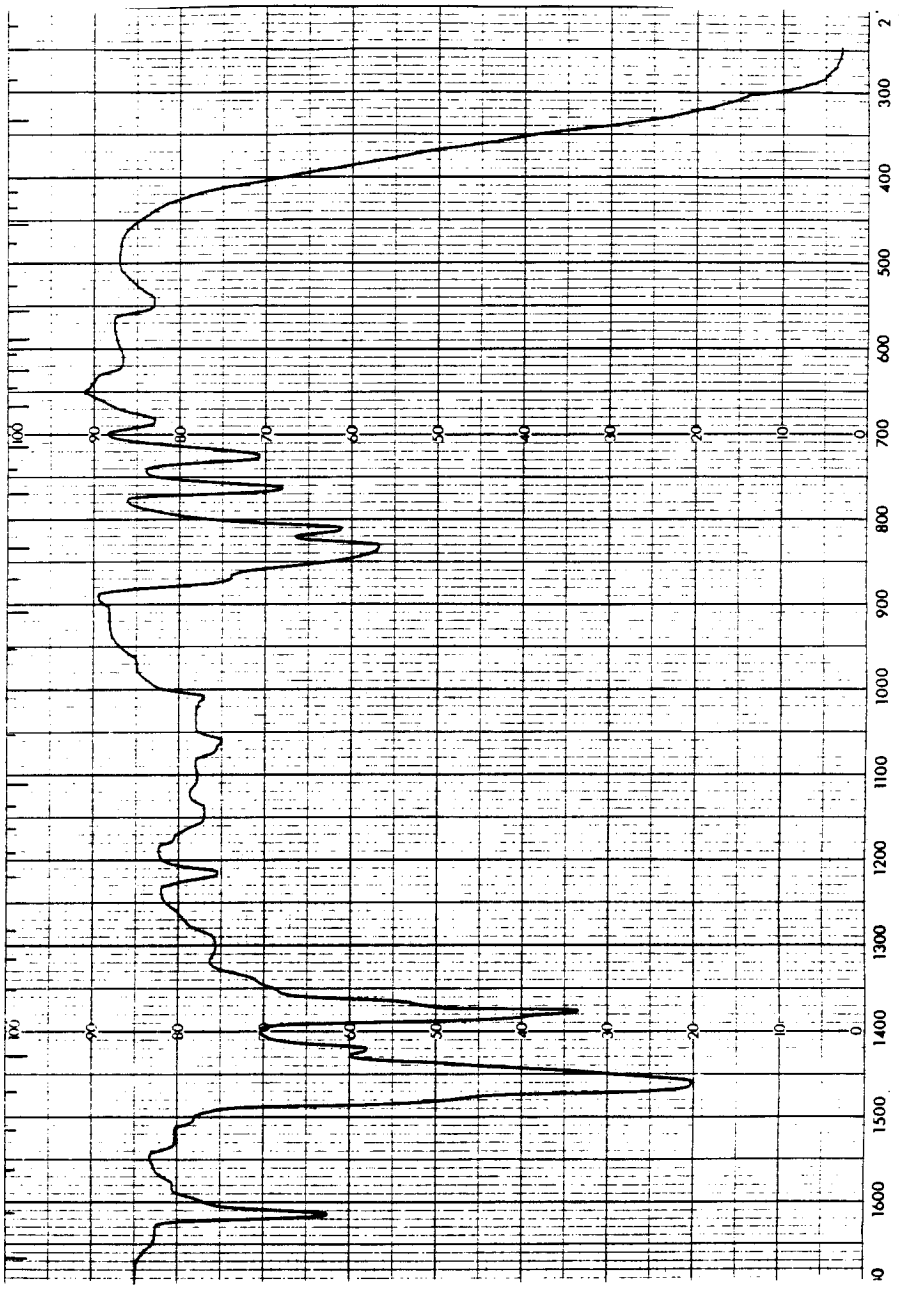

Figure A1.4. IR spectrum of *trans*-$[ReO_2(4\text{-pic})_4][PF_6]$.

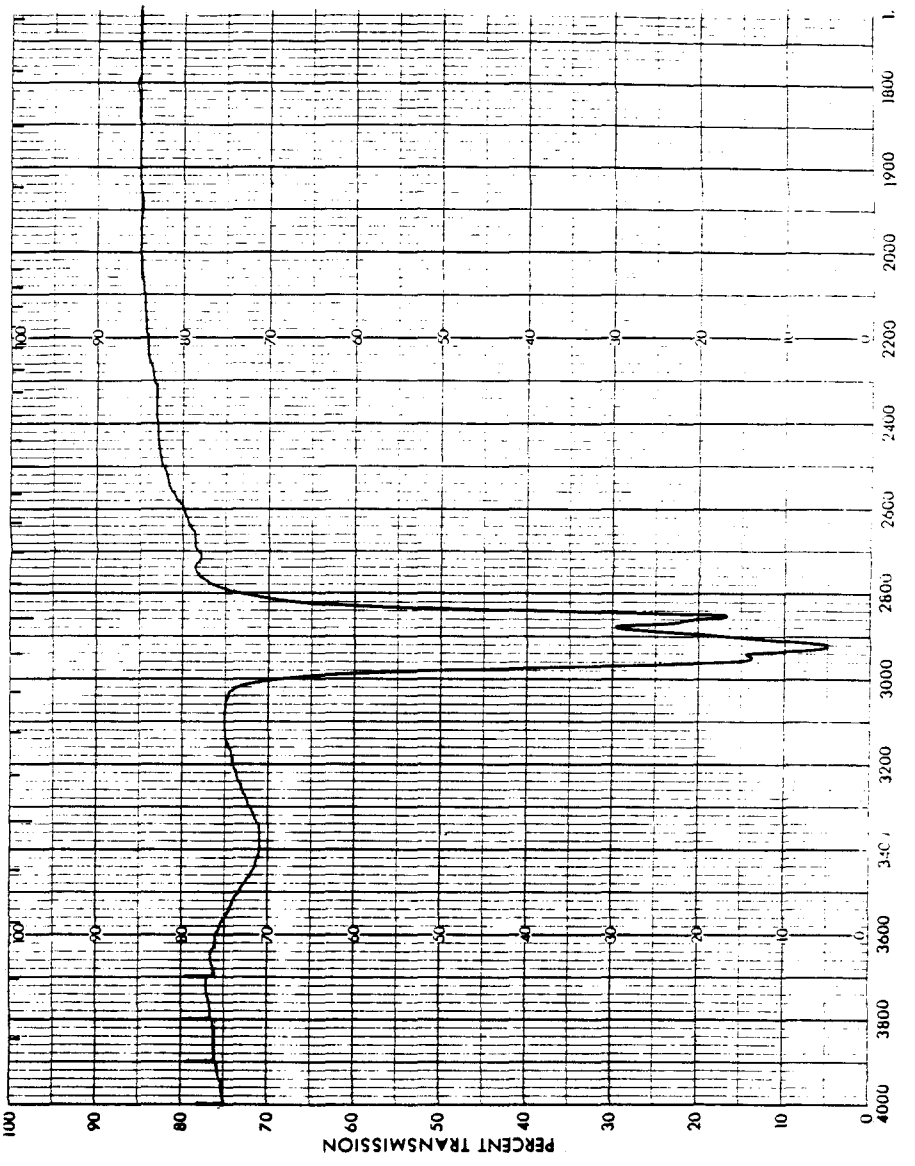

Figure A1.4. (Cont'd)

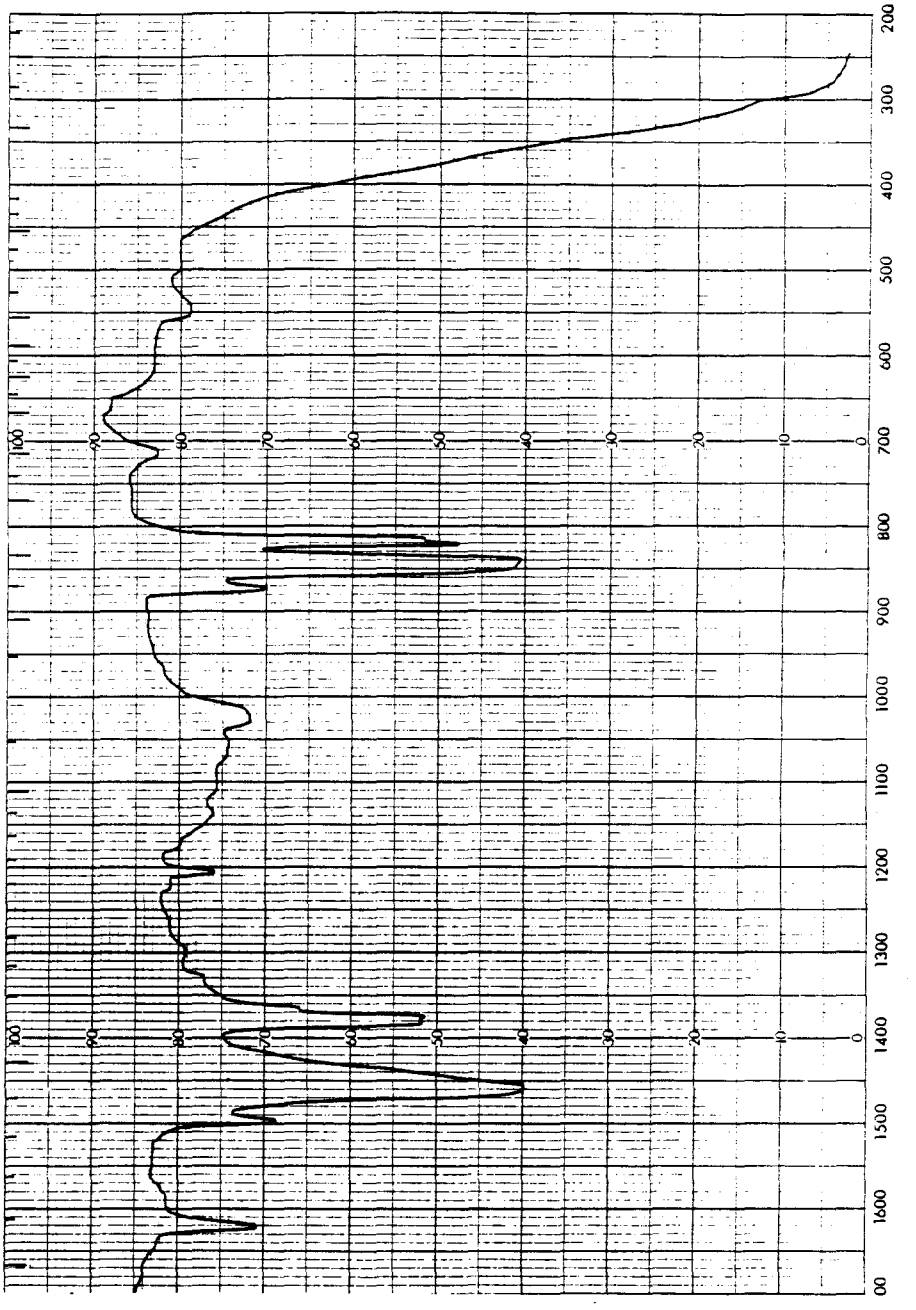

Figure A1.5. IR spectrum of *trans*-[ReO_2(3,5-lut)$_4$][PF_6].

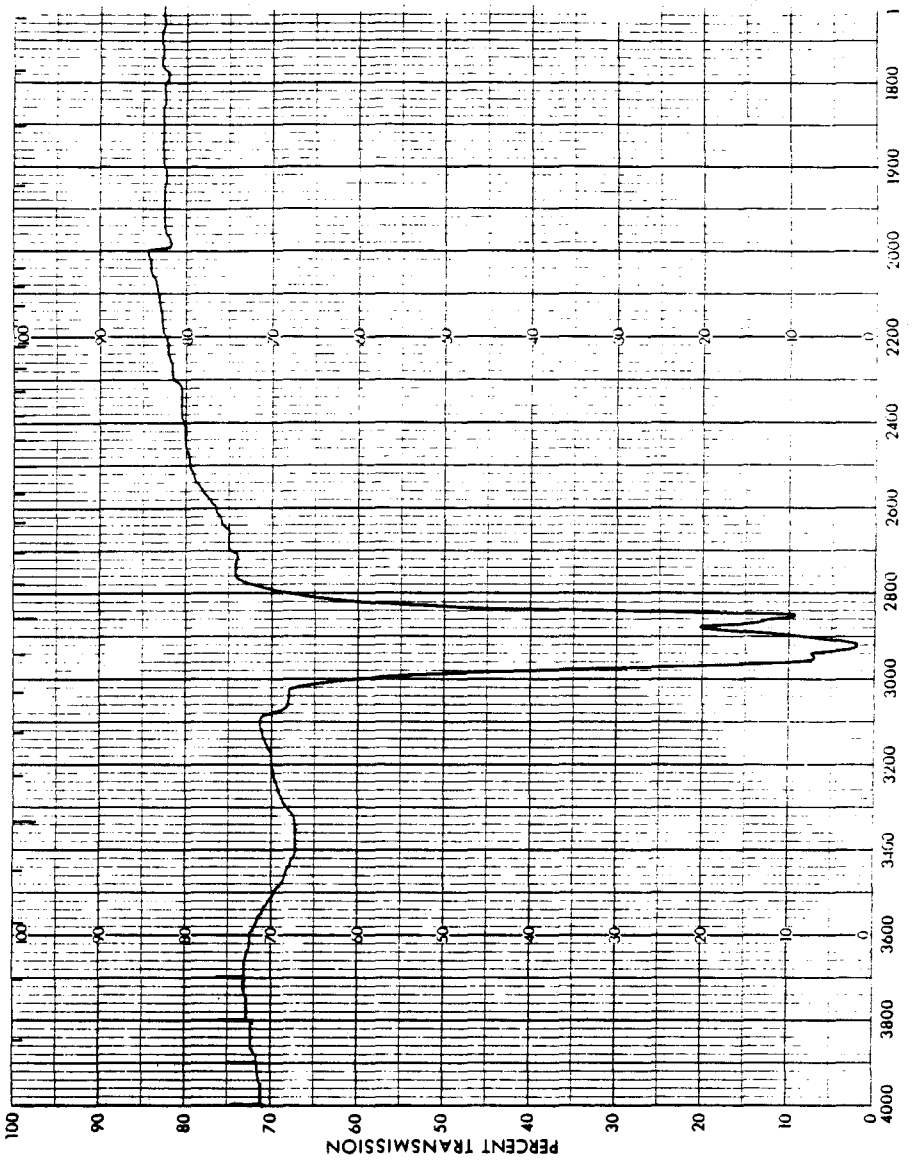

Figure A1.5. (Cont'd)

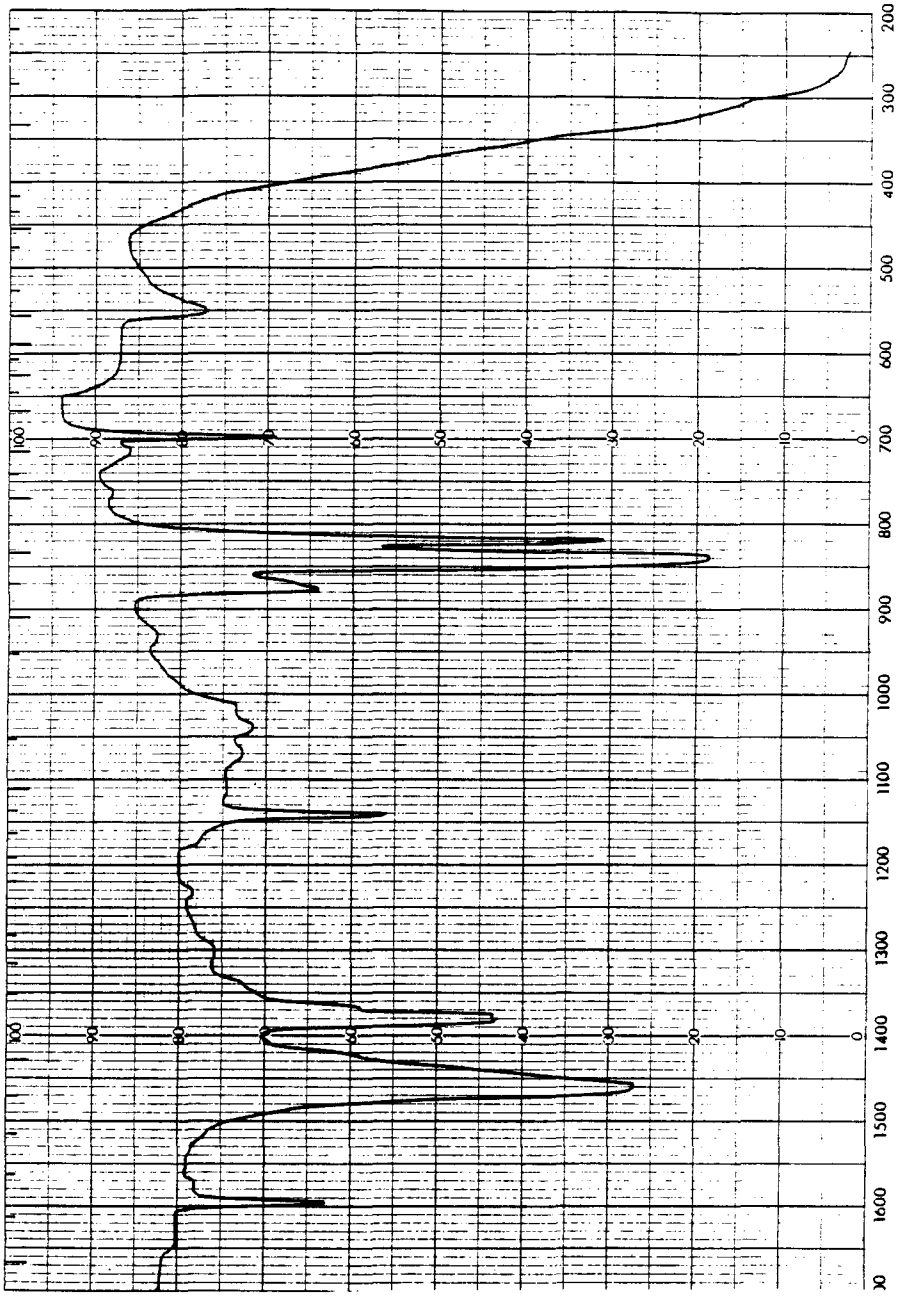

Figure A1.6. IR spectrum of *trans*-$[ReO_2(4\text{-}MeOpy)_4][PF_6]$.

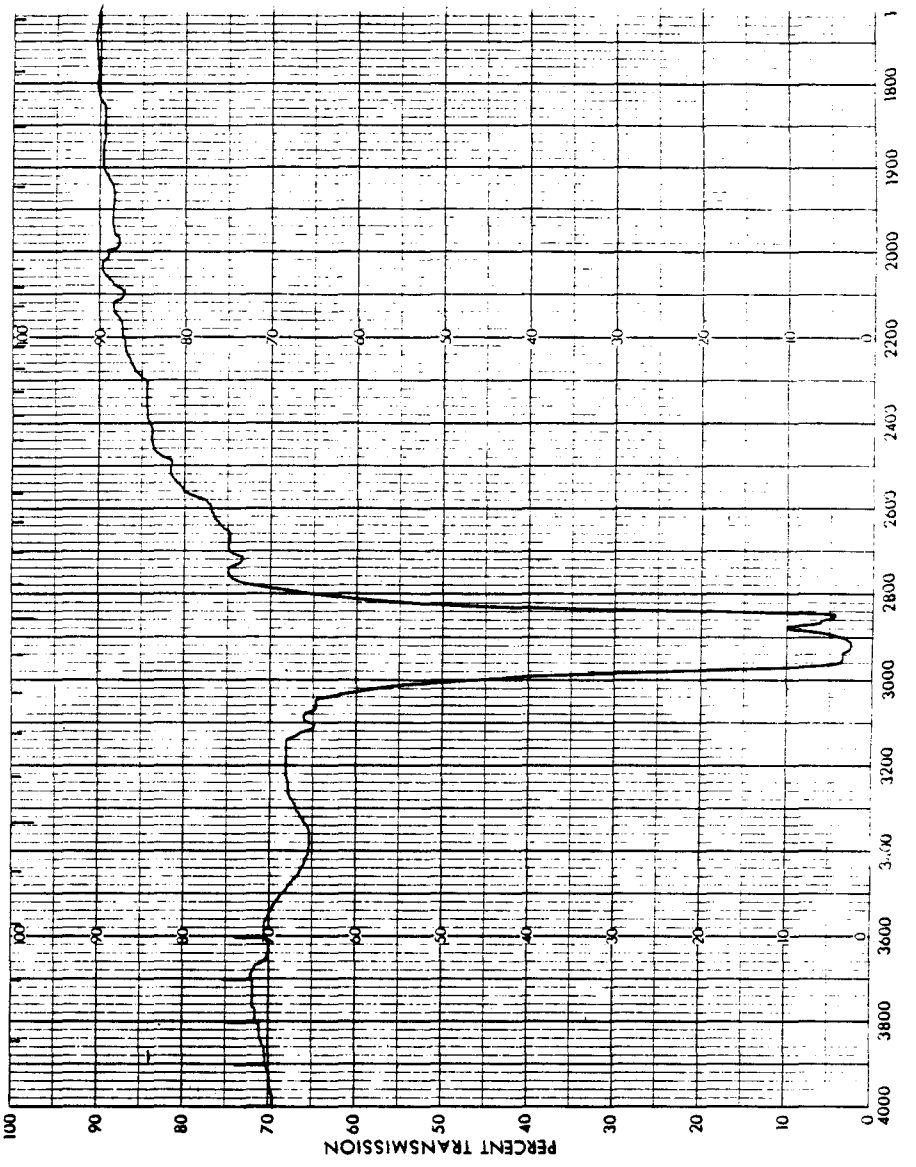

Figure A1.6. (Cont'd)

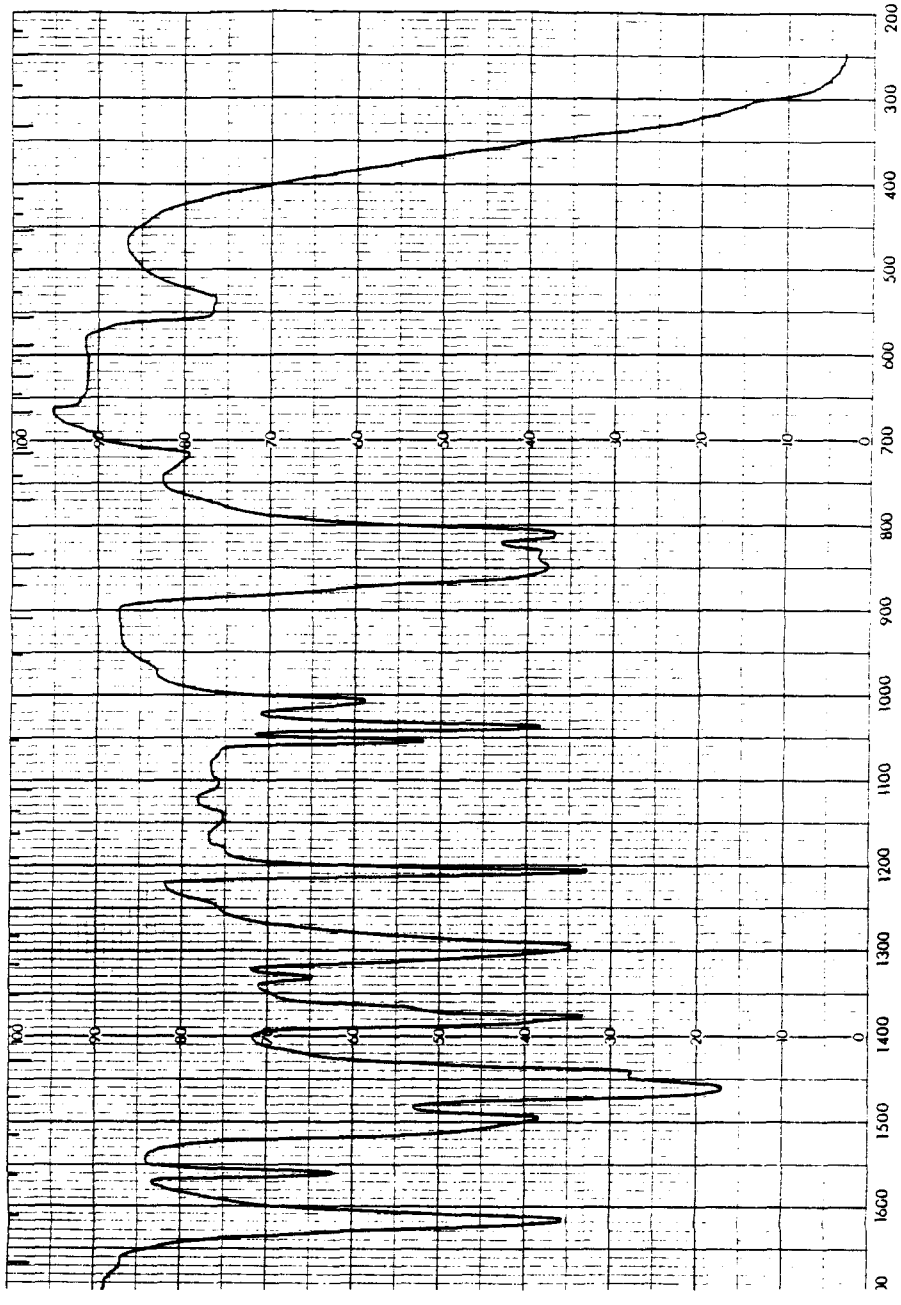

Figure A1.7. IR spectrum of *trans*-[ReO_2(3-Medmap)$_4$][PF_6].

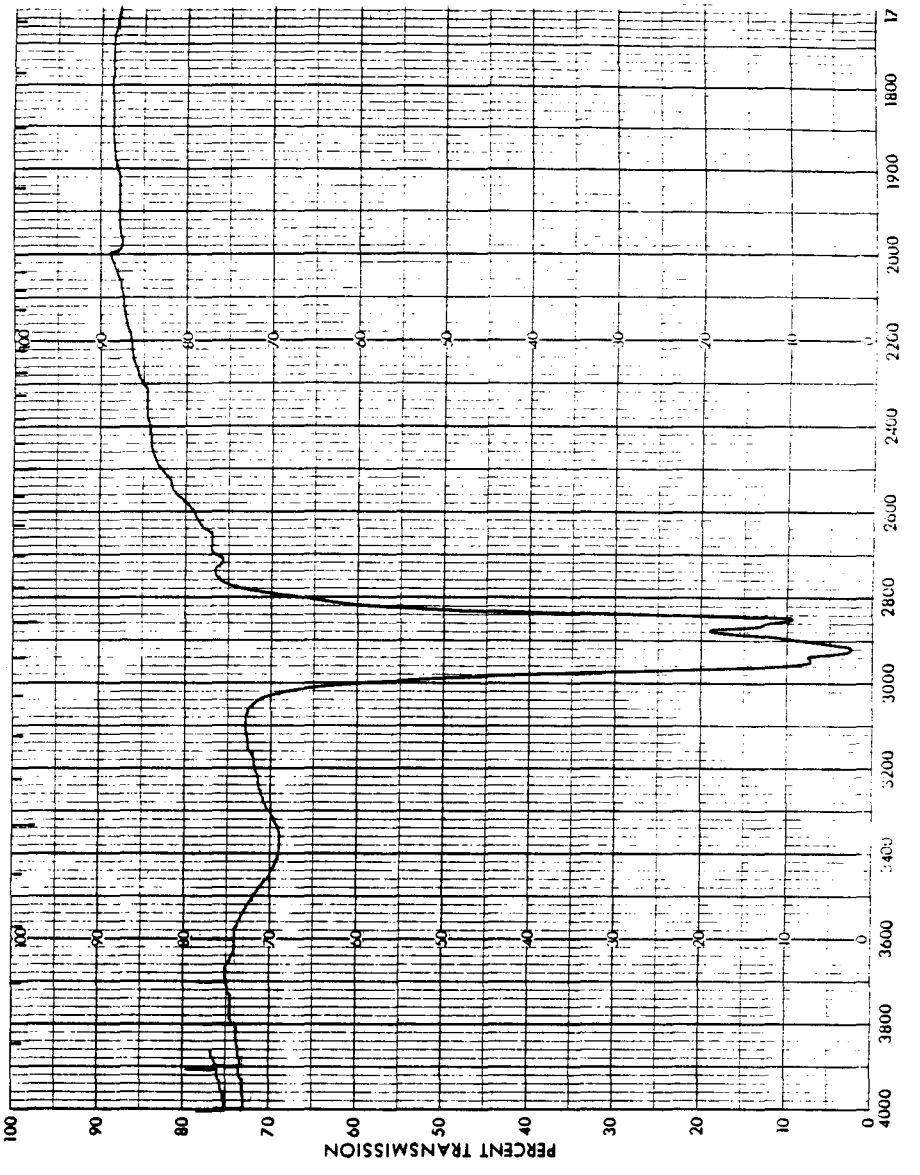

Figure A1.7. (Cont'd)

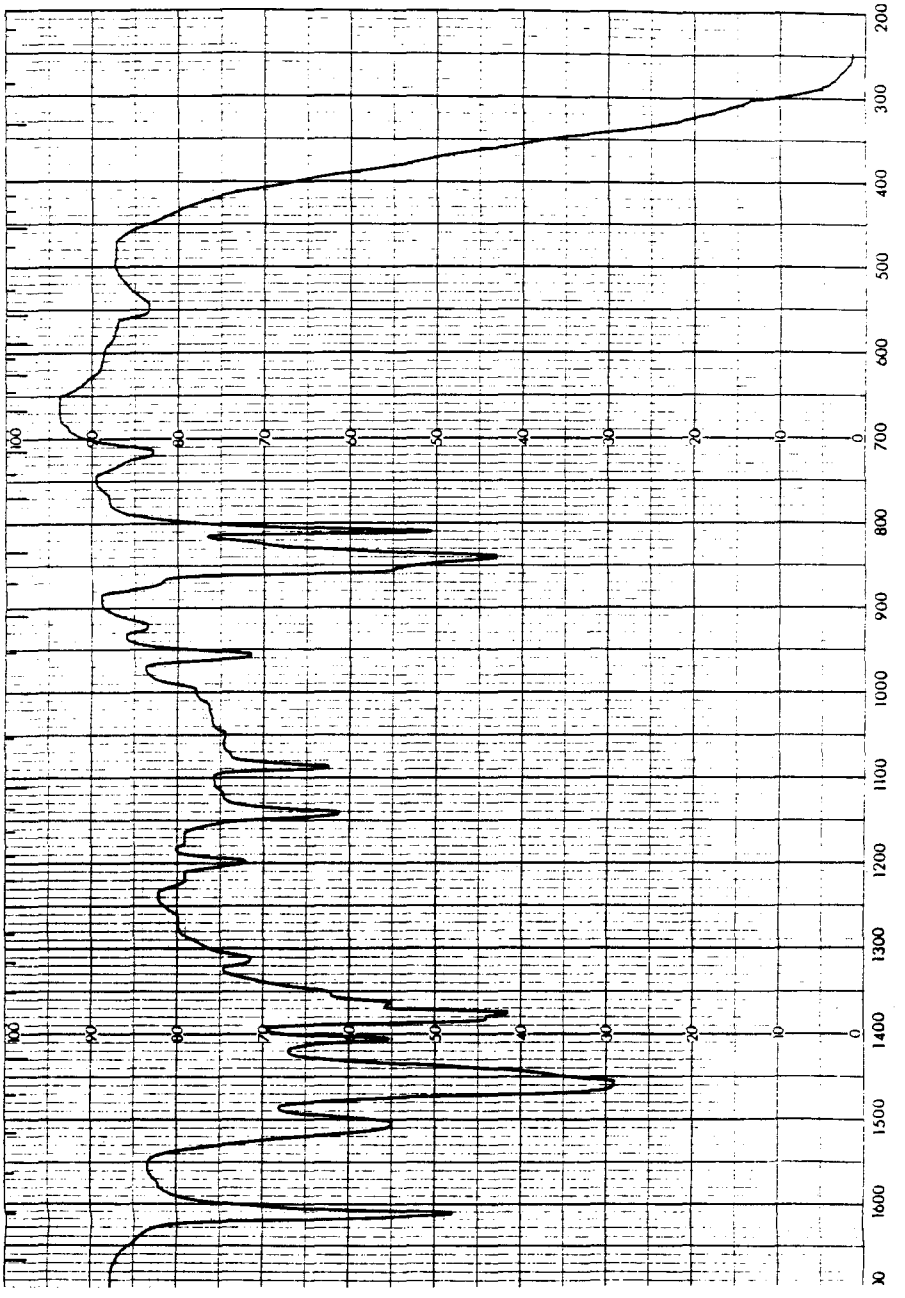

Figure A1.8. IR spectrum of *trans*-$[ReO_2(dmap)_4][PF_6]$.

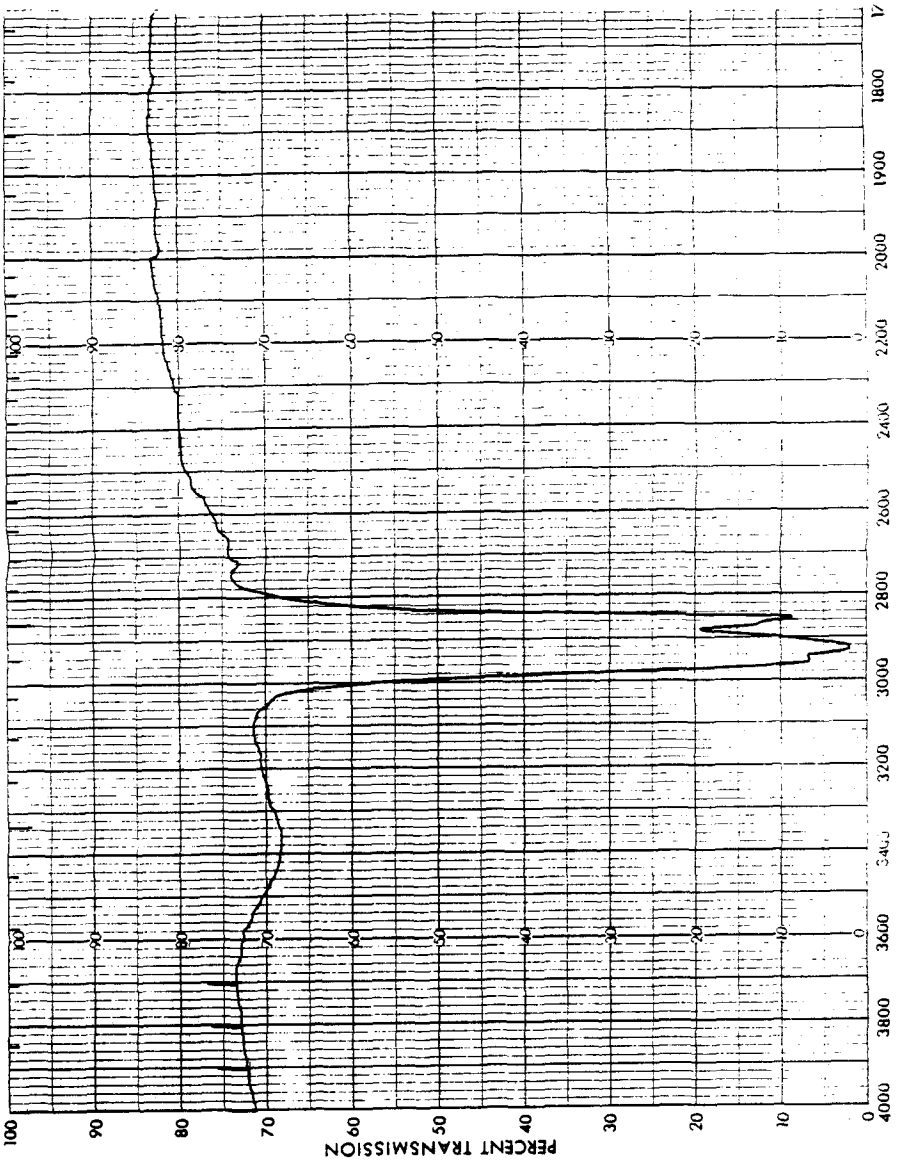

Figure A1.8. (Cont'd)

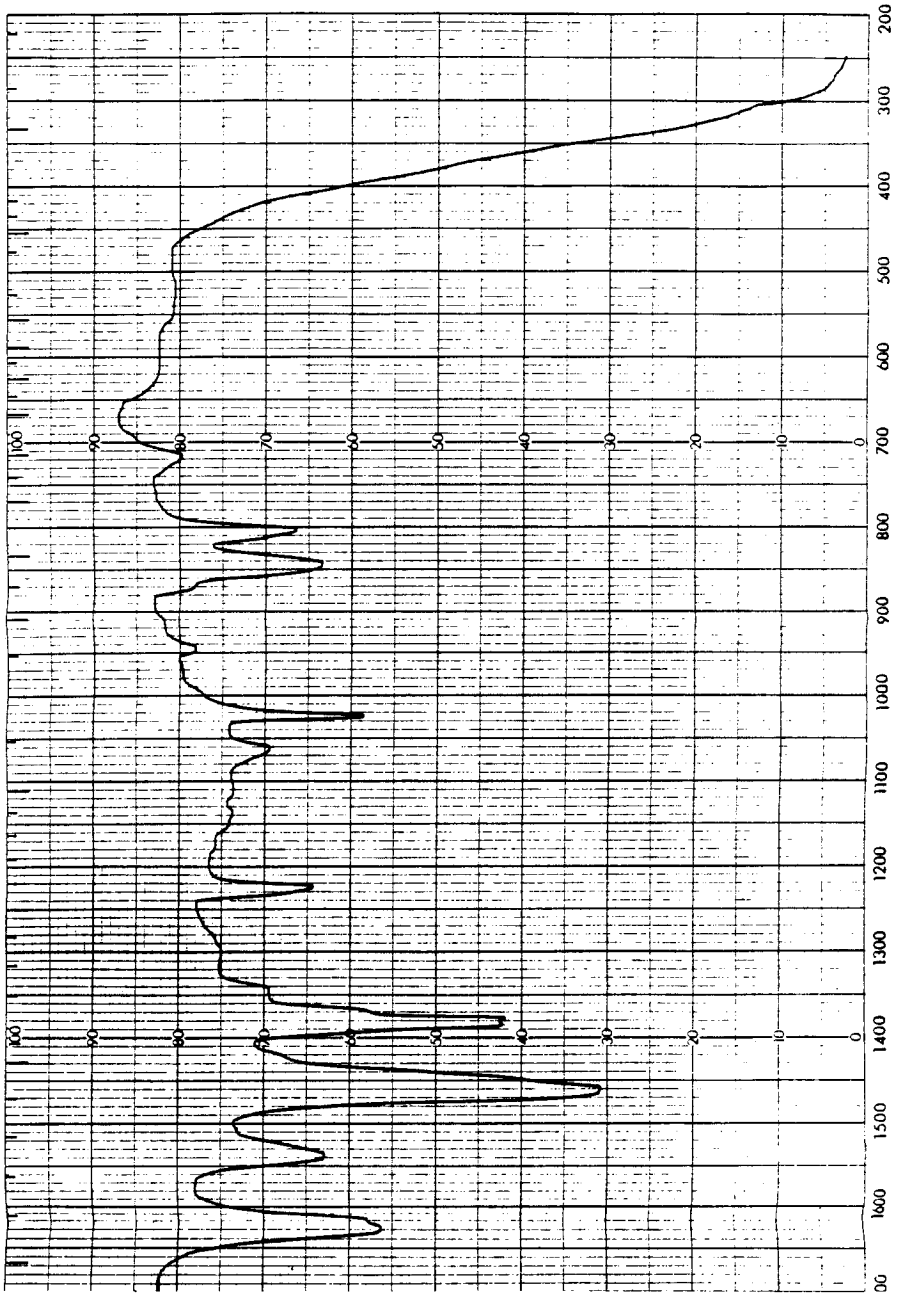

Figure A1.9. IR spectrum of *trans*-[ReO_2(4-pyrrpy)$_4$][PF_6].

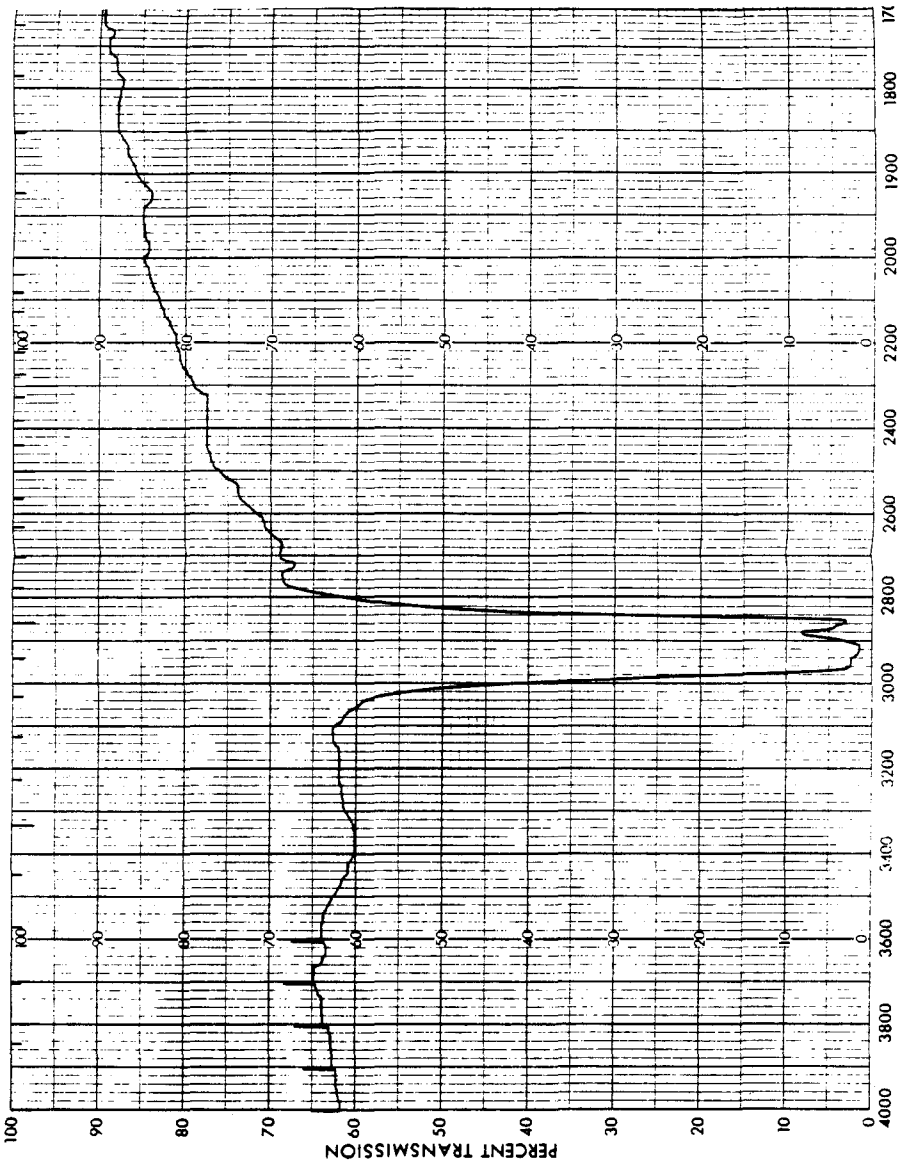

Figure A1.9. (Cont'd)

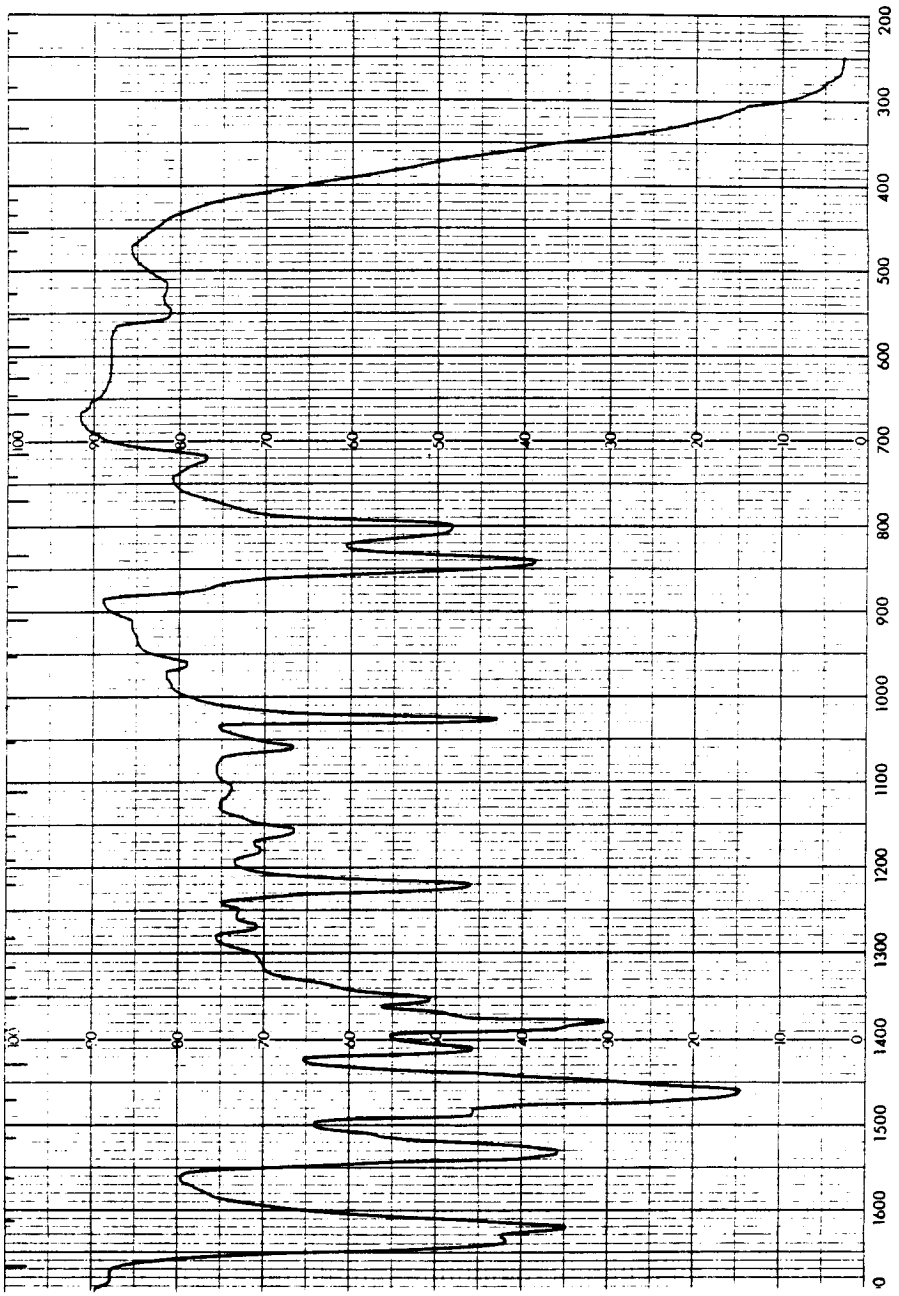

Figure A1.10. IR spectrum of *trans*-$[ReO_2(dmap)_4][PF_6]_2$.

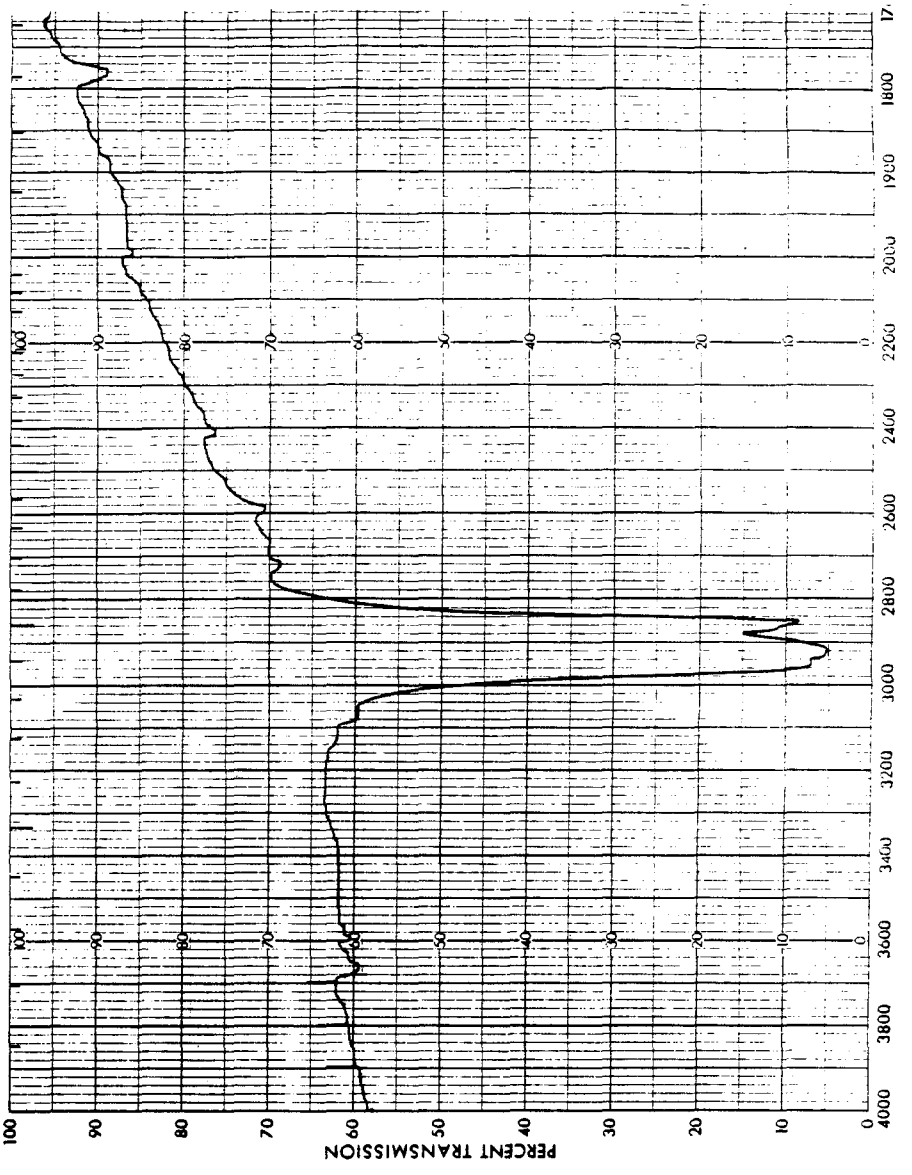

Figure A1.10. (Cont'd)

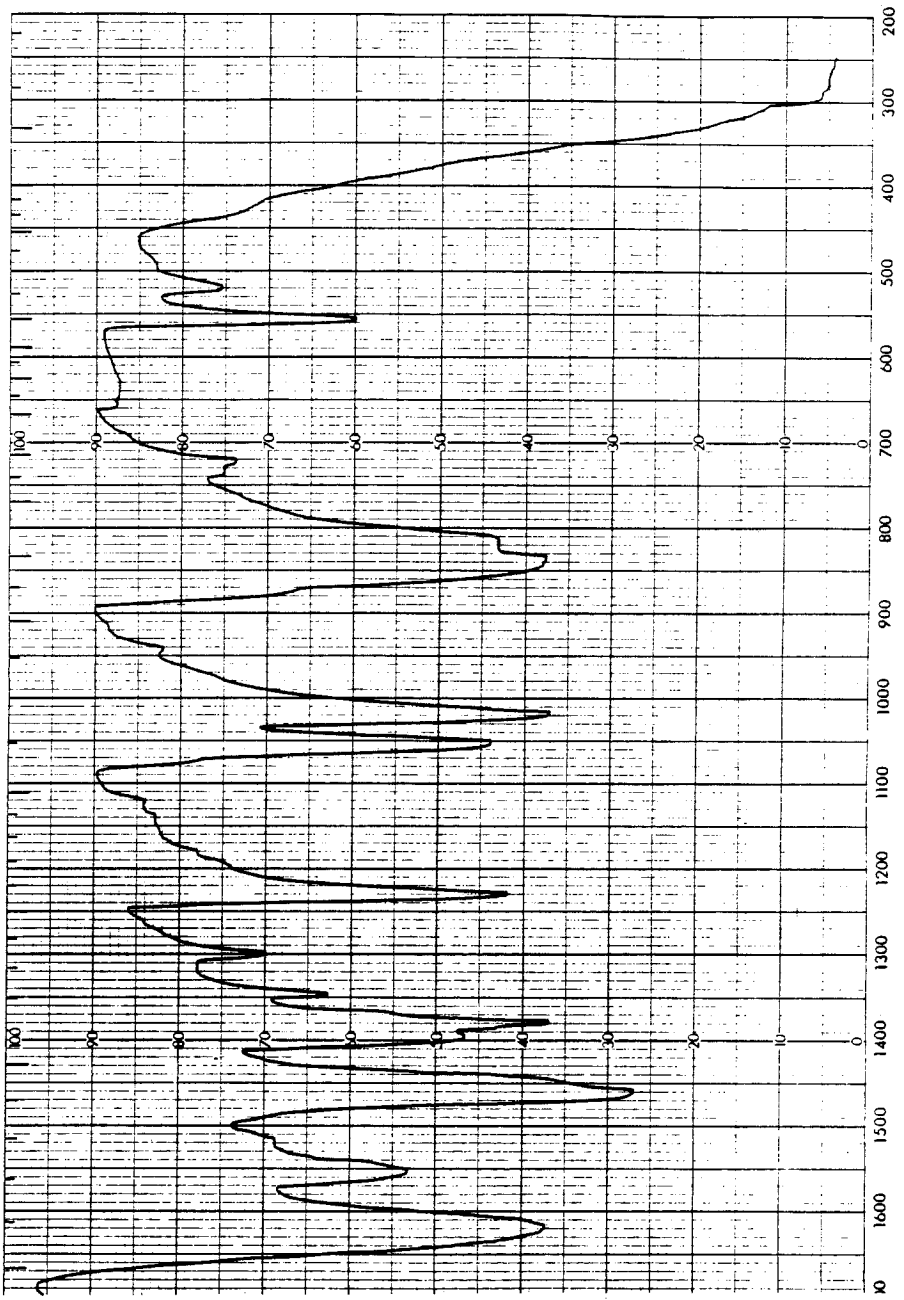

Figure A1.11. IR spectrum of *trans*-[$ReO_2(py)_3(PPh_3)$]I.

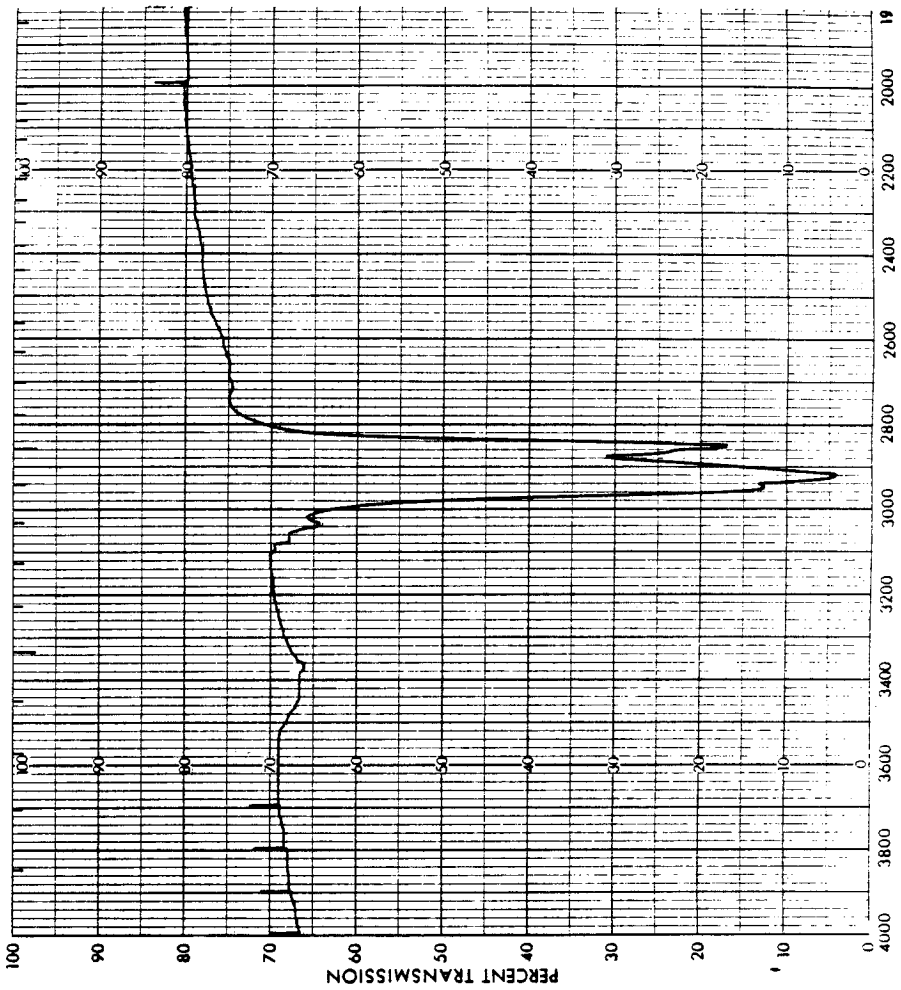

Figure A1.11. (Cont'd)

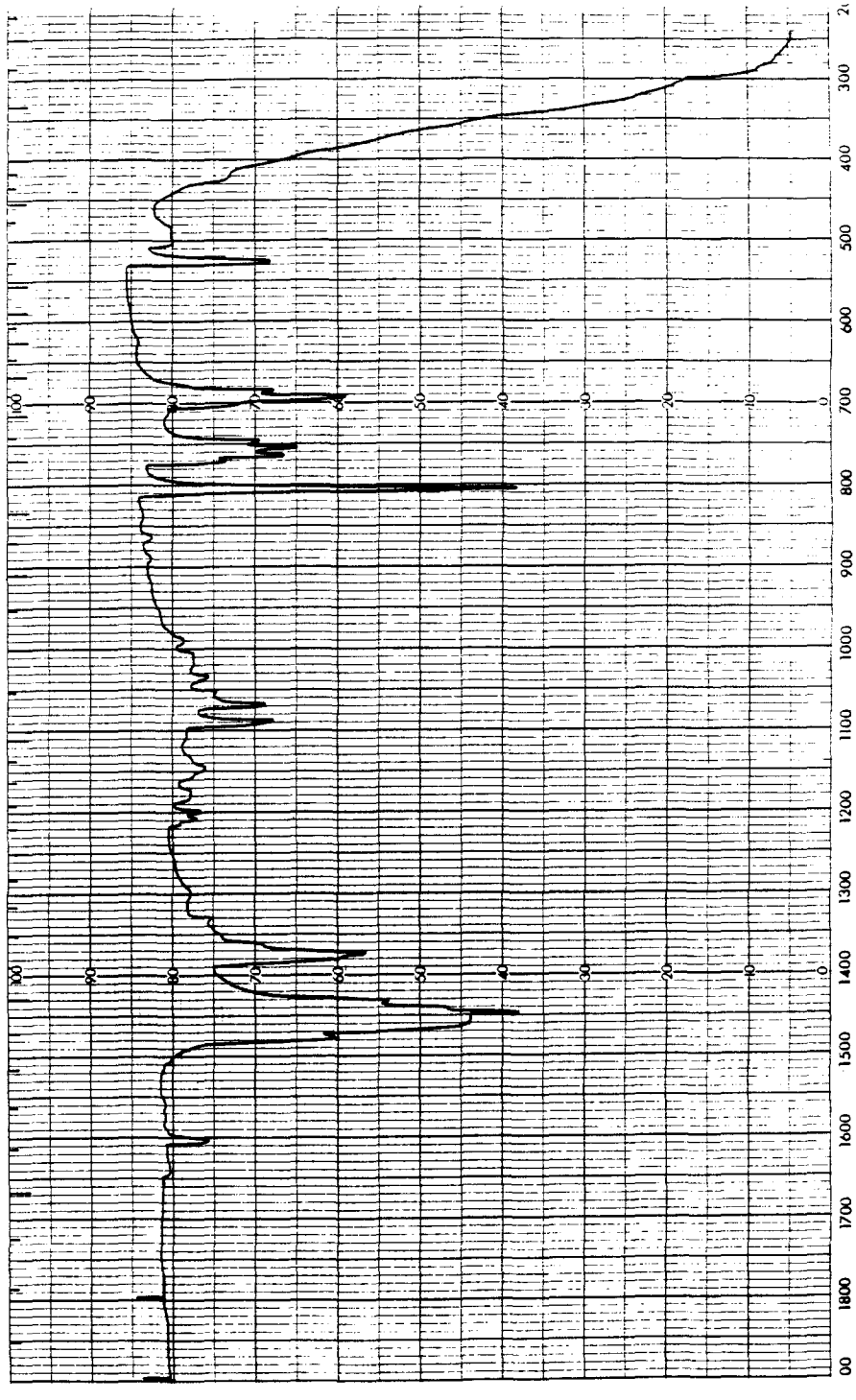

Figure A1.12. IR spectrum of *trans*-[$ReO_2(diphos)_2$][PF_6]•toluene.

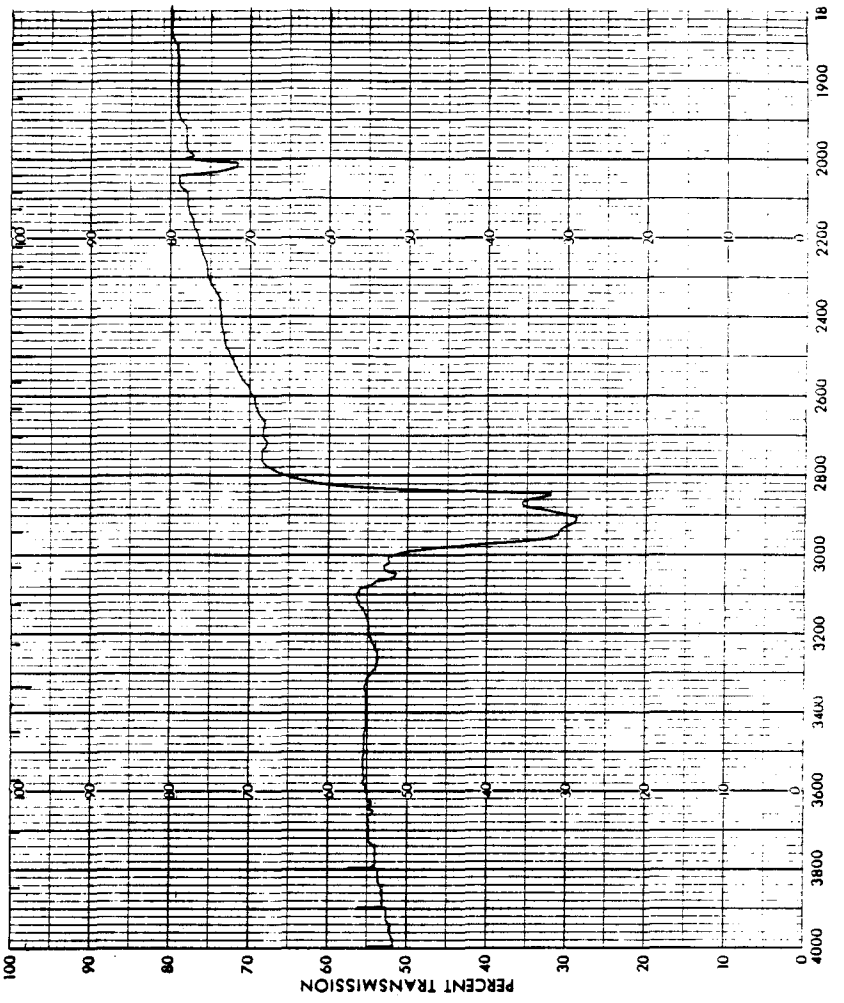

Figure A1.12. (Cont'd)

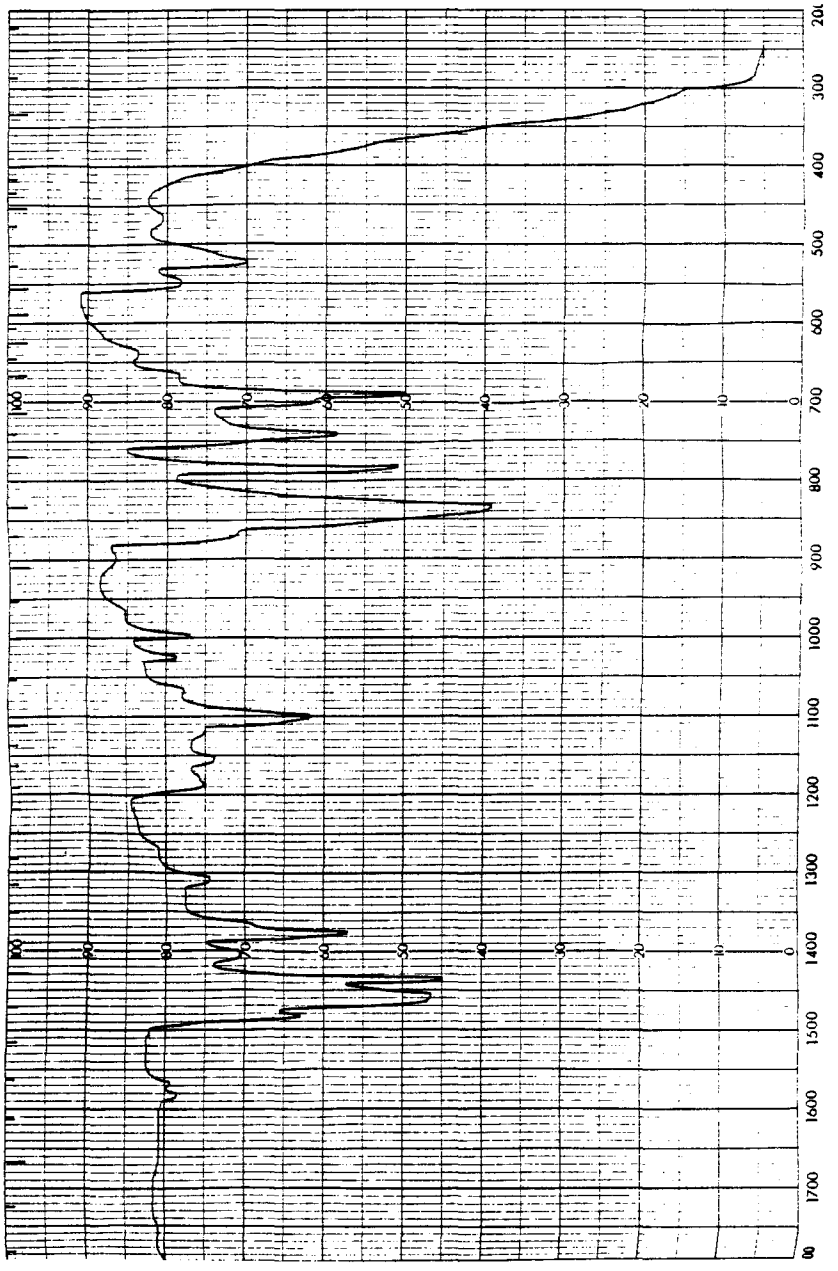

Figure A1.13. IR spectrum of diphos.

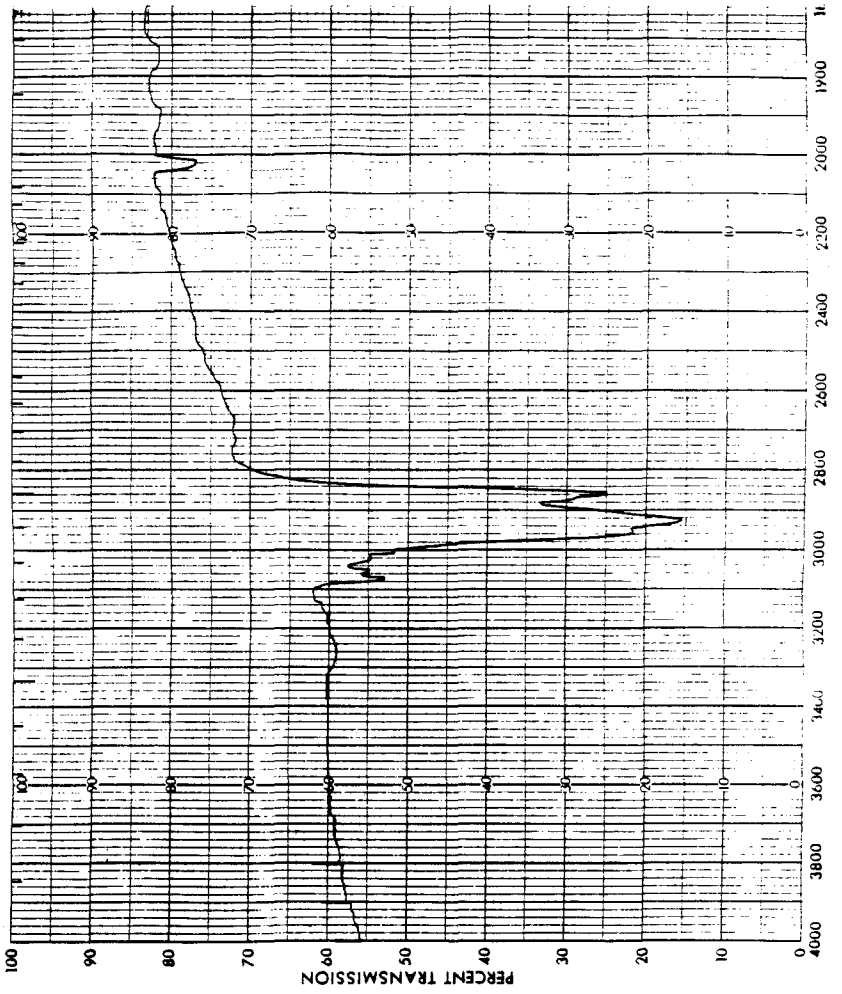

Figure A1.13. (Cont'd)

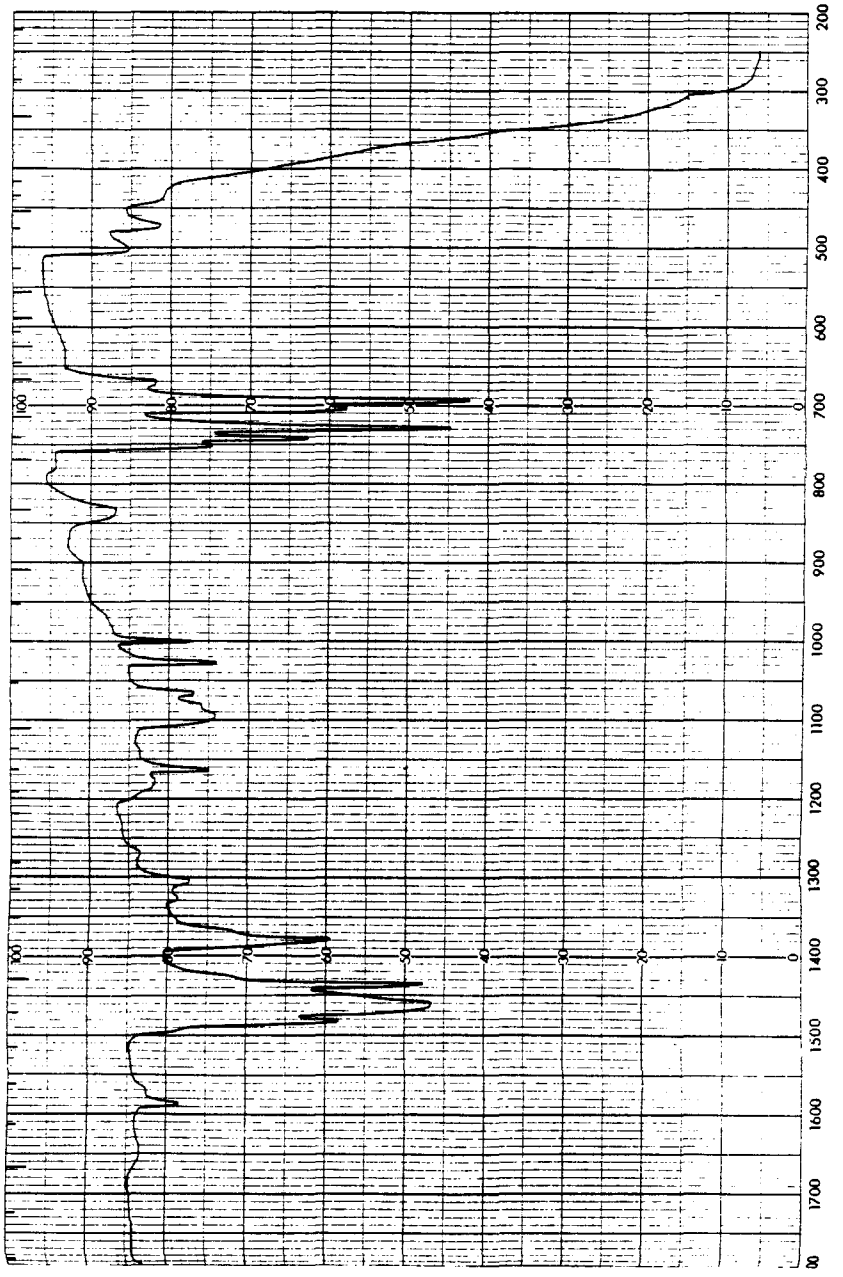

Figure A1.14. IR spectrum of *trans*-$[ReO_2(dppen)_2][PF_6]$.

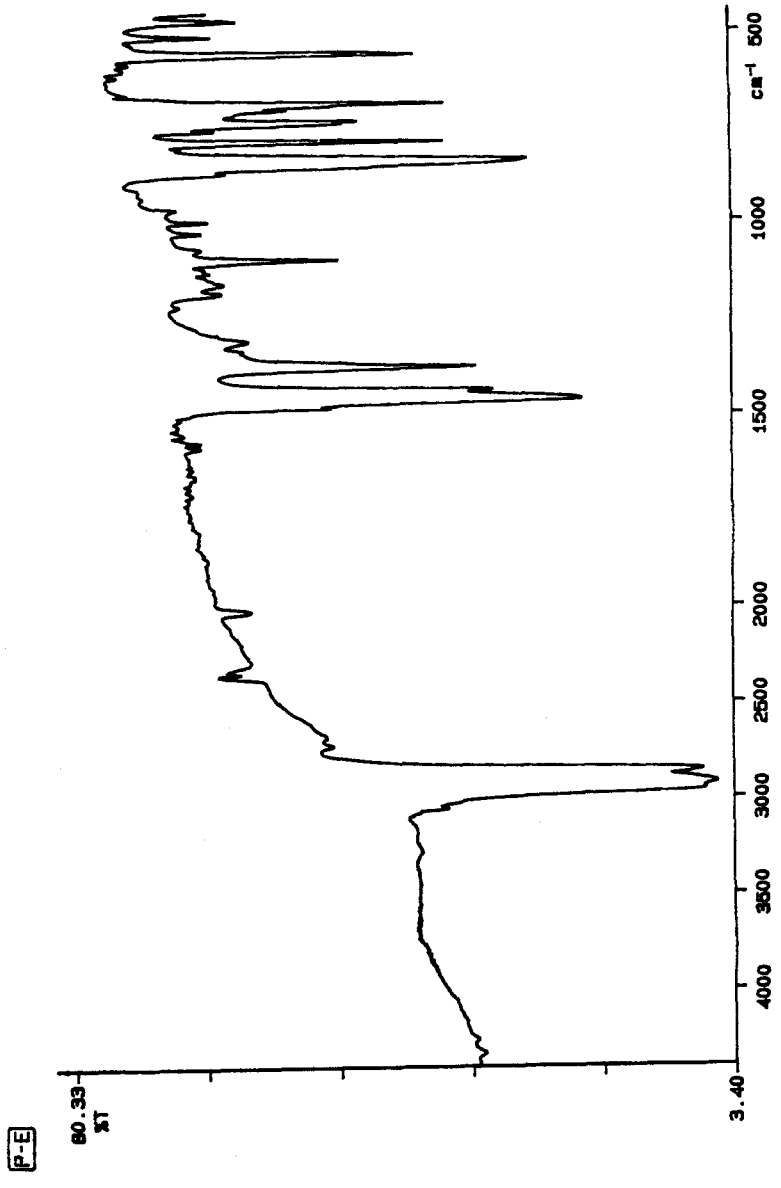

Figure A1.15. IR spectrum of dppen.

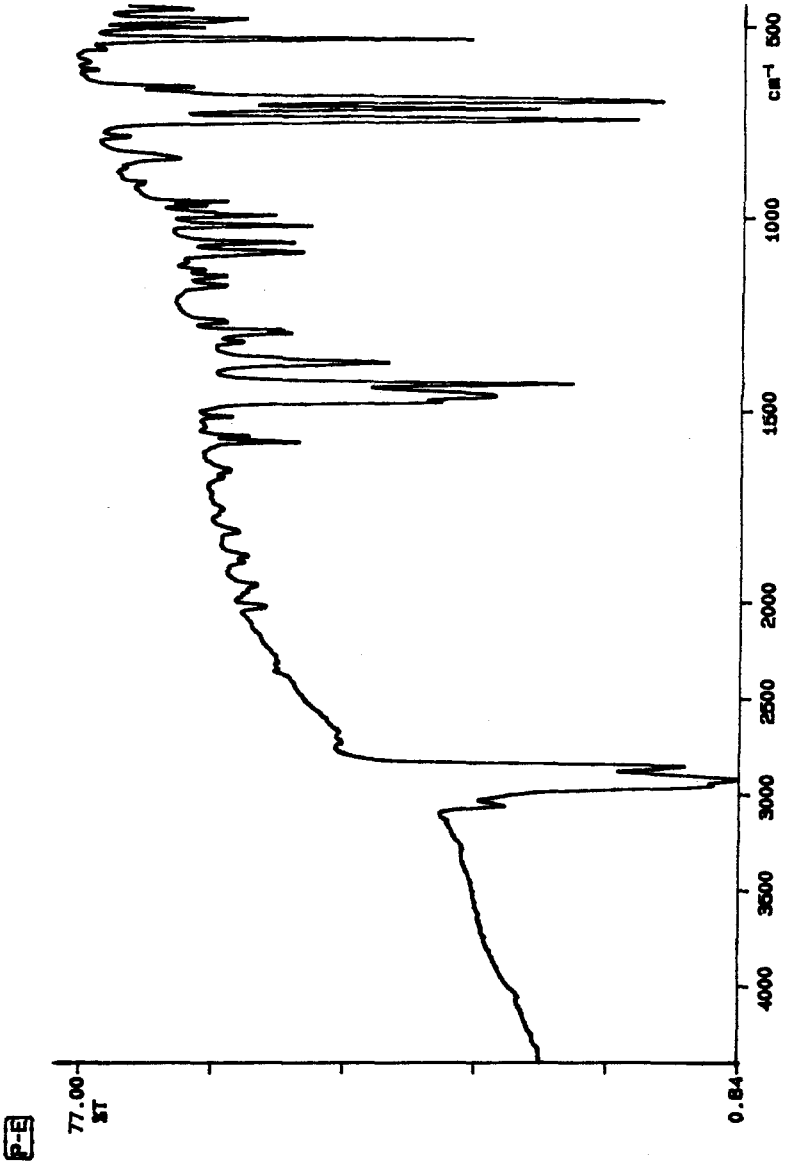

Figure A1.16. IR spectrum of *trans*-$[ReO_2(en)_2][PF_6]$.

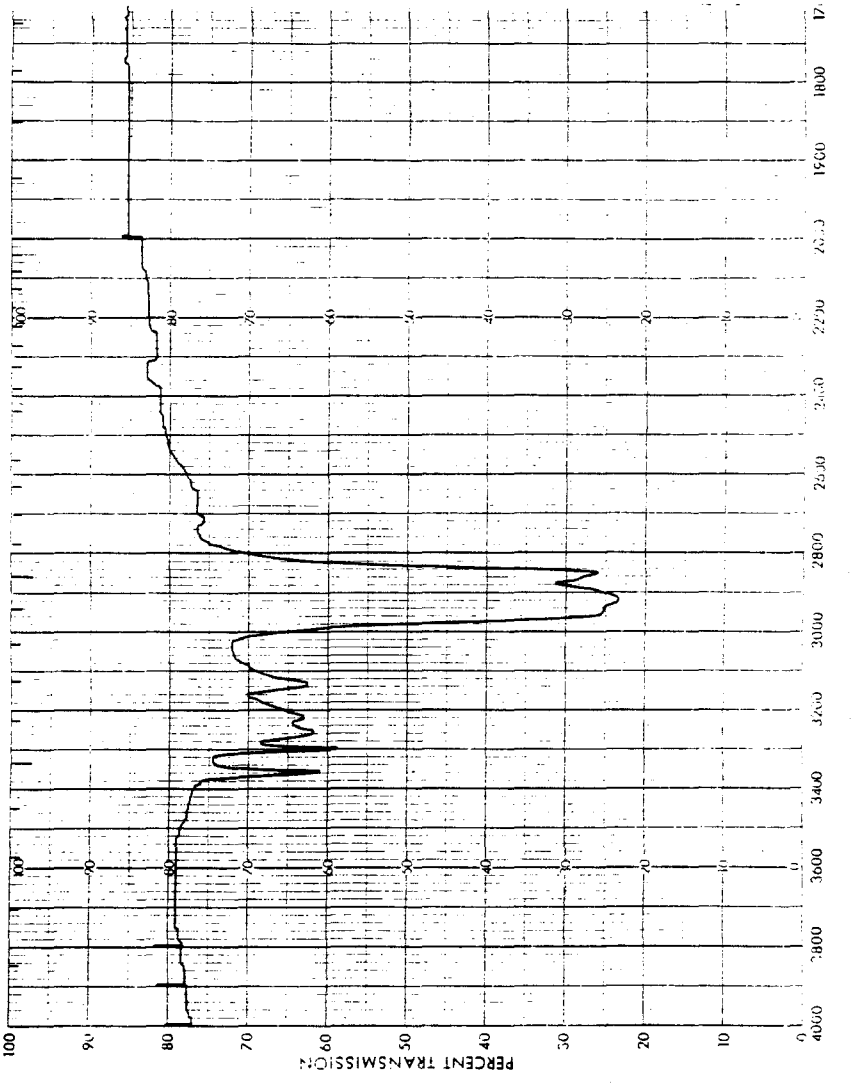

Figure A1.16. (Cont'd)

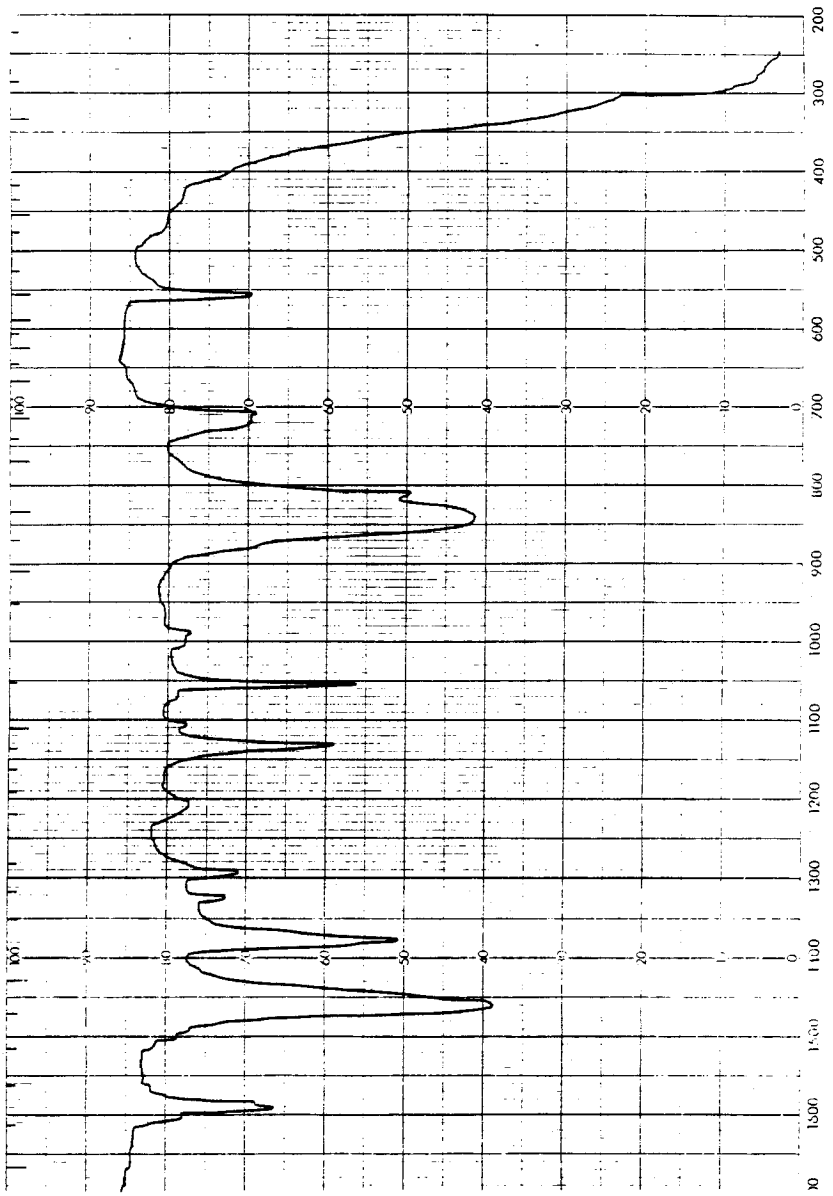

Figure A1.17. IR spectrum of PPh_3.

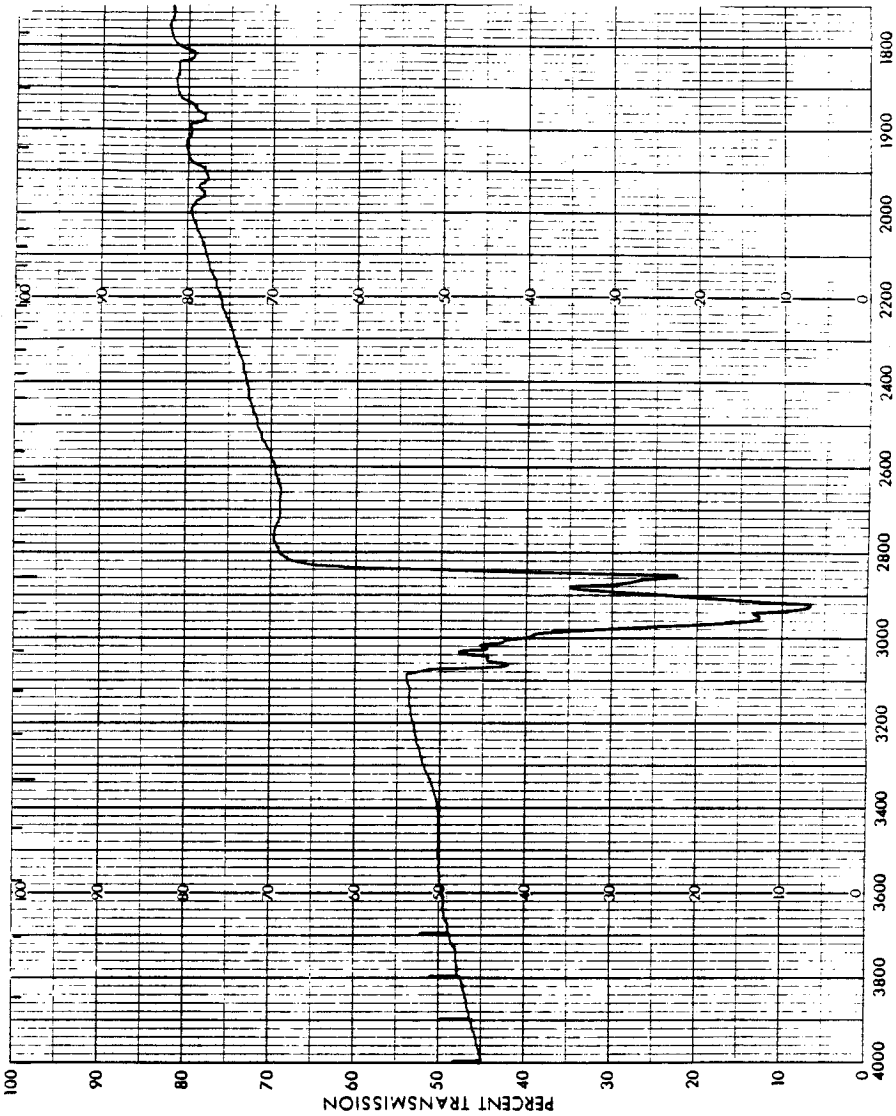

Figure A1.17. (Cont'd)

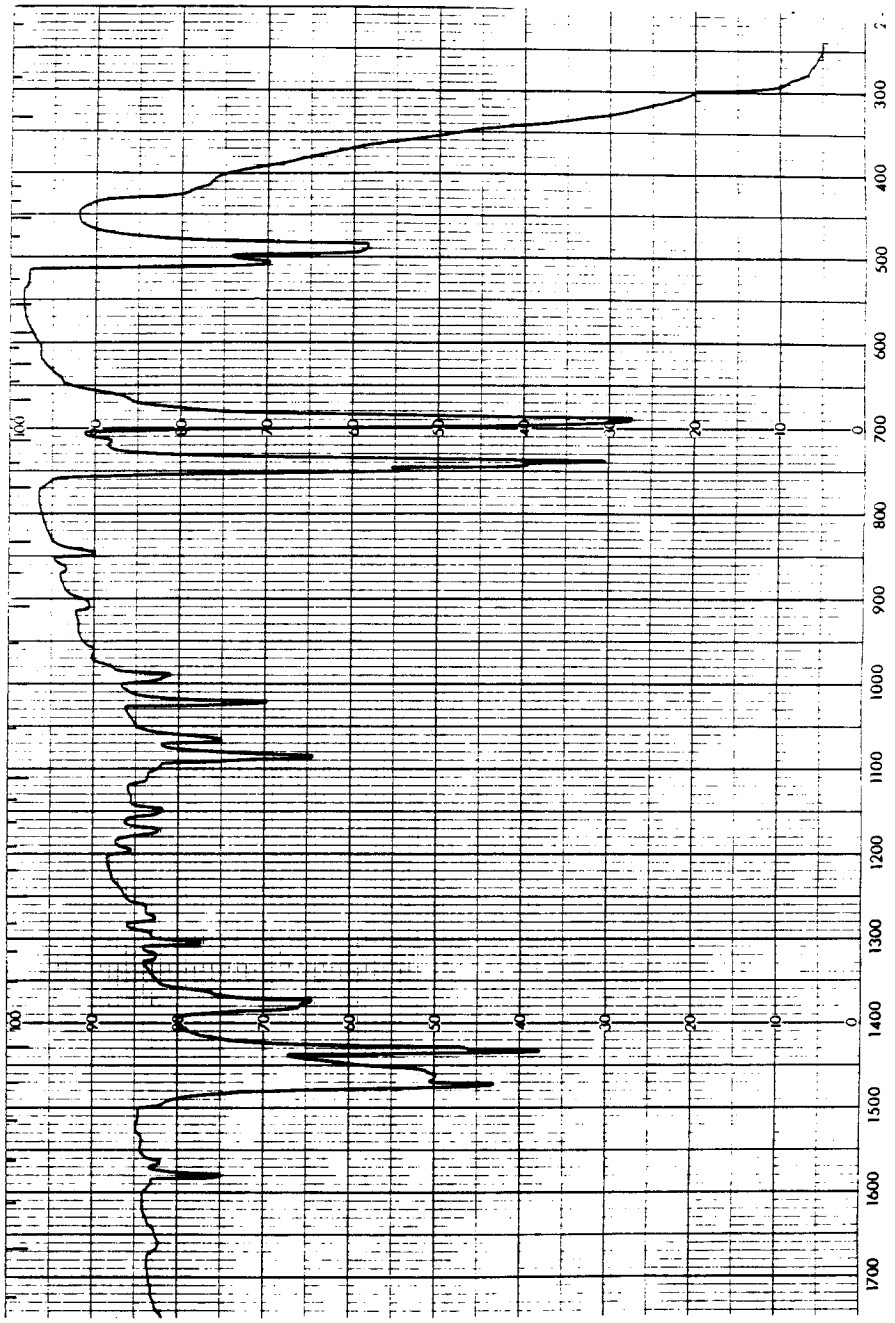

Figure A1.18. IR spectrum of $O=PPh_3$.

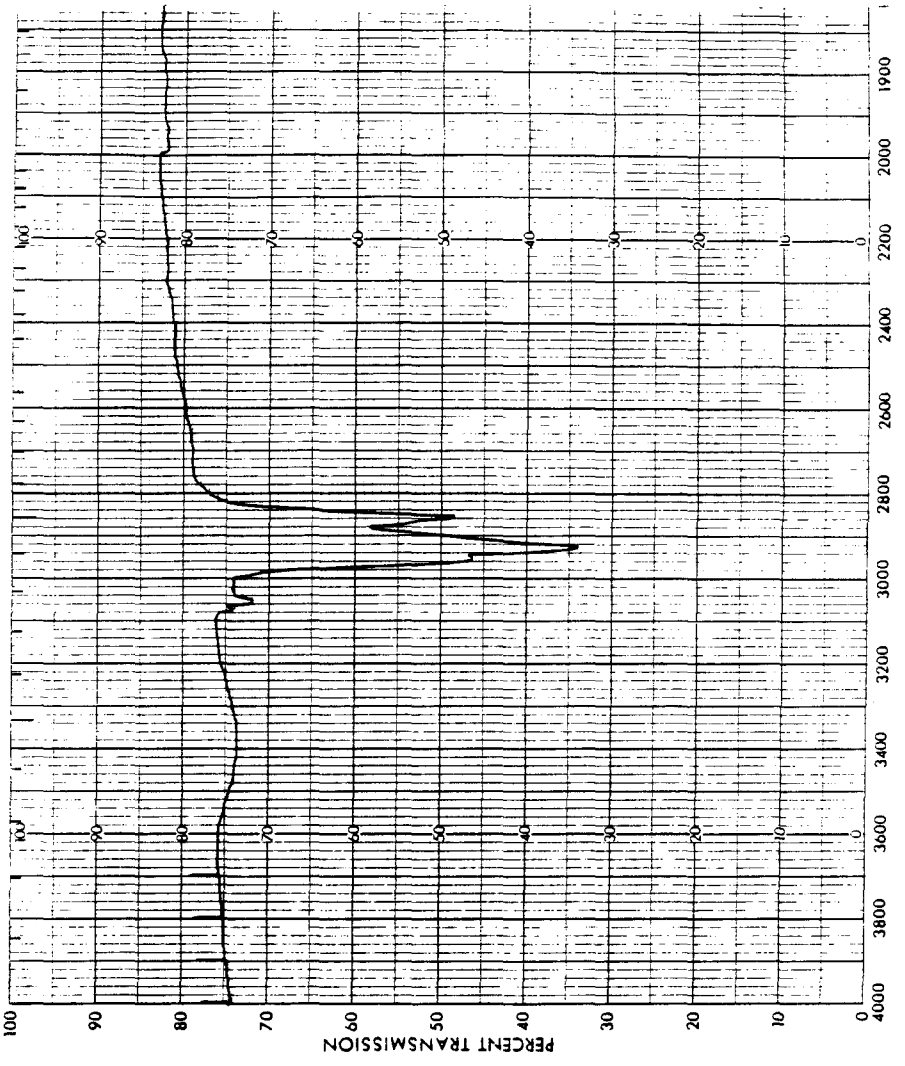

Figure A1.18. (Cont'd)

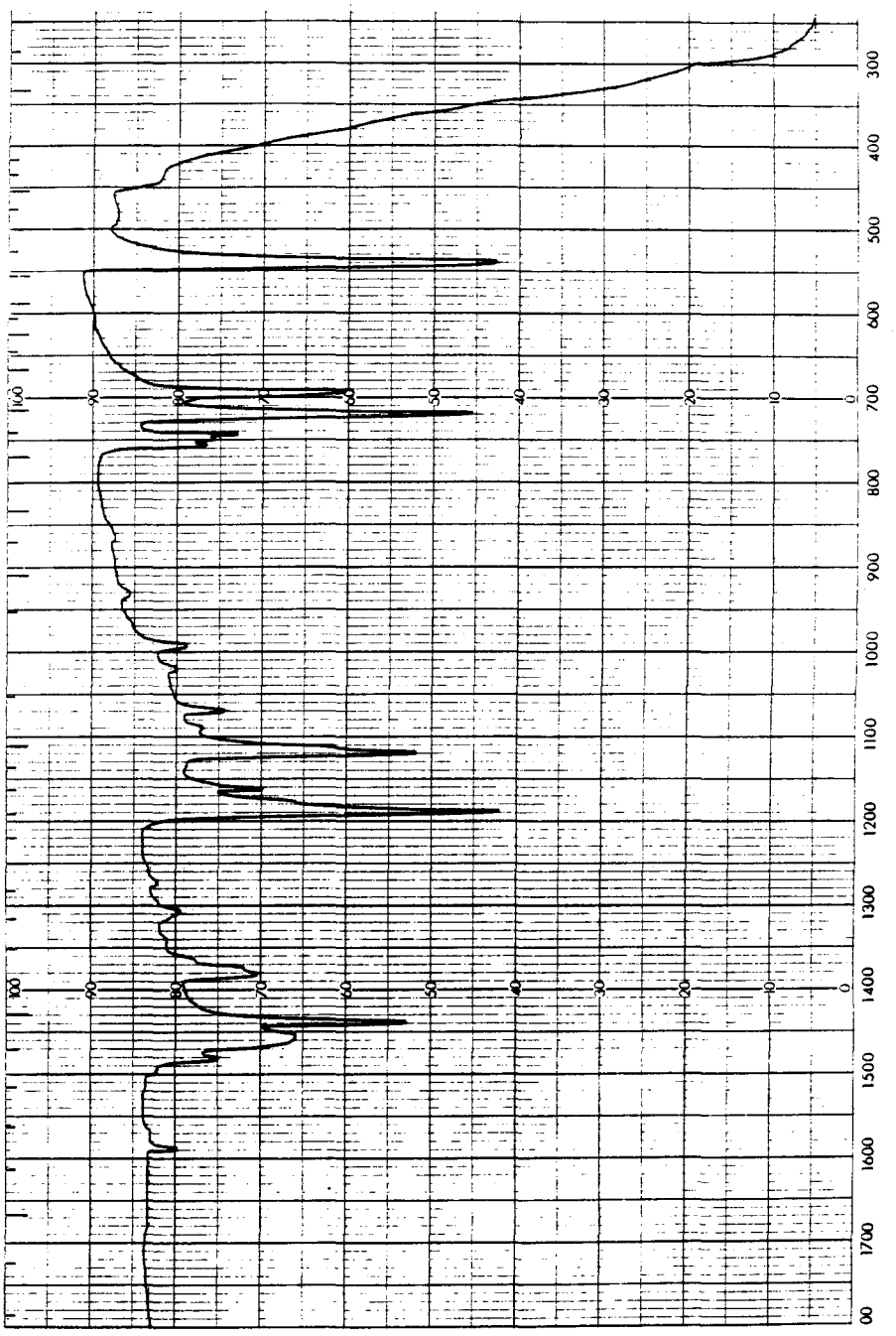

Figure A1.19. IR spectrum of 4-MeOpy.

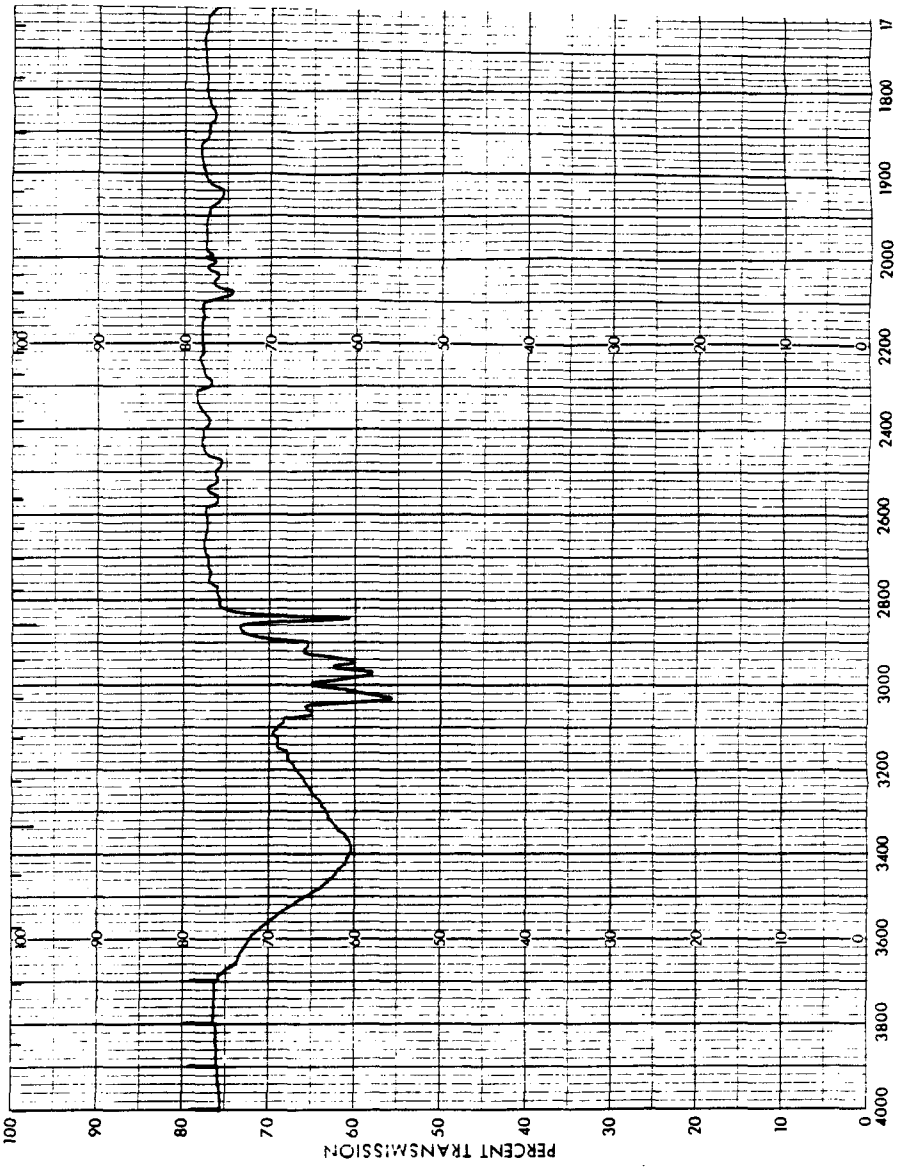

Figure A1.19. (Cont'd)

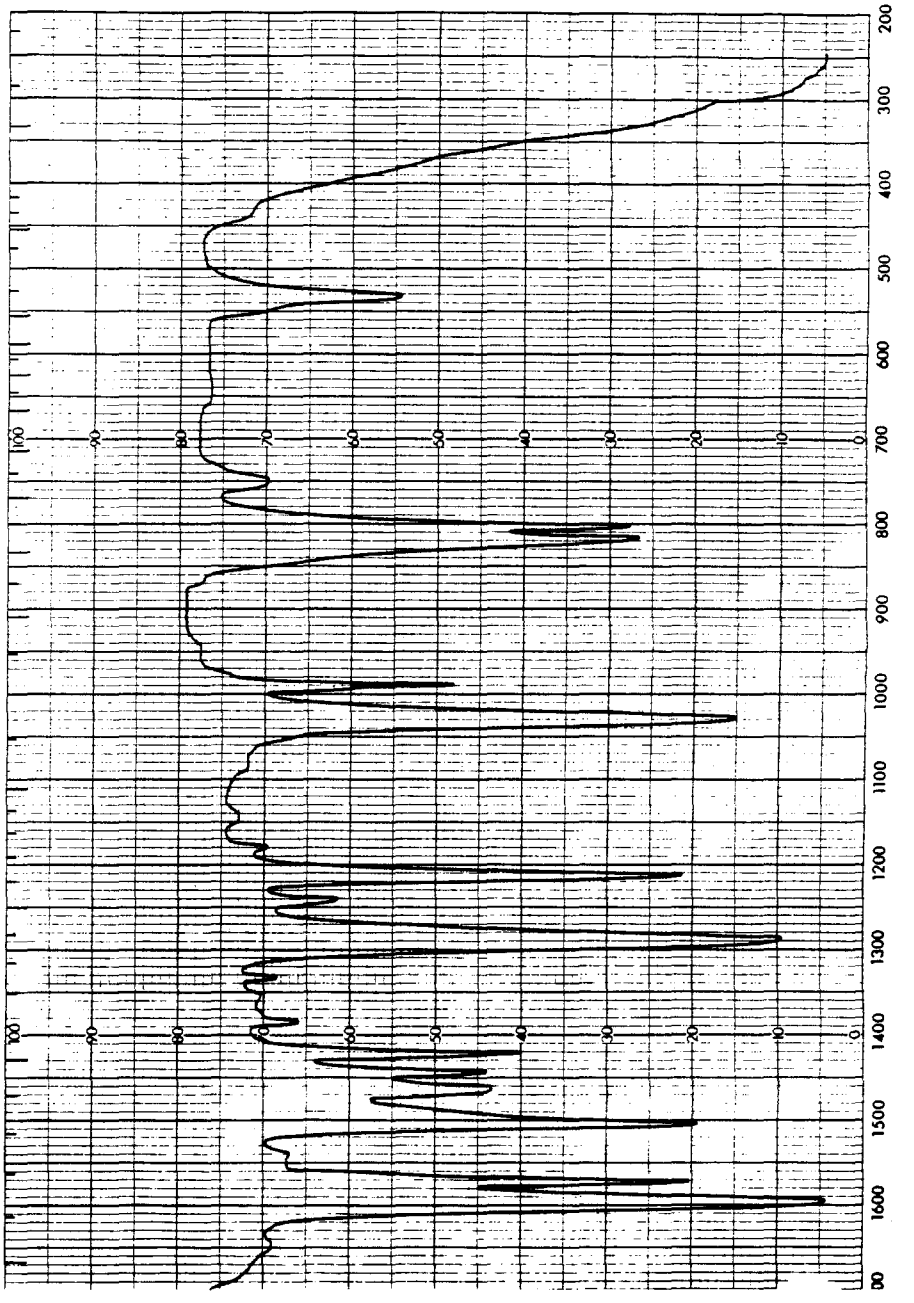

Appendix 2. Supplimentary Material for the X-ray Crystal Structure Determination of *trans*-$[ReO_2(dmap)_4][PF_6]_2$.

Table A2.1. Crystal and Intensity Collection Data for *trans*-$[ReO_2(dmap)_4][PF_6]_2$.

Formula: $ReO_2C_{28}N_8P_2F_{12}H_{40}$	Formula weight: 996.813
Crystal color: Azure	Habit: Prismatic
Crystal size: $0.16 \times 0.21 \times 0.41$ mm	
Space group: $P\bar{1}$ (#2)	
$a = 8.307(3)$Å	$\alpha = 96.24(6)°$
$b = 10.911(5)$Å	$\beta = 108.28(6)°$
$c = 11.907(11)$Å	$\gamma = 99.42(6)°$
$V = 996.1(11)$Å^3	$Z = 1$
$\rho_{calc} = 1.662$ g cm^{-3}	
$\mu = 34.09$ cm^{-1} ($\mu r_{max} = 2.66$)	Transmission coeff. $= 0.51 - 0.64$
CAD-4 diffractometer	θ-2θ scan
$\lambda = 0.7107$Å	Graphite monochromator
2θ range: 2°–50°	Octants collected: $\pm h, \pm k, \pm l$
$T = 293$°K	
Number of reflections measured: 7608	
Number of independent reflections: 3499	
Number with $F_o^2 > 0$: 3498	
Number with $F_o^2 > 3\sigma(F_o^2)$: 3482	
Number of reflections used in refinement: 3499	
Goodness of fit for merging data: 1.29	
Final R-index: 0.0389 for 3498 reflections with $F_o^2 > 0$	
Final R-index: 0.0385 for 3482 reflections with $F_o^2 > 3\sigma(F_o^2)$	
Final goodness of fit: 2.77 for 241 parameters and 3499 reflections	

Table A2.2. Anisotropic Thermal Displacement Parameters x 10^4

for *trans*-[$ReO_2(dmap)_4$][PF_6]$_2$.

Atom	U_{11}	U_{22}	U_{33}	U_{12}	U_{13}	U_{23}
Re	314(2)	665(2)	426(2)	114(1)	105(1)	7(1)
O	372(19)	783(27)	534(21)	114(18)	135(16)	28(19)
N11	385(23)	701(30)	431(23)	113(21)	131(19)	7(21)
C11	373(28)	828(42)	513(32)	158(27)	102(24)	12(29)
C12	496(33)	909(46)	468(31)	162(31)	87(26)	−14(30)
C13	512(33)	927(47)	510(33)	181(32)	188(27)	43(31)
C14	411(31)	1148(56)	557(35)	154(33)	152(27)	−12(35)
C15	379(29)	1042(50)	470(31)	99(30)	141(24)	−21(31)
N12	591(34)	1762(68)	505(31)	308(38)	197(26)	−118(35)
C16	775(54)	2620(133)	578(45)	374(67)	187(40)	−264(60)
C17	624(51)	3700(188)	709(53)	466(78)	307(43)	−230(77)
N21	472(25)	598(30)	554(26)	131(22)	178(21)	20(22)
C21	517(34)	743(43)	607(36)	193(30)	130(28)	57(31)
C22	730(44)	777(47)	660(39)	286(37)	212(34)	104(34)
C23	804(46)	716(45)	784(44)	287(38)	439(39)	39(36)
C24	642(41)	640(44)	992(53)	61(34)	284(39)	−40(38)
C25	494(34)	685(42)	711(40)	78(30)	120(29)	3(32)
N22	876(48)	479(37)	825(46)	199(34)	456(39)	168(33)
C26	1561(93)	783(58)	1717(95)	275(60)	1046(81)	193(59)
C27	2025(121)	755(59)	1661(101)	338(67)	1072(96)	221(62)
P	483(10)	1595(23)	840(14)	237(13)	163(10)	−325(15)
F1	1552(74)	3968(164)	2118(89)	676(86)	−37(65)	−1263(100)
F2	1318(69)	2395(106)	4313(171)	0(68)	−396(87)	1011(115)
F3	1904(93)	3329(142)	2605(109)	348(87)	1125(85)	532(100)
F4	2028(94)	3583(150)	2441(103)	398(94)	−19(82)	−1703(103)
F5	2933(156)	1877(101)	4623(208)	306(97)	−341(146)	1237(124)
F6	1723(90)	4121(182)	3360(145)	199(99)	1402(99)	−470(134)

The form of the displacement factor is:

$$\exp -2\pi^2(U_{11}h^2a^{*2} + U_{22}k^2b^{*2} + U_{33}\ell^2c^{*2} + 2U_{12}hka^*b^* + 2U_{13}h\ell a^*c^* + 2U_{23}k\ell b^*c^*)$$

Table A2.3. Assigned Hydrogen Parameters for *trans*-$[ReO_2(dmap)_4][PF_6]_2$.

x, y and $z \times 10^4$

Atom	x	y	z	B
H16A	−2547	1956	5814	11.2
H16B	−1201	1202	5615	11.2
H16C	−1105	2570	5356	11.2
H17A	−5095	1367	4543	15.2
H17B	−5349	1590	3240	15.2
H17C	−5356	242	3543	15.2
H26A	2801	6944	−1225	10.7
H26B	3050	6472	−11	10.7
H26C	3722	5829	−952	10.7
H27A	503	6461	−2507	12.0
H27B	−71	5042	−3072	12.0
H27C	−1047	5626	−2303	12.0
HC11	1254	1011	2716	5.2
HC12	241	1478	4242	5.7
HC14	−4639	460	1817	6.4
HC15	−3472	−63	393	5.7
HC21	−1996	1673	−1627	5.6
HC22	−1599	3582	−2180	6.4
HC24	3120	4512	422	6.9
HC25	2616	2558	914	5.7

Table A2.4. Complete Distances and Angles for *trans*-$[ReO_2(dmap)_4][PF_6]_2$.

Distance(Å)		Angle(°)	
Re –O	1.764(4)	O –Re –N11	90.0(2)
Re –N11	2.108(4)	O –Re –N21	90.0(2)
Re –N21	2.120(5)	N11 –Re –N21	91.9(2)
N11 –C11	1.346(7)	C15 –N11 –C11	115.2(5)
N11 –C15	1.351(8)	C12 –C11 –N11	124.5(5)
C11 –C12	1.361(9)	HC11 –C11 –N11	117.7
C11 –HC11	0.951	HC11 –C11 –C12	117.8
C12 –C13	1.401(9)	C13 –C12 –C11	120.6(6)
C12 –HC12	0.951	HC12 –C12 –C11	119.5
C13 –C14	1.419(9)	HC12 –C12 –C13	119.9
C13 –N12	1.319(9)	C14 –C13 –C12	114.7(6)
C14 –C15	1.352(9)	N12 –C13 –C12	123.1(6)
C14 –HC14	0.951	N12 –C13 –C14	122.2(6)
C15 –HC15	0.951	C15 –C14 –C13	120.5(6)
N12 –C16	1.451(12)	HC14 –C14 –C13	119.7
N12 –C17	1.457(13)	HC14 –C14 –C15	119.8
C16 –H16A	0.950	C14 –C15 –N11	124.4(6)
C16 –H16B	0.953	HC15 –C15 –N11	117.8
C16 –H16C	0.952	HC15 –C15 –C14	117.8
C17 –H17A	0.949	C16 –N12 –C13	121.1(7)
C17 –H17B	0.941	C17 –N12 –C13	120.7(7)
C17 –H17C	0.961	C17 –N12 –C16	118.1(7)
N21 –C21	1.368(8)	H16A –C16 –N12	109.8
N21 –C25	1.352(8)	H16B –C16 –N12	109.7
C21 –C22	1.343(10)	H16C –C16 –N12	109.6
C21 –HC21	0.949	H16B –C16 –H16A	109.3
C22 –C23	1.408(10)	H16C –C16 –H16A	109.3
C22 –HC22	0.952	H16C –C16 –H16B	109.1
C23 –C24	1.418(11)	H17A –C17 –N12	109.6
C23 –N22	1.298(10)	H17B –C17 –N12	110.1
C24 –C25	1.362(10)	H17C –C17 –N12	108.8
C24 –HC24	0.951	H17B –C17 –H17A	110.3
C25 –HC25	0.949	H17C –C17 –H17A	108.6
N22 –C26	1.438(13)	H17C –C17 –H17B	109.3
N22 –C27	1.394(14)	C25 –N21 –C21	115.8(5)
C26 –H26A	0.948	C22 –C21 –N21	123.5(6)
C26 –H26B	0.948	HC21 –C21 –N21	118.5
C26 –H26C	0.952	HC21 –C21 –C22	118.0
C27 –H27A	0.949	C23 –C22 –C21	121.7(7)
C27 –H27B	0.952	HC22 –C22 –C21	119.4
C27 –H27C	0.951	HC22 –C22 –C23	118.9
P –F1	1.458(11)	C24 –C23 –C22	114.2(7)
P –F2	1.480(12)	N22 –C23 –C22	123.6(7)
P –F3	1.521(12)	N22 –C23 –C24	122.2(7)
P –F4	1.457(12)	C25 –C24 –C23	121.0(7)
P –F5	1.415(15)	HC24 –C24 –C23	119.3
P –F6	1.482(14)	HC24 –C24 –C25	119.7

Table A2.4. (Cont'd)

Angle(°)

C24	-C25	-N21	123.5(6)
HC25	-C25	-N21	118.5
HC25	-C25	-C24	118.1
C26	-N22	-C23	122.6(8)
C27	-N22	-C23	121.6(8)
C27	-N22	-C26	115.2(8)
H26A	-C26	-N22	109.4
H26B	-C26	-N22	109.5
H26C	-C26	-N22	109.2
H26B	-C26	-H26A	109.8
H26C	-C26	-H26A	109.4
H26C	-C26	-H26B	109.4
H27A	-C27	-N22	109.7
H27B	-C27	-N22	109.5
H27C	-C27	-N22	109.6
H27B	-C27	-H27A	109.4
H27C	-C27	-H27A	109.5
H27C	-C27	-H27B	109.2
F2	-P	-F1	86.2(7)
F3	-P	-F1	95.3(6)
F4	-P	-F1	177.4(7)
F5	-P	-F1	88.1(8)
F6	-P	-F1	85.5(7)
F3	-P	-F2	81.7(7)
F4	-P	-F2	91.9(7)
F5	-P	-F2	170.3(8)
F6	-P	-F2	97.0(7)
F4	-P	-F3	86.3(7)
F5	-P	-F3	91.1(8)
F6	-P	-F3	178.4(7)
F5	-P	-F4	94.1(8)
F6	-P	-F4	92.9(7)
F6	-P	-F5	90.3(8)

Table A2.5. Observed and Calculated Structure Factors for *trans*-$[ReO_2(dmap)_4][PF_6]_2$.
The columns contain, in order, ℓ, $10F_{obs}$, $10F_{calc}$ and $10\left(\frac{F^2_{obs}-F^2_{calc}}{\sigma F^2_{obs}}\right)$.
A minus sign preceding F_{obs} indicates that F^2_{obs} is negative.

-9	1	1	
1	168	150	39
2	163	152	24
3	202	207	-10
4	176	166	21
5	172	159	28
6	213	214	-3
7	174	166	19
8	181	166	33
9	177	175	4

-9	2	1	
1	228	235	-18
2	176	166	22
3	227	223	8
4	256	253	5
5	172	153	41
6	191	180	26
7	239	243	-9
8	192	186	13
9	185	173	26

-9	3	1	
1	148	147	3
2	188	184	8
3	188	168	46
4	238	224	33
5	243	247	-9
6	170	160	23
7	199	189	24
8	183	182	3
9	144	124	40

-9	4	1	
1	112	94	34
2	153	157	-11
3	172	171	2
4	121	99	40
5	179	177	2
6	211	214	-8
7	180	167	29
8	172	172	0

-9	5	1	
1	161	149	26
2	149	135	29
3	206	201	11
4	184	186	-2
5	147	135	24
6	197	201	-10
7	193	193	0

-9	6	1	
1	159	168	-20
2	169	159	21
3	129	122	13
4	171	171	-1
5	154	152	5
6	137	128	18

-9	7	1	
2	163	165	-3
3	152	143	17
4	144	135	16

-8	1	1	
1	308	317	-18
2	168	157	25
3	192	189	7
4	300	297	7
5	228	221	14
6	287	273	31
7	299	309	-21
8	230	232	-4
9	140	128	26
10	155	159	-7
11	108	108	0

-8	2	1	
1	276	281	-11
2	319	321	-4
3	209	216	-16
4	206	207	-2
5	261	273	-26
6	250	248	4
7	230	225	9
8	272	284	-27
9	172	172	0
10	161	147	30
11	121	135	-31

-8	3	1	
1	102	87	24
2	192	183	18
3	294	287	15
4	181	168	25
5	253	255	-2
6	311	333	-49
7	224	212	25
8	170	165	13
9	177	180	-7
10	140	133	15
11	105	98	13

-8	4	1	
1	209	207	4
2	143	140	6
3	229	222	14
4	231	230	2
5	225	218	13
6	254	254	0
7	273	283	-22
8	160	149	25
9	159	154	13
10	156	170	-33

-8	5	1	
1	196	197	-1
2	221	217	7
3	149	132	28
4	208	198	20
5	281	289	-18
6	198	189	18
7	210	213	-6
8	183	181	6
9	115	97	34

-8	6	1	
1	166	145	45
2	222	226	-8
3	175	172	5
4	144	134	16
5	224	222	4
6	206	200	15
7	120	120	1
8	139	146	-14
9	154	156	-5

-8	7	1	
1	170	166	9
2	179	156	48
3	185	181	8
4	230	222	16
5	195	190	10
6	193	201	-20
7	163	154	17
8	99	86	22

-8	8	1	
1	140	151	-22
2	130	132	-5
3	122	112	18
4	201	194	13
5	170	171	-1
6	133	130	4

-8	9	1	
1	111	108	5
2	113	108	7
3	114	109	8
4	153	141	24

-7	1	1	
1	285	303	-45
2	440	419	41
3	283	293	-23
4	314	320	-15
5	332	339	-16
6	241	255	-35
7	315	310	10
8	250	268	-41
9	217	226	-21
10	158	147	22
11	145	149	-9
12	143	142	2

-7	2	1	
1	306	332	-66
2	303	322	-48
3	480	476	7
4	302	312	-25
5	83	74	15
6	296	311	-36
7	265	268	-5
8	183	187	-8
9	258	268	-23
10	186	180	13
11	124	121	6
12	156	150	12

-7	3	1	
1	366	365	1
2	207	214	-18
3	335	336	-2
4	403	394	19
5	103	98	9
6	284	283	4
7	299	320	-48
8	221	224	-6
9	185	194	-18
10	212	212	0
11	177	175	3
12	117	112	9

-7	4	1	
1	286	310	-56
2	362	372	-20
3	288	294	-13
4	218	231	-30
5	271	268	6
6	268	267	2
7	173	184	-23
8	259	266	-15
9	184	190	-12
10	147	148	-3
11	209	208	1

-7	5	1	
1	201	193	17
2	264	278	-31
3	315	313	3
4	75	66	12
5	210	208	3
6	315	313	3
7	163	161	4
8	144	166	-41
9	163	166	-5
10	89	72	30
11	86	87	-1

-7	6	1	
1	271	283	-26
2	261	253	16
3	244	260	-36
4	148	143	9
5	168	159	18
6	193	188	9
7	203	204	-3
8	171	158	29
9	169	167	3
10	187	185	4

-7	7	1	
1	246	254	-15
2	265	268	-7
3	173	154	36
4	185	188	-6
5	265	269	-8
6	169	162	14
7	179	182	-7
8	182	184	-4
9	104	92	22

-7	8	1	
1	201	181	37
2	220	230	-19
3	130	137	-11
4	135	123	19
5	195	194	1
6	157	157	0
7	122	122	0
8	153	150	4

-7	9	1	
1	154	150	7
2	123	119	9
3	96	106	-19
4	145	142	7
5	125	123	4
6	121	125	-7

-7	10	1	
1	96	113	-33
2	49	62	-20
3	21	51	-28
4	109	114	-9

-6	1	1	
1	365	378	-32
2	303	320	-45
3	594	568	42
4	360	395	-85
5	316	329	-31
6	232	247	-40

7	273	293	-51
8	201	199	5
9	205	210	-11
10	274	280	-13
11	186	184	3
12	145	147	-2
13	143	138	12

-6 2 l

1	549	517	57
2	398	411	-29
3	310	335	-64
4	547	541	12
5	288	304	-44
6	53	24	39
7	360	365	-10
8	266	267	-2
9	162	175	-28
10	302	313	-24
11	185	190	-9
12	148	137	23
13	124	127	-6

-6 3 l

1	329	359	-77
2	625	599	41
3	351	370	-44
4	380	388	-18
5	333	326	17
6	187	180	16
7	269	279	-24
8	335	323	26
9	277	290	-30
10	250	262	-26
11	203	199	11
12	178	175	6

-6 4 l

1	272	277	-13
2	362	386	-55
3	483	467	31
4	342	342	1
5	102	111	-18
6	286	266	48
7	160	161	-1
8	94	99	-10
9	301	304	-5
10	232	243	-24
11	146	153	-17
12	176	180	-11

-6 5 l

1	372	367	11
2	232	232	1
3	288	288	0
4	297	291	13
5	93	84	16
6	231	245	-34
7	308	298	21
8	158	162	-6
9	180	180	-1
10	155	155	0
11	102	104	-3

-6 6 l

1	352	370	-42
2	380	391	-22
3	308	303	10
4	176	192	-39
5	210	201	21
6	160	165	-9
7	147	147	0
8	256	249	16
9	228	223	11
10	152	155	-6
11	165	170	-10

-6 7 l

1	260	243	39
2	274	288	-31
3	273	279	-12
4	127	115	22
5	196	208	-25
6	242	247	-13
7	158	146	21
8	212	210	3
9	205	209	-9
10	113	106	12

-6 8 l

1	242	239	7
2	235	226	19
3	202	208	-14
4	142	147	-9
5	157	144	24
6	154	167	-24
7	173	171	5
8	173	156	35
9	141	144	-7

-6 9 l

1	166	170	-8
2	163	169	-12
3	107	93	20
4	115	121	-9
5	124	133	-18
6	70	70	0
7	125	117	17
8	147	144	8

-6 10 l

1	100	100	0
2	90	96	-11
3	41	60	-42
4	73	85	-19
5	122	126	-8
6	118	112	9

-6 11 l

1	148	154	-12
2	105	116	-21
3	84	90	-9
4	84	84	0

-5 1 l

1	559	541	33
2	451	470	-42
3	255	243	34
4	521	536	-28
5	411	420	-20
6	265	251	37
7	333	326	17
8	315	317	-4
9	163	174	-27
10	203	204	-3
11	284	289	-12
12	137	135	4
13	114	116	-4

-5 2 l

1	382	398	-40
2	527	516	21
3	463	450	27
4	304	301	8
5	542	538	8
6	389	383	12
7	252	267	-42
8	381	376	10
9	320	299	47
10	188	200	-27
11	265	272	-14
12	181	184	-7
13	116	113	6

-5 3 l

1	476	480	-7
2	351	362	-29
3	582	566	26
4	303	302	3
5	268	287	-52
6	402	391	24
7	415	411	7
8	272	302	-78
9	341	324	36
10	319	322	-4
11	165	173	-17
12	149	144	10
13	102	106	-8

-5 4 l

1	472	444	54
2	305	313	-21
3	320	352	-84
4	450	417	67
5	284	283	2
6	125	140	-39
7	262	228	80
8	153	146	16
9	87	112	-42
10	303	302	1
11	190	196	-13
12	130	122	17

-5 5 l

1	300	311	-26
2	393	356	78
3	207	219	-32
4	230	248	-47
5	329	309	47
6	286	284	5
7	238	264	-68
8	308	297	23
9	202	204	-4
10	157	161	-7
11	140	148	-18
12	102	106	-7

-5 6 l

1	271	283	-31
2	337	348	-26
3	375	362	27
4	275	274	1
5	234	245	-29
6	338	335	6
7	201	191	22
8	139	144	-10
9	265	262	5
10	171	168	7
11	105	105	-1

-5 7 l

1	319	319	0
2	228	227	1
3	253	259	-14
4	288	280	19
5	207	192	34
6	221	227	-14
7	241	248	-15
8	171	172	-2
9	201	194	18
10	161	158	8

-5 8 l

1	231	232	-1
2	220	222	-2
3	164	156	16
4	164	166	-5
5	202	218	-36
6	180	169	23
7	160	159	2
8	190	193	-5
9	163	149	29

-5 9 l

1	115	126	-17
2	168	173	-9
3	171	174	-5
4	133	129	7
5	154	152	2
6	123	124	-2
7	91	76	24
8	131	128	5

-5 10 l

1	112	114	-3
2	99	88	16
3	126	108	29
4	120	124	-7
5	124	124	-1
6	125	130	-10
7	127	124	7

-5 11 l

1	132	134	-5
2	104	116	-24
3	93	90	5
4	105	106	0
5	84	95	-25

-5 12 l

1	80	71	17

-4 1 l

1	92	94	-4
2	570	561	16
3	415	433	-44
4	395	376	47
5	424	445	-50
6	473	484	-23
7	321	329	-21
8	395	387	18
9	347	345	3
10	176	181	-13
11	196	203	-15
12	185	183	3
13	130	117	28

-4 2 l

1	379	385	-14
2	433	432	1
3	496	507	-24
4	652	639	20
5	558	541	32
6	611	601	17
7	586	572	24
8	294	312	-48
9	314	301	32
10	258	240	41

11	184	193	-18
12	170	166	11
13	170	176	-13

-4 3 1

1	554	521	59
2	444	447	-7
3	349	356	-17
4	224	227	-9
5	210	204	18
6	246	265	-56
7	522	514	16
8	443	437	12
9	214	241	-72
10	245	241	9
11	220	219	1
12	108	94	28
13	98	107	-18

-4 4 1

1	231	241	-29
2	373	341	73
3	428	438	-22
4	340	360	-52
5	429	422	15
6	356	337	46
7	152	179	-74
8	275	254	51
9	201	197	9
10	148	156	-17
11	183	186	-7
12	163	163	1

-4 5 1

1	341	351	-27
2	327	341	-37
3	439	409	63
4	290	284	15
5	250	265	-42
6	445	425	39
7	329	326	7
8	198	212	-34
9	230	226	8
10	197	205	-19
11	108	106	3
12	142	138	7

-4 6 1

1	411	367	91
2	321	332	-27
3	283	297	-37
4	368	358	23
5	331	320	26
6	288	296	-18
7	319	324	-11
8	198	187	25
9	116	121	-7
10	173	174	-2
11	111	109	5

-4 7 1

1	286	286	0
2	374	353	46
3	237	248	-28
4	278	281	-8
5	358	359	-1
6	257	238	44
7	211	210	3
8	215	229	-31
9	176	170	13
10	118	117	2

-4 8 1

1	190	198	-17
2	225	215	24
3	179	176	4
4	129	119	21
5	193	183	23
6	220	230	-22
7	171	160	21
8	137	130	15
9	165	163	5
10	110	111	0

-4 9 1

1	167	179	-27
2	149	159	-21
3	200	188	25
4	220	220	1
5	162	157	10
6	133	137	-6
7	135	137	-5
8	115	105	19
9	105	105	-1

-4 10 1

1	167	157	19
2	129	137	-15
3	119	116	5
4	162	146	28
5	136	144	-18
6	115	110	10
7	103	103	0

-4 11 1

1	97	105	-13
2	103	98	10
3	93	97	-7
4	110	98	22
5	101	102	-2

-4 12 1

1	91	92	-1
2	91	79	20
3	98	87	19

-3 1 1

1	520	516	6
2	475	482	-14
3	758	754	5
4	880	869	14
5	595	575	46
6	412	429	-42
7	472	464	16
8	273	295	-60
9	272	266	15
10	369	372	-6
11	205	201	9
12	177	181	-9
13	146	140	13

-3 2 1

1	306	310	-11
2	377	380	-7
3	542	524	36
4	972	989	-19
5	747	736	17
6	616	615	0
7	494	490	7
8	373	356	39
9	189	198	-25
10	216	208	21
11	233	239	-12
12	164	164	0
13	143	140	6

-3 3 1

1	287	267	59
2	502	502	0
3	474	485	-24
4	469	441	81
5	115	123	-24
6	297	295	4
7	247	261	-41
8	285	276	21
9	371	369	4
10	165	169	-9
11	201	204	-7
12	148	157	-21
13	126	112	28

-3 4 1

1	278	301	-70
2	340	352	-33
3	586	561	44
4	540	540	0
5	357	348	24
6	427	431	-8
7	322	318	11
8	119	123	-9
9	290	297	-17
10	234	232	4
11	161	161	0
12	133	137	-8

-3 5 1

1	512	461	97
2	469	466	6
3	582	584	-2
4	479	490	-22
5	339	330	24
6	212	217	-13
7	257	268	-29
8	247	240	16
9	160	166	-13
10	194	202	-18
11	167	176	-21
12	115	103	23

-3 6 1

1	383	383	-1
2	561	537	42
3	456	468	-26
4	263	274	-29
5	396	406	-23
6	326	308	43
7	128	125	6
8	230	238	-18
9	162	168	-13
10	125	115	22
11	112	125	-29

-3 7 1

1	183	203	-58
2	309	306	6
3	430	413	35
4	269	273	-10
5	257	256	2
6	271	280	-19
7	186	178	18
8	196	200	-7
9	206	207	-2
10	155	155	0

-3 8 1

1	309	303	14
2	251	266	-38
3	204	200	7
4	203	199	9
5	172	168	8
6	141	136	9
7	165	176	-22
8	170	151	40
9	127	119	18
10	133	134	-2

-3 9 1

1	242	225	39
2	254	261	-17
3	168	179	-23
4	197	189	17
5	187	188	-2
6	101	92	13
7	114	115	0
8	148	147	1
9	109	107	3

-3 10 1

1	141	156	-29
2	181	172	17
3	138	149	-20
4	122	115	11
5	107	95	22
6	74	84	-22
7	81	82	0

-3 11 1

1	119	132	-21
2	91	101	-12
3	109	105	8
4	117	123	-11
5	84	89	-8
6	80	78	3

-3 12 1

1	125	121	9
2	97	97	0
3	82	81	1

-2 1 1

1	985	1025	-47
2	1605	1515	57
3	1228	1266	-36
4	905	918	-15
5	865	827	48
6	420	420	1
7	313	307	18
8	452	436	32
9	105	114	-21
10	269	267	5
11	319	326	-16
12	204	201	6
13	156	147	20

-2 2 1

1	143	121	81
2	252	276	-89
3	319	304	42
4	791	740	69
5	802	826	-33
6	555	556	-2
7	345	346	0
8	270	260	27
9	139	136	7
10	235	244	-23
11	206	199	16
12	232	226	12
13	157	160	-6

-2 3 l

1	437	436	1
2	706	652	81
3	521	508	26
4	591	607	-29
5	349	322	70
6	289	303	-41
7	458	467	-18
8	109	111	-3
9	156	145	25
10	325	342	-39
11	193	191	4
12	188	179	22
13	175	170	12

-2 4 l

1	619	562	95
2	582	606	-46
3	436	436	0
4	628	612	27
5	474	476	-2
6	227	209	53
7	362	365	-7
8	178	186	-21
9	195	185	23
10	254	255	-2
11	207	211	-7
12	147	140	16

-2 5 l

1	422	419	7
2	522	505	34
3	598	582	29
4	417	406	24
5	371	390	-46
6	322	309	32
7	115	103	27
8	74	85	-19
9	246	253	-16
10	186	179	16
11	172	178	-15
12	159	158	3

-2 6 l

1	523	517	11
2	477	480	-7
3	606	587	32
4	390	397	-15
5	233	230	8
6	374	383	-19
7	195	192	8
8	80	72	12
9	209	213	-10
10	183	167	36
11	115	114	2

-2 7 l

1	289	272	44
2	221	246	-74
3	293	294	-2
4	370	361	20
5	249	249	0
6	181	176	12
7	140	143	-7
8	181	182	-2
9	196	189	16
10	174	173	2

-2 8 l

1	287	268	44
2	351	338	29
3	233	237	-10
4	176	167	20
5	237	246	-21
6	171	174	-6
7	101	85	26
8	176	170	13
9	165	151	31

-2 9 l

1	192	208	-37
2	240	221	42
3	206	211	-13
4	147	152	-11
5	147	145	4
6	101	103	-4
7	67	70	-8
8	118	118	0

-2 10 l

1	162	164	-3
2	149	159	-21
3	154	154	39
4	110	117	-11
5	58	69	-15
6	-8	29	-18
7	57	67	-17

-2 11 l

1	134	126	12
2	110	120	-16
3	104	106	-3
4	142	138	9
5	118	127	-18

-2 12 l

1	128	116	23
2	100	102	-4
3	81	83	-5

-1 1 l

1	164	163	2
2	1036	1100	-72
3	1705	1596	64
4	788	776	17
5	520	524	-9
6	465	455	22
7	323	337	-38
8	299	297	5
9	369	362	17
10	140	147	-17
11	241	232	19
12	200	200	-2
13	128	127	3

-1 2 l

1	957	931	31
2	256	266	-36
3	325	345	-61
4	509	518	-18
5	409	374	82
6	413	414	-1
7	441	450	-21
8	339	345	-13
9	142	142	1
10	207	218	-26
11	245	234	25
12	172	150	50
13	157	156	1

-1 3 l

1	471	454	38
2	620	604	28
3	468	450	40
4	524	508	30
5	506	526	-43
6	343	337	14
7	354	346	20
8	463	467	-9
9	101	92	19
10	208	204	9
11	246	256	-21
12	157	154	6

-1 4 l

1	530	524	13
2	609	590	33
3	472	472	0
4	184	175	31
5	360	363	-9
6	459	470	-22
7	252	243	22
8	254	263	-23
9	187	185	5
10	190	186	9
11	144	136	17
12	116	123	-15

-1 5 l

1	485	509	-52
2	394	375	44
3	521	515	12
4	446	441	10
5	170	147	61
6	252	267	-39
7	328	323	12
8	86	86	0
9	139	142	-4
10	217	225	-17
11	141	130	23

-1 6 l

1	483	462	44
2	423	436	-29
3	259	269	-28
4	405	381	53
5	372	369	6
6	262	256	15
7	302	303	-3
8	153	157	-9
9	151	143	14
10	155	161	-13
11	127	127	0

-1 7 l

1	221	224	-5
2	307	291	41
3	283	289	-15
4	220	222	-5
5	288	291	-6
6	261	260	1
7	159	156	5
8	141	141	0
9	189	182	15
10	127	119	14

-1 8 l

1	229	235	-17
2	230	221	23
3	256	253	7
4	194	189	11
5	193	178	33
6	230	232	-4
7	140	138	2
8	112	104	17
9	154	147	14

-1 9 l

1	177	178	-1
2	121	121	0
3	114	104	17
4	131	139	-16
5	135	139	-6
6	128	113	24
7	101	90	20
8	102	97	10

-1 10 l

1	158	147	21
2	175	186	-24
3	143	146	-4
4	124	109	23
5	101	106	-10
6	50	60	-23
7	38	46	-9

-1 11 l

1	98	94	6
2	94	94	0
3	100	104	-8
4	128	124	8
5	138	133	9

-1 12 l

1	84	90	-11
2	86	84	5
3	75	76	-1

0 0 l

2	320	336	-51
3	911	855	68
4	221	226	-18
5	385	406	-56
6	522	496	52
7	485	493	-17
8	380	400	-48
9	401	405	-9
10	240	249	-20
11	137	126	20
12	159	148	27
13	103	104	-3

0 1 l

-13	95	95	0
-12	157	155	3
-11	161	155	11
-10	220	223	-8
-9	299	307	-19
-8	383	375	18
-7	255	258	-7
-6	479	495	-35
-5	491	482	19
-4	385	357	70
-3	527	557	-63
-2	1000	961	44
-1	106	81	121
1	1108	1038	70
2	524	463	121
3	435	475	-104
4	371	366	14
5	482	454	59
6	235	247	-38
7	545	538	12
8	335	356	-52
9	290	288	5
10	247	245	4
11	174	187	-27

12	126	114	25	2	225	225	0	-1	296	292	10				
13	96	94	4	3	145	154	-33	0	287	291	-9	-8	15	55	-36
				4	440	436	8	1	253	254	-2	-7	52	64	-18
	0 2 1			5	109	102	17	2	158	156	3	-6	53	59	-12
				6	316	323	-19	3	308	309	-2	-5	77	72	8
-13	139	127	26	7	413	422	-20	4	305	311	-14	-4	128	124	6
-12	147	134	29	8	277	277	0	5	241	232	22	-3	156	149	13
-11	181	172	19	9	166	172	-12	6	251	254	-7	-2	115	132	-26
-10	259	271	-30	10	179	177	5	7	230	233	-5	-1	115	122	-11
-9	245	261	-41	11	90	89	1	8	149	137	25	0	122	108	23
-8	362	379	-42					9	153	144	20	1	82	88	-9
-7	328	307	53		0 5 1							2	75	80	-8
-6	298	304	-18						0 8 1			3	92	88	7
-5	150	129	69	-13	86	76	17					4	102	107	-10
-4	320	333	-41	-12	94	82	26	-11	115	109	12				
-3	257	253	11	-11	181	170	22	-10	120	112	15		0 12 1		
-2	135	117	71	-10	204	218	-33	-9	139	129	17				
-1	1864	1818	26	-9	270	267	8	-8	141	139	5	-6	43	49	-13
0	503	452	107	-8	332	318	31	-7	120	129	-19	-5	82	74	14
1	322	311	34	-7	272	285	-35	-6	183	169	32	-4	86	92	-17
2	837	840	-4	-6	210	218	-23	-5	189	190	-1	-3	60	64	-11
3	192	192	0	-5	317	303	36	-4	167	169	-4	-2	62	56	11
4	314	299	43	-4	299	310	-34	-3	329	334	-11	-1	42	64	-29
5	664	691	-44	-3	405	371	77	-2	338	345	-14	0	38	49	-12
6	291	291	0	-2	818	823	-8	-1	200	206	-15	1	49	52	-4
7	345	345	0	-1	861	868	-8	0	191	193	-4	2	64	71	-22
8	459	456	5	0	556	535	40	1	200	186	33				
9	310	325	-38	1	496	473	46	2	156	169	-34		1 -12 1		
10	184	181	7	2	391	396	-11	3	182	172	21				
11	217	221	-6	3	191	198	-21	4	207	213	-13	0	88	83	12
12	149	145	10	4	442	441	1	5	201	201	0	1	84	77	15
				5	415	412	6	6	173	163	19	2	50	60	-23
	0 3 1			6	210	211	-1	7	160	155	12	3	52	50	2
				7	240	243	-9	8	111	113	-3	4	74	76	-2
-13	140	124	35	8	247	259	-29					5	63	77	-39
-12	127	126	3	9	149	139	19		0 9 1			6	37	50	-28
-11	176	174	3	10	152	153	-1								
-10	282	295	-30	11	135	136	-2	-11	95	78	43		1 -11 1		
-9	301	306	-14					-10	90	86	7				
-8	268	274	-16		0 6 1			-9	92	105	-26	0	103	117	-22
-7	299	316	-49					-8	119	114	8	1	139	136	5
-6	350	349	2	-12	80	91	-20	-7	107	118	-18	2	135	128	11
-5	286	293	-21	-11	140	128	21	-6	95	107	-24	3	127	146	-34
-4	443	400	95	-10	130	122	14	-5	115	102	23	4	153	142	20
-3	461	475	-33	-9	104	98	13	-4	168	170	-2	5	88	85	5
-2	491	488	6	-8	137	133	10	-3	203	224	-51	6	61	61	0
-1	1640	1609	21	-7	222	218	10	-2	189	186	5	7	74	66	14
0	825	782	58	-6	223	229	-16	-1	192	183	22	8	42	55	-19
1	151	169	-73	-5	280	273	17	0	173	176	-7				
2	451	443	19	-4	257	268	-31	1	102	99	5		1 -10 1		
3	472	463	19	-3	335	323	30	2	80	78	2				
4	277	265	35	-2	567	579	-22	3	87	76	15	0	120	126	-11
5	375	377	-3	-1	270	284	-42	4	88	88	0	1	134	143	-18
6	631	608	36	0	312	303	24	5	133	135	-4	2	119	112	11
7	326	339	-32	1	325	342	-46	6	127	130	-6	3	121	130	-16
8	277	279	-3	2	326	311	37	7	107	94	30	4	145	174	-62
9	269	275	-14	3	306	305	2					5	142	131	21
10	177	169	17	4	175	188	-35		0 10 1			6	108	110	-3
11	151	151	1	5	331	330	2					7	81	94	-17
12	144	148	-9	6	355	353	3	-10	88	63	47	8	67	64	5
				7	244	245	-2	-9	78	68	16	9	68	63	7
	0 4 1			8	204	201	7	-8	67	64	7				
				9	189	176	29	-7	90	90	0		1 -9 1		
-13	102	101	3	10	123	118	9	-6	119	129	-18				
-12	114	117	-6					-5	113	130	-28	0	210	195	35
-11	189	189	0		0 7 1			-4	163	170	-13	1	150	156	-14
-10	241	241	0					-3	176	184	-19	2	160	167	-15
-9	286	297	-25	-12	94	88	10	-2	105	113	-15	3	221	218	7
-8	269	281	-34	-11	141	131	21	-1	117	118	0	4	179	182	-7
-7	304	310	-15	-10	145	147	-3	0	134	133	1	5	119	135	-31
-6	341	335	15	-9	158	162	-8	1	129	129	-1	6	137	127	19
-5	317	326	-24	-8	126	142	-33	2	168	171	-6	7	106	116	-16
-4	505	475	59	-7	124	104	40	3	179	190	-23	8	109	105	6
-3	450	442	16	-6	137	143	-14	4	151	143	16	9	118	107	21
-2	750	750	0	-5	172	174	-4	5	122	110	24	10	94	97	-5
-1	997	960	42	-4	234	211	61	6	114	101	24				
0	350	364	-38	-3	346	379	-82						1 -8 1		
1	584	573	20	-2	470	441	58		0 11 1						

0	287	287	0	0	71	2	101	-12	182	180	5	8	202	198	9
1	245	235	23	1	912	875	46	-11	145	152	-15	9	125	123	4
2	237	231	13	2	897	825	87	-10	158	161	-7	10	169	167	4
3	309	334	-61	3	181	183	-9	-9	269	267	5	11	150	147	5
4	202	195	16	4	474	473	0	-8	234	252	-54				
5	152	147	11	5	466	437	61	-7	360	350	26		1 4 1		
6	197	212	-39	6	160	187	-89	-6	369	386	9				
7	161	162	-2	7	359	361	-5	-5	439	423	35	-13	139	143	-9
8	126	135	-17	8	334	337	-7	-4	658	664	-10	-12	138	130	14
9	137	138	-1	9	290	278	28	-3	178	154	96	-11	169	162	15
10	135	111	48	10	214	220	-12	-2	429	430	-3	-10	254	257	-7
11	96	86	26	11	186	192	-12	-1	1026	1005	23	-9	216	224	-22
				12	146	130	36	0	587	529	105	-8	292	287	12
	1 -7 1							1	239	258	-76	-7	331	335	-11
					1 -2 1			2	792	812	-28	-6	357	369	-31
0	286	278	21					3	579	561	33	-5	568	523	80
1	249	272	-67	0	433	451	-46	4	222	212	33	-4	582	618	-64
2	324	321	7	1	652	584	112	5	355	372	-45	-3	758	711	66
3	399	369	67	2	873	846	33	6	491	497	-11	-2	506	497	19
4	232	260	-79	3	513	519	-12	7	304	314	-26	-1	696	707	-16
5	155	135	49	4	363	365	-7	8	429	419	20	0	523	486	71
6	81	73	13	5	169	183	-50	9	273	281	-20	1	471	470	3
7	67	67	-2	6	192	205	-45	10	165	155	22	2	567	553	25
8	140	114	54	7	301	307	-14	11	182	181	3	3	73	54	44
9	141	149	-16	8	327	330	-5	12	141	134	14	4	115	124	-25
10	140	150	-18	9	299	315	-38					5	452	457	-12
11	124	118	13	10	193	185	18		1 2 1			6	260	260	0
				11	155	155	0					7	249	253	-9
	1 -6 1			12	168	153	34	-13	178	159	42	8	266	265	4
								-12	199	201	-4	9	158	159	-2
0	340	316	58		1 -1 1			-11	87	83	6	10	138	122	35
1	217	214	8					-10	214	214	1	11	106	114	-18
2	403	426	-53	0	1165	1012	127	-9	310	306	10				
3	407	389	41	1	958	1046	-110	-8	265	270	-14		1 5 1		
4	240	240	0	2	112	66	155	-7	357	376	-49				
5	374	379	-12	3	682	647	55	-6	430	406	54	-13	111	99	23
6	297	270	65	4	715	711	4	-5	401	423	-57	-12	56	47	17
7	177	184	-16	5	335	339	-9	-4	668	630	62	-11	98	94	6
8	199	198	3	6	561	526	63	-3	706	664	64	-10	204	213	-21
9	153	147	14	7	433	438	-10	-2	147	154	-32	-9	232	242	-27
10	131	130	2	8	285	291	-14	-1	135	131	17	-8	277	279	-5
11	131	122	19	9	276	270	14	0	1389	1338	41	-7	358	338	45
12	116	98	35	10	227	232	-11	1	381	399	-48	-6	263	289	-74
				11	136	133	5	2	460	446	31	-5	311	315	-10
	1 -5 1			12	143	136	13	3	815	785	39	-4	329	317	30
								4	257	278	-68	-3	305	271	91
0	550	546	8		1 0 1			5	342	331	28	-2	484	463	44
1	636	577	96					6	572	564	13	-1	606	596	16
2	815	799	21	-13	116	112	7	7	405	415	-22	0	407	389	42
3	507	519	-24	-12	196	197	0	8	253	260	-19	1	262	290	-87
4	344	321	58	-11	218	217	0	9	330	329	3	2	444	429	31
5	356	375	-49	-10	84	68	24	10	226	230	-10	3	413	397	35
6	285	299	-36	-9	372	391	-43	11	192	177	35	4	251	254	-9
7	234	233	1	-8	489	468	41	12	154	142	27	5	317	327	-25
8	282	284	-4	-7	514	504	19					6	380	386	-14
9	266	266	0	-6	445	469	-56		1 3 1			7	214	215	-4
10	193	195	-4	-5	525	521	9					8	176	172	9
11	140	133	15	-4	539	534	9	-13	165	146	41	9	177	174	6
12	101	103	-4	-3	176	218	-203	-12	173	169	7	10	139	134	10
				-2	1348	1284	49	-11	91	106	-25				
	1 -4 1			-1	599	556	78	-10	227	229	-4		1 6 1		
				0	724	814	-150	-9	306	306	0				
0	564	533	57	1	2121	2091	15	-8	326	312	33	-13	102	89	24
1	476	471	10	2	571	560	21	-7	299	311	-32	-12	60	67	-17
2	782	751	43	3	390	401	-29	-6	433	424	19	-11	89	102	-19
3	425	418	16	4	591	582	16	-5	476	466	22	-10	117	110	9
4	419	418	2	5	225	244	-65	-4	402	404	-5	-9	114	107	14
5	284	294	-31	6	394	415	-54	-3	401	390	27	-8	123	141	-40
6	243	233	29	7	499	470	56	-2	502	504	-4	-7	209	207	5
7	372	362	22	8	434	437	-6	-1	637	591	76	-6	299	279	49
8	287	296	-21	9	189	206	-41	0	567	586	-38	-5	285	275	25
9	261	267	-16	10	194	203	-19	1	436	429	17	-4	269	280	-29
10	217	224	-16	11	153	163	-20	2	319	311	22	-3	234	254	-60
11	159	147	22	12	122	114	16	3	388	408	-51	-2	378	349	74
12	102	100	4					4	451	462	-25	-1	368	373	-12
					1 1 1			5	393	385	17	0	317	310	19
	1 -3 1							6	287	295	-21	1	447	435	25
				-13	137	135	4	7	462	450	24	2	265	279	-39

3	264	263	3
4	359	359	0
5	255	248	18
6	265	275	-23
7	218	226	-18
8	154	145	16
9	144	138	12

1 7 1

-12	74	64	19
-11	130	120	21
-10	115	130	-26
-9	144	143	2
-8	198	193	10
-7	158	183	-61
-6	214	199	36
-5	279	289	-24
-4	261	266	-13
-3	260	264	-11
-2	327	324	7
-1	308	294	33
0	267	271	-10
1	323	320	6
2	240	244	-11
3	180	172	17
4	271	274	-5
5	258	270	-27
6	206	194	25
7	168	164	7
8	149	147	4
9	103	106	-4

1 8 1

-11	123	105	34
-10	110	112	-3
-9	113	113	1
-8	134	127	12
-7	150	146	9
-6	152	160	-18
-5	186	180	15
-4	194	186	20
-3	201	208	-17
-2	222	227	-12
-1	155	126	65
0	98	106	-16
1	118	113	10
2	153	135	38
3	170	172	-5
4	174	166	18
5	198	188	20
6	154	150	8
7	88	83	10
8	105	87	34

1 9 1

-11	84	68	24
-10	86	74	21
-9	110	109	3
-8	128	133	-8
-7	128	129	-3
-6	124	131	-13
-5	92	107	-24
-4	127	116	21
-3	174	174	0
-2	167	177	-22
-1	197	186	24
0	229	227	4
1	156	166	-20
2	85	78	10
3	101	106	-6
4	117	119	-3
5	127	116	23
6	122	117	8

1 10 1

-10	68	58	20
-9	88	73	33
-8	89	79	21
-7	91	93	-2
-6	137	135	4
-5	151	155	-7
-4	123	146	-42
-3	153	157	-7
-2	139	134	8
-1	98	111	-22
0	125	124	2
1	137	134	5
2	135	148	-13
3	152	153	-2
4	154	147	16
5	116	111	10

1 11 1

-8	65	65	1
-7	63	74	-21
-6	63	68	-7
-5	71	62	18
-4	88	86	3
-3	95	95	0
-2	102	88	20
-1	96	99	-4
0	91	101	-18
1	83	83	0
2	81	83	-4
3	86	84	4

1 12 1

-6	27	48	-19
-5	45	58	-17
-4	75	73	3
-3	64	68	-8
-2	63	59	7
-1	59	66	-18
0	50	57	-14
1	33	44	-10

2 -12 1

0	117	117	0
1	112	101	21
2	68	69	-2
3	28	51	-24
4	63	59	6
5	62	67	-7
6	35	55	-33

2 -11 1

0	105	110	-7
1	105	123	-29
2	128	123	10
3	113	111	3
4	114	110	6
5	81	83	-2
6	66	65	2
7	73	71	4

2 -10 1

0	151	136	30
1	119	120	0
2	118	121	-5
3	111	110	0
4	106	123	-27
5	130	127	4
6	127	116	18
7	107	111	-8
8	74	86	-20
9	84	67	35

2 -9 1

0	231	234	-9
1	194	185	20
2	137	136	0
3	181	201	-47
4	205	207	-6
5	160	161	-1
6	143	161	-36
7	151	144	13
8	118	100	34
9	87	87	0
10	97	87	24

2 -8 1

0	231	234	-6
1	238	251	-35
2	177	164	33
3	120	99	41
4	121	143	-48
5	143	134	18
6	186	188	-4
7	179	199	-45
8	136	139	-5
9	120	109	22
10	89	89	0

2 -7 1

0	216	227	-31
1	235	215	53
2	290	315	-67
3	310	285	62
4	219	205	34
5	191	208	-46
6	166	155	27
7	103	102	1
8	124	110	25
9	131	135	-6
10	131	125	13
11	103	104	0

2 -6 1

0	446	435	24
1	303	290	35
2	263	257	17
3	409	434	-59
4	293	275	46
5	290	301	-28
6	382	379	7
7	232	223	21
8	151	160	-19
9	150	159	-20
10	161	140	46
11	114	105	18

2 -5 1

0	411	416	-11
1	484	488	-8
2	307	283	65
3	319	319	0
4	488	470	36
5	398	383	33
6	330	344	-35
7	260	267	-16
8	230	221	22
9	193	176	38
10	163	167	-7
11	112	105	13

2 -4 1

0	406	399	15
1	399	395	8
2	645	599	75
3	323	327	-10
4	370	393	-58
5	541	524	32
6	312	324	-29
7	262	252	25
8	290	303	-31
9	220	224	-8
10	178	173	9
11	115	112	5
12	97	83	25

2 -3 1

0	546	547	0
1	100	87	43
2	269	281	-40
3	323	316	21
4	268	271	-8
5	498	484	28
6	382	378	8
7	231	242	-32
8	251	248	6
9	277	279	-5
10	188	185	7
11	131	127	9
12	132	126	13

2 -2 1

0	730	658	105
1	663	688	-41
2	382	343	98
3	676	636	63
4	587	573	25
5	358	390	-85
6	259	243	45
7	356	357	-3
8	221	231	-26
9	237	249	-29
10	168	176	-18
11	117	111	12
12	117	116	3

2 -1 1

0	110	128	-79
1	779	741	53
2	499	509	-22
3	600	616	-29
4	702	672	46
5	627	609	30
6	260	294	-102
7	351	336	35
8	319	317	5
9	199	197	2
10	133	132	2
11	134	136	-5
12	114	111	6

2 0 1

-13	172	170	4
-12	168	159	17
-11	243	250	-16
-10	168	173	-12
-9	140	126	35
-8	350	381	-79
-7	418	413	11
-6	531	512	38
-5	781	762	26
-4	563	554	16
-3	690	677	20
-2	93	14	173
-1	1034	1000	37
0	612	595	30
1	245	245	-1
2	290	298	-24
3	546	521	49

4	630	618	21	-4	560	580	-38	-6	269	279	-26	2	145	150	-9			
5	417	423	-13	-3	280	272	21	-5	307	289	44	3	126	108	30			
6	425	425	0	-2	469	465	8	-4	272	258	36	4	128	123	9			
7	220	226	-19	-1	471	478	-16	-3	302	308	-15	5	129	125	7			
8	318	323	-12	0	197	191	22	-2	305	315	-27							
9	219	231	-27	1	121	125	-14	-1	309	302	16		2	10	1			
10	106	100	9	2	395	415	-50	0	222	241	-53							
11	128	124	8	3	457	434	49	1	379	376	7	-9	85	76	20			
				4	241	254	-39	2	439	444	-10	-8	103	85	37			
	2	1	1	5	471	483	-26	3	246	244	4	-7	92	88	8			
				6	294	290	8	4	258	263	-12	-6	95	99	-6			
-14	127	116	22	7	197	207	-25	5	273	285	-28	-5	119	117	3			
-13	165	157	18	8	182	197	-36	6	228	217	24	-4	132	131	1			
-12	194	194	0	9	103	99	6	7	173	169	6	-3	110	127	-29			
-11	207	210	-5	10	94	87	15	8	146	137	20	-2	124	122	3			
-10	97	95	4					9	112	106	11	-1	118	123	-6			
-9	272	258	36		2	4	1					0	121	123	-2			
-8	245	245	2						2	7	1	1	122	117	9			
-7	266	297	-96	-13	162	145	36					2	127	116	23			
-6	614	597	30	-12	179	188	-18	-12	67	63	7	3	98	106	-16			
-5	542	569	-54	-11	143	137	10	-11	101	82	34	4	84	89	-9			
-4	325	309	46	-10	222	217	11	-10	110	114	-6							
-3	722	698	37	-9	233	244	-27	-9	109	127	-32		2	11	1			
-2	333	341	-24	-8	178	200	-60	-8	192	189	6							
-1	297	314	-55	-7	422	399	51	-7	246	242	8	-8	64	68	-8			
0	751	715	52	-6	471	474	-7	-6	200	218	-45	-7	73	72	1			
1	408	434	-70	-5	390	410	-49	-5	210	215	-10	-6	72	71	1			
2	674	646	45	-4	596	568	48	-4	215	215	-1	-5	62	66	-8			
3	550	570	-38	-3	540	541	-3	-3	179	186	-16	-4	74	73	2			
4	625	627	-2	-2	415	405	24	-2	158	165	-18	-3	72	74	-5			
5	258	273	-44	-1	372	373	-4	-1	248	223	63	-2	56	63	-12			
6	535	519	29	0	470	469	1	0	269	271	-4	-1	78	72	8			
7	409	418	-20	1	377	387	-26	1	256	255	1	0	95	93	4			
8	275	294	-49	2	439	442	-5	2	304	287	38	1	79	90	-26			
9	227	224	6	3	563	563	0	3	227	231	-10	2	85	78	12			
10	182	170	25	4	209	200	25	4	182	165	37							
11	137	123	31	5	216	224	-21	5	169	165	8		2	12	1			
				6	309	318	-21	6	177	180	-4							
	2	2	1	7	242	257	-36	7	104	106	-4	-4	25	48	-25			
				8	144	141	5	8	98	90	14	-3	35	50	-24			
-14	136	127	20	9	145	142	7					-2	51	57	-14			
-13	148	143	11	10	113	122	-20		2	8	1							
-12	218	211	13										3	-12	1			
-11	204	203	0		2	5	1	-11	83	88	-10							
-10	77	69	12					-10	107	102	9	0	119	116	4			
-9	253	268	-41	-13	102	93	19	-9	94	107	-19	1	86	97	-20			
-8	327	311	39	-12	94	77	29	-8	108	128	-34	2	73	68	10			
-7	286	284	7	-11	46	49	-4	-7	139	137	5	3	34	53	-22			
-6	563	564	-3	-10	141	133	17	-6	166	157	20	4	55	60	-10			
-5	572	561	21	-9	214	212	2	-5	144	160	-35	5	83	62	38			
-4	535	539	-9	-8	235	250	-40	-4	178	181	-6							
-3	490	493	-7	-7	288	307	-48	-3	223	210	31		3	-11	1			
-2	690	663	42	-6	357	352	12	-2	157	171	-31							
-1	306	304	8	-5	314	316	-4	-1	101	91	19	0	123	118	7			
0	451	482	-74	-4	251	270	-55	0	111	87	40	1	77	93	-22			
1	549	502	88	-3	329	349	-53	1	115	124	-17	2	85	98	-19			
2	660	652	12	-2	410	398	31	2	114	116	-2	3	99	108	-12			
3	606	600	9	-1	353	346	19	3	142	147	-11	4	104	100	6			
4	601	610	-17	0	335	340	-13	4	162	164	-4	5	74	83	-16			
5	335	341	-13	1	446	429	35	5	140	131	18	6	78	74	6			
6	181	193	-35	2	320	321	-2	6	133	127	14	7	80	70	15			
7	367	357	23	3	338	349	-25	7	93	86	13							
8	294	312	-42	4	380	375	10						3	-10	1			
9	159	162	-6	5	257	248	23		2	9	1							
10	197	192	10	6	227	226	1					0	145	153	-14			
11	174	175	-2	7	253	257	-8	-11	66	62	6	1	152	142	19			
				8	139	136	6	-10	69	71	-4	2	120	121	-1			
	2	3	1	9	105	105	-1	-9	109	107	4	3	130	137	-14			
								-8	163	159	6	4	117	126	-15			
-13	168	157	25		2	6	1	-7	146	154	-15	5	128	114	24			
-12	190	182	15					-6	125	127	-4	6	109	114	-9			
-11	138	135	6	-13	99	98	1	-5	120	120	0	7	104	110	-13			
-10	147	150	-5	-12	90	75	27	-4	105	118	-24	8	100	94	11			
-9	239	241	-5	-11	97	87	15	-3	133	128	9							
-8	302	316	-38	-10	118	125	-10	-2	166	152	29		3	-9	1			
-7	479	473	13	-9	126	119	13	-1	165	182	-40							
-6	592	596	-7	-8	207	208	-1	0	214	209	10	0	134	141	-16			
-5	594	588	9	-7	274	297	-57	1	202	210	-21	1	120	134	-30			

2	147	147	0	10	179	168	26						7	187	188	-3		
3	195	187	17	11	109	106	5	-14	126	115	22		8	149	149	-1		
4	204	218	-32					-13	121	119	3		9	141	137	8		
5	182	193	-22		3	-3	1	-12	158	154	6		10	128	121	13		
6	155	159	-7					-11	206	211	-12							
7	139	128	24	0	511	489	44	-10	195	190	12			3	4	1		
8	99	92	13	1	641	618	37	-9	209	222	-36							
9	62	66	-5	2	220	236	-55	-8	391	379	26		-13	106	99	14		
				3	245	249	-10	-7	319	309	28		-12	157	156	2		
	3	-8	1	4	473	471	5	-6	364	371	-19		-11	186	193	-14		
				5	308	322	-38	-5	794	780	20		-10	184	187	-6		
0	253	232	50	6	305	306	-3	-4	381	386	-14		-9	245	244	2		
1	141	137	8	7	268	278	-23	-3	259	267	-26		-8	245	249	-9		
2	175	188	-34	8	204	203	1	-2	502	476	53		-7	224	243	-56		
3	138	124	30	9	168	169	0	-1	769	751	26		-6	438	420	38		
4	71	69	2	10	202	204	-3	0	661	676	-24		-5	427	433	-15		
5	120	129	-19	11	131	127	8	1	517	494	44		-4	276	290	-41		
6	173	165	16					2	520	512	14		-3	258	261	-6		
7	152	162	-20		3	-2	1	3	496	488	17		-2	494	490	7		
8	126	128	-4					4	494	503	-19		-1	319	320	-5		
9	95	89	10	0	547	521	51	5	433	438	-11		0	328	349	-54		
10	68	64	6	1	669	661	14	6	284	297	-32		1	532	519	24		
				2	684	667	26	7	344	345	0		2	357	354	8		
	3	-7	1	3	497	483	29	8	316	328	-28		3	273	289	-43		
				4	499	477	44	9	202	203	-2		4	350	361	-25		
0	275	273	3	5	475	470	10	10	157	145	27		5	254	250	11		
1	233	219	36	6	224	232	-23						6	174	168	13		
2	247	250	-6	7	240	231	22		3	2	1		7	218	223	-12		
3	331	333	-5	8	236	242	-14						8	178	178	1		
4	286	260	62	9	183	184	0	-14	119	100	36		9	102	102	0		
5	189	194	-11	10	161	157	8	-13	137	139	-3							
6	175	190	-33	11	127	123	7	-12	128	138	-17			3	5	1		
7	175	160	33					-11	216	216	-1							
8	128	118	16		3	-1	1	-10	241	246	-13		-13	69	75	-11		
9	118	115	5					-9	257	248	22		-12	90	86	7		
10	116	103	26	0	599	570	52	-8	322	332	-27		-11	114	104	17		
				1	615	591	43	-7	385	391	-15		-10	155	155	0		
	3	-6	1	2	528	554	-52	-6	309	323	-38		-9	178	187	-22		
				3	528	523	10	-5	457	456	0		-8	229	214	35		
0	246	261	-43	4	440	434	15	-4	573	573	-1		-7	259	279	-51		
1	433	423	21	5	463	457	13	-3	207	213	-22		-6	254	269	-40		
2	409	396	29	6	340	333	15	-2	85	76	26		-5	306	298	20		
3	290	290	-1	7	198	206	-21	-1	459	463	-8		-4	273	282	-25		
4	363	379	-36	8	157	159	-4	0	505	512	-16		-3	174	170	10		
5	316	309	16	9	228	237	-21	1	564	564	0		-2	391	404	-31		
6	249	248	2	10	139	135	9	2	552	550	3		-1	501	492	18		
7	215	226	-26	11	107	98	17	3	501	483	35		0	324	330	-14		
8	152	149	6					4	335	337	-5		1	375	374	1		
9	129	120	15		3	0	1	5	287	296	-24		2	438	426	25		
10	118	120	-3					6	263	267	-9		3	289	284	11		
				-14	117	100	34	7	108	104	8		4	204	202	5		
	3	-5	1	-13	117	117	1	8	241	246	-10		5	243	263	-46		
				-12	192	198	-11	9	205	209	-8		6	190	179	21		
0	246	251	-14	-11	134	147	-26	10	124	124	0		7	179	175	8		
1	357	360	-5	-10	226	224	5						8	168	168	0		
2	548	526	40	-9	283	275	18		3	3	1							
3	310	315	-12	-8	311	294	44							3	6	1		
4	304	303	4	-7	284	305	-62	-14	126	117	18							
5	452	431	41	-6	356	361	-13	-13	171	153	41		-13	78	77	0		
6	322	317	12	-5	615	587	48	-12	144	159	-27		-12	94	93	2		
7	204	208	-8	-4	548	512	69	-11	159	160	-1		-11	115	107	13		
8	186	179	16	-3	617	616	3	-10	181	186	-13		-10	169	156	26		
9	135	129	11	-2	291	282	25	-9	303	300	6		-9	156	167	-26		
10	129	115	29	-1	461	480	-44	-8	278	285	-16		-8	176	172	9		
11	120	113	15	0	577	571	11	-7	397	390	15		-7	265	267	-5		
				1	505	501	7	-6	657	655	4		-6	249	267	-46		
	3	-4	1	2	603	574	50	-5	437	458	-49		-5	194	196	-3		
				3	519	523	-8	-4	416	401	33		-4	224	217	18		
0	369	330	95	4	528	531	-4	-3	400	415	-36		-3	314	313	3		
1	304	309	-16	5	350	363	-33	-2	383	385	-2		-2	330	333	-8		
2	376	375	3	6	319	304	37	-1	468	453	32		-1	358	343	35		
3	617	576	67	7	323	321	3	0	450	450	1		0	361	366	-11		
4	351	361	-25	8	145	146	-1	1	305	322	-49		1	246	262	-40		
5	319	321	-6	9	211	208	7	2	282	294	-34		2	252	253	-1		
6	404	399	11	10	166	164	4	3	394	408	-33		3	274	284	-24		
7	240	241	-1	11	125	112	26	4	332	328	9		4	191	184	15		
8	213	208	11					5	173	162	27		5	181	177	10		
9	186	191	-11		3	1	1	6	276	283	-16		6	189	191	-4		

7	163	157	13	2	67	71	-7
8	121	112	17				
				3	11	1	
	3	7	1				
				-7	52	56	-10
-12	90	80	18	-6	34	52	-23
-11	83	82	1	-5	39	57	-34
-10	103	98	7	-4	63	73	-27
-9	125	121	8	-3	83	74	16
-8	138	162	-51	-2	77	71	9
-7	211	201	25	-1	83	78	10
-6	214	207	16	0	98	80	28
-5	166	168	-4				
-4	82	81	2	4	-12	1	
-3	125	108	34				
-2	122	129	-15	0	108	103	10
-1	106	124	-36	1	72	88	-26
0	247	227	46	2	46	65	-37
1	244	256	-30	3	51	54	-5
2	168	171	-6				
3	176	160	33	4	-11	1	
4	156	154	3				
5	103	99	7	0	109	109	0
6	111	110	0	1	102	96	11
7	123	125	-4	2	81	77	6
				3	90	93	-6
	3	8	1	4	112	109	4
				5	94	93	3
-11	103	94	16	6	85	82	9
-10	108	112	-8				
-9	113	102	16	4	-10	1	
-8	109	113	-7				
-7	114	121	-13	0	148	154	-11
-6	118	114	7	1	164	176	-26
-5	130	123	12	2	165	163	3
-4	140	148	-16	3	157	156	3
-3	208	211	-9	4	122	143	-34
-2	237	218	43	5	119	108	22
-1	160	171	-25	6	114	99	28
0	133	129	7	7	89	93	-7
1	164	137	52				
2	144	145	-2	4	-9	1	
3	119	117	2				
4	132	128	7	0	143	126	34
5	128	126	5	1	55	59	-6
6	97	102	-6	2	83	93	-16
				3	177	181	-9
	3	9	1	4	195	189	13
				5	156	167	-22
-10	83	72	27	6	151	145	14
-9	96	91	8	7	89	92	-5
-8	137	130	14	8	60	59	4
-7	148	148	0				
-6	118	128	-17	4	-8	1	
-5	117	107	17				
-4	131	127	8	0	239	238	1
-3	142	148	-12	1	197	186	25
-2	145	143	4	2	154	138	35
-1	170	170	0	3	177	186	-21
0	160	182	-41	4	149	139	21
1	138	140	-3	5	137	130	12
2	135	125	19	6	157	157	-1
3	108	110	-4	7	138	122	34
4	87	86	1	8	84	91	-13
				9	71	77	-14
	3	10	1				
				4	-7	1	
-9	78	73	12				
-8	82	79	4	0	229	237	-20
-7	76	76	0	1	257	265	-19
-6	76	73	4	2	316	308	20
-5	71	67	5	3	274	273	3
-4	97	86	19	4	261	255	14
-3	111	108	4	5	236	228	18
-2	107	112	-11	6	161	170	-18
-1	123	118	10	7	122	128	-10
0	127	114	26	8	123	120	7
1	79	89	-18	9	99	98	2

				4	-6	1	
0	280	277	6				
1	178	185	-18				
2	482	465	33				
3	400	383	35				
4	235	253	-44				
5	296	293	8				
6	192	185	14				
7	128	114	24				
8	105	121	-26				
9	117	118	-1				
				4	-5	1	
0	470	430	80				
1	362	362	-1				
2	374	382	-18				
3	479	458	42				
4	373	359	32				
5	297	302	-11				
6	225	232	-16				
7	173	175	-5				
8	119	120	-1				
9	133	121	25				
10	126	114	25				
				4	-4	1	
0	57	53	9				
1	489	476	26				
2	380	386	-14				
3	317	311	16				
4	476	477	-2				
5	293	300	-17				
6	179	174	13				
7	214	224	-23				
8	193	189	10				
9	165	151	33				
10	153	151	3				
				4	-3	1	
0	209	220	-34				
1	583	554	52				
2	581	569	21				
3	278	286	-23				
4	390	371	43				
5	328	325	6				
6	206	213	-17				
7	162	158	9				
8	196	207	-25				
9	174	166	18				
10	159	147	26				
				4	-2	1	
0	549	562	-25				
1	634	599	58				
2	547	553	-10				
3	567	562	10				
4	394	393	3				
5	185	176	25				
6	266	269	-7				
7	159	157	4				
8	151	160	-20				
9	185	182	6				
10	157	148	20				
				4	-1	1	
0	539	555	-32				
1	575	565	18				
2	482	458	49				
3	527	540	-26				
4	404	397	14				
5	144	143	2				

6	169	162	16
7	216	225	-21
8	157	164	-15
9	167	162	12
10	169	169	0
	4	0	1
-14	103	102	3
-13	105	106	-3
-12	157	156	1
-11	183	200	-39
-10	190	200	-23
-9	235	241	-17
-8	460	465	-9
-7	347	339	21
-6	214	207	20
-5	478	487	-18
-4	541	526	28
-3	350	329	54
-2	494	495	-1
-1	270	283	-41
0	686	680	8
1	549	569	-40
2	483	464	40
3	630	628	2
4	409	408	2
5	406	409	-6
6	179	190	-25
7	230	214	36
8	221	230	-19
9	180	168	27
10	158	152	12
	4	1	1
-14	108	104	7
-13	137	139	-5
-12	169	162	14
-11	155	148	14
-10	247	256	-20
-9	255	246	21
-8	276	284	-21
-7	432	423	19
-6	323	308	36
-5	256	254	3
-4	439	453	-32
-3	506	483	46
-2	266	278	-35
-1	562	555	12
0	755	723	46
1	592	598	-10
2	476	482	-13
3	488	470	36
4	129	138	-23
5	292	290	4
6	306	312	-13
7	221	227	-14
8	231	232	-1
9	209	213	-12
	4	2	1
-14	99	86	22
-13	126	119	14
-12	155	167	-24
-11	168	163	10
-10	251	250	1
-9	380	384	-9
-8	353	346	15
-7	307	310	-8
-6	419	426	-15
-5	322	333	-30
-4	201	201	-1
-3	505	507	-3
-2	113	115	-4
-1	235	254	-60
0	440	444	-9

1	408	400	18	3	235	245	-23	-2	137	133	7	1	284	291	-16
2	451	463	-26	4	192	183	20	-1	129	117	23	2	262	249	31
3	380	397	-41	5	163	150	25	0	156	140	35	3	307	315	-19
4	236	226	25	6	185	181	8	1	104	109	-9	4	202	216	-34
5	88	88	0	7	167	164	7	2	51	61	-22	5	190	189	2
6	180	172	19									6	197	190	14
7	192	198	-13		4	6	1		4	10	1	7	109	99	20
8	161	154	15									8	94	91	4
9	174	167	14	-12	86	79	12	-8	60	68	-18				
				-11	119	122	-7	-7	65	70	-9		5	-5	1
	4	3	1	-10	150	151	-2	-6	78	70	12				
				-9	169	173	-9	-5	54	63	-16	0	316	314	4
-13	166	146	43	-8	168	178	-21	-4	54	69	-22	1	393	386	15
-12	143	145	-3	-7	148	153	-11	-3	92	90	3	2	347	362	-35
-11	157	168	-22	-6	163	152	24	-2	99	100	-1	3	266	251	35
-10	200	195	12	-5	142	150	-18	-1	104	108	-7	4	257	260	-9
-9	278	278	0	-4	126	127	-1	0	117	103	25	5	319	324	-13
-8	347	362	-36	-3	208	198	23					6	209	204	11
-7	278	297	-51	-2	347	356	-20		5	-12	1	7	120	134	-25
-6	341	330	25	-1	257	273	-39					8	133	133	0
-5	485	476	17	0	273	252	48	0	71	79	-18	9	109	104	9
-4	253	259	-16	1	333	327	14	1	88	86	3				
-3	205	212	-23	2	168	165	6						5	-4	1
-2	362	371	-22	3	109	103	10		5	-11	1				
-1	489	496	-14	4	153	154	-1					0	234	256	-64
0	362	379	-44	5	142	134	18	0	113	117	-8	1	170	168	5
1	424	410	29	6	131	123	17	1	100	106	-12	2	427	427	0
2	480	468	23					2	94	90	8	3	280	293	-33
3	186	189	-8		4	7	1	3	93	77	27	4	225	214	26
4	249	251	-4					4	99	92	13	5	352	368	-37
5	200	202	-2	-12	80	73	19					6	191	197	-11
6	143	134	16	-11	83	85	-4		5	-10	1	7	144	135	17
7	185	183	4	-10	93	87	12					8	165	167	-5
8	182	182	-1	-9	107	97	14	0	149	156	-13	9	143	138	11
				-8	135	130	8	1	170	174	-8				
	4	4	1	-7	148	158	-20	2	158	166	-16		5	-3	1
				-6	161	163	-3	3	144	145	-1				
-13	111	104	14	-5	174	173	2	4	121	119	4	0	551	521	54
-12	108	106	2	-4	110	121	-21	5	84	80	10	1	301	315	-36
-11	164	159	10	-3	73	69	6	6	79	75	7	2	339	331	21
-10	202	209	-14	-2	151	131	41					3	318	320	-4
-9	198	201	-6	-1	154	161	-15		5	-9	1	4	301	308	-18
-8	229	224	10	0	152	159	-14					5	303	289	32
-7	263	275	-30	1	223	207	33	0	118	125	-13	6	168	182	-32
-6	214	238	-68	2	147	159	-22	1	105	111	-9	7	174	166	17
-5	286	266	50	3	99	92	9	2	91	78	17	8	144	135	20
-4	428	422	14	4	100	93	13	3	117	129	-19	9	142	140	5
-3	243	244	-3	5	107	109	-4	4	150	151	-1				
-2	264	260	10					5	111	111	1		5	-2	1
-1	535	527	15		4	8	1	6	100	110	-19				
0	353	366	-31					7	114	96	33	0	350	374	-63
1	296	311	-41	-11	100	91	15					1	486	482	10
2	442	442	0	-10	113	110	5		5	-8	1	2	304	308	-11
3	221	211	24	-9	116	114	4					3	202	190	30
4	143	146	-8	-8	114	108	10	0	200	195	9	4	426	439	-29
5	206	215	-20	-7	110	113	-5	1	206	210	-8	5	225	237	-29
6	188	187	3	-6	116	120	-7	2	174	172	3	6	103	103	1
7	155	141	31	-5	122	119	5	3	164	160	8	7	191	194	-7
8	161	157	6	-4	139	131	14	4	136	149	-26	8	149	144	11
				-3	158	185	-59	5	149	132	33	9	121	114	13
	4	5	1	-2	181	190	-24	6	168	152	36				
				-1	185	174	22	7	122	118	9		5	-1	1
-13	86	90	-7	0	180	187	-14								
-12	89	94	-8	1	156	146	18		5	-7	1	0	298	315	-50
-11	125	121	7	2	122	108	28					1	507	520	-26
-10	183	171	24	3	107	115	-15	0	328	327	3	2	472	457	29
-9	201	208	-16	4	94	97	-4	1	237	233	9	3	252	254	-6
-8	199	195	9					2	229	242	-32	4	394	395	0
-7	232	220	28		4	9	1	3	254	249	12	5	241	242	-3
-6	294	297	-7					4	165	159	12	6	125	130	-10
-5	255	260	-13	-10	82	64	28	5	155	163	-16	7	156	149	13
-4	310	294	38	-9	81	77	7	6	200	197	6	8	176	184	-18
-3	279	291	-29	-8	92	91	2	7	123	117	13	9	166	159	16
-2	255	274	-51	-7	106	98	15	8	98	91	12				
-1	346	341	9	-6	103	108	-10						5	0	1
0	398	403	-10	-5	95	107	-16		5	-6	1				
1	334	352	-43	-4	115	109	9					-13	116	125	-19
2	272	280	-18	-3	155	140	28	0	383	378	10	-12	162	166	-7

trans[ReO2(DMAP)4](PF6)2 Page 12

-11	211	203	19	-8	178	176	5	2	205	207	-4	1	189	174	30
-10	214	214	1	-7	330	322	19	3	104	104	0	2	147	154	-12
-9	257	256	1	-6	278	295	-46	4	102	93	16	3	152	153	-1
-8	212	214	-4	-5	295	286	20	5	133	130	5	4	123	123	0
-7	303	312	-23	-4	394	396	-4					5	93	101	-15
-6	410	405	10	-3	347	350	-8		5	7	1	6	136	122	28
-5	237	226	31	-2	219	228	-24								
-4	626	647	-36	-1	349	352	-7	-11	71	77	-10		6	-7	1
-3	631	598	54	0	347	344	7	-10	75	70	11				
-2	416	415	1	1	164	186	-57	-9	50	66	-27	0	277	285	-18
-1	439	451	-28	2	346	347	-1	-8	114	104	15	1	241	256	-36
0	406	387	44	3	368	365	6	-7	146	138	14	2	166	159	15
1	377	391	-33	4	112	112	-1	-6	152	159	-14	3	152	151	2
2	332	351	-49	5	191	177	31	-5	151	167	-32	4	124	126	-3
3	524	514	19	6	171	176	-12	-4	174	162	28	5	87	90	-6
4	426	444	-39	7	114	109	10	-3	137	143	-13	6	144	152	-19
5	235	238	-8					-2	123	124	-1	7	155	149	13
6	284	290	-15		5	4	1	-1	149	126	40				
7	176	173	6					0	146	149	-5		6	-6	1
8	153	138	33	-13	124	115	18	1	174	174	0				
				-12	146	136	21	2	160	147	29	0	288	267	48
	5	1	1	-11	127	121	9	3	120	115	10	1	275	286	-27
				-10	163	163	0	4	102	98	7	2	237	258	-52
-13	127	125	4	-9	172	181	-19					3	194	181	28
-12	224	231	-14	-8	158	163	-11		5	8	1	4	147	156	-19
-11	211	207	7	-7	260	245	35					5	144	139	9
-10	180	174	13	-6	289	299	-24	-10	84	73	32	6	179	169	23
-9	264	275	-27	-5	254	263	-24	-9	86	86	0	7	142	134	19
-8	224	220	10	-4	265	267	-4	-8	106	113	-15				
-7	158	155	5	-3	392	403	-24	-7	122	119	4		6	-5	1
-6	402	415	-29	-2	304	307	-5	-6	143	133	18				
-5	319	320	-4	-1	273	270	7	-5	151	144	12	0	308	327	-45
-4	184	182	5	0	354	347	16	-4	131	126	7	1	235	222	32
-3	391	406	-35	1	247	245	4	-3	148	135	22	2	260	275	-35
-2	538	522	29	2	271	280	-20	-2	133	146	-22	3	200	226	-65
-1	320	338	-47	3	277	287	-21	-1	100	104	-6	4	172	147	53
0	429	441	-27	4	168	170	-4	0	132	116	32	5	195	209	-31
1	440	409	63	5	148	136	27	1	153	155	-5	6	245	248	-7
2	157	170	-36	6	153	155	-3	2	108	101	14	7	146	140	15
3	376	391	-34												
4	329	329	-1		5	5	1		5	9	1		6	-4	1
5	107	106	2												
6	213	203	22	-12	128	115	26	-8	89	78	16	0	382	376	13
7	213	223	-25	-11	122	120	4	-7	81	79	2	1	258	273	-38
8	149	143	13	-10	135	133	3	-6	85	87	-4	2	205	182	55
				-9	131	118	23	-5	103	103	0	3	229	245	-39
	5	2	1	-8	142	146	-10	-4	90	103	-23	4	168	185	-40
				-7	193	190	5	-3	101	99	2	5	231	222	21
-13	121	112	19	-6	245	243	4	-2	99	91	15	6	245	246	-2
-12	207	193	34	-5	325	336	-23	-1	61	71	-16	7	172	163	21
-11	187	204	-36	-4	307	314	-16	0	79	78	2				
-10	220	214	15	-3	285	269	36						6	-3	1
-9	261	255	12	-2	301	303	-5		6	-11	1				
-8	289	294	-13	-1	232	249	-40					0	252	266	-39
-7	269	273	-12	0	179	175	8	0	151	144	13	1	396	384	25
-6	242	241	2	1	246	250	-8	1	115	112	6	2	210	217	-20
-5	425	434	-19	2	287	294	-16	2	95	88	12	3	164	150	33
-4	394	385	19	3	167	168	-2					4	192	201	-22
-3	256	261	-14	4	175	171	10		6	-10	1	5	279	287	-19
-2	394	403	-20	5	167	158	19					6	191	177	30
-1	313	313	1	6	114	110	6	0	121	121	1	7	156	158	-4
0	261	280	-52					1	156	152	8				
1	299	309	-25		5	6	1	2	128	132	-9		6	-2	1
2	302	275	61					3	94	102	-17				
3	296	310	-35	-12	76	66	22	4	81	87	-9	0	254	276	-60
4	205	205	0	-11	107	95	21					1	209	217	-20
5	179	185	-14	-10	132	125	14		6	-9	1	2	243	241	4
6	135	126	17	-9	114	110	6					3	140	137	7
7	153	147	12	-8	141	143	-4	0	147	126	37	4	133	141	-18
8	178	178	1	-7	145	158	-27	1	128	128	0	5	306	321	-34
				-6	111	107	6	2	122	120	3	6	194	196	-4
	5	3	1	-5	111	104	12	3	116	104	23	7	156	141	33
				-4	142	156	-30	4	99	106	-13				
-13	153	146	16	-3	126	141	-28	5	90	85	9		6	-1	1
-12	188	166	50	-2	191	183	16								
-11	148	136	22	-1	226	229	-6		6	-8	1	0	536	511	45
-10	187	192	-12	0	127	139	-23					1	311	320	-20
-9	202	200	4	1	171	157	27	0	218	229	-23	2	272	296	-64

3	316	307	20				
4	256	275	-45	-13	104	104	0
5	253	240	27	-12	163	159	10
6	216	219	-6	-11	161	149	28
7	192	182	23	-10	145	158	13
				-9	201	204	-5
	6	0	1	-8	123	121	2
				-7	125	117	16
-13	134	120	30	-6	339	333	13
-12	142	141	1	-5	333	329	8
-11	215	216	-1	-4	315	301	31
-10	183	170	29	-3	363	366	-5
-9	189	200	-28	-2	302	297	10
-8	265	274	-21	-1	212	213	-1
-7	84	61	37	0	234	233	1
-6	205	214	-25	1	221	207	31
-5	526	518	13	2	116	125	-17
-4	348	345	6	3	269	273	-9
-3	559	562	-4	4	232	230	4
-2	570	546	41	5	133	129	8
-1	256	266	-27	6	158	149	19
0	316	330	-34				
1	332	298	77		6	4	1
2	182	194	-29				
3	204	217	-33	-12	148	127	45
4	420	437	-34	-11	132	125	15
5	257	264	-14	-10	131	131	0
6	188	177	26	-9	180	169	21
7	208	204	10	-8	153	151	4
				-7	214	217	-5
	6	1	1	-6	299	285	31
				-5	313	310	5
-13	149	136	28	-4	296	291	12
-12	158	156	4	-3	257	249	16
-11	250	259	-19	-2	270	281	-23
-10	193	196	-6	-1	243	257	-32
-9	172	166	12	0	179	176	4
-8	256	264	-20	1	210	203	15
-7	111	112	-2	2	212	216	-8
-6	185	185	0	3	221	211	23
-5	386	393	-16	4	204	191	31
-4	393	382	23	5	175	171	9
-3	260	263	-7				
-2	350	362	-28		6	5	1
-1	366	356	22				
0	196	209	-34	-12	120	117	5
1	185	201	-42	-11	113	108	9
2	242	222	46	-10	130	121	19
3	119	132	-27	-9	91	84	10
4	272	271	1	-8	52	37	12
5	256	254	3	-7	146	141	9
6	175	164	24	-6	203	201	5
7	172	154	39	-5	248	237	23
				-4	284	290	-12
	6	2	1	-3	235	233	4
				-2	184	170	28
-13	132	117	31	-1	191	186	12
-12	166	156	21	0	124	136	-21
-11	196	198	-2	1	95	97	-1
-10	183	197	-31	2	203	199	8
-9	223	222	2	3	196	196	-1
-8	196	182	33	4	137	130	14
-7	144	143	2				
-6	299	296	5		6	6	1
-5	260	256	9				
-4	392	395	-6	-11	82	69	30
-3	393	389	8	-10	98	99	-2
-2	245	237	19	-9	92	86	11
-1	306	316	-25	-8	79	79	-1
0	297	281	37	-7	145	141	6
1	141	142	-2	-6	142	148	-11
2	169	175	-12	-5	124	122	2
3	292	283	21	-4	153	135	31
4	198	202	-7	-3	151	159	-14
5	187	179	18	-2	126	141	-26
6	207	208	-1	-1	138	120	31
				0	120	123	-4
	6	3	1	1	97	106	-18
2	143	135	17				
3	147	142	10	0	216	212	8
				1	232	239	-16
	6	7	1	2	223	235	-27
				3	162	146	32
-10	96	78	33	4	178	180	-4
-9	73	59	25	5	180	182	-4
-8	97	89	18	6	175	158	38
-7	129	130	-3				
-6	152	144	17		7	-3	1
-5	157	162	-10				
-4	147	149	-4	0	212	221	-24
-3	134	128	12	1	137	133	8
-2	140	136	7	2	222	233	-26
-1	104	111	-12	3	186	188	-4
0	109	92	30	4	160	140	44
1	122	129	-14	5	186	190	-11
				6	175	168	15
	6	8	1				
					7	-2	1
-8	92	85	12				
-7	115	116	-3	0	359	338	44
-6	120	116	8	1	227	223	9
-5	132	120	22	2	124	124	0
-4	104	110	-11	3	195	199	-10
-3	80	84	-11	4	190	186	8
-2	85	83	4	5	190	177	29
-1	75	80	-9	6	182	187	-11
	7	-10	1		7	-1	1
0	105	102	5	0	232	249	-43
1	100	103	-5	1	409	401	17
				2	264	264	0
	7	-9	1	3	197	202	-11
				4	261	252	21
0	141	144	-6	5	212	206	13
1	126	124	5	6	149	138	25
2	109	115	-10				
3	116	108	16		7	0	1
	7	-8	1	-12	128	113	31
				-11	143	140	7
0	173	164	18	-10	181	178	5
1	169	166	8	-9	174	163	25
2	124	117	15	-8	209	225	-37
3	116	118	-3	-7	283	294	-27
4	125	123	3	-6	83	61	33
				-5	261	274	-30
	7	-7	1	-4	431	424	13
				-3	239	244	-12
0	219	194	51	-2	306	321	-36
1	196	192	9	-1	340	336	10
2	144	154	-22	0	161	163	-3
3	123	108	31	1	177	188	-27
4	96	101	-9	2	271	263	17
5	104	108	-6	3	197	195	3
				4	196	190	14
	7	-6	1	5	224	219	12
0	275	280	-11		7	1	1
1	215	186	60				
2	206	193	27	-12	140	134	12
3	184	190	-12	-11	154	140	32
4	137	130	15	-10	182	194	-25
5	129	126	6	-9	191	192	-1
				-8	217	201	36
	7	-5	1	-7	222	231	-20
				-6	164	160	9
0	290	296	-15	-5	243	235	19
1	220	239	-45	-4	302	304	-4
2	197	176	44	-3	309	311	-3
3	191	191	0	-2	240	242	-4
4	179	182	-8	-1	217	216	3
5	157	144	29	0	268	259	21
6	176	168	18	1	129	133	-9
				2	159	160	-2
	7	-4	1	3	244	235	19

4	191	186	11						8 0 1			-1	142	133	18
5	163	151	26	-9	110	100	19					0	155	144	22
				-8	86	84	4	-11	104	94	18				
	7 2 1			-7	100	104	-7	-10	142	132	20		8 5 1		
				-6	128	124	8	-9	175	181	-13				
-12	124	116	16	-5	129	127	3	-8	200	186	28	-8	113	105	15
-11	141	136	12	-4	137	131	12	-7	239	238	1	-7	83	89	-9
-10	163	148	32	-3	144	128	32	-6	252	255	-5	-6	100	96	6
-9	207	198	20	-2	132	132	0	-5	182	159	45	-5	117	110	13
-8	251	251	0	-1	110	117	-14	-4	196	193	5	-4	99	101	-4
-7	146	146	-1	0	104	102	3	-3	235	231	8	-3	115	113	3
-6	199	193	13					-2	147	136	19	-2	135	134	1
-5	289	289	0		7 7 1			-1	195	200	-10				
-4	222	209	27					0	244	254	-20		9 -6 1		
-3	258	270	-27	-7	111	104	12	1	187	183	10				
-2	284	294	-23	-6	96	103	-13	2	141	139	5	0	131	116	29
-1	161	155	11	-5	110	102	13	3	234	225	19				
0	217	217	0	-4	122	122	0						9 -5 1		
1	225	219	13	-3	103	106	-5		8 1 1						
2	147	134	24	-2	100	93	12					0	157	165	-18
3	174	167	16					-11	140	129	23				
4	212	209	6		8 -8 1			-10	131	119	25		9 -4 1		
								-9	188	182	13				
	7 3 1			0	88	92	-7	-8	218	210	18	0	160	167	-15
				1	114	104	18	-7	211	195	31	1	196	203	-15
-12	110	102	15					-6	190	189	1				
-11	145	145	-1		8 -7 1			-5	211	215	-7		9 -3 1		
-10	163	159	10					-4	164	155	17				
-9	182	181	2	0	161	167	-14	-3	176	166	21	0	146	127	40
-8	220	216	8	1	167	147	43	-2	223	232	-19	1	188	186	2
-7	127	125	3	2	132	135	-6	-1	191	190	2				
-6	179	178	2					0	180	170	22		9 -2 1		
-5	268	278	-21		8 -6 1			1	208	209	-1				
-4	265	259	11					2	157	155	6	0	234	241	-17
-3	254	239	31	0	181	176	11	3	181	170	24	1	182	168	30
-2	259	264	-10	1	225	220	10								
-1	227	226	3	2	166	155	24		8 2 1				9 -1 1		
0	170	158	24	3	155	151	8								
1	195	187	17					-11	123	113	13	0	230	236	-14
2	203	200	7		8 -5 1			-10	123	122	3	1	209	201	16
3	145	145	0					-9	151	145	14				
4	149	145	8	0	182	160	42	-8	215	204	27		9 0 1		
				1	227	222	12	-7	223	225	-5				
	7 4 1			2	200	203	-8	-6	178	162	29	-9	152	140	26
				3	156	145	23	-5	217	201	31	-8	202	189	29
-11	99	89	18					-4	192	197	-9	-7	145	138	15
-10	130	119	23		8 -4 1			-3	138	128	16	-6	159	151	17
-9	167	165	4					-2	195	200	-9	-5	196	199	-5
-8	188	174	28	0	235	249	-31	-1	219	231	-30	-4	171	161	19
-7	183	181	3	1	193	174	43	0	153	152	1	-3	122	125	-7
-6	238	236	4	2	197	192	10	1	135	137	-3	-2	157	172	-35
-5	225	212	25	3	164	166	-5	2	182	187	-11	-1	171	170	2
-4	220	220	0	4	144	129	30					0	174	160	32
-3	209	223	-29						8 3 1						
-2	179	163	31		8 -3 1								9 1 1		
-1	198	195	5					-10	173	161	25				
0	176	186	-24	0	216	231	-33	-9	197	185	26	-9	148	138	21
1	154	147	15	1	185	192	-13	-8	196	185	26	-8	174	158	35
2	179	175	9	2	161	143	41	-7	205	185	44	-7	168	163	11
3	189	178	25	3	159	170	-26	-6	173	169	9	-6	135	126	17
				4	189	188	2	-5	167	153	28	-5	161	153	15
	7 5 1							-4	172	170	3	-4	173	186	-27
					8 -2 1			-3	180	187	-16	-3	113	121	-16
-10	108	101	13					-2	203	189	30	-2	130	126	9
-9	117	119	-3	0	239	247	-15	-1	206	200	13	-1	196	201	-10
-8	57	63	-11	1	246	257	-25	0	196	193	4				
-7	74	69	9	2	200	196	8	1	126	122	9		9 2 1		
-6	152	151	1	3	147	139	18								
-5	144	155	-19	4	210	201	19		8 4 1			-8	132	120	24
-4	162	156	11									-7	153	143	21
-3	190	181	17		8 -1 1			-9	145	129	32	-6	175	169	14
-2	127	134	-14					-8	157	157	0	-5	173	154	37
-1	105	102	5	0	271	266	11	-7	140	142	-3	-4	160	157	7
0	125	124	1	1	215	209	15	-6	169	163	13	-3	162	162	-1
1	143	130	26	2	238	238	0	-5	142	145	-5	-2	142	135	15
2	135	119	31	3	210	207	6	-4	105	98	12				
				4	172	152	31	-3	152	140	24		9 3 1		
	7 6 1							-2	168	166	5				

-6	145	132	24	-5	158	150	16	-4	133	119	26	-3	144	133	15